DEVELOPMENT, VERIFICATION, AND DESIGN ANALYSIS

OF THE BOREHOLE FLUID THERMAL MASS MODEL FOR

APPROXIMATING SHORT TERM BOREHOLE THERMAL

RESPONSE

by

THOMAS RAY YOUNG

Bachelor of Science

Oklahoma State University

Stillwater, Oklahoma

2001

Submitted to the Faculty of the
Graduate College of the
Oklahoma State University
in partial fulfillment of
the requirements for
the degree of
MASTERS OF SCIENCE
Oklahoma State University
December, 2004

DEVELOPMENT, VERIFICATION, AND DESIGN ANALYSIS

OF THE BOREHOLE FLUID THERMAL MASS MODEL FOR

APPROXIMATING SHORT TERM BOREHOLE THERMAL

RESPONSE

Thesis Approved:

Dr. Spitler
Thesis Advisor

Dr. Delahoussaye

Dr. Fisher

Dr. Emsile
Dean of Graduate College

ACKNOWLEDGEMENTS

In order to give credit where it is due, my conscience requires that, at the very least, I mention God who sent his son Jesus Christ to die in my place, for my sins, and gives eternal life to everyone who believes in Jesus. Without the grace, mercy, strength and wisdom God has provided me in various ways, this thesis would never have been finished. He deserves ALL the honor and glory.

Also I am indebted to Dr. Spitler for his willingness to take me on as one of his students. His expertise and experience were invaluable and his willingness to continue working with me after I took a job and left Stillwater is very much appreciated

I would like to thank Dr. Delahoussaye for his mentoring early on in my research. Dr. Delahoussaye was essential in helping me gain the programming skills and practical understanding that I needed to succeed.

To Aditya, Hayder, and Liu I appreciate your friendships, learned from your expertise, and enjoyed working with you greatly. I would especially like to thank Xiaowei for the hours he spent running simulation and examining my work.

I would also like to thank my wife Rachel who provided moral support through a listening ear and plenty of cookies and brownies.

I would like to thank my parents for instilling in me moral values and a good work ethic. Also, thank you for your prayers and financial support.

I should also mention my Sunday school class for all there prayers and moral support. Hardly a Sunday went by without someone asking me how the thesis was going.

TABLE OF CONTENTS

LIST OF TABLES

LIST OF FIGURES

1   INTRODUCTION

"As long as the earth endures, seedtime and harvest, cold and heat, summer and winter, day and night will never cease." (Genesis 8:22, NIV) The basic needs of man which include keeping warm in winter and cool in summer have remained constant throughout history. The technology used to meet the needs has changed. People and animals have historically used caves and manmade holes as shelter from the elements. In this way humans have been extracting heat from the earth to keep warm in winter and using the earth to keep cool in summer for centuries. Modern man uses more refined methods for extracting and rejecting heat from the ground such as ground source heat pump (GSHP) systems.

The term "ground source heat pump (GSHP)" refers to heat pump systems that use either the ground or a water reservoir as a heat source or sink. GSHP systems are either open-loop or closed-loop. Open-loop GSHP systems use a pump to circulate groundwater through the heat pump heat exchanger. A closed-loop GSHP system uses a water pump to circulate fluid through pipes buried horizontally or inserted into boreholes in the ground. The buried closed loop version of the GSHP is commonly referred to as a ground loop heat exchanger (GLHE).

The physical properties of boreholes are very important to the study of GLHE systems. Boreholes typically range between 46 to 122 meters (150 to 400 ft) deep and are typically around 10 to 15 cm (4 to 6 inches) in diameter. A borehole system can be

composed of anywhere from 1 to over 100 boreholes. Each borehole in a multi-borehole system is typically placed at least 4.5 m (15 ft) from all other boreholes. Figure 1-1 shows a vertical cross section of three boreholes. Each borehole is connected to the other boreholes with pipes that are typically buried 1-2 meters (3-6 ft) under the top surface.
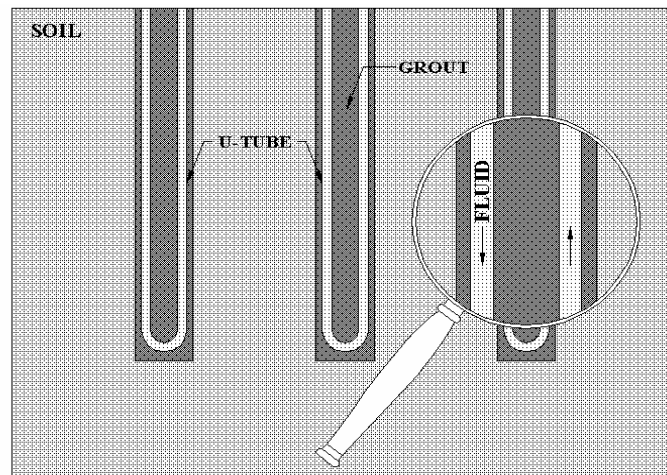
Figure 1-1 Borehole system

After the U-tube is inserted, the borehole will usually be backfilled with grout. The grout is used to prevent contamination of aquifers. Figure 1-1 shows 3 ideal boreholes. The grout is often a bentonite clay mixture, with the possibility of having thermally-enhanced additives. The grout usually has a thermal conductivity significantly lower than the surrounding ground. The circulating fluid is water or a water-antifreeze mixture. Each borehole is shown in this picture to be parallel with the other boreholes and perpendicular to the surface of the ground. In reality, drilling rigs do not drill perfectly straight, causing the path of a borehole to deviate, especially in deep boreholes.

The U-tube as shown in Figure 1-1 has equal spacing between the two legs of the U-tube throughout the borehole. In real systems, however, the U-tube leg spacing does

not necessarily remain constant throughout the length of the borehole. Spacers are

sometimes employed to force the tubes towards the borehole wall.

Figure 1-2 shows a two dimensional horizontal cross section of a single borehole.

The U-tube leg spacing is called the shank spacing and is defined as the shortest distance

between the outer pipe walls of each leg of the U-tube.
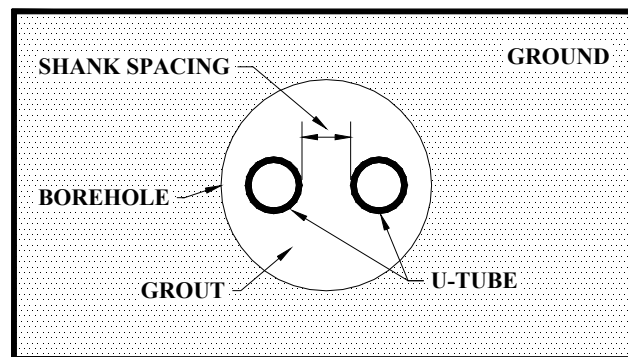
Figure 1-2 Borehole Cross Section

As previously mentioned, the size of a borehole heat exchanger system can range

from one borehole to over a hundred. For small buildings one borehole may suffice but

for large commercial buildings over 100 boreholes are sometimes required. This can

make the initial investment quite costly. The main advantage of a GSHP system over an

air-source heat pump system is that it rejects heat to the ground in the summer, when the

ground is cooler than the air, and extracts heat from the ground during the winter, when

the ground is warmer than the air.

A GSHP system will very seldom reject the same amount of heat as it extracts on

an annual basis. In cold climates, for envelope-dominated buildings, the GSHP system

will extract much more heat from the ground than it rejects to the ground. In this case,

the ground surrounding the boreholes gradually declines in temperature. Over time, the

reduction in the ground temperature around the boreholes will decrease the performance

3

of the heat pump in heating mode. In cold climates, the fluid circulating in the boreholes might drop below freezing, requiring the addition of antifreeze in the system. Similarly in warm climates, since more heat is rejected to the ground than extracted from the ground, the ground temperature will rise. This will impair the performance of the heat pump in cooling mode. The actual annual imbalance depends not only on climate but also on the building internal heat gains and building design.

The thermal loads over a number of years must be accounted for when designing a GSHP system. This is necessary to determine the impact of any annual heat imbalance. If a borehole heat exchanger (BHE) is over-designed, the initial construction costs may be excessive. If the system is under-designed, the BHE may not meet the long term heating or cooling needs of the user.

Research has been conducted for the purpose of applying GSHP technology to other areas besides buildings. Chiasson and Spitler (2001 and 2000) at Oklahoma State University have conducted research applying GSHP technology to highway bridges. The system uses pipes embedded in the road pavement to circulate fluid from a GSHP to eliminate ice or snow formation. The potential benefits of this new application include safer driving conditions and longer lasting bridges and roads due to reduced corrosion.

Engineers who are attempting to design a GSHP system for a specific application can use programs such as GLHEPRO (Spitler 2000) to describe a potential system composed of a specific ground loop heat exchanger and heat pump and then simulate the systems response to monthly and peak, heating and cooling loads. Using programs such as GLHEPRO, engineers can also optimize the depth of a specific borehole heat exchanger configuration.

1.1 BACKGROUND

Regardless of the GSHP application, the thermal response of the GLHE plays an important part in the design and simulation of GSHP systems. Since thermal loading on typical GLHE systems is of long duration, design methodologies have focused, in some detail, on long time step responses to monthly loads. (Eskilson, 1987) However, short time responses have typically been modeled only crudely using analytical models such as the cylinder source. These short time responses can be very important in determining the effect of daily peak loads. Daily peak loads occur in all applications but may be dominant in applications such as church buildings, concert halls, and the Smart Bridge application. To model the short-time response, it is important to accurately represent such details as the borehole radius, U-tube diameter and shank spacing, as well as the thermal properties and mass of the circulating fluid, U-tube and grout. This thesis presents a new methodology for modeling the short time GLHE thermal response. This is particularly important for systems with peak-load-dominant loading conditions.

1.2 LITERATURE REVIEW

The literature review describes different methods that have been developed to model borehole heat exchangers. The methods are divided into two categories: steady state and transient.

Quasi-steady state conditions occur in two-dimensional borehole cross sections, as shown in Figure 1-2 when the circulating fluid, U-tubes and grout within a borehole do not change temperature (relative to each other) with time for a constant heat flux. If the internal borehole temperature differences are constant, the borehole resistance, defined as the resistance between the circulating fluid and the borehole, is also constant. Thus,

when a borehole's internal temperature differences have stabilized for a constant heat flux, the borehole resistance can be modeled as a constant.

Transient modeling of borehole heat exchangers might be broken into three different regions. The first region deals with transients that occur within the borehole before the borehole reaches steady state. For this transient region, the borehole may be modeled as having infinite length since surface and bottom end effects can be neglected. Two dimensional geometric and thermal properties of the borehole influence the temperature response in the first region. The second region occurs after the internal geometric and thermal properties of the borehole cease to influence the temperature response and before the surface and bottom end effects influence the temperature response. The third transient region occurs when three dimensional effects such as borehole to borehole interaction, surface and bottom end effects influence the temperature response.

The borehole transient resistance or g-function is broken into two zones called the short time step (STS) g-function (Yavuzturk, 1999) and the long time step (LTS) g-function. (Eskilson, 1987) The short and the long time step g-functions relate to the three regions described above in that the short time step g-function represents region one and two and the long time step g-function represents region two and three. Thus it is important to note that the short and long time step g-function can both represent region 2. This allows the two g-functions to be integrated into one continuous g-function curve, allowing the borehole transient resistance to be known for small times, such as 0.5 hours, to large times, such as 100 years. Short and long time step g-functions are discussed in

detail in section 1.2.2.3 and 1.2.2.2 respectively. The next two sections, however, will discuss the current literature for steady state and transient borehole modeling.

1.2.1 Steady State Modeling of Boreholes

This section discusses borehole resistance since it is an important part of transient analysis. The borehole resistance is the thermal resistance between the fluid and the borehole wall. Figure 1-3 shows a cross-section of a borehole and a corresponding thermal delta circuit.
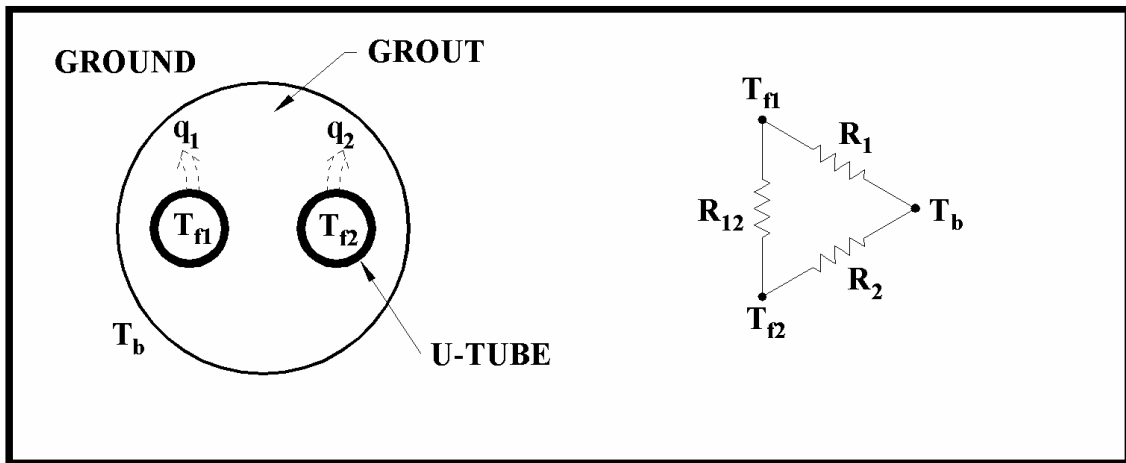
Figure 1-3 Cross-section of the Borehole and the Corresponding Thermal Δ-Circuit (Hellström, 1991 p.78)

T_{f1} and T_{f2} (°C or °F) represent the fluid temperature in each leg of the U-tube

and q_1 and q_2 $\left[\dfrac{W}{m} \ or \ \dfrac{Btu}{hr \cdot ft} \right]$ the heat flux (heat transfer rate per unit length of borehole)

from the circulating fluid. T_b represents the average temperature on the borehole wall.

As shown in the delta circuit in Figure 1-3, the thermal resistance between T_{f1} and T_b is

R_1 $\left[\dfrac{mK}{W} \ or \dfrac{hr \cdot ft \cdot {}^{\circ} F}{Btu} \right]$ and the thermal resistance between T_{f2} and T_b is R_2

$\left[\dfrac{mK}{W} \, or \, \dfrac{hr \cdot ft \cdot ^{\circ} F}{Btu} \right]$. R_{12} represents the "short circuit" resistance for heat flow between T_{f1}

and T_{f2}. However, if the fluid temperatures in each leg of the U-tube are approximately

equal, which occurs at the bottom of the borehole, the resistance R_{12} can be neglected in

the Δ-circuit. The R_{12} resistance is often neglected for the entire borehole. This has the

effect of decoupling one leg of the U-tube from the other, greatly simplifying the system.

Figure 1-4 shows a decoupled borehole system with a circuit diagram defining R_1

and R_2.
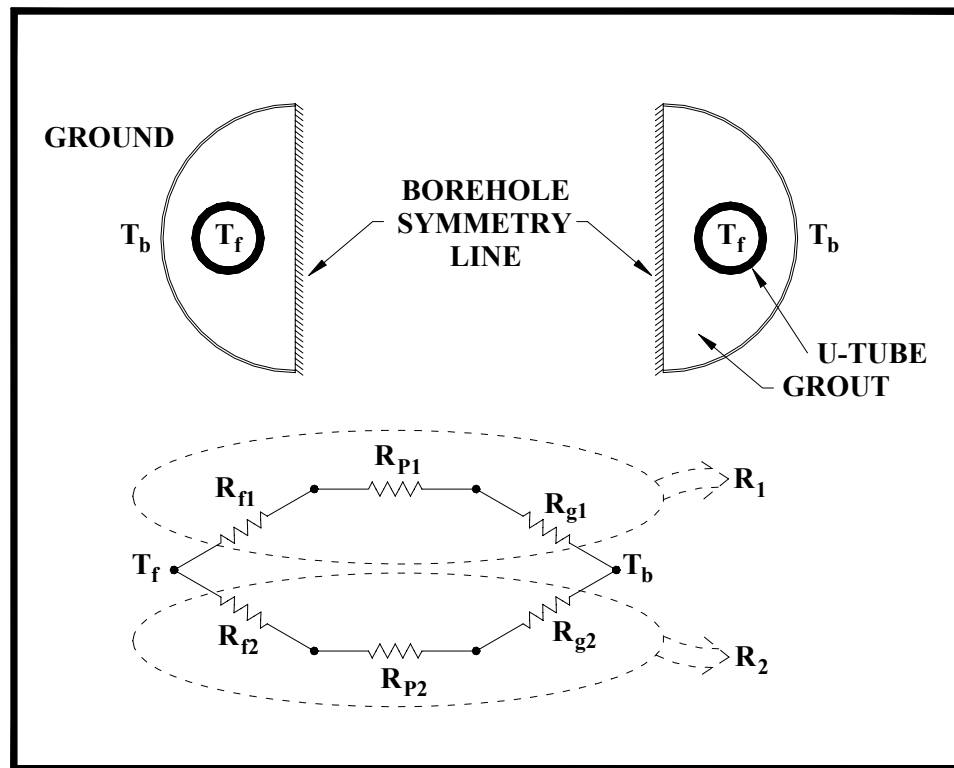
Figure 1-4 Cross Section of a Borehole with Symmetry Line and the Corresponding Thermal Circuit.

In decoupling the borehole, the assumption is made that the grout, pipe, and fluid

for each half of the borehole have the same geometry and thermal properties. This

8

assumption means that $R_{f1} = R_{f2}$, $R_{p1} = R_{p2}$, and $R_{g1} = R_{g2}$. Thus R_1 and R_2, from the circuit in Figure 1-3, are equal. However, the total resistance of the grout is not typically written in terms of the grout resistance for half of the borehole. The overall grout resistance is instead lumped in one R_g term.

With these assumptions the borehole resistance circuit shown in Figure 1-4 can easily be reduced to produce Equation 1-1. This equation describes the overall borehole resistance.

$$R_{total} = R_{grout} + \frac{R_{pipe} + R_{fluid}}{2}$$ (1-1)

where,

R_{total} = borehole thermal resistance $\left(\dfrac{mK}{W}\right)$ or $\left(\dfrac{h \cdot ft \cdot {}^\circ F}{Btu}\right)$

R_{grout} = grout thermal resistance $\left(\dfrac{mK}{W}\right)$ or $\left(\dfrac{h \cdot ft \cdot {}^\circ F}{Btu}\right)$

R_{pipe} = pipe thermal resistance for one tube $\left(\dfrac{mK}{W}\right)$ or $\left(\dfrac{h \cdot ft \cdot {}^\circ F}{Btu}\right)$

R_{fluid} = fluid thermal resistance for one tube $\left(\dfrac{mK}{W}\right)$ or $\left(\dfrac{h \cdot ft \cdot {}^\circ F}{Btu}\right)$

The two major contributors to the borehole resistance are the grout and pipe resistance. The fluid resistance contributes typically less than one percent to the overall steady state borehole resistance for turbulent flow. For laminar flow the contribution made by the fluid resistance is much greater and can exceed twenty percent of R_{total}.

The pipe resistance can be calculated with Equation 1–2 (Drake and Eckert, 1972).

$$R_{pipe} = \frac{\ln\left(\dfrac{r_2}{r_1}\right)}{2\pi k}$$

where,

R_{pipe} = pipe thermal resistance $\left(\dfrac{mK}{W}\right)$ or $\left(\dfrac{h \cdot ft \cdot °F}{Btu}\right)$

k = Conductivity of the pipe $\left(\dfrac{W}{mK}\right)$ or $\left(\dfrac{Btu}{h \cdot ft \cdot °F}\right)$

r_2 = outside diameter (m) or (ft)

r_1 = Inside diameter (m) or (ft)

The fluid resistance can be calculated using Equation 1-3 (Drake and Eckert, 1972).

$$R_{fluid} = \frac{1}{2\pi r_1 h}$$

where,

R_{fluid} = fluid thermal resistance $\left(\dfrac{mK}{W}\right)$ or $\left(\dfrac{h \cdot ft \cdot °F}{Btu}\right)$

h = convection coefficient of the fluid $\left(\dfrac{W}{m^2 K}\right)$ or $\left(\dfrac{Btu}{h \cdot ft^2 \cdot °F}\right)$

r_1 = U-tube inside diameter (m) or (ft)

The grout resistance can be calculated from the average temperature profile at the borehole wall and the surface of the U-tubes with Equation 1-4 (Hellström, 1991), presuming these temperatures are available.

$$R_{grout} = \frac{T_{U-tube} - T_{BH-Wall}}{Q} \qquad \textbf{(1-4)}$$

where,

R_{grout} = grout thermal resistance $\left(\dfrac{mK}{W}\right)$ or $\left(\dfrac{h \cdot ft \cdot {}^\circ F}{Btu}\right)$

Q = Heat flux per unit length of U-tube $\left(\dfrac{W}{m}\right)$ or $\left(\dfrac{Btu}{h \cdot ft}\right)$

T_{U-tube} = Average temperature at outer surface of U-tube (K) or (°F)

$T_{BH-Wall}$ = Average borehole wall temperature (K) or (°F)

The grout resistance is the most complicated component of the borehole resistance. Unlike the pipe and fluid resistance, the apparent grout resistance will change significantly over the first few hours of heat injection or extraction.

There are several methods of calculating the grout thermal resistance. The methods that are used to directly calculate the steady state borehole resistance are the Gu and O'Neal (a, 1998) approximate diameter equation, the Paul (1996) method, and the multipole (Bennet and Claesson, 1987) method. Other methods calculate the transient heat transfer between the fluid and surrounding ground, but may be applied to calculate the borehole resistance, include the cylinder source (Ingersoll, 1948) method, and the finite volume method (Yavuzturk, 1999).

1.2.1.1 Line Source Model

The line source developed by Kelvin and later solved by Ingersoll and Plass (1948), is the most basic model for calculating heat transfer between a line source and the earth. In this model the borehole geometry is neglected and modeled as a line source or sink of infinite length, surrounded by an infinite homogenous medium. Thus, with

11

respect to modeling a borehole, the line source model neglects the end temperature effects.

Equation 1-5 is the general equation that Ingersoll and Plass (1948) used to model the temperature at any point in an infinite medium from a line source or sink. The medium is assumed to be at a uniform temperature at time zero.

$$\Delta T = \frac{q}{4\pi k_{soil}} \int_{x}^{\infty} \frac{e^{-\beta}}{\beta} d\beta \tag{1-5}$$

where,

$$x = \frac{r^2}{4\alpha_{soil}t} \tag{1-6}$$

ΔT = change in ground temperature at a distance r from the line source (°C) or (°F)

q = heat transfer rate per length of line source $\left(\dfrac{W}{m}\right)$ or $\left(\dfrac{Btu}{h \cdot ft}\right)$

t = time duration of heat input q (s)

r = radius from the line source (m) or (ft)

α_{soil} = soil thermal diffusivity $\left(\dfrac{m^2}{s}\right)$ or $\left(\dfrac{ft^2}{s}\right)$

k_{soil} = conductivity of the soil $\left(\dfrac{W}{mK}\right)$ or $\left(\dfrac{Btu}{h \cdot ft \cdot °F}\right)$

The integral in Equation 1-5 can be approximated with Equation 1-7 for an mth stage of refinement.

$$I(x) = -\gamma - \ln(x) - \sum_{n=1}^{m} \frac{(-1)^n x^n}{n \cdot n!}$$

<div align="right">(1-7)</div>

where,

x = Defined by Equation 1–6

γ = 0.5772156649 = Euler's Constant

Equation 1-7 shows the general form of the line source for the mth stage of refinement. In most references the second stage of refinement is used. This method is only accurate for large times. For a typical borehole this equates to times greater than approximately 10 hours.

For small times, less than 10 hours, the Gauss-Laguerre quadrature approximation, as shown in Equation 1-8, is given. This approximation uses the fourth order Gauss-Laguerre quadrature to solve the infinite integral in Equation 1-5.

$$I_{quad}(x) = e^{-x}\left(w_{41} \cdot \frac{1}{x + z_{41}} + w_{42} \cdot \frac{1}{x + z_{42}} + w_{43} \cdot \frac{1}{x + z_{43}} + w_{44} \cdot \frac{1}{x + z_{44}} \right)$$

<div align="right">(1-8)</div>

where,

$w_{41} = 0.6031541043$ $z_{41} = 0.322547689619$

$w_{42} = 0.357418692438$ $z_{42} = 1.745761101158$

$w_{43} = 0.0388879085150$ $z_{43} = 4.536620296921$

$w_{44} = 0.00053929470561$ $z_{44} = 9.395070912301$

The Gauss – Laguerre quadrature approximation shown here should be used for small times, approximately less than 10 hours.

Equation 1-9 is a modification of Equation 1-5 and shows how to use the line source to model the borehole fluid temperature. Without the borehole resistance ($q \cdot R_{bh}$)

<div align="center">13</div>

the borehole temperature (T) would be the temperature at the borehole wall radius and not the fluid temperature.

$$T(t) = \frac{q}{4\pi k_{soil}} \cdot I\left(\frac{r_{bh}^2}{4\alpha_{soil}t}\right) + q \cdot R_{bh} + T_{ff}$$

<div align="right">(1-9)</div>

T = Borehole fluid temperature (°C) or (°F)

t = time duration of heat input (s)

T_{ff} = far field temperature of the soil (°C) or (°F)

q = heat transfer rate per length of line source $\left(\dfrac{W}{m}\right)$ or $\left(\dfrac{Btu}{h \cdot ft}\right)$

r_{bh} = radius of the borehole (m) or (ft)

R_{bh} = steady state borehole resistance $\left(\dfrac{mK}{W}\right)$ or $\left(\dfrac{h \cdot ft \cdot °F}{Btu}\right)$

α_{soil} = soil thermal diffusivity $\left(\dfrac{m^2}{s}\right)$ or $\left(\dfrac{ft^2}{s}\right)$

k_{soil} = conductivity of the soil $\left(\dfrac{W}{mK}\right)$ or $\left(\dfrac{Btu}{h \cdot ft \cdot °F}\right)$

Equation 1-9 differs from Equation 1.5 in that it uses the steady state borehole resistance to model the heat transfer from the borehole wall to the fluid; the line source model is used to model the heat transfer between the borehole wall and the far field. This usage of the line source requires that the steady state borehole resistance is known. Since the steady state resistance is used the line source will have error for short times before the borehole reaches steady state resistance. For most boreholes the error in the steady state borehole resistance is negligible at 2 hours.

The line source model is very easy to use and requires relatively few calculations compared to other methods. However, the drawback to this model is that the borehole

internal geometry, thermal properties, and the mass of the fluid are not modeled. The

resulting inaccuracies will be examined in Chapter 4.

1.2.1.2 Gu-O'Neal Equivalent Diameter Model

The Gu and O'Neal (1998 a) equivalent diameter method is a very simple method

of calculating the steady state borehole thermal resistance. It yields a steady state

borehole resistance value that is adequate for most simple calculations.

This method is represented by an algebraic equation for combining the U-tube

fluid into one circular region inside the center of the borehole such that the resistance

between the equivalent diameter and borehole wall is equal to the steady state borehole

resistance of the grout. Equation 1–10 is used to calculate the equivalent diameter. As

can be seen the equivalent diameter is based solely on the diameter of the U-tube and the

center to center distance between the two legs.

$$D_{eq} = \sqrt{2D \cdot L_s} \qquad D \le L_s \le r_{BH} \qquad\qquad \textbf{(1-10)}$$

where,

D_{eq} =   Equivalent diameter (m) or (ft)

r_{BH} =   radius of the borehole (m) or (ft)

D =   diameter of the U-tube (m) or (ft)

L_s =   center to center distance between the two legs (m) or (ft)

Figure 1-5 shows three actual configurations and their equivalent diameters. "d"

shows the equivalent diameter for configuration "a"; "e" for "b"; and "f" for "c".
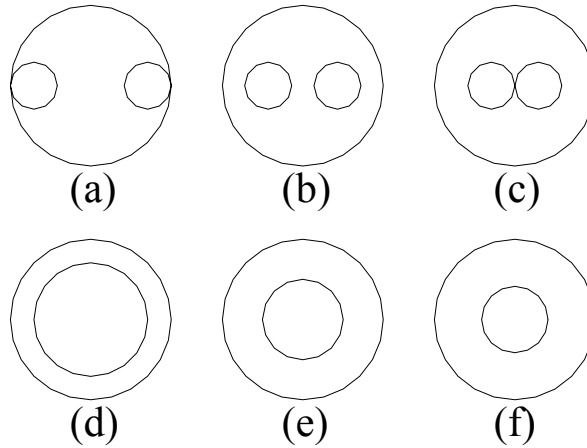
Figure 1-5 Actual Geometry vs Equivalent Diameter Approximation

To calculate the grout resistance, Equation 1-11, which is the general equation for radial heat conduction through a cylinder, should be employed.

$$R_{grout} = \frac{\ln\left(\dfrac{D_{bh}}{D_{eq}}\right)}{2\pi k_{grout}}$$

(1-11)

where,

R_{grout} = grout thermal resistance $\left(\dfrac{mK}{W}\right)$ or $\left(\dfrac{h \cdot ft \cdot {}^{\circ}F}{Btu}\right)$

k_{grout} = conductivity of the grout $\left(\dfrac{W}{mK}\right)$ or $\left(\dfrac{Btu}{h \cdot ft \cdot {}^{\circ}F}\right)$

D_{bh} = diameter of the borehole (m) or (ft)

D_{eq} = equivalent diameter using Gu-O'Neal's method (m) or (ft)

The steady state resistance of the grout can be used in Equation 1.1 to calculate the overall borehole resistance.

1.2.1.3 Paul Model

An experimentally and analytically based method for calculating steady state borehole resistance was developed at South Dakota State University by Paul (1996). The Paul method for calculating the steady state borehole resistance was created using both experimental data and a two dimensional finite element program for modeling a borehole cross section. Several different borehole parameters were modeled such as shank spacing, borehole diameter, U-tube diameter, grout conductivity, and soil conductivity.

The test apparatus used a single layer thick coil of wire wrapped around each side of the U-tube to form an electrical resistance heater. This provided a uniform, constant flux heat input for the system. A real borehole will not have uniform flux at the pipe wall. Heat was input until steady state temperature conditions at the borehole wall radius and along the circumference of the U-tube were reached. The borehole resistance was then calculated from the temperatures and the flux.

A two dimensional finite element model was created using ANSYS, a UNIX based software package, for the purpose of extending the range of borehole diameters and pipe sizes that the steady state borehole resistance could be solved for. The ANSYS cases could be run much faster than the experimental apparatus; this allowed for more cases to be run.

Experimental results from the test apparatus and the ANSYS model were compared for validation purposes. From the results, shape factor correlations were created to model the complex geometry of the borehole. Equation 1-12 is the resulting shape factor equation for calculating the steady state grout resistance.

17

$$R_{grout} = \frac{1}{K_{grout} \cdot S} \quad , \quad S = \beta_0 \cdot \left(\frac{d_b}{d_{U-tube}} \right)^{\beta_1}$$

(1-12)

where,

R_{grout} =   Equivalent diameter (m) or (ft)

K_{grout} =   Conductivity of the grout $\left(\frac{W}{mk} \right)$ or $\left(\frac{Btu}{h \cdot ft \cdot °F} \right)$

S   =   Shape factor (dimensionless)

β_0 and β_1 =   Curve fit coefficients (dimensionless)

d_b =   Diameter of the borehole (m) or (ft)

d_{U-tube} =   Outside diameter of the U-tube (m) or (ft)

Equation fit coefficients are given by Paul (1996) for four different shank

spacings; A0, A1, B and C. The shank spacings are described in Figure 1-6.

Index	Spacing Condition	
A0	S1 = 0	
A1	S1=.123 in (.3124 cm)	
B	S1 = S2	
C	S2 = 0.118 in (.300 cm)	
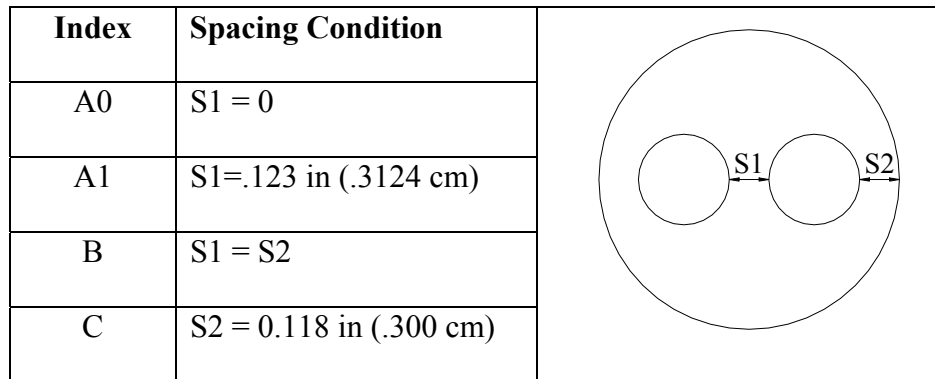
Figure 1-6 Types of shank spacing used in the Paul borehole resistance approximation.

The β_0 and β_1 values for the shank spacing described in Figure 1-6 are given in Table 1-

6.

Table 1-1 Paul Curve Fit Parameters used to Calculate the Steady State Grout Resistance

	A0	A1	B	C
β_0	14.450872	20.100377	17.44268	21.90587
β_1	-0.8176	-0.94467	-0.605154	-0.3796
R	0.997096	0.992558	0.999673	0.9698754

The R value indicates the accuracy of the curve with respect to the experimental or

ANSYS model. An R value of 1 indicates a perfect fit.

The grout resistance found using this method should be applied within Equation

1-1 to determine the overall borehole resistance.

1.2.1.4 Cylinder Source Model

The cylinder source model, created by Ingersoll and Plass (1948), uses an

infinitely long cylinder inside an infinite medium with constant properties and solves the

analytical solution of the 2-D heat conduction equation. The cylinder source solution for

the g-function and temperature change at the borehole wall can be calculated with

Equations 1-13, 14, and 15.

$$\Delta T = \frac{q}{k_{soil}} \cdot G\left(F_o, \frac{r}{r_o}\right) \quad , \quad F_o = \frac{\alpha_{soil} \cdot t}{r^2}$$

(1-13)
(1-14)

$$G\left(F_o, \frac{r}{r_o}\right) = \frac{1}{\pi^2} \int_0^\infty \left(e^{-\beta^2 \cdot F_o} - 1\right) \left[\frac{J_0\left(\frac{r}{r_o} \cdot \beta\right) Y_1(\beta) - J_1(\beta) Y_0\left(\frac{r}{r_o} \cdot \beta\right)}{\left(J_1^2(\beta) + Y_1^2(\beta)\right)\beta^2} \right] d\beta$$

(1-15)

where,

ΔT	=	temperature difference between the steady state temperature of the ground and the temperature at the borehole wall (°C) or (°F)
q	=	heat flux per unit length of the borehole $\left(\frac{W}{m}\right)$ or $\left(\frac{Btu}{h \cdot ft}\right)$
F_o	=	Fourier number (dimensionless)
r	=	inner cylinder radius (equivalent U-tube radius) (m) or (ft)
r_o	=	outer cylinder radius (borehole radius) (m) or (ft)
J_0, J_1, Y_0, Y_1	=	Bessel functions of the zero and first orders
t	=	time (s)

The variable "r" is the location at which a temperature is desired from the cylinder source located at r_o. $G(F_o, r/r_o)$ is a function of time and distance only. To apply the cylinder source equation for modeling the fluid temperature within a borehole, Equation 1-16 can be used, setting r equal to the equivalent U-tube radius and r_o equal to the borehole radius.

$$T(t) = \frac{q}{k_{soil}} \cdot G\left(F_o, \frac{r}{r_o}\right) + q \cdot R_{bh} + T_{ff}$$

(1-16)

where,

$T(t)$ =   borehole fluid temperature (°C) or (°F)

q =   heat flux per unit length of the borehole $\left(\dfrac{W}{m}\right)$ or $\left(\dfrac{Btu}{h \cdot ft}\right)$

F_o =   Fourier number (dimensionless)

r =   inner radius (equivalent U-tube radius) (m) or (ft)

r_o =   outer cylinder radius (borehole radius) (m) or (ft)

T_{ff} =   far field temperature of the soil (°C) or (°F)

t =   time (s)

R_{bh} =   steady state borehole resistance $\left(\dfrac{mK}{W}\right)$ or $\left(\dfrac{h \cdot ft \cdot °F}{Btu}\right)$

k_{soil} =   soil conductivity $\left(\dfrac{W}{mK}\right)$ or $\left(\dfrac{h \cdot ft \cdot °F}{Btu}\right)$

The cylinder source can be used to model the steady state borehole resistance using Equation 1-1. The U-tube and fluid resistances can be calculated as shown in section 1.2.1 in Equations 1-2 and 1-3.

A comparison of borehole resistance calculation methods, including the cylinder source method, is shown in chapter 2. Also a correction factor was created that increases the accuracy of the cylinder source greatly for boreholes with a large shank spacing. As will be shown in chapter 2, even without the correction factor, the cylinder source with superposition technique is a reasonably accurate method for calculating the grout resistance.

1.2.1.5 Multipole

The multipole (Bennet, et al. 1987) method is used to model conductive heat flow in and between pipes of differing radius. In the multipole model, the tubes are located inside a homogenous circular region that is inside another homogenous circular region. The multipole method is not constrained to calculating the steady state borehole resistance for a borehole with only one U-tube. Furthermore, the tubes do not need to be symmetrical about any axis. This is advantageous since some boreholes have two U-tubes. The model is also able to calculate borehole resistance for U-tubes that are not equidistant from the center of the borehole. To show the capabilities of the model Figure 1-7 has been created showing an asymmetric borehole with three pipes. The pipes have temperatures, T_{f1}, T_{f2}, and T_{f3}.
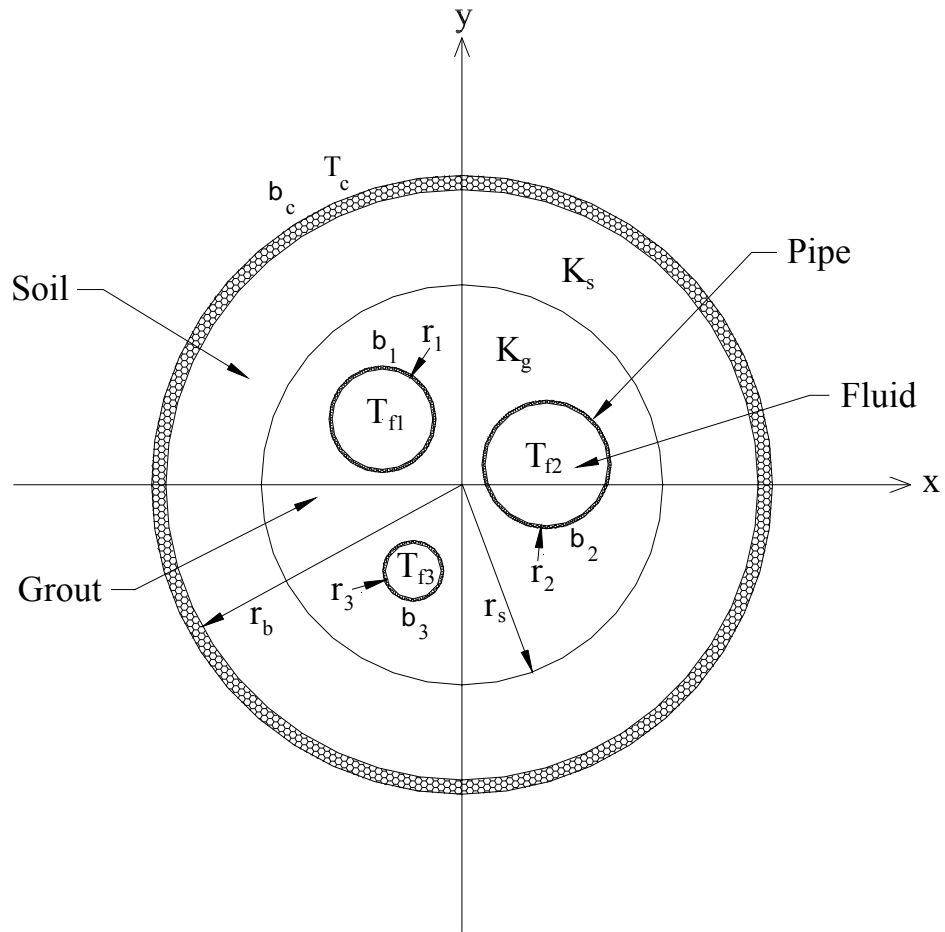
Figure 1-7 Example of a 2D System for the Multipole Method.

The inner circular region represents the grout and the outer region represents the soil for the borehole system. For calculating borehole resistance, r_b can be set to 100 m (328 ft). The inputs to the multipole method are shown in Table 1-2.

Table 1-2 Variable Input List for the Multipole Method.

K_g	Thermal conductivity in the inner region $\left(\dfrac{W}{mk}\right)$ or $\left(\dfrac{Btu}{h \cdot ft \cdot {}^\circ F}\right)$
K_s	Thermal conductivity in the outer region $\left(\dfrac{W}{mk}\right)$ or $\left(\dfrac{Btu}{h \cdot ft \cdot {}^\circ F}\right)$
N	Number of pipes
J	Order of multipole
r_b	Radius of the outer region (m) or (ft)
r_s	Radius of the inner region (m) or (ft)
β_c	Thermal resistance coefficient at the outer circle (nondimensional)
T_c	Temperature of the outer region (K) or (°F)
The following are input for each pipe indexed by i	
x_i, y_i	Location of each innermost pipe (m) or (ft)
r_i	Radius of each pipe (m) or (ft)
β_i	Thermal resistance coefficient for each pipe (nondimensional)
T_{fi}	Fluid temperature (K) or (°F)

In Table 1-2 the non-dimensional variable β_i is used to input the pipe thermal resistances. This is shown in Equation 1-17.

$$\beta = 2\pi Rk \qquad\qquad (1\text{-}17)$$

where,

R =   Thermal resistance of the pipe $\left(\dfrac{Km}{W}\right)$ or $\left(\dfrac{h \cdot ft \cdot °F}{Btu}\right)$

k =   Grout conductivity $\left(\dfrac{W}{mk}\right)$ or $\left(\dfrac{Btu}{h \cdot ft \cdot °F}\right)$

β =   resistance coefficient (Nondimensional)

The general equation that the multipole method solves is the steady state two-dimensional heat conduction equation, Equation 1-18:

$$\frac{\partial^2 T}{\partial x^2} + \frac{\partial^2 T}{\partial y^2} = 0 \qquad\qquad (1\text{-}18)$$

where,

T =   Temperature (°C) or (°F)

x   =   Distance in the x direction (m) or (ft)

y   =   Distance in the y direction (m) or (ft)

When solving the differential equation several assumptions are made. The temperature is constant inside of the pipe walls and the fluid convective resistance. The temperature around the outer region is constant. The system is at steady state.

Multipoles were created using the line source model. They are called multipoles because for each line source there is a line sink at a mirror point. This can be seen in Equation 1-19, the temperature equation for a zeroth order multipole, where the line sink q_n is at (x_n, y_n) in the first term and the mirror sink of strength $\sigma \cdot q_n$ is located at the mirror point $(x_n r_b^2 / r_n^2, y_n r_b^2 / r_n^2)$ in the second term. A zeroth order multipole has one source and one sink.

$$0 \le r \le r_b: \tag{1-19}$$

$$T(x, y) = \frac{q_n}{2\pi k_b} \left\{ \ln\left(\frac{r_b}{\sqrt{(x-x_n)^2 + (y-y_n)^2}} \right) + \sigma \cdot \ln\left(\frac{r_b / r_n}{\sqrt{(x-x_n \frac{r_b^2}{r_n^2})^2 + (y-y_n \frac{r_b^2}{r_n^2})^2}} \right) \right\}$$

$$\sigma = \frac{k_b - k}{k_b + k}, \qquad -1 \le \sigma \le 1$$

where,

$T(x, y)$ = Temperature (K) or (°F)

q_n = Heat flux per unit length $\left(\dfrac{W}{m} \right)$ or $\left(\dfrac{Btu}{h \cdot ft} \right)$

k_b = Conductivity of the inner region $\left(\dfrac{W}{mk} \right)$ or $\left(\dfrac{Btu}{h \cdot ft \cdot °F} \right)$

k = Conductivity of the outer region $\left(\dfrac{W}{mk} \right)$ or $\left(\dfrac{Btu}{h \cdot ft \cdot °F} \right)$

x_n = Location of the line source in the x direction (m) or (ft)

y_n = Location of the line source in the y direction (m) or (ft)

r_b = Radius of the inner region (m) or (ft)

r_n = Radius of the line source (m) or (ft)

To give a graphical perspective on the location of the source and sink Figure 1.8 is given. As can be seen in Figure 1.8 the sink lies on the same radius line as the source.
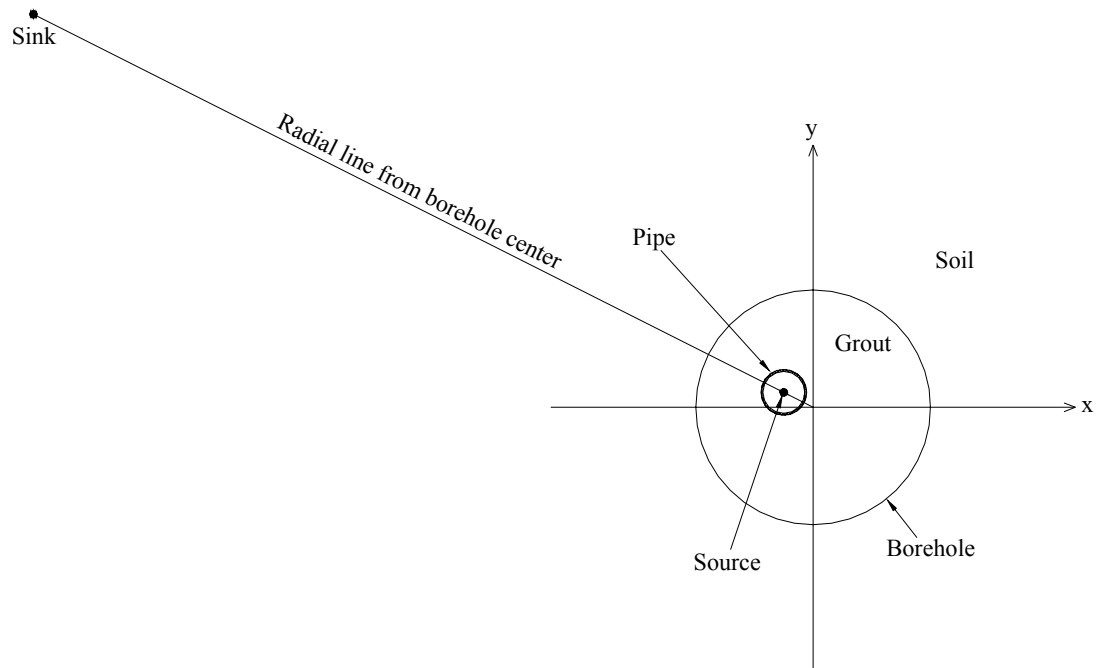
Figure 1-8 Source and Sink Location for a Single Pipe

Equation 1-19 is the zeroth order multipole equation; to produce a more accurate solution more sources and sinks can be utilized for each pipe. To do this requires a simplification of Equation 1-19 by use of polar notation. Writing Equation 1-19 in polar notation yields Equation 1-20 where $\text{Re}(W_{n0})$ is the real component of the zero order multipole.

$$T(x, y) = \frac{q_n}{2\pi k_b} \cdot \text{Re}(W_{n0})$$

where,

$T(x, y)$ = Temperature (K) or (°F)

q_n = Heat flux per unit length $\left(\dfrac{W}{m}\right)$ or $\left(\dfrac{Btu}{h \cdot ft}\right)$

k_b = Conductivity of the inner region $\left(\dfrac{W}{mk}\right)$ or $\left(\dfrac{Btu}{h \cdot ft \cdot °F}\right)$

$\text{Re}(W_{n0})$ = Real component of the zero order multipole

For higher order multipoles, derivatives are taken of the W_{n0} as shown in

Equation 1-21.

$$W_{nj} = \frac{1}{(j-1)!} \cdot \frac{\partial^j}{\partial z_n^j}(W_{no})$$

where,

W_{nj} = j^{th} order multipole of nth line source

j = Order of multipole

z_n = Location of pipe n in polar coordinates

W_{no} = zero order multipole

Both the real and imaginary components of W_{nj} satisfy the continuous radial flux

boundary condition at $r = r_b$. The constant temperature condition of each of the pipes

and the outer radius r_s is satisfied using a Fourier series expansion. Using this method

the temperature for any point within r_s can be found. Equation 1-22 and 23 show the

general solution for the temperature inside the outer cylinder radius for orders of

multipoles greater than zero. For a borehole this becomes the borehole wall temperature.

$$T = T_o + \text{Re}\left[\sum_{n=1}^{N} P_n \cdot W_{no} + \sum_{n=1}^{N} \sum_j P_{nj} \cdot r_{pn}^{j} \cdot W_{nj} + \sum_j P_{cj} \cdot r_c^{-j} \cdot W_{cj} \right] \qquad \textbf{(1-22)}$$

$$P_n = \frac{q_n}{2\pi \cdot k_b} \qquad \textbf{(1-23)}$$

where,

T = Temperature at the borehole wall (K) or (°F)

T_o = Far field temperature (K) or (°F)

n = counter variable

j = Order of multipole

N = number of pipe

W_{no} = zero order multipole

W_{cj} = Multipole of the outer cylinder

W_{nj} = j^{th} order Multipole of nth line source

r_{pn} = Radius of the innermost pipes (m) or (ft)

r_c = Radius of the cylinder encircling the innermost pipes (m) or (ft)

The final equations, shown in Chapter 8 (Bennet, et al. 1987), are an elaboration

of Equation 1-22. In the paper three equations are presented which must be solved

iteratively. In Chapter 11 (Bennet, et al. 1987) Fortran 77 code is conveniently given

which solves the equations.

28

The multipole method can produce highly accurate steady state temperature profiles of a borehole and soil. Figure 1-9 shows the two dimensional steady state temperature inside and around a typical borehole. For this figure the borehole fluid temperature was set to 10 °C (18 °F) above a zero far field temperature and a tenth order multipole was used. This method requires a constant temperature boundary condition inside the fluid convective resistance inside the U-tubes. This is a reasonable assumption if the fluid in the U-tubes is in the turbulent flow regime.
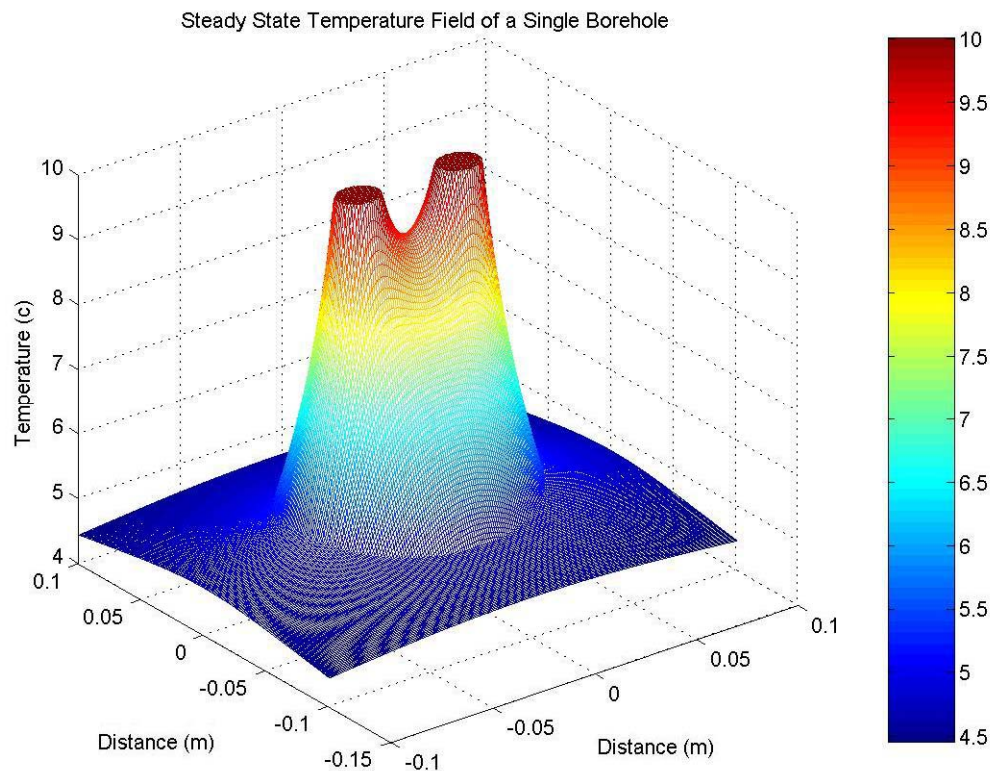
Figure 1-9 Steady State Temperature Field for a Borehole Heat Exchanger

A tenth order multipole produces four or five digits of accuracy. Since the multipole method is very fast on computers above 400 megahertz, a tenth order multipole should be used for most problems.

As can be seen in Figure 1-9, the difference in grout and soil conductivity creates a slope discontinuity at the borehole radius, where the inner circular region representing the grout meets the outer region representing the soil.

A typical steady state temperature profile at the borehole wall is shown in Figure 1-10.
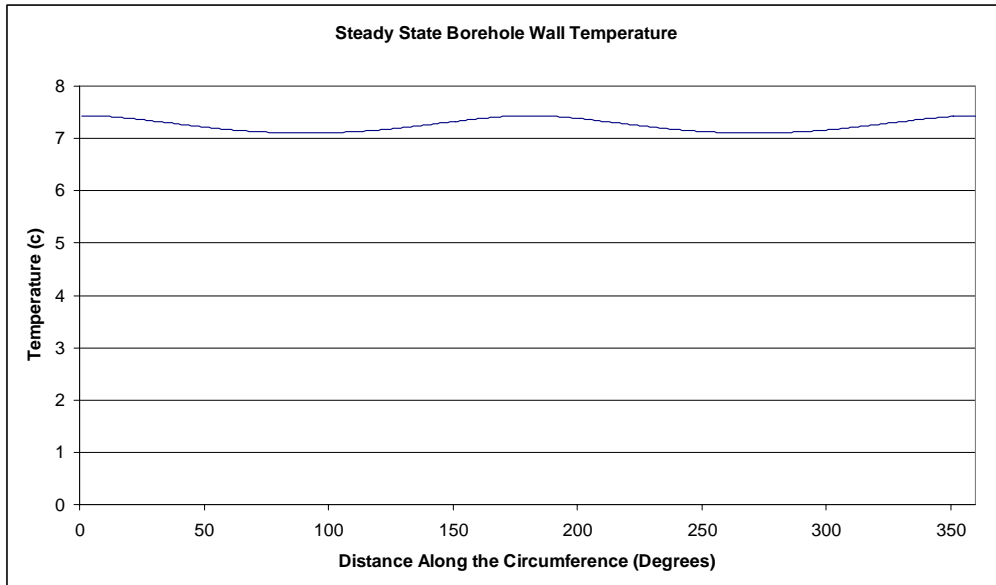
Figure 1-10 Temperature Change Around the Borehole Circumference

To calculate the steady state borehole resistance a temperature is specified for each leg of the U-tube. The multipole method is then used to calculate a heat flux out of each U-tube and the temperature around the circumference of the borehole radius should be averaged. Since the multipole program solves for temperatures very quickly, using 360 points at the borehole radius is feasible and will produce a high degree of accuracy.

Once an average temperature at the borehole radius is found and it can then be used with the flux in Equation 1-24 to find the steady state borehole resistance.

$$R_{BH} = \frac{T_{fluid} - T_{bh}}{q_{U-tube1} + q_{U-tube2}} \qquad \textbf{(1-24)}$$

where,

$$R_{BH} \quad = \quad \text{borehole thermal resistance } \left(\frac{mK}{W}\right) \text{ or } \left(\frac{h \cdot ft \cdot °F}{Btu}\right)$$

$$T_{fluid} \quad = \quad \text{average temperature at the U-tube pipe wall (K) or (°F)}$$

$$T_{bh} \quad = \quad \text{average temperature at the borehole radius (K) or (°F)}$$

$$q_{U-tube1} \quad = \quad \text{heat flux from U-tube leg one } \left(\frac{W}{m}\right) \text{ or } \left(\frac{Btu}{h \cdot ft}\right)$$

$$q_{U-tube2} \quad = \quad \text{heat flux from U-tube leg two } \left(\frac{W}{m}\right) \text{ or } \left(\frac{Btu}{h \cdot ft}\right)$$

1.2.2   Transient Modeling of Borehole Heat Exchangers

Transient heat transfer in boreholes occurs when the heat flux entering the borehole through the fluid does not equal the heat flux leaving the borehole via the borehole wall. Borehole transients have a significant effect on the borehole fluid temperature response after any change in heat extraction or rejection rate. For a step change in the heat flux, the time for which transient effects are significant is determined primarily by the grout thermal conductivity and the borehole geometry such as the shank spacing and radius of the borehole. In general, a small grout thermal conductivity or a large borehole radius will lengthen the transient region.

In most actual systems, the heat flux applied to a borehole through the circulating fluid changes continuously throughout operation. Thus borehole transients need to be modeled not only at the beginning of a simulation but throughout the simulation.

Several analytical two dimensional models exist and have been used to model boreholes such as the line source (Ingersoll and Plass, 1948) and cylinder source (Ingersoll, 1948). These methods have very limited capability for modeling the internal borehole transients especially for transient heat pulse changes in the first 10 hours. This section, describes the buried electrical cable (Carslaw and Jaeger, 1947) analytical model, and presents the General Elliptical Multi-block Solver (GEMS2D) and Yavuzturk's (1999) pie sector finite volume method programs. The application of the buried electrical cable model to borehole heat exchangers is covered in Chapter 3. This section also covers Eskilson's (1987) three dimensional model of boreholes and its coupling with the two dimensional analytical or finite volume methods via borehole resistance.

1.2.2.1. Buried Electrical Cable Model

The buried electrical cable (BEC) model (Carslaw and Jaeger 1947) is an analytical model used to describe the heat flow out of a cable buried in the ground. An electrical cable consists of three main parts, a metal core surrounded by insulation and then an outer protective sheath. A diagram of a buried electrical cable is shown in Figure 1-11 along with a circuit diagram of the system. Implicit in this method are the assumptions that the core and sheath thermal capacities have finite thermal capacities but are perfect conductors and that the insulation has negligible heat capacity, but a fixed thermal resistance.

The most significant difference between the buried electrical cable model and other analytical models such as the line source and cylinder source is that this model incorporates the thermal capacity of the sheath and core in calculating the temperature profile of the core. As seen in the circuit diagram in Figure 1-11 the core and sheath

thermal capacities are represented as S_1 and S_2. The insulation resistance is represented as R_s.

In the circuit a heat flux can be applied creating a temperature differential between the core and soil. The heat flux is absorbed by the capacitances S_1 and S_2.
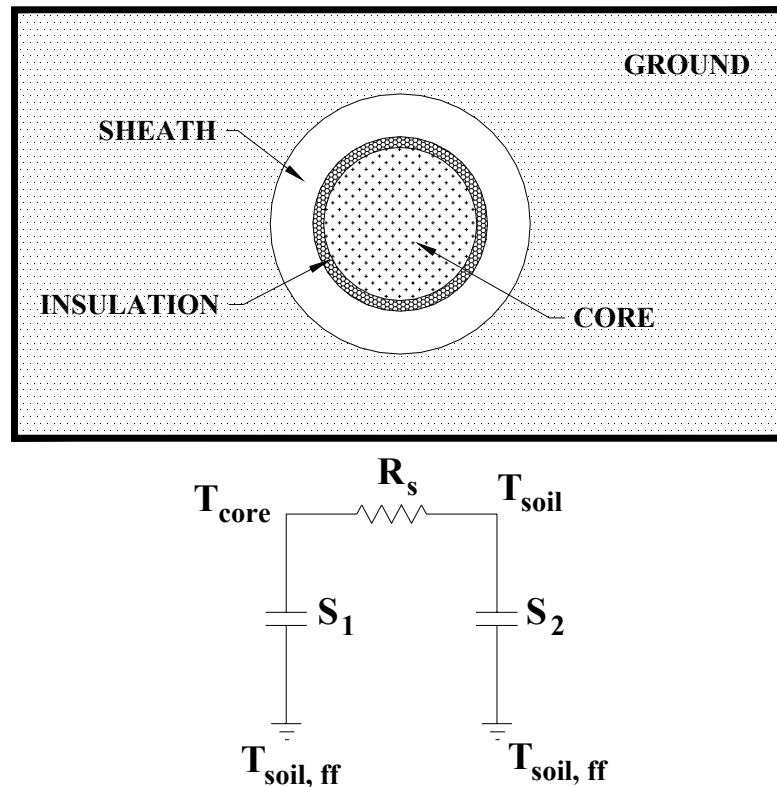
Figure 1-11 Diagram of a Buried Electrical Cable and Circuit

The analytical equations, given as Equations 1-25 and 1-26, for this system are more complicated and require more computational time than the cylinder source and the line source equations.

$$\Delta T = \frac{q}{k_{soil}} G(t) \tag{1-25}$$

$$G(t) = \frac{2a_1^2 a_2^2}{\pi^3} \int_0^\infty \left[\frac{1 - e^{-u^2\left(\alpha\frac{t}{a^2}\right)}}{u^3 \cdot \Delta} \right] du \tag{1-26}$$

$$a_1 = \frac{2\pi r_b^2 \rho C_p}{S_1} \quad , \quad a_2 = \frac{2\pi r_b^2 \rho C_p}{S_2} \quad , \quad h = 2\pi \cdot R_s k_{soil}$$

$$\Delta = \left[\left[u\left(a_1 + a_2 - hu^2\right) J_0(u) - a_2\left(a_1 - hu^2\right) J_1(u) \right]^2 + \left[u\left(a_1 + a_2 - hu^2\right) Y_0(u) - a_2\left(a_1 - hu^2\right) Y_1(u) \right]^2 \right]$$

where,

t = time (s)

r_b = outer radius of the sheath (m) or (ft)

k_{soil} = Conduc1tivity of the soil $\left(\frac{W}{mK}\right)$ or $\left(\frac{Btu}{h \cdot ft \cdot °F}\right)$

ρ = density of the soil $\left(\frac{kg}{m^3}\right)$ or $\left(\frac{lbm}{ft^3}\right)$

C_p = specific heat of the soil $\left(\frac{J}{kgK}\right)$ or $\left(\frac{Btu}{kg \cdot °F}\right)$

R_s = insulation thermal resistance $\left(\frac{Km}{W}\right)$ or $\left(\frac{h \cdot ft \cdot °F}{Btu}\right)$

S_1 = core thermal capacity $\left(\frac{J}{mK}\right)$ or $\left(\frac{Btu}{ft \cdot °F}\right)$

S_2 = sheath thermal capacity $\left(\frac{J}{mK}\right)$ or $\left(\frac{Btu}{ft \cdot °F}\right)$

α_{soil} = soil thermal diffusivity $\left(\frac{m^2}{s}\right)$ or $\left(\frac{ft^2}{s}\right)$

$J_0, J_1,$
Y_0, Y_1 = Y and J type Bessel functions of zero and first orders

Equation 1-26 will produce a buried electrical cable g-function for a particular time.

It should be noted that this is the only analytical model presented here which takes into account the thermal mass of the heat generation medium, which in the case of a buried electrical cable is the core. However, there is potential for this model to be modified to model a borehole and account for the fluid mass inside a borehole. The application of the BEC analytical equation in modeling a borehole system is discussed in detail in Chapter 3.

1.2.2.2. G-function Model: Long Time Step

The long time step (LTS) g-function (Eskilson 1987) represents the nondimensionalized borehole response for times when three-dimensional effects such as borehole to borehole interaction, surface and bottom end effects influence the borehole fluid temperature response. G-functions are plotted against the natural log of scaled time where the scaling factor is dependent on the depth of the borehole and the soil thermal diffusivity. As developed by Eskilson (1987), the borehole transient resistance or g-function can be non-dimensionalized with respect to the soil and scaled with respect to the steady state borehole resistance to form a g-function.

Both long and short time step g-functions can be produced using Equation 1-27 (Eskilson 1987). In Equation 1-27 the $T_{borehole}$ term represents the time-varying average temperature at the borehole wall and must be calculated with a numerical or analytical procedure. T_{ground} is the far field temperature and usually remains constant. This g-function represents the non-dimensionalized resistance between the ground and borehole wall. Equation 1-28 includes the borehole resistance term.

$$g\left(\frac{t}{t_s},\frac{r_b}{H}\right) = \frac{2\pi k_{soil}}{Q}\left(T_{borehole} - T_{ground}\right)$$

<div align="right">(1-27)</div>

$$g\left(\frac{t}{t_s},\frac{r_b}{H}\right) = \frac{2\pi k_{soil}}{Q}\left(T_{borehole} - T_{ground}\right) + 2\pi k_{soil} R_{BH}$$

<div align="right">(1-28)</div>

where,

g =   g-function value (dimensionless)

Q =   flux per unit length $\left(\dfrac{W}{m}\right)$ or $\left(\dfrac{Btu}{h \cdot ft}\right)$

k_{soil} =   thermal conductivity of the soil $\left(\dfrac{W}{m \cdot K}\right)$ or $\left(\dfrac{Btu}{ft \cdot °F}\right)$

$T_{borehole}$ =   average temperature at the borehole wall (°C) or (°F)

T_{ground} =   far field temperature of the ground (°C) or (°F)

As can be seen from Equation 1-28, the g-function has two major parameters t/t_s

and r_b/H. For a specific borehole configuration, the first parameter is the major

contributor to the g-function and the second is a factor that corrects the g-function

according to the borehole radius (r_b) to depth (H). The r_b/H correction factor is

relatively minor since it changes the g-values on the order of one percent or less. The

main parameter, in Equation 1-27, that requires significant calculation time is the average

temperature at the borehole wall radius ($T_{borehole}$).

G-functions are plotted against the natural log of non-dimensionalized time. The

term t_s is called the time scale factor, and can be calculated using Equation 1-29

(Eskilson 1987).

$$t_s = \frac{H^2}{9\alpha_{soil}}$$ (1-29)

where,

t_s =   time scale factor (s)

H   =   depth of the borehole (m) or (ft)

α_{soil} =   soil thermal diffusivity $\left(\dfrac{m^2}{s}\right)$ or $\left(\dfrac{ft^2}{s}\right)$

The g-function defined by Equation 1-27 represents the ground thermal resistance
and not the borehole resistance. This is beneficial because it allows a single long time
step g-function to be useful for any borehole geometry and soil conductivity as discussed
by Eskilson (1987). The g-function in Equation 1-28 is only valid for the specific
borehole for which the borehole resistance was calculated.

An example of a combined long and short time step g-function for a single
borehole system is shown in Figure 1-12 and 1-13. In these figures, the g-function is
plotted against log scale time. Figure 1-12 was created with Equation 1-27 and Figure 1-
13 with Equation 1-28.
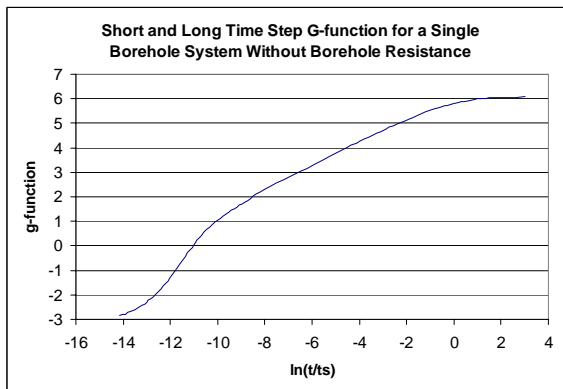
Figure 1-12 Short and long time step g-function without borehole resistance
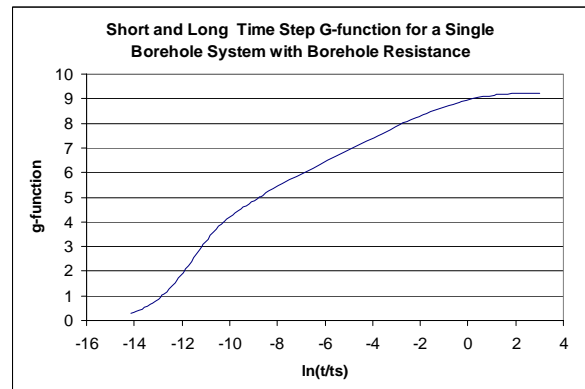
Figure 1-13 Short and long time step g-functions with borehole resistance

As can be seen in Figure 1-13 the g-function approaches zero at small times. This indicates that as time approaches zero the resistance asymptotically approaches zero due to the steady state temperature profile of the soil. Looking at Figure 1-12 might give the impression, however, that for small times the resistance is negative but this is an illusion created by subtracting the borehole resistance. When the borehole resistance is added back in, as shown in Figure 1-13, the resistance approaches zero at short times. At large times, G-functions will plateau. This occurs because of borehole end effects.

Using Equation 1-30 an average fluid temperature can be calculated if the g-function is known.

$$T_{borehole} = \left(\frac{Q}{2\pi k_{soil}} \right) \cdot g\left(\frac{t}{t_s}, \frac{r_b}{H} \right) + T_{ground} \qquad \textbf{(1-30)}$$

where,

$T_{borehole}$ = average temperature at the borehole wall radius (°C) or (°F)

T_{ground} = far field temperature of the ground (°C) or (°F)

g = g-function value (dimensionless)

Q = flux per unit length $\left(\dfrac{W}{m} \right)$ or $\left(\dfrac{Btu}{hr \cdot ft} \right)$

k_{soil} = thermal conductivity of the soil $\left(\dfrac{W}{m \cdot K} \right)$ or $\left(\dfrac{Btu}{ft \cdot °F} \right)$

There are no published analytical solutions that approximate the g-functions for multiple borehole systems. This is due to multiple borehole systems dependence on not only the depth of the borehole, but also on the distance between each borehole. The interaction between boreholes is difficult or impossible to analytically model. With the

38

boreholes dissipating different unknown amounts of heat, it is difficult to analytically

model the average borehole wall temperature of the system. However, it can be resolved

using superposition.

In order to create long time step g-functions for multiple borehole systems

Eskilson (1987) created a Fortran 77 program which uses a variable mesh finite

difference method with cylindrically symmetric coordinates. The program is described in

detail for a single borehole in Eskilson (1987). The program has the ability to input a

constant heat flux per unit length of borehole and calculates the resulting temperature at

the borehole radius ($T_{borehole}$) for various times. The borehole wall temperature ($T_{borehole}$)

is then used in Equation 1-27 to calculate the LTS g-function. An example of the type of

variable mesh grid that Eskilson used is shown in Figure 1-14
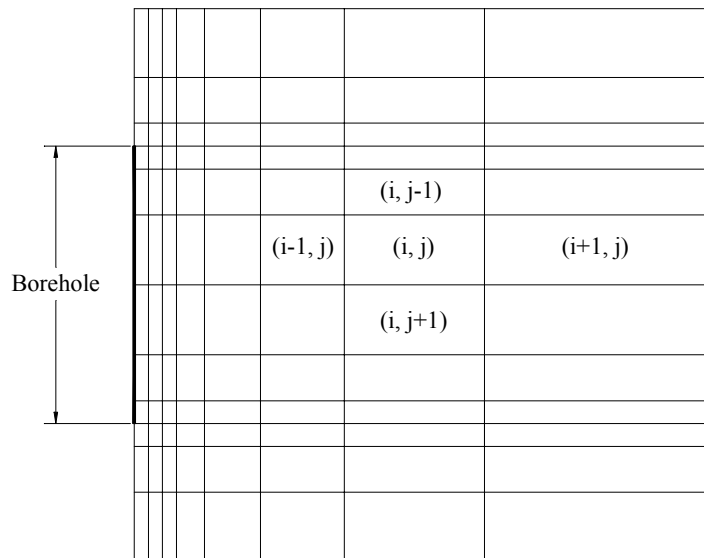
**Figure 1-14 Two-dimensional radial-axial mesh for a heat extraction
borehole in the ground (Eskilson, 1987)**

In Figure 1-14 each cell is a rectangular cross section of a ring. Temperatures are

calculated at the center of each cell; however, logarithmic interpolation can be used to

find the temperature at other points in the soil. Eskilson gives a detailed analysis of appropriate mesh sizes in the radial and axial direction since the mesh determines the accuracy of the solution. In general, small cells provide good numerical accuracy and the temperatures are valid for smaller times. However, small cells create longer computational times for a computer. Eskilson suggests using no smaller cells than necessary for a particular problem. Although computer technology has improved since 1987, mesh size is still important for large simulations.

In the examples Eskilson used, the upper part of the borehole is thermally insulated to a depth of 5 meters (16.4 ft) and the overall borehole depth is 115 m (377 ft). Mesh comparisons for short times of 25 years and long times of 237 and 947 years were conducted. In the end, heuristics were created for determining the appropriate mesh size in the radial and axial direction.

To solve the thermal performance for a system with multiple boreholes, Eskilson (1987) used the superposition technique. Two different examples are given (Eskilson, 1987): a 4x4 borehole configuration, with 10 m (33 ft) spacing, and a 12x10 borehole configuration, with 4 m (13 ft) spacing, with the simplest type of loading condition where the heat flux at the borehole wall is constant per unit length of the borehole. To validate the accuracy of the program the line source was used in conjunction with superposition.

Eskilson's program was used to produce the LTS g-function curves shown in Figure 1-15. It can intuitively be determined that a tighter borehole field will produce more overall resistance and as the boreholes are spaced farther apart, all multiple borehole systems will approach the single borehole case. This can be seen in Figure 1-15.
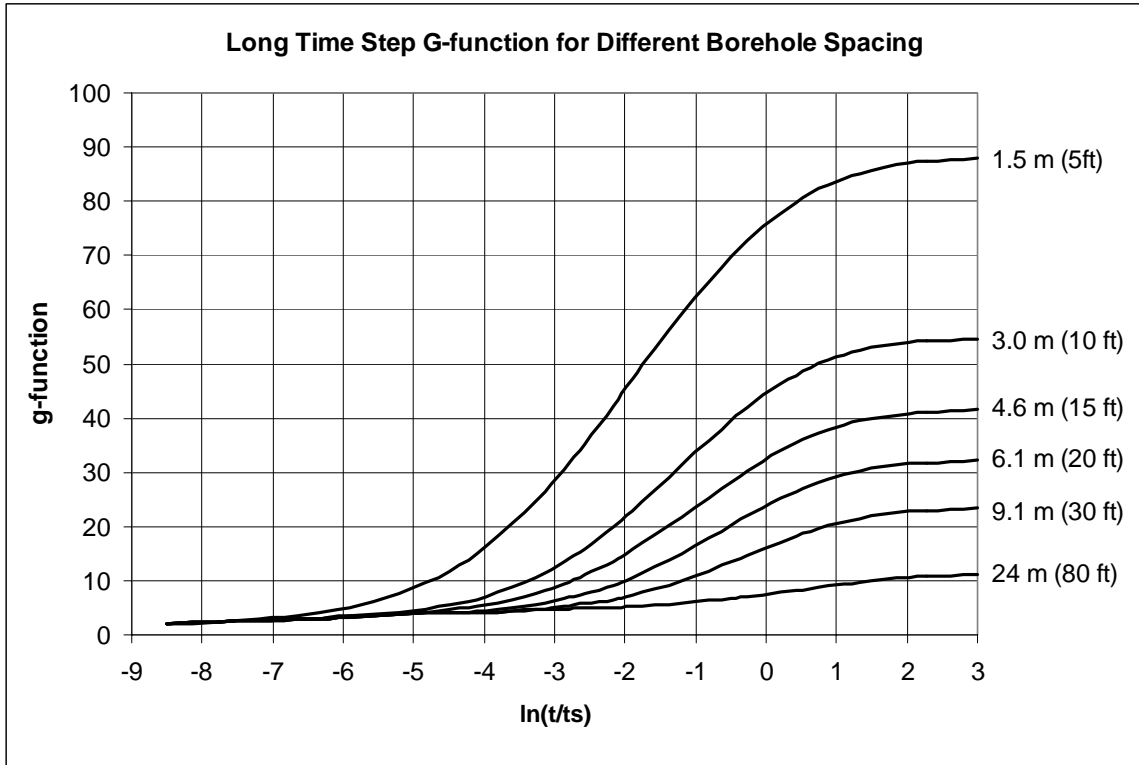
Figure 1-15 Long Time Step g-function for a 64 Borehole System in an 8x8 Configuration with Varying Borehole Spacing

Since none of the internal properties of the borehole are significant, the long time step g-function might initially seem simple to solve. Because of three dimensional effects, the g-function for multiple borehole systems is deceptively complicated to solve.

1.2.2.3. G-function Model: Short Time Step

The short time step (STS) g-function describes the transients that occur within the borehole before the borehole reaches steady state conditions. For this transient region, the borehole is modeled as having infinite length since surface and bottom end effects can be neglected. The STS g-function can be approximated using the line source or the cylinder source as described in section 1.2.1.1 and 1.2.1.4, respectively, to calculate a fluid temperature profile versus time which could be input into Equation 1-31 to yield a

g-function. Equation 1-31 calculates a g-function in terms of the fluid temperature and the steady state borehole resistance. Unlike the long time step g-function, this g-function is only valid for the specific borehole internal geometry (shank spacing, borehole radius… etc.) and conductivities that the T_{fluid} and R_{BH} was generated with.

$$g\left(\frac{t}{t_s}, \frac{r_b}{H}\right) = \frac{2\pi k_{soil}}{Q}\left(T_{fluid} - (R_{BH}Q) - T_{ground}\right) \tag{1-31}$$

where,

g = g-function value (dimensionless)

Q = flux per unit length $\left(\dfrac{W}{m}\right)$ or $\left(\dfrac{Btu}{h \cdot ft}\right)$

k_{soil} = thermal conductivity of the soil $\left(\dfrac{W}{m \cdot K}\right)$ or $\left(\dfrac{Btu}{ft \cdot^\circ F}\right)$

T_{ground} = far field temperature of the ground (°C) or (°F)

T_{fluid} = average temperature of the circulating fluid (°C) or (°F)

R_{BH} = borehole resistance $\left(\dfrac{mK}{W}\right)$ or $\left(\dfrac{h \cdot ft \cdot^\circ F}{Btu}\right)$

Another method which is capable of generating greater accuracy than analytical methods is the finite volume model (Patankar, 1980). Two programs that have implemented this model will be discussed. The first is called the General Elliptical Multi-block Solver (GEMS2D) and was developed by Rees (2001). Applications of GEMS2D are reported by Spitler, et al. (1999) and Rees, et al. (2002). This program solves the general convection diffusion equation using a boundary fitted grid. GEMS2D is capable of solving both steady state and transient problems. Boundary fitted grids enable GEMS2D to be applied in solving heat transfer problems with complex geometries such as U-tubes within a borehole. Figure 1-16 shows a GEMS2D boundary fitted grid for half of a borehole, since the geometry is symmetrical.
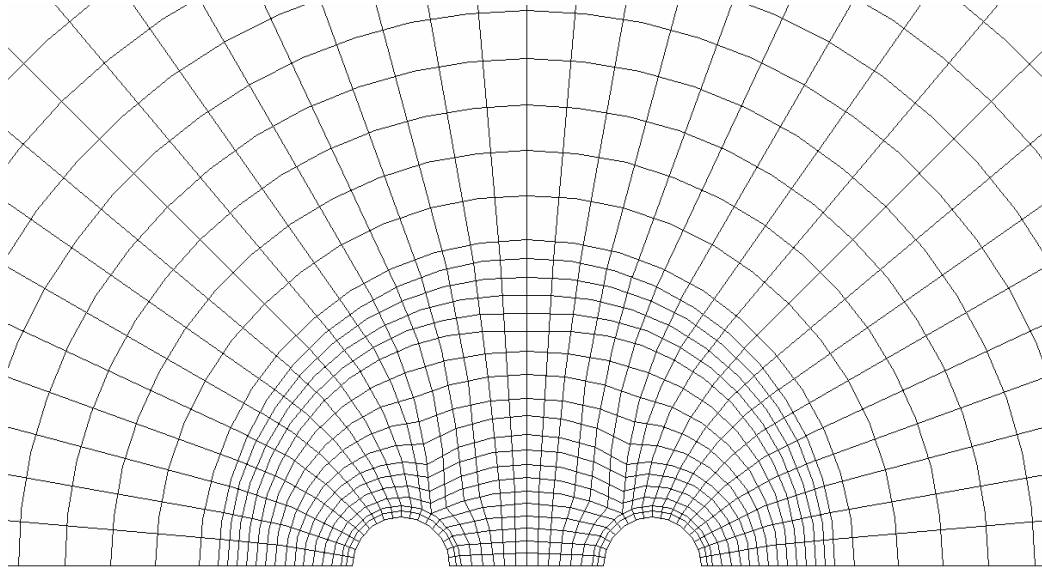
Figure 1-16 Grid for a cross section of a borehole

A complicated grid such as that shown in Figure 1-16 will require several different blocks to be created and then connected together. Each block is composed of many cells. The cells in each block can then be assigned properties such as conductivity and heat capacity. Different cells within a single block can be assigned different properties. A detailed description of how the GEMS2D program was applied to borehole heat conduction with fluid mass is given in Section 4.1.

GEMS2D is capable of calculating the steady state borehole resistance and the transient temperature profile at the borehole wall. The g-function can be calculated from the average borehole wall temperature ($T_{borehole}$) using Equation 1-31.

GEMS2D is written in the Fortran 90/95 language. A grid generation tool was also written to automate the creation of grids for the GEMS2D simulator. Using a text input file, the grid for convection-diffusion heat transfer problems can be created with the grid generation tool. In the text file, blocks and boundaries are created and thermal properties of each block are specified. After the grid is created, GEMS2D can then be

used to simulate the system. The GEMS2D outputs are given in an output text file.

Temperatures at each node at each time increment can be given for transient simulations.

The second program was developed by Yavuzturk, et al. (1999) and also uses the

two dimensional finite volume model, but with a polar grid. It is specifically developed

for modeling the heat flow out of a U-tube borehole heat exchanger. Like GEMS2D,

Yavuzturk's program is able to model both the transient and steady state solutions for the

temperature field within and around a borehole.

To model the geometry of a borehole heat exchanger Yavuzturk uses an

approximation for the borehole U-tube geometry called the pie sector approximation

(Yavuzturk and Spitler, 1999). The pie-sector approximates the cross section of the U-

tubes via two "pie-shaped" wedges. Figure 1-17 shows the grid that Yavuzturk's

program creates. Only half the borehole is shown since the system is symmetrical. The

pie shaped wedge shown in this figure is representative of one leg of the U-tube. It is

shown bolded, in the figure, while the actual circular U-tube geometry is shown for both

legs without bolding.
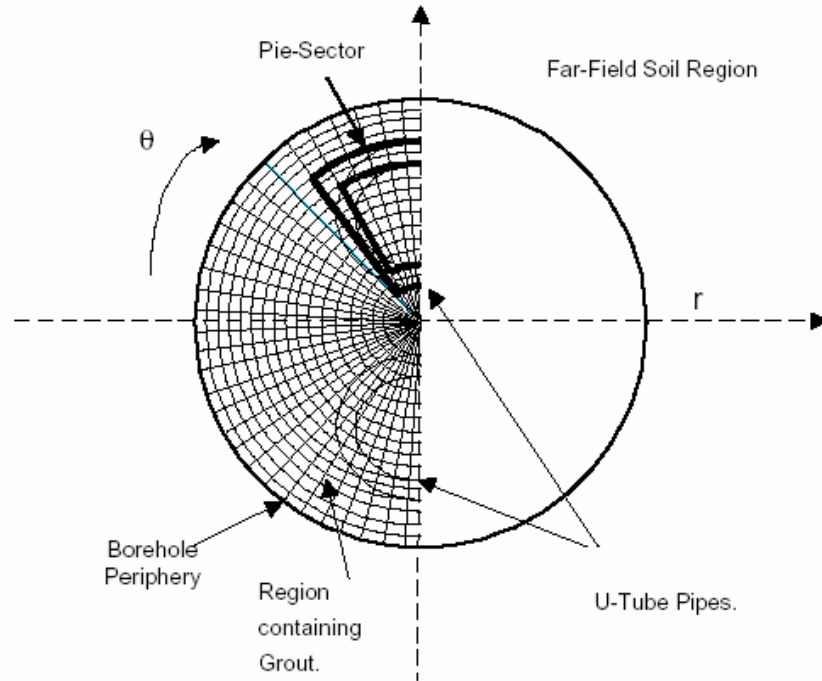
Figure 1-17 Grid for Pie-Sector Approximation (Yavuzturk, 1999)

The grid resolution and pie sector approximation for the U-tube geometry is determined by an automated parametric grid generation algorithm and is a function of the borehole and U-tube pipe geometry. The algorithm matches the inside perimeter of the circular pipe to the inside perimeter of the pie sector and also creates identical heat flux and resistance conditions near the pipe wall between the circular pipe and the pie sector approximation. The fluid resistance is approximated by adjusting the thermal conductivity of the U-tube pipe wall. The total radius of the grid is 3.6 m or (12 ft) so that longer simulation times can be conducted. At this radius, the boundary condition is set to a constant far field temperature.

The model was primarily written in the Fortran 77 programming language. Inputs to the model are simple since grid generation is automated. The inputs include shank spacing, U-tube diameter, borehole diameter, convection coefficient, the volumetric heat

capacity of the soil, grout and U-tubes, and the conductivity of the soil, grout and U-tubes. These inputs are provided in a text file. The outputs are given in an output text file.

Since the U-tube geometry is not modeled as accurately as in GEMS2D, the pie-sector approximation will generally be less accurate than GEMS2D. The benefit of Yavuzturk's program is that it requires approximately half the simulation time as GEMS2D.

The resulting simulation model, discussed in detail in Yavuzturk and Spitler (1999), uses Eskilson's LTS g-functions simulation methodology with Yavuzturk's STS g-functions simulation methodology. The model has been incorporated into a commercially available GLHE design tool called GLHEPRO (Spitler, 2000). GLHEPRO Version 3 is discussed in detail in section 1.2.3.

The simulation model has also been implemented and proved useful in several studies (Yavuzturk and Spitler, 2000, Ramamoorthy, et al. 2001, and Chiasson, 1999). Hybrid GSHP systems use ~~other~~ heat rejection equipment, such as cooling towers, fluid coolers, shallow ponds (Chiasson, et al. 2000; Ramamoorthy, et al. 2001) or pavement heating systems (Chiasson, et al. 2000). For example, several operating and control strategies of a cooling tower hybrid GSHP system are discussed in Yavuzturk and Spitler (2000), and are compared with hourly simulations performed in TRNSYS (SEL 1997). A goal of these studies is to show that hybrid GSHP systems can reduce the size of the GLHE system which in turn can reduce the first cost of the system and the necessary land area.

Spitler, et al. (2000) which gives a summary of research and developments in grounds source heat pump systems, design, modeling, and applications for commercial and institutional buildings. Presented in this paper are design methodologies for determining hourly and minutely responses for GLHE designs.

1.2.3 **GLHEPRO Version 3 Design Tool**

GLHEPRO Version 3 (Spitler, 2000) combines a Microsoft windows graphical user interface and a ground loop heat exchanger simulation. The software package developed by Marshall and Spitler is based on the methods developed by Eskilson (1987) at the University of Lund, Sweden. GLHEPRO Version 3 has a library of heat pump performance curves and has the capability of adding user defined heat pump performance curves. GLHEPRO Version 3 also has the flexibility of using SI or English units.

GLHEPRO Version 3 uses the long time step g-functions developed by Eskilson (1987). As discussed earlier, Eskilson (1987) created a 2 dimensional finite difference program that omits the internal borehole properties such as shank spacing, grout and U-tubes properties. This was done by assuming a steady-state heat transfer process inside the borehole and modeling the transient process outside the borehole using a finite difference technique, so that the temperature at the borehole wall ($T_{borehole}$) was found. Equation 1-31 can then be used to create the g-function. GLHEPRO Version 3 uses data from Eskilson's finite difference program to model the long time step g-function for over 250 different borehole configurations. The fluid temperature is found by using the temperature at the borehole wall in conjunction with the borehole steady state resistance. The method used in GLHEPRO Version 3 to calculate the short time step response is the

line source (Ingersoll, 1948). The Paul (1996) method was used to calculate the borehole resistance for a specific borehole geometry.

GLHEPRO Version 3 received inputs for peak and monthly, heating and cooling loads along with borehole internal geometric and thermal properties and borehole configuration. GLHEPRO Version 3 has the capability of outputting the maximum and minimum monthly fluid temperature entering the heat pump and the energy consumption of the system. GLHEPRO Version 3 also has a sizing mode which requires maximum and minimum limits for the entering fluid temperature to the heat pump. The sizing program will find the minimum depth required for a specific borehole configuration to be within the maximum and minimum user defined fluid temperature limits.

1.3   OBJECTIVES

The primary objective is to develop and implement a method whereby engineers can more accurately model peak-load-dominant systems without time consuming numerical modeling. Implicit within this main objective are the following specific objectives:

1. Determine an appropriate method for calculating the steady state borehole resistance and implement it in GLHEPRO.

2. Enhance short-time-step (STS) GLHE simulation methodology to account for thermal mass of the fluid to yield more accurate designs via simulations.

3. Develop an automated method for producing the combined short and long time step g-function.

4. Evaluate the impact of the more accurate g-function calculation methodologies on the simulation of GLHE systems.

5. Evaluate the impact of the more accurate g-function methodologies on the simulation of GSHP.

2   COMPARISON OF BOREHOLE RESISTANCE CALCULATION METHODS

A small change in the steady state borehole resistance has a significant impact on the borehole fluid temperature profile. Since the short time step (STS) g-function is derived directly from the borehole fluid temperature it includes the borehole resistance. In order to be consistent with the long time step (LTS) g-function, it is necessary to adjust the STS g-function to subtract the non-dimensional temperature rise due to the borehole resistance. This, in turn, requires accurate knowledge of the borehole resistance. Furthermore, as discussed in Chapter 3, the borehole fluid thermal mass (BFTM) model, which is developed in this thesis for calculating the STS g-function, requires the steady state borehole resistance to be known. Thus, there was a need for comparing different borehole resistance calculation methods for the purpose of choosing one for the BFTM model. This chapter provides a comparison between different methods for calculating the steady state borehole thermal resistance.

Both numerical and analytical methods can be used to determine the steady state resistance of the borehole. The numerical methods require much more computational effort but are generally more accurate than approximate analytical methods such as the Gu and O'Neal (a 1998) equivalent diameter method.

The general equation for borehole resistance comes from summing the three resistances (fluid, pipe, and grout) between the fluid inside the U-tube and the borehole wall as discussed in section 1.2.1. The fluid resistance is typically calculated with a convection correlation. The pipe resistance is determined as a cylindrical conductive resistance. The grout resistance is more difficult to determine, due to the complex geometry.

The methods that are compared in this chapter for calculating the grout resistance are the multipole method, the Paul (1996) method, the Gu and O'Neal (a 1998) approximate diameter method, and the cylinder source method (Ingersoll, 1948, 1954). The two numerical programs that are used to calculate the borehole resistance are GEMS2D (Rees, 2001) and Yavuzturk's (Yavuzturk and Spitler, 1999) pie sector approximation which both use the finite volume method.

2.1 Borehole Resistance Transient and Steady State

For the first few hours of constant heat injection or extraction the borehole resistance is transient. Figure 2-1 shows how the borehole resistance changes over the first 12 hours after a constant flux is applied. Figure 2-1 was generated from the average fluid temperature and the average temperature at the borehole wall radius using Equation 2-1.

$$R_{total} = \frac{\left(T_f - T_{borehole}\right)}{Q} \tag{2-1}$$

where,

R_{total} =   borehole resistance $\left(\dfrac{Km}{W}\right)$ or $\left(\dfrac{h \cdot ft \cdot {}^\circ F}{Btu}\right)$

T_f =   Average fluid temperature (K) or (°F)

$T_{borehole}$ =   Average temperature at the borehole wall radius (K) or (°F)

Q =   flux per unit length $\left(\dfrac{W}{m}\right)$ or $\left(\dfrac{Btu}{h \cdot ft}\right)$

This figure comes from a GEMS2D simulation where the borehole was 11.4 cm (4.5 in) diameter, with a 1.6 cm (0.63 in) shank spacing, standard bentonite grout, a pipe

conductivity of 0.39 (W/(m·K)) (0.225 Btu/(h·ft·°F)), and a fluid convection coefficient

of 1690 ($W / (m^2 K)$) (298 ($Btu / (h \cdot ft^2 \cdot °F)$)) As can be seen the borehole resistance is

almost constant after about 12 hours. For typical boreholes there is usually less than a

2% difference between the steady state value and the value at 10 hours. This is indicated

by Figure 2-2.
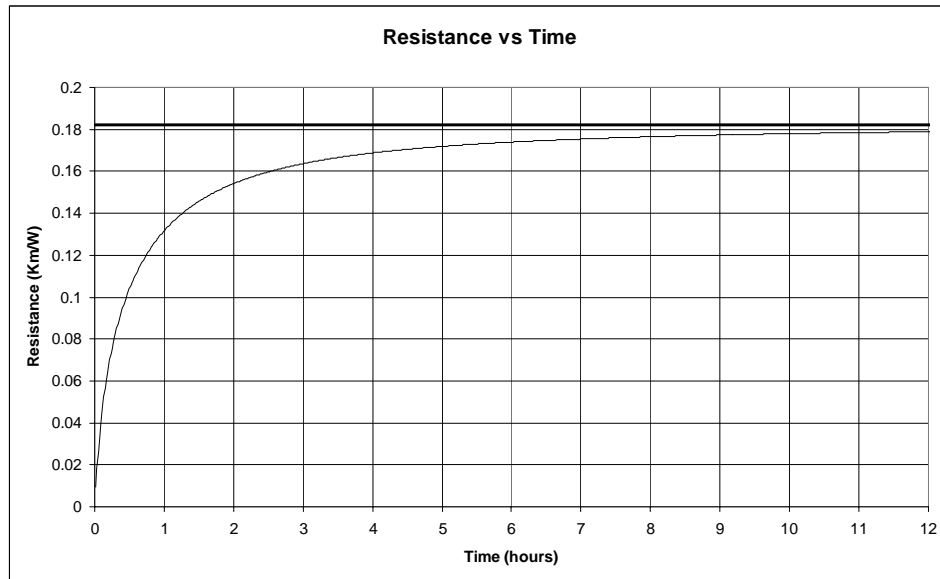
Figure 2-1 Transient Borehole Resistance Profile vs Time
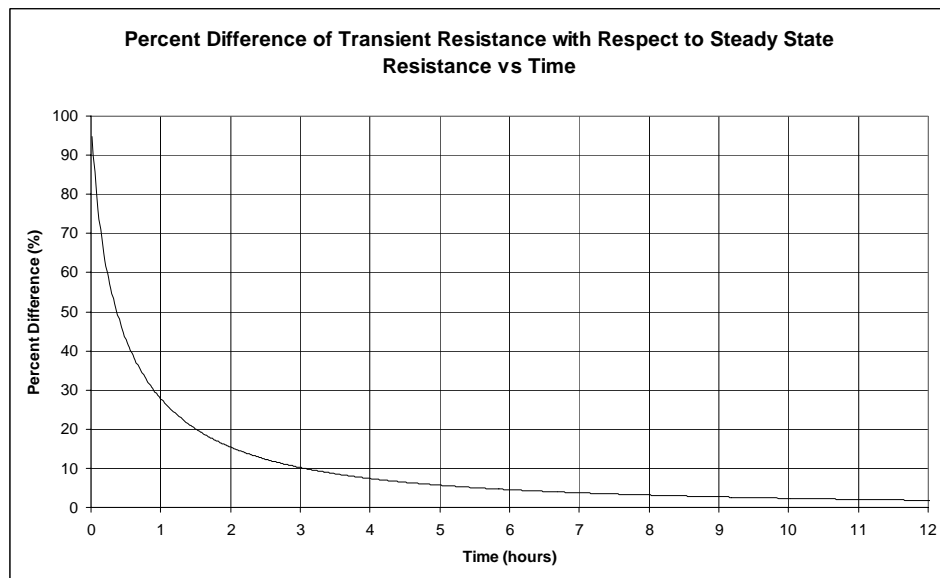
Figure 2-2 Percent Difference in Transient Borehole Resistance with respect to Steady State borehole resistance

The rate at which the resistance approaches the steady state value is dependent on the geometry and thermal properties within the borehole. A borehole with a low grout or pipe conductivity requires more time for the borehole to reach steady state.

2.2   Borehole Resistance Calculation from Analytical and Empirical Methods

The analytical methods that are compared in this thesis include the multipole method, the Gu and O'Neal approximate diameter method, and the cylinder source method. The Paul method is also included in this section because it is based on curve fits to numerical and analytical data and is not strictly numerically based. The literature review in sections 1.2.1.1 through 1.2.1.4 describes how each method, except for the cylinder source, can be used to model the steady state borehole resistance. An application of the cylinder source for calculating the steady state borehole resistance is described in this section.

The Gu and O'Neal method and the Paul method are much simpler to calculate than the multipole and cylinder source methods; however the multipole and cylinder source methods produce more accurate solutions.

The Gu and O'Neal method was used exactly as described in section 1.2.1.2 and the Paul method was used exactly as described in section 1.2.1.3. Thus, with regards to these methods, no further explanation is necessary in this chapter. However, because of the complexity of the cylinder source and multipole methods, additional explanation is provided here in addition to what has been previously described in the literature review in sections 1.2.1.4 and 1.2.1.5 respectively.

The cylinder source solution can be used to model steady state resistance by using the principal of superposition. To model the grout resistance using Equation 1-4, the temperature rise from the flux exiting each leg of the U-tube can be superimposed to calculate the average U-tube outside wall temperature and also the average borehole wall temperature. Implicit in this method is the assumption that the soil conductivity, which is different from grout conductivity, has relatively little influence on the borehole thermal resistance. This method will be explained in greater detail using Figure 2-3 which shows the cylinder source locations for the calculation of the U-tube average outside wall temperature.

Figure 2-3 (a) shows a cylinder source located at $(x,y) = (0,0)$ in an infinite medium of grout. The circle labeled borehole in Figure 2-3 (a) is shown to indicate the cylinder source location inside the borehole. The cylinder source in Figure 2-3 (a) is the location where the U-tube temperature (T_{U-tube}) will be calculated for Equation 1-4. A circle showing the borehole radius is shown, however the cylinder source method does not make a distinction between conductivities or thermal properties nor does it account for the existence of the other U-tube since the medium is infinite.

For the purpose of calculating borehole resistance, the conductivity of the soil (k_{soil}) in Equation 1-13 should be replaced with the conductivity of the grout (k_{grout}). In Figure 2-3 (a) the temperature rise at the U–tube radius should be calculated using r = r_o in Equation 1-13. Since the temperature rise will not vary it is unnecessary to calculate several temperatures along the U-tube circumference and average them.
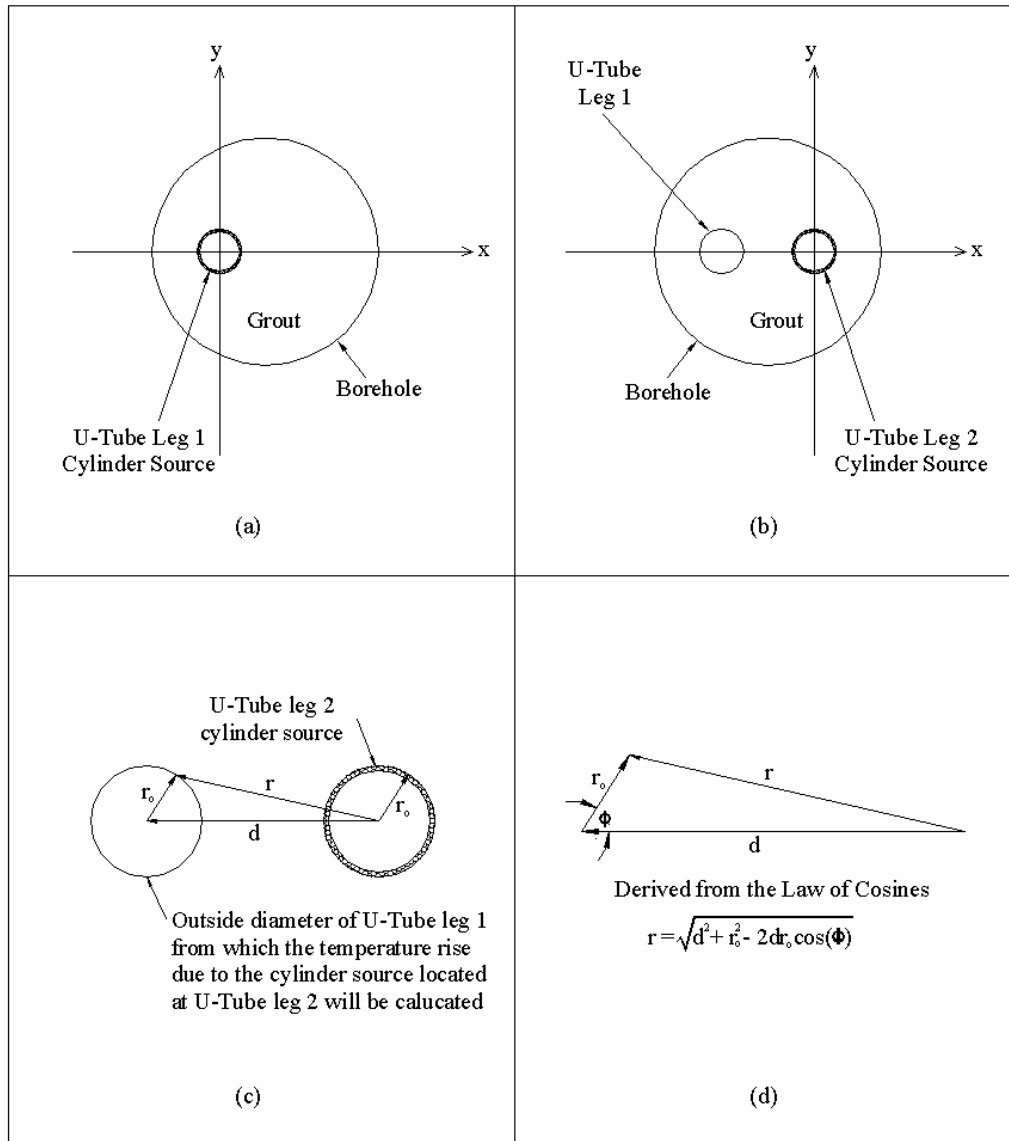
Figure 2-3 Cylinder Source Diagram for Calculating the U-tube Outside Wall Temperature for use in the Steady State Borehole Resistance Calculation

Figure 2-3 (b) is similar to (a) except it models the cylinder source at the other leg of the U-tube. Similar to Figure 2-3 (a), the cylinder source in (b) is also surrounded by an infinite medium of grout. To show where the temperature rise will be calculated, a circle is drawn showing U-tube leg 1, however neither the fluid nor the U-tube leg 1 pipe exists in the infinite and continuous medium surrounding the cylinder source. A larger

view of the U-tubes in Figure 2-3 (b) is shown in Figure 2-3 (c) and the geometry of how to calculate the radius (r) for Equation 1-13 is shown in Figure 2-3 (d). The temperature rise from the cylinder source at U-tube leg 2 should be calculated for several points along the circumference of U-tube leg 1. The average temperature should then be calculated. This can be done by calculating "r" with the equation shown in Figure 2-3 (d) for several different Φ angles. To calculate the overall temperature rise at the U-tube radius the average temperature increase from each U-tube cylinder source should be superimposed to yield the overall temperature.

Equation 2-5 calculates the resistance between the U-tube OD and radius infinity. In a real system this is analogous to calculating the combined grout and soil resistance except the soil properties are the same as grout. Likewise Equation 2-6 calculates the resistance between borehole OD and radius infinity also using grout properties. Equation 2-7 finds the resistance of the grout that is located between the U-tube and the borehole radius by subtracting the resistance calculated in Equation 2-6 from that calculated in Equation 2-5.

In a similar manner the average temperature at the borehole radius can be found by averaging the temperature rises created by a cylinder source located at each U-tube leg. If the borehole is symmetrical down the middle then the calculation shown in Equation 2-6 will calculate the resistance between the borehole wall and an infinite radius.

$$r_{BH}(\theta) = \sqrt{d^2 + r_{borehole}^2 - 2r_{borehole}d\cos(\theta)} \qquad (2\text{-}2)$$

$$r_{U-tube}(\theta) = \sqrt{(d/2)^2 + r_{UT}^2 - 2r_{UT}(d/2)\cos(\theta)} \qquad (2\text{-}3)$$

$$R(r, r_o, \alpha, k) = \frac{1}{k} \cdot G\left(F_o, \frac{r}{r_o}, k\right) \qquad (2\text{-}4)$$

$$R_{U-tube} = \frac{1}{2N} \cdot \sum_{\theta=0}^{N-1}\left[R(r_{u-tube}(\theta \cdot \frac{360}{N}), r_{UT}, \alpha_{grout}, k_{grout}) + R(r_{UT}, r_{UT}, \alpha_{grout}, k_{grout})\right] \qquad (2\text{-}5)$$

$$R_{BH} = \frac{1}{N} \cdot \sum_{\theta=0}^{N-1}\left[R(r_{BH}(\theta \cdot \frac{360}{N}), r_{UT}, \alpha_{grout}, k_{grout})\right] \qquad (2\text{-}6)$$

$$R_{grout} = R_{U-tube} - R_{BH} \qquad (2\text{-}7)$$

where,

R_{grout} = borehole grout resistance $\left(\dfrac{mK}{W}\right)$ or $\left(\dfrac{h \cdot ft \cdot {}^\circ F}{Btu}\right)$

R_{U-tube} = resistance between U-tube OD and radius infinity $\left(\dfrac{mK}{W}\right)$ or $\left(\dfrac{h \cdot ft \cdot {}^\circ F}{Btu}\right)$

R_{BH} = resistance between borehole OD and radius infinity $\left(\dfrac{mK}{W}\right)$ or $\left(\dfrac{h \cdot ft \cdot {}^\circ F}{Btu}\right)$

N = number of points to calculate the resistance around the circumference of the borehole or the U-tube (dimensionless)

θ = dummy variable used for counting from 0 to N (dimensionless)

r_{UT} = radius of the U-tube (m) or (in)

α_{grout} = thermal diffusivity of the grout $\left(\dfrac{m^2}{s}\right)$ or $\left(\dfrac{ft^2}{s}\right)$

k_{grout} = grout conductivity $\left(\dfrac{W}{mk}\right)$ or $\left(\dfrac{Btu}{h \cdot ft \cdot {}^\circ F}\right)$

$R(r, r_o, \alpha, k)$ = general function for resistance as a function of G() from Equation 1-15

$r_{U-tube}(\theta)$ = radial distance from the center of the cylinder source and the outside diameter of the other leg of the U-tube (m) or (in)

$r_{BH}(\theta)$ = radial distance from the center of the cylinder source and the outside diameter of the other leg of the U-tube (m) or (in)

d = the distance between the two centers of the left and right U-tube legs (m) or (in)

$r_{borehole}$ = borehole radius (m) or (in)

As shown in Equation 2-7, to calculate the grout resistance the resistance between the borehole wall and infinity is subtracted from the resistance between the U-tube OD and infinity. Thus, Equations 2-2 through 2-7 can be applied to yield a solution for the steady state borehole resistance.

In order to use the cylinder source to calculate steady state resistance a Fourier number should be calculated and the number of points to solve for around the borehole and U-tube radiuses should be established. The time that was used to calculate the Fourier number was 80,000 hours which causes the solution to converge to five or more digits. The number of points that was chosen for finding the average temperature of both the U-tube and borehole wall was 90. As the number of points was increased from 8 to180, the solution converged to five or more digits at 90 points. Other parameters that were chosen were the integration bounds in Equation 1-15 which are between zero and infinity. It was found that an upper integration bound of 10,000 produces 4 or more significant digits of convergence as compared to an integration bound of 100,000 which gives more than 8.

The multipole resistance was found using a modified version of the Fortran 77 source code given in Bennet and Claesson (1987). Within the multipole method, the borehole resistance is found by establishing a temperature at the U-tube wall and then calculating a heat flux and a temperature profile around the circumference of the borehole wall. The temperature at the borehole was calculated by taking an average of 180 points along the circumference of the borehole wall. Averaging 180 points versus averaging 360 points produced a temperature difference of less than 0.00001 °C (0.000018 °F) difference. The resistance can be calculated by using Equation 1-1.

2.3 Borehole Resistance Calculation using Numerical Methods

As described in section 1.2.2.3, GEMS2D closely approximates the borehole geometry using a boundary fitted grid, whereas Yavuzturk approximates the borehole geometry using a pie shaped wedge in a parametric grid to represent the U-tubes. In this chapter, GEMS2D is used as a standard for the borehole resistance calculation since it correlates very closely with another highly accurate method, the multipole method. This will be shown in section 2.5. GEMS2D has also proven to be a very accurate two dimensional finite volume program for other simulations. The disadvantage of GEMS2D is that it is approximately half as fast as Yavuzturk's finite volume model program.

In both GEMS2D and Yavuzturk's pie sector approximation the average borehole wall temperature was subtracted from the given fluid temperature. This is shown in Equation 2-1. With constant flux and large times, typically greater than 10 hours, Equation 2-1 produces the steady state borehole resistance. A comparison of the steady state borehole resistances that GEMS2D and Yavuzturk's pie sector approximation produce is shown in section 2.4.

2.4 Numerical Methods: Comparison between GEMS2D and the Pie-Sector Approximation for Calculating Steady State Resistance

Table 2-1 shows the baseline borehole system configuration that was used for the comparison. By varying individual parameters, this borehole configuration produced Table 2-2 which shows the steady state borehole resistance for both GEMS2D and the pie sector approximation. The conductivities that were varied in this comparison are the soil, grout and pipe conductivity.

59

The conductivities that were shown cover most typical borehole configurations.

Also the borehole diameters that were chosen are 11.4 cm (4.5 in), 15.2 cm (6 in) and

19.1 cm (7.5 in) which also cover typical borehole configurations. As the borehole

diameter was changed the shank spacing was held constant at 0.16 cm (0.067 in). The

final parameter that was varied was the fluid flow rate at 0.000189 m^3/s (3 gpm),

0.000379 m^3/s (6 gpm), and 0.000568 m^3/s (9 gpm). This also covers the range of most

boreholes.

Table 2-1 Borehole Properties (Base Case)

Borehole System Table	English Units	SI Units
Diameter	4.5 (in)	114.3 (mm)
Shank Spacing	0.067 (in)	1.7 (mm)
U-tube OD	1.05 (in)	26.67 (mm)
U-tube ID	0.824 (in)	20.93 (mm)
k_{soil}	$1.2 \left(\dfrac{Btu}{h \cdot ft \cdot °F} \right)$	$2.077 \left(\dfrac{W}{m \cdot °K} \right)$
k_{grout}	$0.4 \left(\dfrac{Btu}{h \cdot ft \cdot °F} \right)$	$0.692 \left(\dfrac{W}{m \cdot °K} \right)$
k_{pipe}	$0.8 \left(\dfrac{Btu}{h \cdot ft \cdot °F} \right)$	$1.38 \left(\dfrac{W}{m \cdot °K} \right)$
k_{fluid}	$0.8 \left(\dfrac{Btu}{h \cdot ft \cdot °F} \right)$	$1.38 \left(\dfrac{W}{m \cdot °K} \right)$
Fluid Volumetric Heat	$62.4 \left(\dfrac{Btu}{ft^3 \cdot °F} \right)$	$4.18 \left(\dfrac{MJ}{m^3 \cdot K} \right)$
Flow Rate	3 (gpm)	$0.000189 \ (m^3/s)$

Table 2-2 Borehole Resistance Comparison between GEMS2D and the pie sector approximation

Varied Input			Borehole Resistance				%
Inputs	English	SI	Pie Sector		GEMS2D		Diff.
			$(°F/h \cdot Btu)$	(K/W)	$(°F/h \cdot Btu)$	(K/W)	%
k_{soil}	$0.8 \left(\dfrac{Btu}{h \cdot ft \cdot °F} \right)$	$1.38 \left(\dfrac{W}{m \cdot °K} \right)$	0.3615	0.685	0.3603	0.683	-0.333
k_{soil}	$1.2 \left(\dfrac{Btu}{h \cdot ft \cdot °F} \right)$	$2.07 \left(\dfrac{W}{m \cdot °K} \right)$	0.3608	0.684	0.3588	0.680	-0.559
k_{soil}	$1.6 \left(\dfrac{Btu}{h \cdot ft \cdot °F} \right)$	$2.77 \left(\dfrac{W}{m \cdot °K} \right)$	0.3604	0.683	0.3580	0.679	-0.671
k_{grout}	$0.2 \left(\dfrac{Btu}{h \cdot ft \cdot °F} \right)$	$0.346 \left(\dfrac{W}{m \cdot °K} \right)$	0.6778	1.28	0.6481	1.23	-4.48
k_{grout}	$0.4 \left(\dfrac{Btu}{h \cdot ft \cdot °F} \right)$	$0.692 \left(\dfrac{W}{m \cdot °K} \right)$	0.3608	0.684	0.3588	0.680	-0.559
k_{grout}	$0.8 \left(\dfrac{Btu}{h \cdot ft \cdot °F} \right)$	$1.38 \left(\dfrac{W}{m \cdot °K} \right)$	0.1982	0.376	0.2143	0.406	7.79
k_{pipe}	$0.4 \left(\dfrac{Btu}{h \cdot ft \cdot °F} \right)$	$.692 \left(\dfrac{W}{m \cdot °K} \right)$	0.3898	0.739	0.4284	0.812	9.43
k_{pipe}	$0.8 \left(\dfrac{Btu}{h \cdot ft \cdot °F} \right)$	$1.38 \left(\dfrac{W}{m \cdot °K} \right)$	0.3608	0.684	0.3588	0.680	-0.559
k_{pipe}	$1.2 \left(\dfrac{Btu}{h \cdot ft \cdot °F} \right)$	$2.07 \left(\dfrac{W}{m \cdot °K} \right)$	0.3494	0.662	0.3329	0.631	-4.84
Dia.	4.5 (in)	11.4 (cm)	0.3608	0.684	0.3588	0.680	-0.559
Dia.	6 (in)	15.2 (cm)	0.4259	0.807	0.3138	0.595	-30.3
Dia.	7.5 (in)	19.1 (cm)	0.4758	0.902	0.2785	0.528	-52.3
Flow Rate	3 (gpm)	$0.000189\ (m^3/s)$	0.3608	0.684	0.3588	0.680	-0.559
Flow Rate	6 (gpm)	$0.000379\ (m^3/s)$	0.3585	0.680	0.3570	0.677	-0.413
Flow Rate	9 (gpm)	$0.000568\ (m^3/s)$	0.3576	0.678	0.3563	0.675	-0.358

Several observations can be made between the steady state resistance obtained from GEMS2D and the pie sector approximation in Table 2-2. The pie sector approximation deviates from the GEMS2D solution when the grout geometric properties are changed. By changing the diameter of the borehole without changing the shank spacing or the U-tube diameter the grout geometry is being changed. This test measures

61

how accurately the automated grid generation algorithm approximates the actual geometry of the borehole with the pie sector approximation. The resistance is overestimated by more than 50% in the 19.1 cm (7.5 in) diameter case.

When the conductivity of the pipe or grout are changed from the standard of 1.38 and 0.692 $\left(\frac{W}{m\cdot°K}\right)$ (0.8 and 0.4 $\left(\frac{Btu}{h\cdot ft\cdot°F}\right)$) respectively the relative percent difference increases substantially. This error is accounted for because, when the conductive properties of the grout and pipe are increased or decreased, the effects of the geometric differences between the two programs are magnified.

Changing the conductivity of the soil does not appreciably change the percent difference between the two programs. This is because soil conductivity has a second order effect on borehole resistance since it is outside the borehole and both programs accurately represent the circular geometry at the borehole wall radius.

Both GEMS2D and the pie sector approximation would be poor choices as the resistance calculator for use with the BFTM model since they are very slow. The pie sector approximation requires on the order of thirty minutes and GEMS2D requires an hour on a 450 MHZ computer. Therefore analytical methods need to be compared to arrive at a reasonable solution. The pie sector approximation will not be considered further since GEMS2D is the more accurate finite volume model program for predicting borehole resistance as shown in section 2.5.

2.5   Comparison of Methods for Calculating Steady State Borehole Resistance

The steady state borehole resistance calculation methods that are compared in this chapter include the Paul (1996) method, the Gu and O'Neal (a 1998) approximate

diameter method, cylinder source, and the multipole methods. The GEMS2D solution is given as a general comparison.

The data for the baseline borehole used in this study are given in Table 2-3. Two different grout types were chosen, standard bentonite and thermally enhanced grout. This will give an understanding for how grout conductivity affects the different borehole resistance calculation methods. For each grout type, resistances were calculated for three different borehole diameters 7.6 cm (3 in), 11.4 cm (4.5 in), and 15.2 cm (6 in). The 7.6 cm (3 in) diameter case is an unrealistic borehole configuration; however it is useful for testing the capabilities of the models. For each borehole diameter, resistances were calculated for four different U-tube shank spacings ranging from 3.2 mm (0.125 in) from the outside wall of each U-tube, to where both U-tubes are touching the borehole outside wall. The parameters that were not varied include the U-tube diameter, U-tube thermal properties, soil thermal properties, and the circulating fluid's convection coefficient.

Table 2-3 Base Line Borehole Properties

Borehole Diameter				Pipe - 1" SDR-11				
D	=	114.30 mm	4.5 in	I.D.	=	27.4 mm	1.08 in	
Grout - Standard Bentonite				O.D.	=	33.4 mm	1.31 in	
K	= 0.75	$\left(\frac{W}{m\cdot{}^\circ K}\right)$	.433 $\left(\frac{Btu}{h\cdot ft\cdot {}^\circ F}\right)$	K	=	$0.390\left(\frac{W}{m\cdot{}^\circ K}\right)$	0.225 $\left(\frac{Btu}{h\cdot ft\cdot {}^\circ F}\right)$	
ρC_p	= 3.90	$\left(\frac{MJ}{m^3 K}\right)$	58.2 $\left(\frac{Btu}{ft^3\cdot {}^\circ F}\right)$	ρC_p	=	$1.77\left(\frac{MJ}{m^3 K}\right)$	26.4 $\left(\frac{Btu}{ft^3\cdot {}^\circ F}\right)$	
Soil - Typical Properties				Spacing				
K	= 2.50	$\left(\frac{W}{m\cdot{}^\circ K}\right)$	1.44 $\left(\frac{Btu}{h\cdot ft\cdot {}^\circ F}\right)$	A	S1=	3.18 mm	1/8 in	
ρC_p	= 2.50	$\left(\frac{MJ}{m^3 K}\right)$	37.3 $\left(\frac{Btu}{ft^3\cdot {}^\circ F}\right)$	B	S1=	S2	S2	
Fluid Convection Coefficient				C3	S2=	3.00 mm	0.12 in	
H	= 1690	$\left(\frac{W}{m^2 K}\right)$	298 $\left(\frac{Btu}{h\cdot ft^2\cdot {}^\circ F}\right)$	C	S2=	0 mm	0 in	
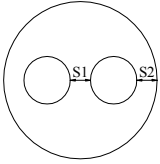
Table 2-4 gives the resistances that were calculated using the given borehole properties with the different methods. Table 2-5 shows the percent error of the steady state borehole resistance with respect to the GEMS2D calculated borehole resistance. Since GEMS2D is not capable of calculating the borehole resistance for the C spacing case, the multipole solution was used for the error calculation.

The general methods for calculating the borehole resistance were shown in the literature review for the cylinder source, the multipole, Gu and O'Neal, and the Paul methods. The cylinder source column shown in Table 2-4 shows data using the cylinder source method described in section 2.2. The multipole data shown in Table 2-4 uses the tenth order multipole solution.

Table 2-4 Steady State Borehole Resistance Comparison
N/A signifies that the method was not suitable for calculating the borehole resistance for this case

Borehole Diameter (mm) (in)	U-tube Spacing	k_{grout} (W/Km) $\left(\dfrac{hr \cdot ft \cdot °F}{Btu}\right)$	Paul (Km/W) $\left(\dfrac{hr \cdot ft \cdot °F}{Btu}\right)$	Gu and O'Neal (Km/W) $\left(\dfrac{hr \cdot ft \cdot °F}{Btu}\right)$	Cylinder Source (Km/W) $\left(\dfrac{hr \cdot ft \cdot °F}{Btu}\right)$	Multipole (Km/W) $\left(\dfrac{hr \cdot ft \cdot °F}{Btu}\right)$	GEMS2D (Km/W) $\left(\dfrac{hr \cdot ft \cdot °F}{Btu}\right)$
76.2 (3)	A	0.75 (0.4333)	0.188 (0.326)	0.136 (0.235)	0.1337 (0.2314)	0.1213 (0.2099)	0.1211 (0.2095)
76.2 (3)	B	0.75 (0.4333)	0.170 (0.294)	0.136 (0.235)	0.1338 (0.2316)	0.1214 (0.2101)	0.1213 (0.2099)
76.2 (3)	C3	0.75 (0.4333)	N/A	0.135 (0.233)	0.1331 (0.2303)	0.1206 (0.2087)	0.1204 (0.2084)
76.2 (3)	C	0.75 (0.4333)	0.127 (0.220)	0.119 (0.206)	0.1170 (0.2025)	0.1025 (0.1774)	N/A
114.3 (4.5)	A	0.75 (0.4333)	0.256 (0.443)	0.222 (0.384)	0.2197 (0.3803)	0.2119 (0.3668)	0.2116 (0.3663)
114.3 (4.5)	B	0.75 (0.4333)	0.205 (0.354)	0.190 (0.329)	0.1882 (0.3258)	0.1823 (0.3155)	0.1822 (0.3154)
114.3 (4.5)	C3	0.75 (0.4333)	N/A	0.146 (0.252)	0.1437 (0.2487)	0.1288 (0.2230)	0.1288 (0.2230)
114.3 (4.5)	C	0.75 (0.4333)	0.141 (0.244)	0.137 (0.238)	0.1355 (0.2346)	0.1149 (0.1989)	N/A
152.4 (6)	A	0.75 (0.4333)	0.322 (0.557)	0.283 (0.489)	0.2807 (0.4859)	0.2737 (0.4737)	0.2734 (0.4733)
152.4 (6)	B	0.75 (0.4333)	0.235 (0.407)	0.227 (0.392)	0.2248 (0.3892)	0.2216 (0.3836)	0.2216 (0.3836)
152.4 (6)	C3	0.75 (0.4333)	N/A	0.163 (0.282)	0.1611 (0.2788)	0.1386 (0.2399)	0.1387 (0.2401)
152.4 (6)	C	0.75 (0.4333)	0.152 (0.263)	0.157 (0.273)	0.1556 (0.2694)	0.1260 (0.2182)	N/A
76.2 (3)	A	1.5 (0.8666)	0.116 (0.201)	0.0896 (0.155)	0.08779 (0.1520)	0.08796 (0.1523)	0.08774 (0.1519)
76.2 (3)	B	1.5 (0.8666)	0.107 (0.185)	0.0896 (0.155)	0.08786 (0.1521)	0.08803 (0.1524)	0.08788 (0.1521)
76.2 (3)	C3	1.5 (0.8666)	N/A	0.0893 (0.155)	0.08743 (0.1513)	0.08763 (0.1517)	0.08740 (0.1513)
76.2 (3)	C	1.5 (0.8666)	0.0853 (0.148)	0.0813 (0.141)	0.07947 (0.1376)	0.07899 (0.1367)	N/A
114.3 (4.5)	A	1.5 (0.8666)	0.150 (0.259)	0.133 (0.230)	0.1308 (0.2264)	0.1317 (0.2280)	0.1315 (0.2276)
114.3 (4.5)	B	1.5 (0.8666)	0.124 (0.215)	0.117 (0.202)	0.1151 (0.1992)	0.1158 (0.2005)	0.1157 (0.2003)
114.3 (4.5)	C3	1.5 (0.8666)	N/A	0.0946 (0.164)	0.09279 (0.1606)	0.09149 (0.1584)	0.09144 (0.1583)
114.3 (4.5)	C	1.5 (0.8666)	0.0922 (0.160)	0.0905 (0.157)	0.08871 (0.1536)	0.08627 (0.1493)	N/A
152.4 (6)	A	1.5 (0.8666)	0.183 (0.316)	0.163 (0.282)	0.1613 (0.2793)	0.1624 (0.2811)	0.1621 (0.2806)
152.4 (6)	B	1.5 (0.8666)	0.139 (0.241)	0.135 (0.234)	0.1334 (0.2309)	0.1345 (0.2328)	0.1344 (0.2327)
152.4 (6)	C3	1.5 (0.8666)	N/A	0.103 (0.179)	0.1015 (0.1757)	0.09828 (0.1701)	0.09833 (0.1702)
152.4 (6)	C	1.5 (0.8666)	0.0978 (0.169)	0.101 (0.174)	0.09876 (0.1710)	0.09413 (0.1629)	N/A

Tables 2-4 and 5 show that the tenth order multipole and GEMS2D correlate very closely yielding a maximum difference of 0.26 percent. In addition, the multipole method is very fast with a computer compared to GEMS2D. It takes less than a second to calculate on a 450 MHz computer whereas the GEMS2D program might require half an hour, depending on the grid, on the same computer.

Table 2-5 Percent Error of Borehole Resistance
N/A signifies that the method was not suitable for calculating the borehole resistance for this case

Bore Diameter mm (in)	Spacing	Kgrout (W / Km) $\left(\frac{hr \cdot ft \cdot {}^\circ F}{Btu}\right)$	Paul	Gu and O'Neal	Cylinder Source	Multipole
76.2 (3)	A	0.75 (0.4333)	55.5	11.9	10.4	0.17
76.2 (3)	B	0.75 (0.4333)	39.9	11.8	10.4	0.11
76.2 (3)	C3	0.75 (0.4333)	N/A	12.0	10.5	0.17
76.2 (3)	C	0.75 (0.4333)	23.8	15.9	14.1	N/A
114.3 (4.5)	A	0.75 (0.4333)	20.8	4.69	3.83	0.12
114.3 (4.5)	B	0.75 (0.4333)	12.3	4.28	3.29	0.03
114.3 (4.5)	C3	0.75 (0.4333)	N/A	12.9	11.5	0.01
114.3 (4.5)	C	0.75 (0.4333)	22.5	19.5	17.9	N/A
152.4 (6)	A	0.75 (0.4333)	17.8	3.35	2.67	0.09
152.4 (6)	B	0.75 (0.4333)	6.14	2.31	1.46	-0.01
152.4 (6)	C3	0.75 (0.4333)	N/A	17.5	16.1	-0.10
152.4 (6)	C	0.75 (0.4333)	20.6	24.9	23.5	N/A
76.2 (3)	A	1.5 (0.8666)	32.2	2.10	0.05	0.25
76.2 (3)	B	1.5 (0.8666)	21.3	2.00	-0.02	0.17
76.2 (3)	C3	1.5 (0.8666)	N/A	2.13	0.04	0.26
76.2 (3)	C	1.5 (0.8666)	7.96	2.86	0.60	N/A
114.3 (4.5)	A	1.5 (0.8666)	13.9	0.86	-0.50	0.20
114.3 (4.5)	B	1.5 (0.8666)	7.25	0.95	-0.59	0.07
114.3 (4.5)	C3	1.5 (0.8666)	N/A	3.43	1.48	0.05
114.3 (4.5)	C	1.5 (0.8666)	6.89	4.89	2.82	N/A
152.4 (6)	A	1.5 (0.8666)	12.8	0.64	-0.48	0.17
152.4 (6)	B	1.5 (0.8666)	3.72	0.57	-0.77	0.02
152.4 (6)	C3	1.5 (0.8666)	N/A	5.03	3.22	-0.05
152.4 (6)	C	1.5 (0.8666)	3.91	6.81	4.92	N/A

Compared to the tenth order multipole method, the Gu and O'Neal approximate diameter method, the cylinder source methods as well as the Paul method typically have greatly reduced accuracy. For all of the models in Table 2-5, the largest errors occur for

66

the 7.6 cm (3 in) diameter U-tube case for both thermally enhanced and non thermally enhanced grout. The Paul method, the Gu and O'Neal method, and the cylinder source method all tend to over predict borehole resistance. The cylinder source is in some cases higher and some cases lower than the actual resistance as can be seen in Table 2-4.

For both the Gu and O'Neal method and the cylinder source method, as the shank spacing increases from "A" (narrowly spaced U-tube) to "C" (widely spaced U-tube) the error increases substantially. For the Gu and O'Neal method, with standard grout, 11.4 cm (4.5 in) diameter with the "A" and "C" shank spacing, borehole errors were 4.7% and 19.5% respectively. For the same condition the cylinder source solution produced errors of 3.8% for the "A" shank spacing and 17.9% for the "C" shank spacing. This increase in error stems from the Gu and O'Neal method and the cylinder source method not taking into account the soil conductivity. As the U-tubes move from very close together to very far apart the impact of soil conductivity on the borehole resistance increases. Thus, as would be expected for the thermally enhanced grout cases, the errors have all substantially decreased for both the Gu and O'Neal and the cylinder source methods, due to the grout and the soil conductivities being closer together.

As stated earlier, the data in Table 2-5 shows that the Gu and O-Neal method has an increase in error as the shank spacing increases. Thus, since the resistance is a direct result of the equivalent diameter (Equation 1-11), the data shows that the equivalent diameter calculation is less accurate for large shank spacings versus small shank spacings.

The Paul method performed poorly in comparison to the other methods. In most cases the error produced by the Paul method was several times that of the other methods

shown in Table 2-5. Also, the error fluctuates differently with shank spacing than the Gu

and O'Neal method and the cylinder source model. As mentioned in section 1.2.1.3 the

experimental model had uniform heat flux around the U-tubes which is not the case in a

real system. This is the cause of some of the error in the Paul method however it

probably does not account for all of the error in the 76.2 mm (3 in) diameter cases shown

in Table 2.5.

2.6 Borehole Resistance and Merging of the Short and Long Time Step G-Function

The steady state borehole resistance parameter is used to separate the long time

step g-function from specific borehole geometries making a single long time step g-

function valid for any specific borehole geometry. This is accomplished by the R_{total}

term in Equation 2-8.

$$g = \frac{2\pi k_{soil}\left(T_f - (R_{total} \cdot Q) - T_{ground}\right)}{Q} \tag{2-8}$$

where,

g = g-function (nondimensionalized)

R_{total} = borehole resistance $\left(\dfrac{Km}{W}\right)$ or $\left(\dfrac{h \cdot ft \cdot °F}{Btu}\right)$

T_f = average fluid temperature (K) or (°F)

T_{ground} = steady state ground temperature (K) or (°F)

Q = flux per unit length $\left(\dfrac{W}{m}\right)$ or $\left(\dfrac{Btu}{h \cdot ft}\right)$

k_{soil} = soil conductivity $\left(\dfrac{W}{m \cdot K}\right)$ or $\left(\dfrac{Btu}{ft \cdot °F}\right)$

The g-function in Equation 2-8 is only a representation of the thermal resistance of the ground. Before the long time step g-function can be used to calculate the fluid temperature the borehole resistance must be calculated using specific borehole parameters and then added to the thermal resistance of the ground. If the resistance calculation is not accurate then the long and short time step g-functions will merge poorly.

Figure 2-1 shows a short time step g-function calculated with the line source for the borehole with properties shown in Table 2-1 with a 11.4 cm (4.5 in) diameter and B shank spacing. The steady state borehole resistance is shown in Table 2-4. In Figure 2-1 the long time step g-function is for a single borehole. As can be seen in Figure 2-1 three different curves have been created for the longtime step g-function using three different methods for calculating borehole resistance. The "LTS: Generalized" curve is the long time step g-function without the borehole resistance.

**Line Source Short Time Step G-function Compared to Long Time Step G-function Translated
Using Different Borehole Resistance Calculation Methods**
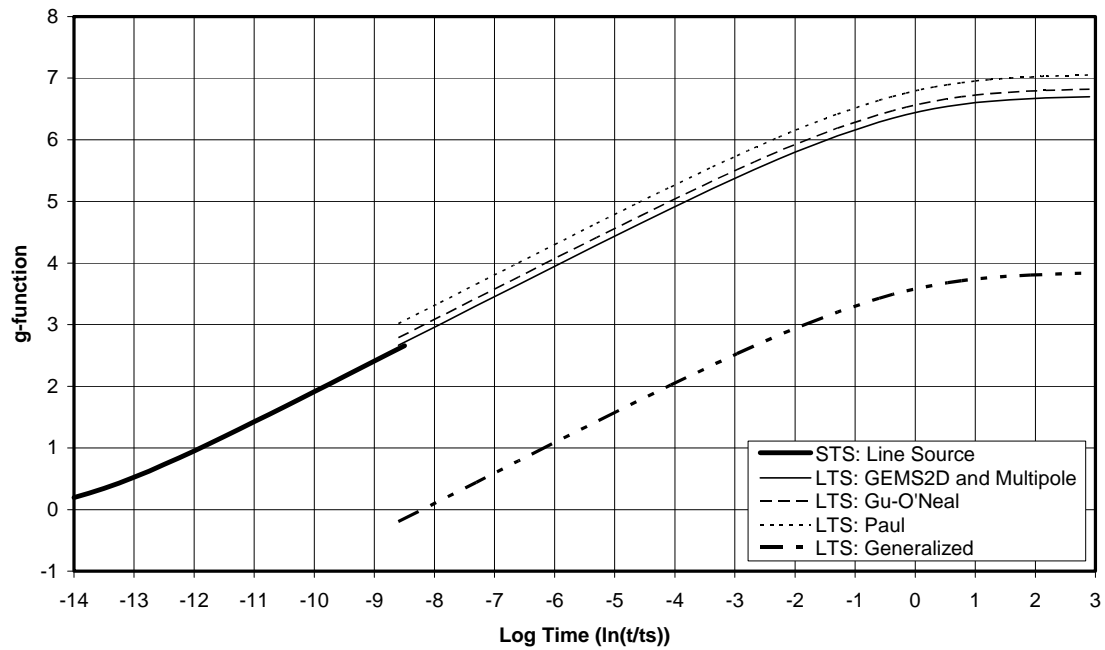
**Figure 2-4 Line Source STS G-function Compared to LTS G-function Using
Different Borehole Resistance Calculation Methods for a Single Borehole System**

As can be seen in Figure 2-3 the LTS and STS g-function merges well using the

resistance calculated with either the GEMS2D or Multipole resistance methods. Also the

LTS g-function using the Gu and O'Neal or the Paul methods matches less well with the

STS g-function. As shown in Table 2-5, the errors in the borehole resistances are 12.3%

for the Paul method and 4.3% for the Gu and O'Neal method. The percent errors shown

for this particular case in Table 2-5 are not the greatest errors. For some cases the

merging between the long and short time step g-functions will be even worse using the

Gu-O'Neal and the Paul methods.

70

2.7   Conclusion

As discussed in the literature review the long and short time step g-functions are produced using different methods. The long time step g-function is produced using superposition with data from a two dimensional radial-axial finite difference model. The short time step g-function is produced with a two dimensional analytical or experimental model of the cross section of the borehole. Before the g-function can be used in a simulation, consistency must be checked between the two methods that produce the short and long time step g-functions and borehole resistance. If the short and long time step g-function do not merge well together this is evidence of a problem with the borehole resistance calculation or with the short or long time step g-function itself.

This study shows that since the Paul method, for most geometries, does not accurately calculate the borehole resistance and therefore does not ensure a good merge of the long and short time step g-function, it should not be used in simulations. The Gu-O'Neal method is superior to the Paul method and might be suitable in a simulation when a very simple method is needed. The user should be aware of the errors involved with this simple calculation as shown in Table 2-5. Of the methods that are compared in this chapter, the multipole method is the best analytical method for the purpose of merging the long and short time step g-function. Also, since the borehole resistance for most simulations will only be computed once, for a given simulation, it is not necessary for the resistance calculator to be exceptionally fast. However using the finite volume methods such as the pie sector approximation or GEMS2D which require fifteen minutes and 30 minutes, respectively, on a 1.4 Ghz computer is not practical. Since the multipole method requires less then a second to calculate on a 450 Mhz Pentium II and attains a

very good correlation with the GEMS2D model it is a very good choice for the borehole

resistance calculator.

3 SHORT TIME STEP G-FUNCTION CREATION AND THE BOREHOLE FLUID THERMAL MASS MODEL (BFTM)

The short time step g-function can be generated by any program or equation that is capable of approximating a transient borehole fluid temperature profile over time. The simplest and fastest method for use in a computer simulation is the line source method. As discussed in Chapter One, this method neglects all of the interior geometry and fluid mass of the borehole and models the borehole as a single heat rejection line of infinite length. Not surprisingly, being the simplest method, it is also one of the least accurate methods for short times less than ten hours where the specific borehole geometry and thermal mass of the fluid are important factors. When the geometry and fluid mass of the borehole are simulated the error of the line source can be seen. This error is shown in Figure 3-1, where the temperature rise calculated with the line source is compared to that calculated with GEMS2D, accounting for the borehole geometry. The BH geometry and thermal properties is the standard case shown in Table 2-3 with the "B" U-tube spacing.
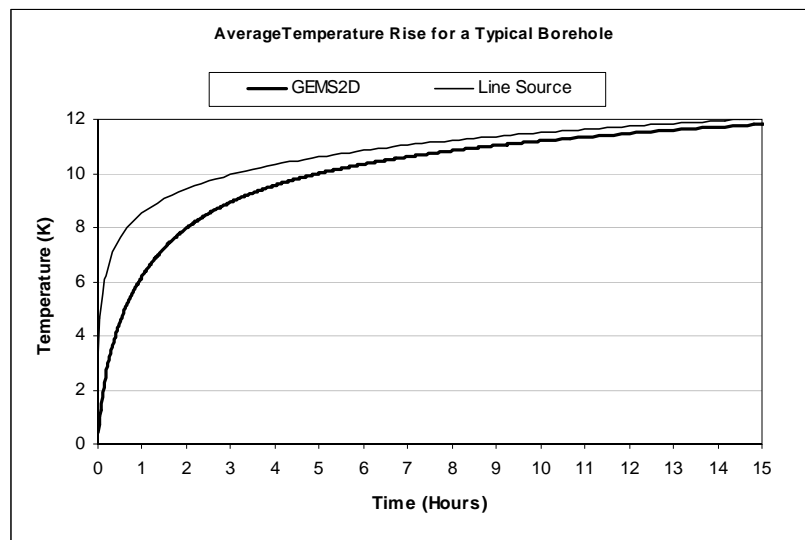
Figure 3-1 Average Fluid Temperature using the line source and GEMS2D model with fluid mass for a heat rejection pulse

The line source typically overestimates the borehole resistance over the first day of simulation creating a higher average fluid temperature in heat extraction.

Since numerical methods such as GEMS2D are very slow at calculating temperature response they are ill-suited for practicing engineers to use while designing a ground loop heat exchanger. Furthermore, the initial step of creating a grid with borehole geometry and properties is time consuming and tedious, GEMS2D would be even more difficult to incorporate in a simulation program. A faster and suitably accurate method is needed. The method that was applied to ground loop heat exchangers comes from the buried electrical cable model (Carslaw and Jaeger, 1947). It is adapted to model a borehole, accounting for the fluid thermal mass. It is therefore referred to as the borehole fluid thermal mass (BFTM) model. The BFTM model is described in detail in this chapter and the GEMS2D numerical validations are shown in Chapter 4.

3.1   Borehole Fluid Thermal Mass Model

The BFTM model uses the buried electrical cable model (BEC) which is described in the literature review in section 1.2.2.1. A diagram of the buried electrical cable is shown in Figure 1-10 where there is a core with infinite conductivity surrounded by insulation which is surrounded by a sheath. In Equation 1-31, each input in the buried electrical cable model has an analogous input with respect to a borehole. Table 3-1 describes the inputs with respect to each model.

Table 3-1 Borehole Properties Table

Number	Buried Electrical Cable Model	Borehole Fluid Thermal Mass Model
1	Insulation Thermal Resistance	Borehole Resistance
2	Outer Radius of the Sheath	Borehole Radius
3	Core Thermal Capacity	Fluid Thermal Capacity
4	Sheath Thermal Capacity	Grout Thermal Capacity
5	Soil Thermal Diffusivity	Same
6	Specific Heat of the Soil	Same
7	Conductivity of the Soil	Same

The first four parameters in Table 3-1 have different meanings in the BFTM model from the BEC model. The soil parameters are the same in both models. In the BEC model the sheath and core are perfect conductors and have no contact resistance. Also, in the BEC model, the core has zero resistance whereas the sheath has a resistance value. Thus, as shown in Table 3-1 the borehole resistance for the BFTM model is analogous to the insulation resistance for the BEC model.

The second parameter in Table 3-1 equates the borehole radius to the buried cable radius. The concept is the same between the two models.

In the buried electrical cable model, the sheath and core are assumed to be thermal masses without resistance or what might be called "lumped capacitances". In the borehole, the fluid, with internal convective transport, behaves as a "lumped capacitance" with grout surrounding the U-tube and fluid. This is indicated in Table 3-1 by the third and fourth parameters where the core thermal capacity is represented as the fluid thermal capacity and the sheath thermal capacity becomes the grout thermal capacity. Placing all of the grout thermal capacity at the outside of the borehole resistance is an approximation. This can be improved upon, as discussed in section 3.2

To maintain the correct thermal mass of the fluid and grout, the cross sectional area of the fluid and grout are maintained from the actual U-tube to the buried electrical cable representation. Thus the area of the fluid in the two legs of the U-tubes equals the core area in the BEC model as shown in Equation 3-1.

$$Area = 2\pi \cdot r_{U-tube}^2 = \pi \cdot r_{core}^2 \qquad \textbf{(3-1)}$$

r_{core} is solved for and shown in Equation 3-2.

$$r_{core} = \sqrt{2}r_{U-tube} \qquad \textbf{(3-2)}$$

where,

r_{core} =   Radius of the core for a BEC (m) or (in)

r_{U-tube} =   Inside radius of U-tube for a borehole (m) or (in)

Using Equation 3-2 for the core radius the equations for the fluid and grout thermal capacities per unit length are as shown in Equation 3-3.

$$S_1 = \lambda_{fluid} \cdot A_{fluid} \quad , \quad S_2 = \lambda_{grout} \cdot A_{grout} \qquad \textbf{(3-3)}$$

where,

S_1 =   Core thermal capacity per unit length $\left(\dfrac{J}{mK}\right)$ or $\left(\dfrac{Btu}{ft \cdot {}^\circ F}\right)$

S_2 =   Sheath thermal capacity per unit length $\left(\dfrac{J}{mK}\right)$ or $\left(\dfrac{Btu}{ft \cdot {}^\circ F}\right)$

A_{fluid} =   Area of the core which represents the fluid $\left(m^2\right)$ or $\left(in^2\right)$

A_{grout} =   Area of the sheath which represents the grout $\left(m^2\right)$ or $\left(in^2\right)$

The area of the fluid and grout are calculated as follows .

$$A_{fluid} = \pi \cdot R_{core}^2 \quad , \quad A_{grout} = \pi \cdot R_{BH}^2 - A_{fluid} \qquad \text{(3-4)}$$

where,

A_{fluid} = Area of the core which represents the fluid (m^2) or (in^2)

A_{grout} = Area of the sheath which represents the grout (m^2) or (in^2)

R_{core} = Core radius (m) or (in)

R_{BH} = Borehole Radius (m) or (in)

This method does not take into account the shank spacing when calculating the core and sheath thermal capacity. The shank spacing comes into the model through the borehole resistance calculation using the multipole method and the grout allocation factor (GAF) discussed in section 3.2.

3.2 Grout Allocation Factor Used to Improve Accuracy

The grout allocation factor (GAF) is used to improve the accuracy of the buried electrical cable model, in order to better account for borehole geometry. It does this by moving part of the thermal capacity of the grout into the core, on the inside of the borehole thermal resistance, as shown in Equation 3-5. The GAF value is actually a fraction of the grout to be moved from the outside of the borehole thermal resistance to the inside of the borehole thermal resistance. The thermal capacities calculated in Equation 3-5 are used in Equation 3-3.

$$S_{1f} = S_1 + S_2 \cdot f \quad , \quad S_{2f} = S_2 \cdot (1-f) \tag{3-5}$$

where,

S_{1f} = Adjusted core thermal capacity per unit length $\left(\dfrac{J}{mK}\right)$ or $\left(\dfrac{Btu}{ft \cdot {}^\circ F}\right)$

S_{2f} = Adjusted sheath thermal capacity per unit length $\left(\dfrac{J}{mK}\right)$ or $\left(\dfrac{Btu}{ft \cdot {}^\circ F}\right)$

S_1 = Core thermal capacity per unit length $\left(\dfrac{J}{mK}\right)$ or $\left(\dfrac{Btu}{ft \cdot {}^\circ F}\right)$

S_2 = Sheath thermal capacity per unit length $\left(\dfrac{J}{mK}\right)$ or $\left(\dfrac{Btu}{ft \cdot {}^\circ F}\right)$

f = Grout allocation factor (no units)

The optimal GAF value was found to vary slightly with varying shank spacing, borehole diameter and fluid multiplication factor. The fluid multiplication factor will be introduced in section 3.3. The optimal GAF values, for a range of cases are given in Chapter 4 along with a description of how they were found.

With a GAF equal to zero, the BFTM model over predicts the fluid temperature for the first 10 hours for most borehole configurations. However, even with a zero GAF, the BFTM model is better than the line source model.

3.3   Fluid Multiplication Factor in the BFTM model

By modeling the fluid mass in a borehole, the BFTM model is a significant improvement over the line source and all other analytical models. It is an improvement not only because the fluid temperature profile is more accurate but because the BFTM model also allows the effects of additional fluid in the system, outside the borehole, to be modeled.

Not only does the fluid in the borehole damp the temperature response, fluid outside the borehole, in the rest of the system, also significantly damps the temperature

response. It is also possible to use a fluid storage tank, or buffer tank, to increase the performance of ground loop heat exchangers in systems that are peak-load-dominant. Extra fluid in the system is modeled by increasing the capacity, S_1, with a fluid multiplication factor.

The fluid multiplication factor is shown in Equation 3-6. The factor increases the thermal capacity of the circulating fluid. Specifying $F_{fluid} = 2$ will double the thermal capacity of the fluid in the system.

$$S_{1mf} = S_1 \cdot F_{fluid} + S_2 \cdot f \tag{3-6}$$

where,

$\quad S_{1mf} \quad = \quad$ Core thermal capacity adjusted for grout allocation factor and extra fluid per unit length $\left(\dfrac{J}{mK} \right)$ or $\left(\dfrac{Btu}{ft \cdot {}^\circ F} \right)$

$\quad F_{fluid} \quad = \quad$ Fluid multiplication factor (no units)

$\quad S_1 \quad = \quad$ Core thermal capacity per unit length $\left(\dfrac{J}{mK} \right)$ or $\left(\dfrac{Btu}{ft \cdot {}^\circ F} \right)$

$\quad S_2 \quad = \quad$ Sheath thermal capacity per unit length $\left(\dfrac{J}{mK} \right)$ or $\left(\dfrac{Btu}{ft \cdot {}^\circ F} \right)$

$\quad f \quad = \quad$ Grout allocation factor (no units)

3.4 Implementation of the BFTM Model

An important concern when implementing the BFTM model is computer processing time. Even though the BFTM model is much faster than a GEMS2D solution it is much slower than the line source solution. This introduces several practical concerns with evaluating the Bessel functions and the integral in Equation 1-31 as well as incorporating the method into a simulator.

3.4.1 Bessel Function Evaluation

The general equations for J and Y type, integer order Bessel functions are shown in Equation 3-7 and 3-8.

$$J_n(x) = \sum_{k=0}^{\infty} \frac{(-1)^k}{k!(n+k)!}\left(\frac{x}{2}\right)^{n+2k} \tag{3-7}$$

$$Y_n(x) = \frac{2}{\pi}\left\{\left[\ln\left(\frac{x}{2}\right)+\gamma\right]J_n(x) - \frac{1}{2}\sum_{k=0}^{n-1}\frac{(n-k-1)!}{k!}\left(\frac{x}{2}\right)^{-(n-2k)} + \frac{1}{2}\sum_{k=0}^{\infty}\left(\frac{(-1)^{k+1}[f(k)+f(n+k)]}{k!(n+k)!}\left(\frac{x}{2}\right)^{n-2k}\right)\right\} \tag{3-8}$$

$$f(k) = \sum_{m=1}^{k} 1/m \quad , \quad \gamma = 0.57722$$

where,

$J_n(x)$ =   J type Bessel function

$Y_n(x)$ =   Y type Bessel function

x   =   Point that the Bessel function is evaluated

γ =   Euler's Constant

N   =   Positive integer

These equations will converge for all "x" values however they are computationally expensive especially for $x \gg 1$. Since these functions will be called many times in evaluating the BEC integral, a faster method was needed.

A faster method for calculating the Bessel function is suggested by Press, et al. (1989). This method uses polynomial equations to approximate the Bessel functions as shown in Equation 3-9, 10, 11, and 12. Since these equations use polynomials they are much easier to program than Equations 3-7 and 3-8 as well as much faster to execute. These were coded into two Fortran functions, one for J type and another for Y type Bessel functions.

$$J_0(x) = \frac{R_1}{S_1} \quad , \quad J_1(x) = \frac{R_2}{S_2}, \text{ for } 0 < x < 8 \qquad \textbf{(3-9)}$$

$$J_n(x) = \sqrt{\frac{2}{\pi x}}\left[P_n\left(\frac{8}{x}\right)\cos(X_n) - Q_n\left(\frac{8}{x}\right)\sin(X_n) \right], \text{ for } 8 < x < \infty \qquad \textbf{(3-10)}$$

$$Y_0(x) = \frac{R_3}{S_3} - \frac{2}{\pi}J_0(x)\ln(x) \quad , \quad Y_1(x) = \frac{R_4}{S_4} - \frac{2}{\pi}\left[J_0(x)\ln(x) - \frac{1}{x} \right], \text{ for } 0 < x < 8 \qquad \textbf{(3-11)}$$

$$Y_n(x) = \sqrt{\frac{2}{\pi x}}\left[P_n\left(\frac{8}{x}\right)\sin(X_n) + Q_n\left(\frac{8}{x}\right)\cos(X_n) \right], \text{ for } 8 < x < \infty \qquad \textbf{(3-12)}$$

$$X_n = x - \frac{2n+1}{4}\pi$$

where,

$J_n(x)$	=	J type Bessel function
$Y_n(x)$	=	Y type Bessel function
x	=	Point that the Bessel function is evaluated
P_0, P_1, Q_0, Q_1 R_1, S_1, R_2, S_2 R_3, S_3, R_4, S_4	=	Polynomial equation coefficients
N	=	Positive integer

3.4.2   BFTM Model - Solving the Integral

The integral in Equation 1-26 has lower and upper limits of 0 and ∞. The complexity of Equation 1-26 makes an analytical solution infeasible. A numerical solution is therefore preferable. This leads to the problem of choosing an upper bound for the integration interval since ∞ cannot be attained with numerical methods. In order

81

to determine an interval that will provide a reasonable numerical solution, Equation 3-13 was created from Equation 1-26 by extracting the quantity that is to be integrated.

$$F(t,u) = \left(\frac{1 - e^{-u^2 \left(\alpha \frac{t}{a^2} \right)}}{u^3 \cdot \Delta} \right)$$

(3-13)

$$\Delta = \left[\left[u\left(a_1 + a_2 - hu^2\right)J_0(u) - a_2\left(a_1 - hu^2\right)J_1(u)\right]^2 + \left[u\left(a_1 + a_2 - hu^2\right)Y_0(u) - a_2\left(a_1 - hu^2\right)Y_1(u)\right]^2 \right]$$

$$a_1 = \frac{2\pi r_b^2 \rho C_p}{S_1} \quad , \quad a_2 = \frac{2\pi r_b^2 \rho C_p}{S_2} \quad , \quad h = 2\pi \cdot R_s k_{soil}$$

where,

$F(t,u)$ = Function to be integrated with respect to u

u = Integration variable (dimensionless)

t = Time (s)

Note: For variable definitions not listed here refer to Equation 1-26

The integration variable in Equation 3-13 is cubed in the denominator. This causes the function to approach zero very rapidly for u > 2 regardless of the specified time. This can be seen graphically in Figure 3-2 which uses the borehole properties shown in Table 2-3 with the "b" spacing. The shape of the curve changes as time increases. For times less than 14 hours the curve has one hump, for times greater than 14 hours a second hump appears and continues to increase in amplitude. Even though Equation 3-13 is complex, the shape that is produced is relatively simple for a range of parameters over time.
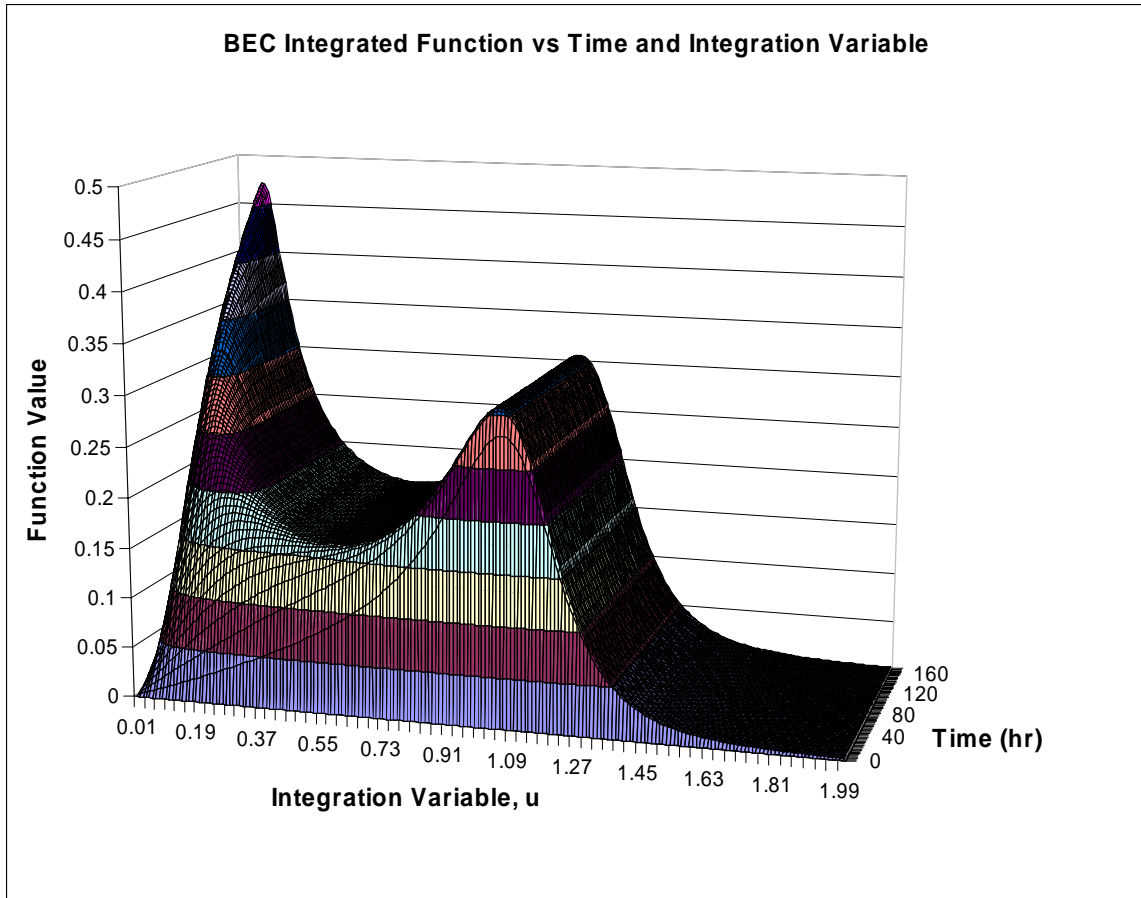
Figure 3-2 Integrated Function in the BEC Model

Through experimentation it was found that integrating from 0 to 10 produced at least four digits of accuracy when compared to integrating from 0 to 10000. Therefore the integration limits of 0 to 10 were chosen for the Fortran model.

3.4.3   Incorporating the Fluid Thermal Mass Model in a Design Program

In a typical GLHE design program the depth of the borehole will be found for a specific borehole system via iteration. Since the short time step g-function is dependent on borehole geometry and not borehole depth, a new STS g-function does not need to be recalculated each iteration when the depth of the borehole system changes. Since g-functions are plotted against log scale time and log scaled time is a function of the borehole depth, the STS g-function will appear to change when depth changes. In reality

the shape of the STS g-function remains the same, but it is being translated horizontally (on the plot) when the depth of the borehole changes. If the depth of the borehole increases the STS g-function is shifted to the right. If the depth of the borehole decreases the STS g-function is shifted to the left.

An equation can be created that can translate the short time step g-function for different depths by using the logarithmically scaled time equation at the old borehole depth as shown in Equation 3-14.

$$LT_{old} = \ln\left(\frac{t}{t_{s,old}}\right) \quad , \quad t_{s,old} = \frac{H_{old}^2}{9 \cdot \alpha} \qquad \text{(3-14)}$$

Where,

LT_{old} =   logarithmically scaled time for prior depth (dimensionless)

t =   actual time (sec)

$t_{s,old}$ =   time scale factor (sec)

H_{old} =   old borehole depth (m) or (ft)

α =   soil thermal diffusivity $\left(\frac{m^2}{s}\right)$ or $\left(\frac{ft^2}{s}\right)$

Solving the above equation for "t" yields $t = t_{s,old} \cdot e^{LT_{old}}$. This equation can be

substituted into $LT_{new} = \ln\left(\frac{t}{t_{s,new}}\right)$, to yield $LT_{new} = \ln\left(\frac{t_{s,old} \cdot e^{LT_{old}}}{t_{s,new}}\right) = \ln\left(\frac{t_{s,old}}{t_{s,new}}\right) + LT_{old}$. Thus

the horizontal shift can be quantified by taking the natural log of the ratio of the time

scale factors. Equation 3-15 results after substituting $\frac{H^2}{9 \cdot \alpha}$ for t_s (old and new) and then

canceling the $9 \cdot \alpha$ terms.

$$LT_{new} = \ln\left(\frac{H_{old}^2}{H_{new}^2}\right) + LT_{old}$$

(3-15)

Where,

LT_{new} =   logarithmically scaled time for new depth

LT_{old} =   logarithmically scaled time for prior depth

H_{new} =   new borehole depth (m)

H_{old} =   old borehole depth (m)

Since $\ln\left(\dfrac{H_{old}^2}{H_{new}^2}\right)$ is a constant for every log time all the points are shifted by the same

amount. Figure 3-3 shows a STS g-function that has been translated from a depth of 91.4

m (300 ft).
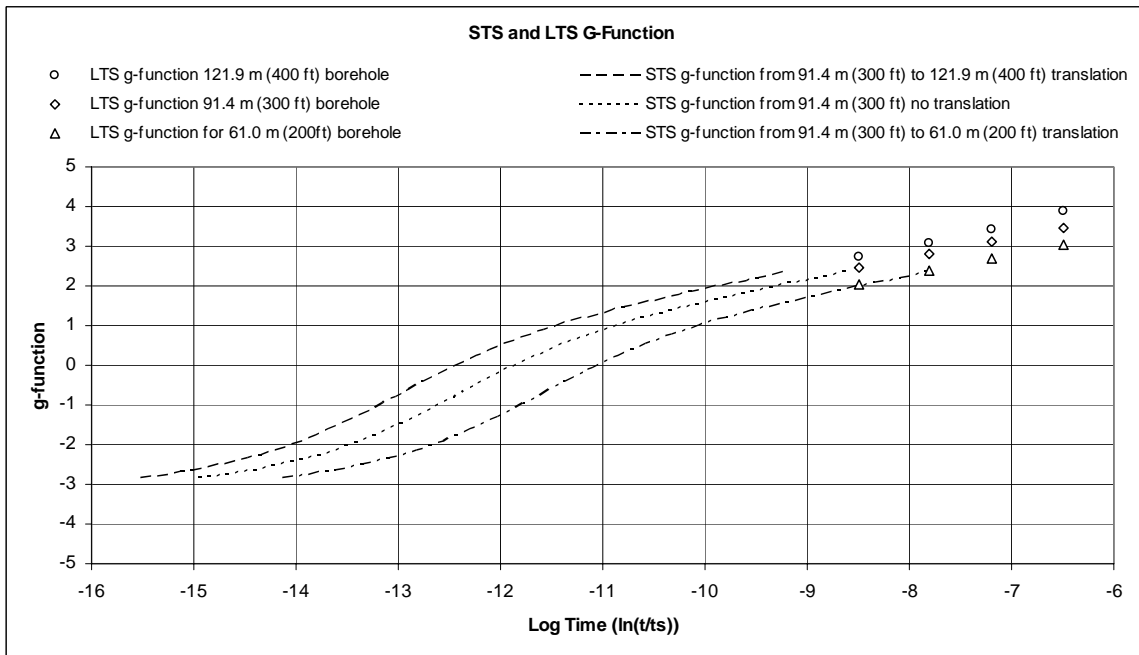
Figure 3-3 STS G-Function Translation

Since the region where the STS and LTS g-function meet is linear with respect to a log scale, the gap that exists in Figure 3-3 with the dashed line and the overlap that exists in Figure 3-3 with the dot-dash line does not create a problem if logarithmic interpolation is used.

The line source solution for deep boreholes is valid for a larger segment of the curve. Thus a STS g-function can be translated as far to the left as desired without losing accuracy since the linear region between the STS and LTS g-function also grows.

If a STS g-function is translated to the right the overlap between the STS and LTS g-function increases causing the linear region joining the short and long time step g-function to become narrow. Thus a STS g-function that is translated from 91.4 m (300 ft) to 15.2 m (50 ft) would have considerable overlap and would not merge perfectly with the LTS g-function.

Even though improper merging occurs for very short boreholes less than 15.2 m (50 ft) the problem can be remedied. An algorithm should be written which interpolates in the STS g-function first. If a time is to large for the STS g-function, the LTS g-function should be interpolated in. This type of algorithm assumes that if proper merging does not occur at where the LTS g-function begins, than the STS g-function will gradually merge with LTS g-function.

3.5 Improving the BFTM Model for Small Times Using Logarithmic Extrapolation

In chapter 4 the BFTM model is validated using over 60 GEMS2D simulations. The comparison in chapter 4 shows that if the borehole diameter is 7.62 cm (3 in) the BFTM model is able to accurately predict the fluid temperature within 0.25 °C (0.45 °F)

for a 2 hour heat pulse. This is a large improvement over the line source model which has 2 °C (3.6 °F) error at 2 hours. However the BFTM model has increasing error for 11.4, 15.2, and 19.1 cm (4.5, 6 and 7.5 in) borehole diameter. For example, the 15.2 and 19.1 cm (6 and 7.5 in) diameter boreholes the error can be as large as 1 °C (1.8 °F) for a two hour heat pulse. The remedy prescribed in this thesis is to use logarithmic extrapolation. This method is possible because g-functions, created from GEMS2D data, are linear with respect to log times between 1 hour and 10 hours. Logarithmic extrapolation is a heuristic approach based on the BFTM model's ability to accurately predict the slope of the GEMS2D g-function for a specific time. This section will describe how logarithmic extrapolation is implemented and Chapter 4 will validate its accuracy.

3.5.1 Implementing Logarithmic Extrapolation

Logarithmic extrapolation uses the G-function curve plotted against non-dimensional logarithmic time. Logarithmic extrapolation only requires the slope and the location on the g-function for a chosen point in time. The general equations for the extrapolated g-function values and the fluid temperature rise are given as Equations 3-16 and 3-17, as a function of time in seconds and the time scale factor.

$$g(t) = m \ln\left(\frac{t}{t_s}\right) + b \tag{3-16}$$

$$T(t) = \frac{Q}{2\pi k} g(t) \tag{3-17}$$

Where,

$g(t)$ = g-function

t = time (seconds)

m = slope of g-function (unitless)

b = Constant (unitless)

t_s = time constant defined in Equation 1-29 (seconds)

$T(t)$ = fluid temperature (°C or °F)

Q = Constant (W/m or BTU/hr·ft)

k = Soil conductivity $\left(\dfrac{W}{mk}\right)$ or $\left(\dfrac{Btu}{h \cdot ft \cdot °F}\right)$

Equation 3-16 and 17 are shown in Figure 3-4 as a temperature and a g-function curve with the BFTM and GEMS2D simulations. Figure 3-4 has a 19.1 cm (7.5 in) borehole, shank spacing of 8.25 cm (3.25 in), soil conductivity of 2.5 W/mk (1.44 Btu/(h·ft·°F)), standard grout and a 76.2 m (250 ft) depth . One hour is -12.1 in logarithmic time for this case. The time used to solve for "m" and "b" in Equation 3-15 is 8 hours. The GAF value used in the BFTM model is 0.255. As can be seen the exponential for the g-function graph is completely linear since the domain is logarithmic.
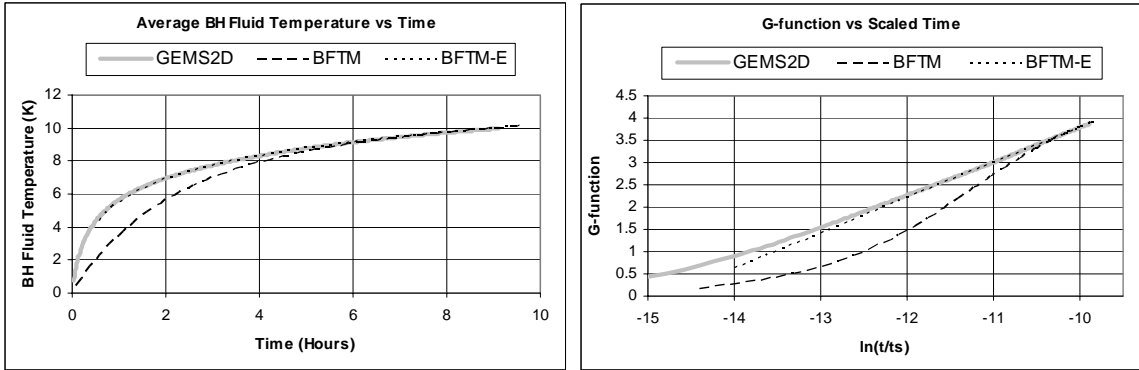
Figure 3-4 BFTM-E, BFTM, and GEMS2D Fluid Temperature and G-function

The GEMS2D g-function has a very linear profile between -13 and -10. The BFTM g-function is not linear and has a rapidly changing slope between -14 and -10.5. The linearity of the GEMS2D g-function is why logaritmic extrapolation is relatively accurate for predicting the fluid temperature even down to 1 hour or less.

The GAF value and the time, below which extrapolation should be done are very important for achieving good accuracy for the extrapolated part. The extrapolation time was chosen to be a function of borehole diameter. The GAF value is a function of borehole diameter, shank spacing, and fluid factor. The GAF values and extrapolation times for the diameters will be given in chapter 4.

4 NUMERICAL VALIDATION OF THE BOREHOLE FLUID THERMAL MASS MODEL USING GEMS2D

This section provides the numerical validation and calibration of the BFTM model using GEMS2D. Over 60 different simulations were conducted in both GEMS2D and with the BFTM model. The numerical validations were conducted by simulating the fluid thermal mass and the borehole geometry in the GEMS2D simulator. The parameters that were varied to determine the accuracy of the model are the borehole diameter, shank spacing, grout conductivity, soil conductivity, grout volumetric heat capacity and fluid factor. GEMS2D simulations were created to validate the accuracy of the fluid factor within the BFTM model and to determine a suitable grout allocation factor (GAF).

The base case borehole properties for the simulations in this chapter are shown in Table 4-1.

Table 4-1 Borehole Properties for GEMS2D to BFTM Model Comparisons.

BH Radius	=	11.4 cm	4.5 in
Soil Conductivity	=	$2.5\ \dfrac{W}{mk}$	$1.44\ \dfrac{Btu}{h\cdot ft\cdot°F}$
Grout Conductivity	=	$0.75\ \dfrac{W}{mk}$	$0.43\ \dfrac{Btu}{h\cdot ft\cdot°F}$
Pipe Conductivity	=	$0.3895\ \dfrac{W}{mk}$	$0.225\ \dfrac{Btu}{h\cdot ft\cdot°F}$
Soil Volumetric Heat Capacity	=	$2.5\ \dfrac{MJ}{km^3}$	$37.3\ \dfrac{Btu}{ft^3\cdot°F}$
Grout Volumetric Heat Capacity	=	$3.9\ \dfrac{MJ}{km^3}$	$58.2\ \dfrac{Btu}{ft^3\cdot°F}$
Fluid Volumetric Heat Capacity	=	$4.185\ \dfrac{MJ}{km^3}$	$62.4\ \dfrac{Btu}{ft^3\cdot°F}$
Fluid Convection Coefficient	=	$1690\ \dfrac{W}{m^2k}$	$298\ \dfrac{Btu}{h\cdot ft^2\cdot°F}$
U-tube Inside Diameter	=	0.02744 m	1.08 in
U-tube Outside Diameter	=	0.03341 m	1.315 in
Shank Spacing	=	0.01583 m	0.623 in
Constant heat flux	=	$40.4\ \dfrac{W}{m}$	$42.0\ \dfrac{Btu}{ft\cdot hr}$

The standard heat flux that was chosen for the simulation is 40.4 W/m (42.0 Btu/(ft*hr)).

Several different borehole geometries were chosen from a 7.6 cm (3 in) diameter borehole to a 19.1 cm (7.5 in) borehole diameter along with different shank spacings. Figure 4-1 shows drawings of the different geometries. The boreholes with a checkmark in the upper right hand corner were simulated with 1x, 2x, and 4x fluid factors
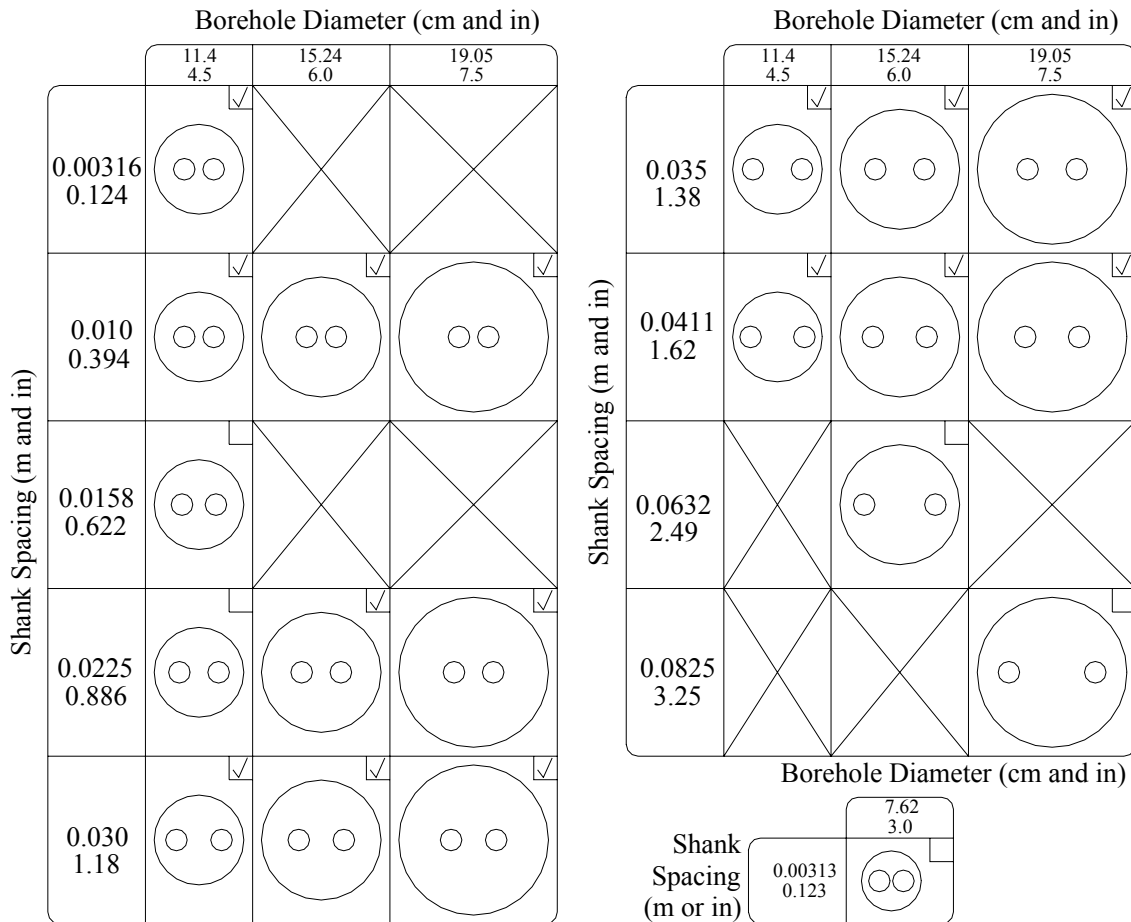
Figure 4-1 Borehole Geometries Simulated with GEMS2D

Section 4.1 describes the GEMS2D simulation in detail. Section 4.2 explains the analysis used to select a grout allocation factor for the BFTM model, a matrix of grout allocation factors used to improve the accuracy of the BFTM model, and a logarithmic extrapolation start time. Sections 4.3 through 4.8 shows a comparison between the BFTM model fluid temperatures and the GEMS2D fluid temperatures for the first ten hours of heat injection.

92

4.1   GEMS2D Simulations

This section describes the GEMS2D simulations that were used to analyze the

accuracy of the BFTM model. The grid that was used is composed of five blocks, as

shown in Figure 4.2.

Block 5

Block 3

Block 1 - fluid and pipe right U-tube
Block 2 - fluid and pipe left U-tube
Block 3 - grout
Block 4 - grout
Block 5 - soil

Block 2   Block 4   Block 1
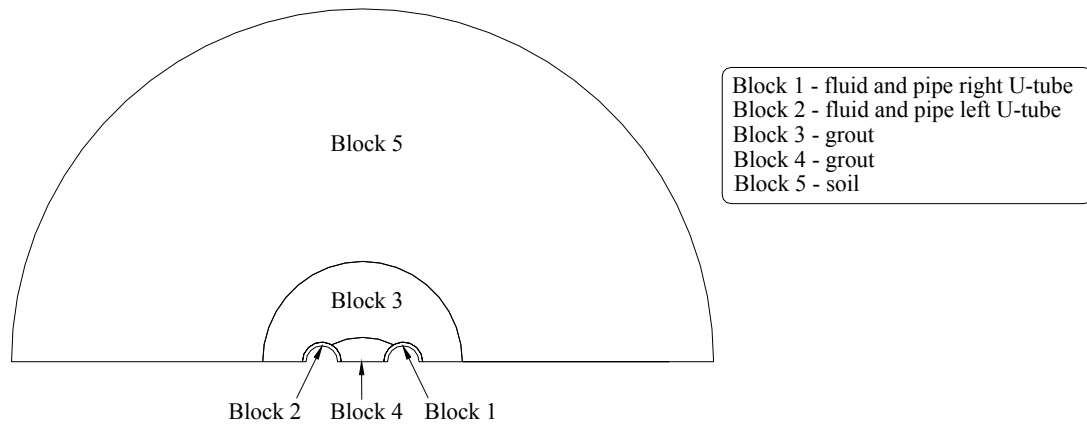
Figure 4-2 Blocks for a Borehole System without Interior Cells for GEMS2D

Blocks 1 through 4 represent the borehole and block 5 represents the soil. Figure

4-2 shows part of the soil. Block 5 extends 2 meters (6.56 ft) from the center of the

borehole. The grid in the blocks can be seen in Figure 4-3. As discussed in the literature

review, GEMS2D is capable of solving complicated two dimensional grids. Figure 4-3

has a symmetry line between the two U-tubes. If the heat fluxes are equal out of both U-

tubes the grid shown in Figure 4-3 can be cut in half, decreasing the simulation time. The

grid shown in Figure 4-3 has the advantage of being able to accept unequal heat fluxes

out of each leg of the U-tube. This condition would occur if the fluid in the two legs of

the U-tube were at different temperatures. Even though this type of simulation was not

conducted, grids like the one in Figure 4-3 were used allowing for that possibility in the

future. Simulations for this chapter ranged between 5 hours to 20+ hours on a 1.8

gigahertz computer for 15 hours of simulation time with temperatures output every 60 seconds.
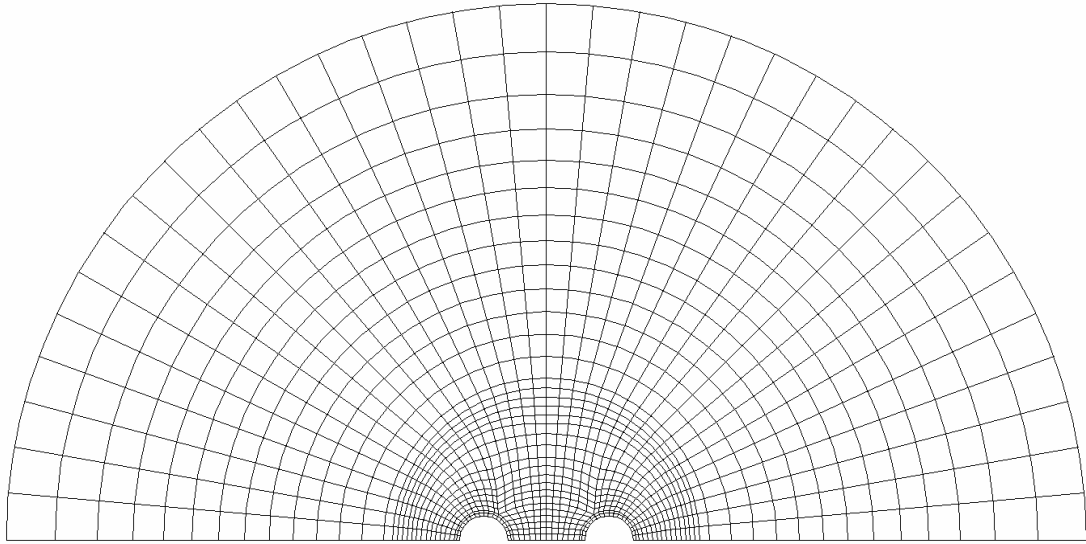
Figure 4-3 GEMS2D Grid of a Borehole with Soil

Blocks 1 and 2, as shown in Figure 4-2, each represent both the fluid and the pipe for the respective legs of the U-tube. Figure 4-4 shows a breakdown of how properties are allocated to the cells of blocks 1 and 2. To represent the fluid, the first three annular regions in block 1 and 2 are given a very large conductivity of 1×10^4 W/mk (0.576×10^4 BTU/h·ft·F) and mass equal to that of the circulating fluid (water, 1000 kg/m^3 or 8.33 lb/gallon). The large conductivity simulates well-mixed flow by creating a constant temperature throughout the first three annuluses of blocks 1 and 2. However, setting the conductivity high causes the GEMS2D program to converge very slowly. The fourth annular region is used to represent the convective resistance and has a conductivity of 1.296 W/mk (0.747 BTU/h·ft·F) and zero volumetric heat capacity. The conductivity is calculated by setting the resistance in the fourth annular region equal to the convective resistance for one leg of the U-tube. Use of this conductivity in the fourth annular region

94

is equivalent to a convective resistance of 0.00686 mK/W (0.0119 h·ft·°F/Btu). The U-tube pipe is represented by the fifth through the eighth annular regions.
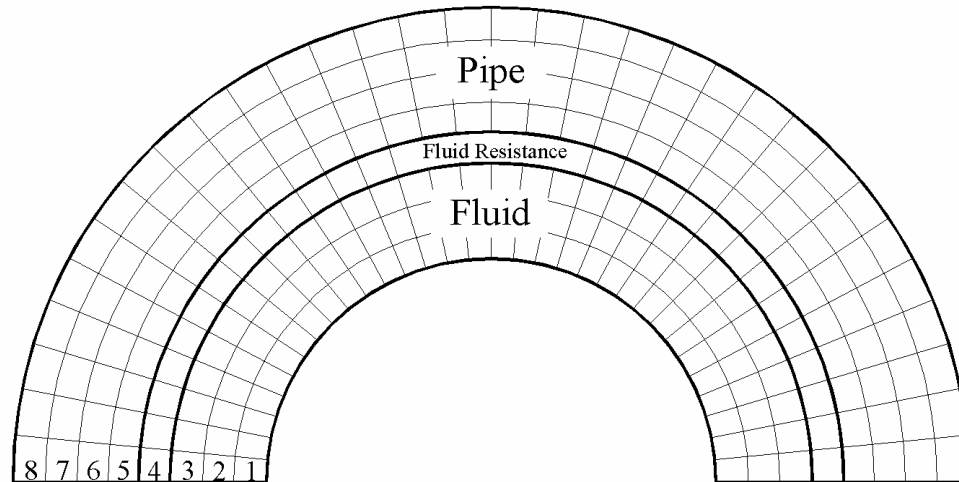
Figure 4-4 GEMS2D Grid of U-tube and Fluid with 8 Annular Regions

On the inner edge of the first annulus there is a constant flux boundary condition set to 20.2 W/m (21.0 Btu/ft*hr) for each leg of the U-tube.

4.2 Finding the Grout Allocation Factor

As mentioned in Chapter 3, the grout allocation factor (GAF) is used to increase the accuracy of the BFTM model. As will be shown in sections 4.3 to 4.8 the GAF is a function of borehole diameter, shank spacing, and fluid factor. The optimal GAF value ranges between 0.29 and 0.185. Figure 4-5 was created using the borehole configuration described in Table 4-1 and shows the effect of GAF on the fluid temperature profile.
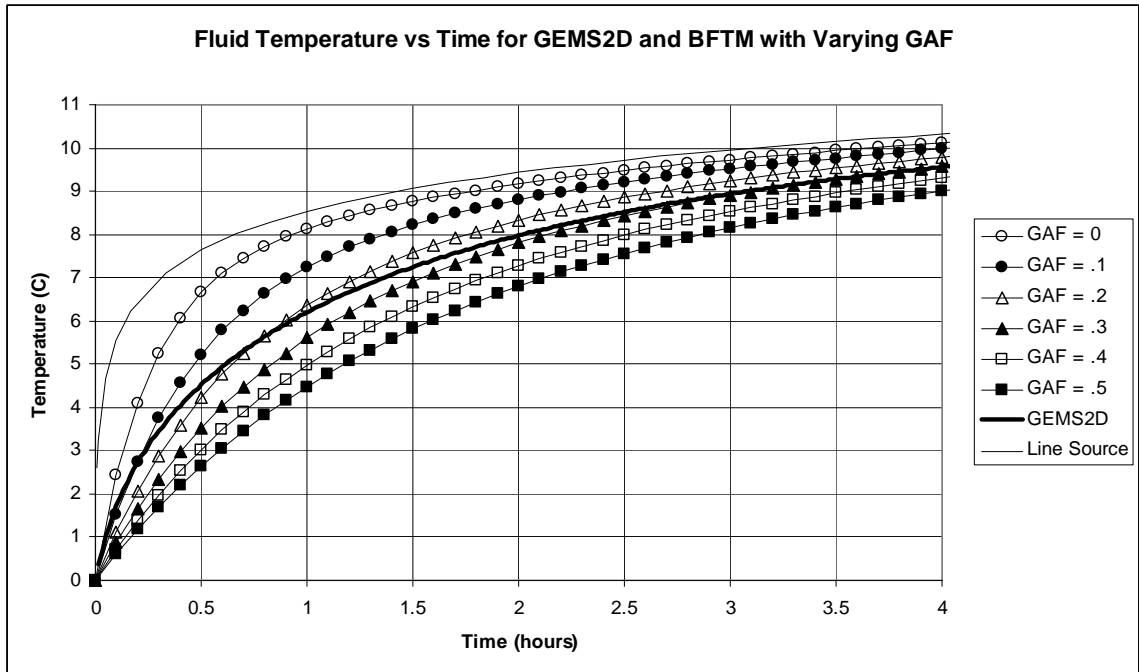
Figure 4-5 Fluid Temperature vs Time of GEMS2D and BFTM with Varying GAF

A specific GAF was found by matching the slope of the GEMS2D g-function with the

slope of the BFTM g-function at a specific time. The time was chosen based on borehole

diameter as discussed below. Figure 4-6 shows the g-function slope for the BFTM model

for a 15.24 cm (6 in.) diameter case with 3.16 cm (1.123 in.) shank spacing. In Figure 4-

6 a horizontal line is plotted for the GEMS2D g-function slope at 5 hours. The GAF that

causes the GEMS2D g-function slope to equal the BFTM g-function slope is the value

chosen to use with exponential extrapolation. For this case the GAF = 0.27.
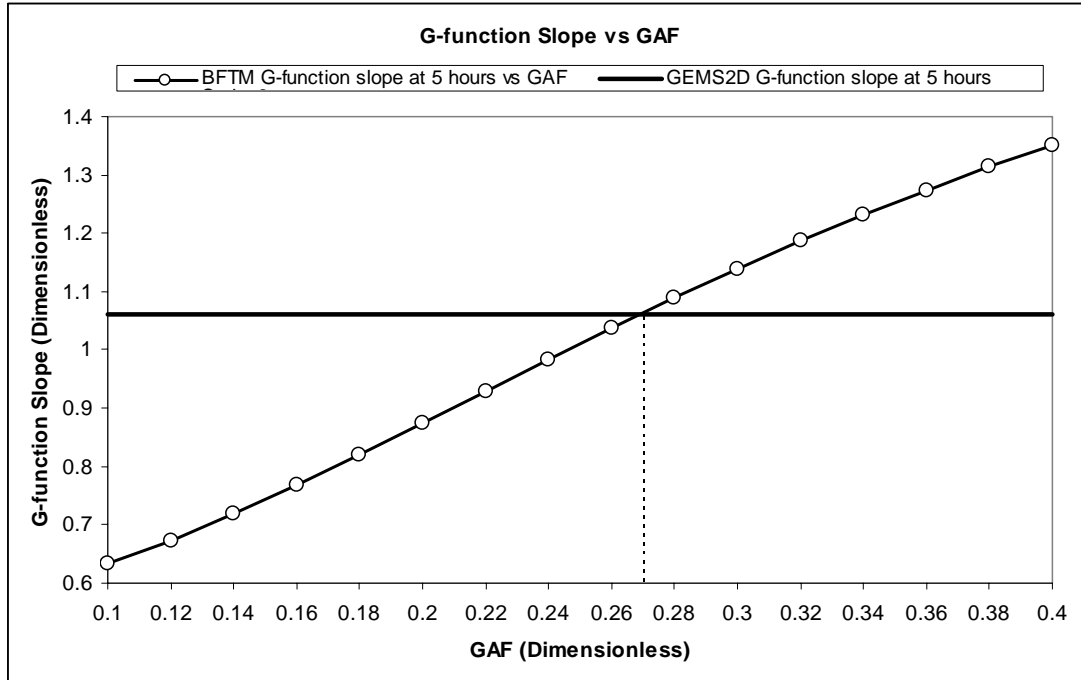
Figure 4-6 G-function Slope vs GAF for the BFTM at 5 Hours

As will be shown in Section 4.3, the time for which slopes are matched is dependent on borehole diameter. A constant time was not feasible since the BFTM model increasingly underestimates the fluid temperature as borehole diameter increases. Table 4-2 shows the times that were chosen.

To show why it is necessary to have the time for extrapolation based on diameter a 15.24 cm (6 in) diameter and 0.0316 m (1.244 in) shank spacing is used as an example. When the slopes between the GEMS2D and the BFTM models g-functions are set to equal each other at 3 hours GAF is equal to 0.158. Figure 4-7a and 4-7b shows that with a slope matching time of 3 hours the error is much larger, for the BFTM curve and the exponential curve than in Figure 4-7c and 4.7d. Figure 4-7c and 4.7d shows the temperature profile and g-function for the recommended slope matching time of 5 hours.

(a)   **(b)**

(c)   **(d)**
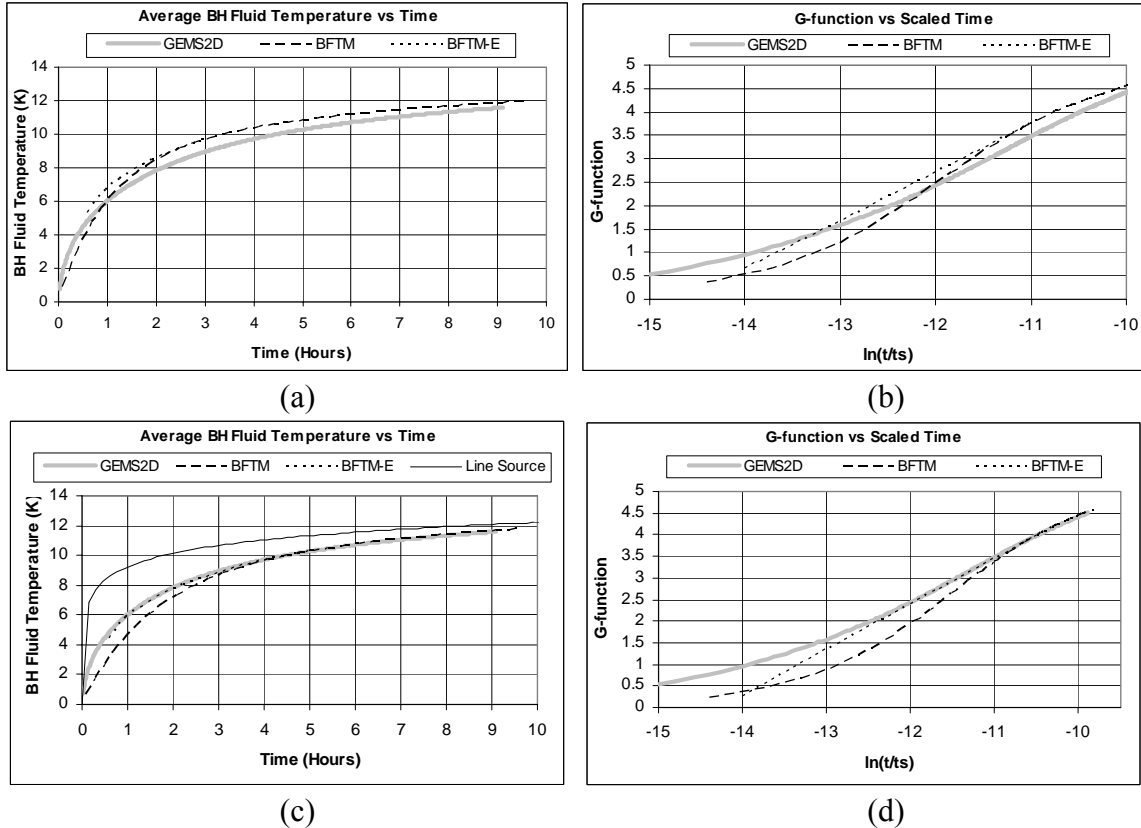
Figure 4-7 Fluid Temperature and G-function for 15.24 cm (6 in) Diameter Borehole Using a Slope Matching Time of 3 Hours for (a) and (b) and 5 hours for (c) and (d)

Table 4-2 Borehole Diameter vs Time for Slope Matching.

BH Diameter	Time (hours)
7.62 cm (3 in)	2
11.4 cm (4.5 in)	3
15.24 cm (6 in)	5
19.05 cm (7.5 in)	8

Using the times shown in Table 4-2, the GAF values for various combinations of borehole diameter, shank spacing and fluid factor were found that cause the same slopes between GEMS2D and the BFTM models. These GAF values are shown in Table 4-3.

98

Table 4-3 GAF Dependent on Borehole Diameter, Shank Spacing and Fluid Factor

BH Diameter = 4.5 in (11.4)			
Shank Spacing (m)	1xfluid	2xfluid	4xfluid
0.00316	0.260	0.240	0.220
0.01	0.285	0.250	0.230
0.0225	0.285	None	None
0.03	0.285	0.250	0.230
0.035	0.290	None	None
0.0411	0.290	0.250	0.230

BH Diameter = 6 in (11.4 cm)			
Shank Spacing (m)	1xfluid	2xfluid	4xfluid
0.01	0.245	0.225	0.200
0.0225	0.270	0.240	0.215
0.03	0.270	0.248	0.230
0.035	0.270	None	None
0.0411	0.270	0.255	0.230
0.0625	0.270	None	None

BH Diameter = 7.5 in (19.1 cm)			
Shank Spacing (m)	1xfluid	2xfluid	4xfluid
0.01	0.220	0.205	0.185
0.0225	0.235	0.225	0.200
0.03	0.245	0.230	0.205
0.035	0.250	None	None
0.0411	0.255	0.239	0.210
0.0825	0.255	None	None

Interpolation within Table 4-3 can yield GAF values for other borehole configurations. As seen in Table 4-3 and described in section 3.2, GAF increases slightly for increasing shank spacing, decreases slightly as fluid factor increases, and decreases as borehole diameter increases.

The borehole diameter influences the GAF value because GAF is defined as a fraction of the grout in the borehole. Since the amount of grout in the borehole changes as a function of the borehole radius squared then the amount of grout allocated to the borehole using GAF also changes by the borehole radius squared. If GAF was a constant for all borehole diameters then more grout would be allocated than what is needed for the given shank spacing for larger boreholes. Thus GAF decreases for larger borehole diameters.

It will be shown in section 4-8 that the BFTM model under predicts the fluid temperature when the GAF is used. As the fluid mass inside the U-tube increases due to

increasing fluid factor the BFTM model underestimates the fluid temperature to a lesser extent. Thus as fluid factor increases, GAF decreases slightly.

The curves in the plots in sections 4.3 through 4.8 have GEMS2D, BFTM and Exponential curves. The GEMS2D curve shows data that comes from the GEMS2D finite volume model program. The BFTM curve shows data that comes from the BFTM model which uses GAF but does not use logarithmic extrapolation. The BFTM-E curve shows data that comes from logarithmic extrapolation between 0.5 hours and the times shown in Table 4-2.

4.3   Borehole Diameter Validation with Line Source Comparison

Figures 4-8 through 4-11 show a comparison between the line source, the BFTM model and the GEMS2D model for different borehole diameters ranging from 7.62 to 19.1 cm (3 to 7.5 inches) with the "B" spacing. The 7.62 cm (3 inch) borehole case is a less common borehole configuration and was created for the purpose of testing the limits of the BFTM model. Each figure contains two plots, one of the temperature rise and another of the g-function resulting from the temperature rise. The g-function plots include borehole resistance and were created using Equation 1-28.

As can be seen in Figure 4-8 through 4-11 the BFTM temperature curves more closely match the curves produced by GEMS2D than those produced by the line source model. The largest fluid temperature difference between the BFTM and the GEMS2D model occurs in Figure 4-11 with the 19.1 cm (7.5 inch) diameter borehole. BFTM model underestimates the temperature of the fluid by approximately 1 °C (1.8 °F) for the 19.1 cm (7.5 in) diameter case at two hours whereas the line source overestimates the

100

temperature by 2.5 °C (4.5 °F). For the smaller diameter boreholes the BFTM model and the line source model are much more accurate.

The BFTM models give increasing underestimation of the fluid temperature as borehole diameter increases. This poses a problem in a design program by significantly underestimating the necessary depth of the borehole system whereas the line source increasingly overestimates the fluid temperature. As discussed in section 3.5, logarithmic extrapolation can be used to greatly improve accuracy for times less than those shown in Table 4-2. The linearly extrapolated value, represented by the BFTM-E curve, is very close only underestimating the fluid temperature by 0.1 °C (0.18 °F) at 2 hours. For all other cases at two hours the BFTM model and the GEMS2D simulation differ less than 0.5 °C (0.9 °F).

Table 4-4 shows the borehole configurations for this section and the borehole resistance that was used with the BFTM model.

Table 4-4 Borehole Resistances and GAF for Diameter Validation Tests

Borehole Diameter	Shank Spacing	Borehole Resistance	Extrapolation Time (hours)	GAF
7.62 cm (3 in)	0.3127 cm (0.1231 in)	0.1213 mK/W $(0.2099\,°F \cdot ft \cdot h/Btu)$	2	0.274
11.4 cm (4.5 in)	1.583 cm (0.6232 in)	0.1822 mK/W $(0.3153\,°F \cdot ft \cdot h/Btu)$	3	0.285
15.24 cm (6 in)	3.16 cm (1.123 in)	0.2215 mK/W $(0.3834\,°F \cdot ft \cdot h/Btu)$	5	0.270
19.05 cm (7.5 in)	4.123 cm (1.623 in)	0.2504 mK/W $(0.4334\,°F \cdot ft \cdot h/Btu)$	8	0.255
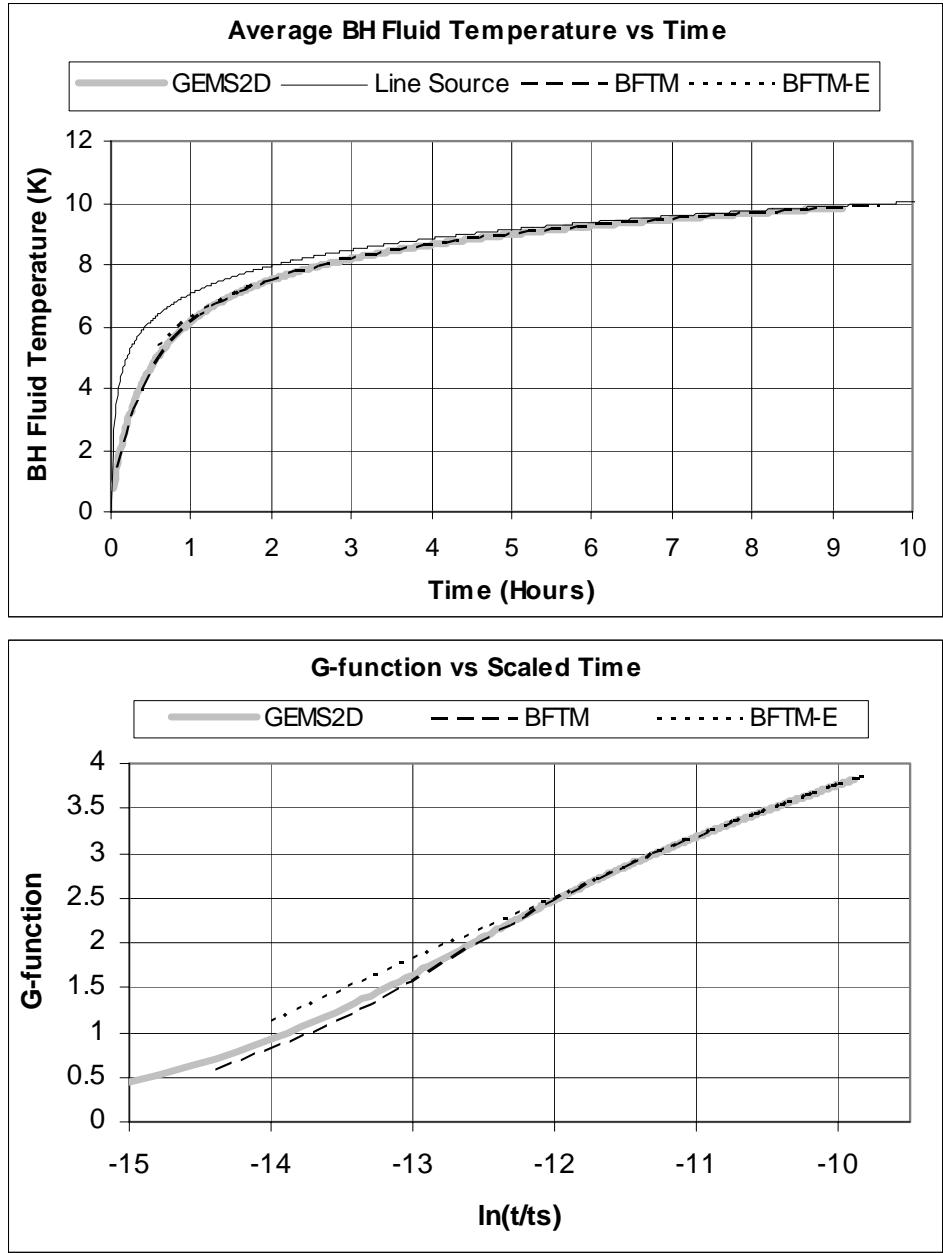
Figure 4-8 Validation of the BFTM Model Using a GEMS2D Simulation with a 7.62 cm (3 in) Borehole
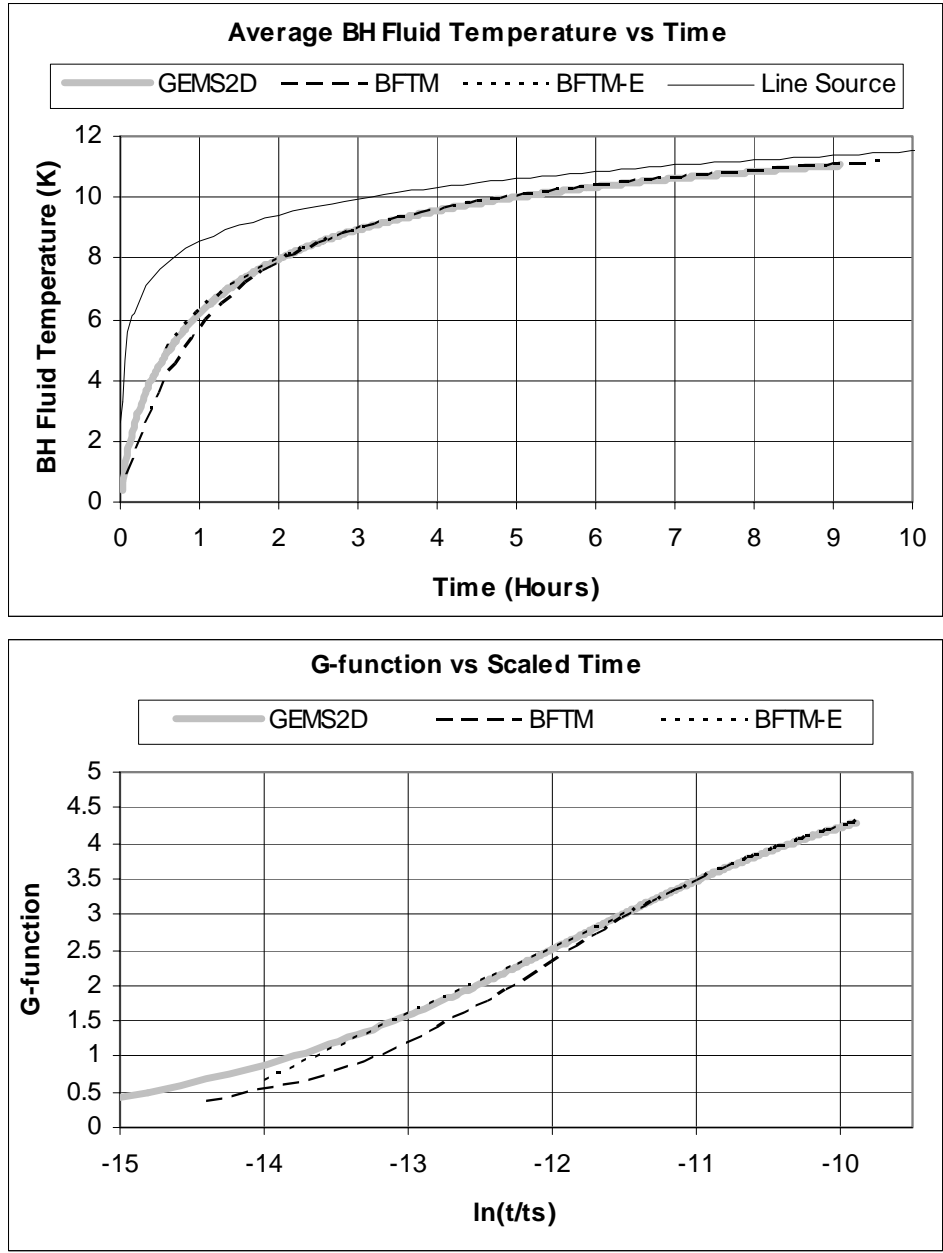
Figure 4-9 Validation of the BFTM Model Using a GEMS2D Simulation with a 11.4 cm (4.5 in) Borehole
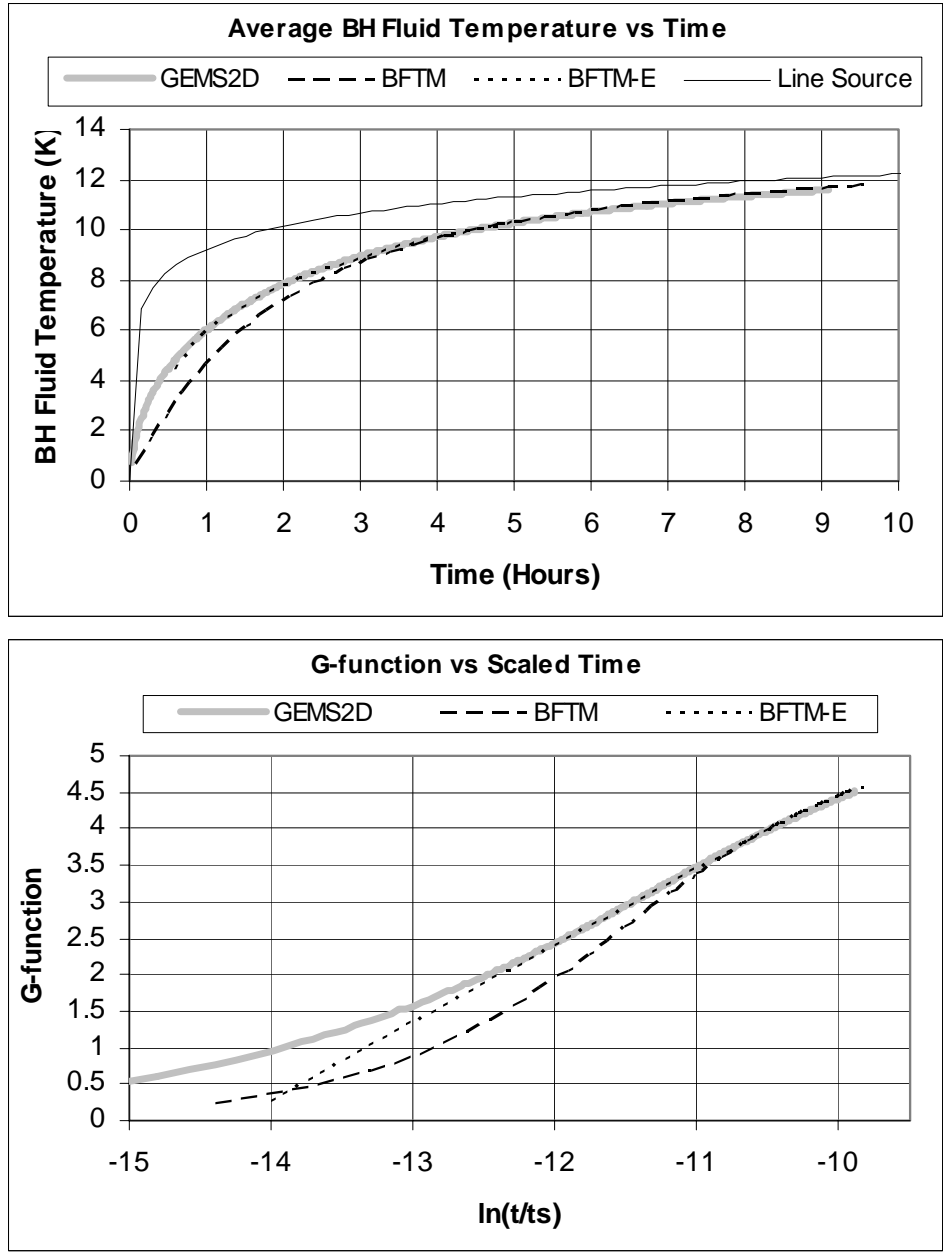
Figure 4-10 Validation of the BFTM Model Using a GEMS2D Simulation with 15.2 cm (6 in) Borehole with 3.16 cm (1.24 in) Shank Spacing
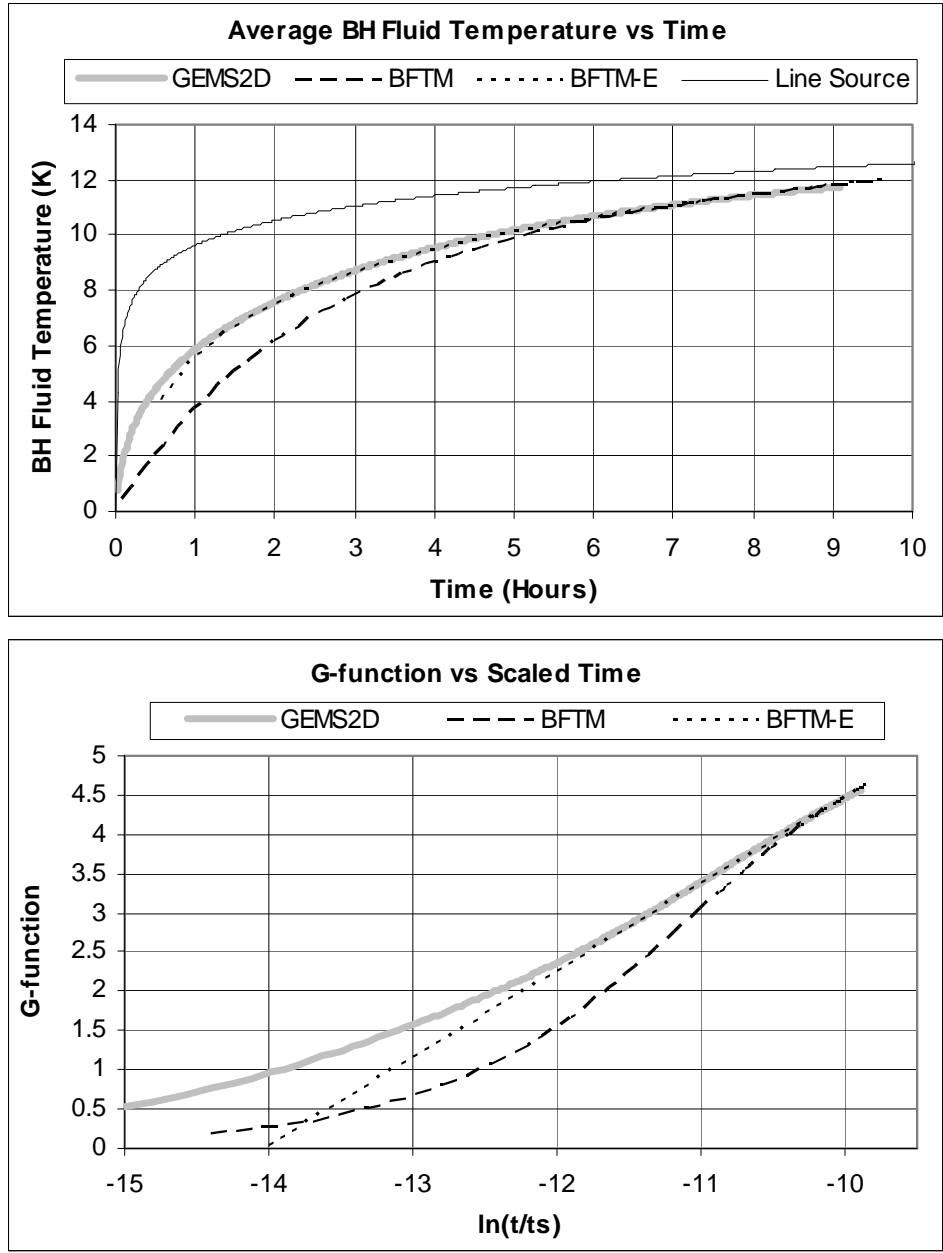
Figure 4-11 Validation of the BFTM Model Using a GEMS2D Simulation with a 19.1 cm (7.5 in) Borehole with a 4.12 cm (1.62 in) Shank Spacing

4.4   Shank Spacing Validation

Section 4.4 shows three different shank spacings for the 11.4cm (4.5 in) diameter

borehole. Figures 4-12 through 4-14 show how the BFTM model performs with different

shank spacing. As can be seen, the method performs very well for all cases. After 2

hours, in all four cases, the temperature profile closely matches the actual temperature. At two hours the largest temperature difference between the BFTM model and GEMS2D was less than 0.25 °C (0.45 °F). In all cases, the BFTM model slightly underestimates the fluid temperature. With exponential extrapolation the error is reduced to well below 0.1 °C (0.18 °F). The exponential curve in the figures ranges from 0.5 to 3 hours since it should only be used for times less than 3 hours for an 11.4 cm (4.5 in) diameter borehole.

Table 4-5 shows the borehole resistance and GAF used in the BFTM model for the three shank spacings.

Table 4-5 Borehole Resistances for Shank Spacing Validation Tests

Shank Spacing	Borehole Resistance	GAF
0.313 cm (0.123 in)	0.2112 mK/W ($0.3655\,°F \cdot ft \cdot h / Btu$)	0.260
2.25 cm (0.89 in)	0.1681 mK/W ($0.2909\,°F \cdot ft \cdot h / Btu$)	0.285
4.12 cm (1.62 in)	0.1285 mK/W ($0.2224\,°F \cdot ft \cdot h / Btu$)	0.290
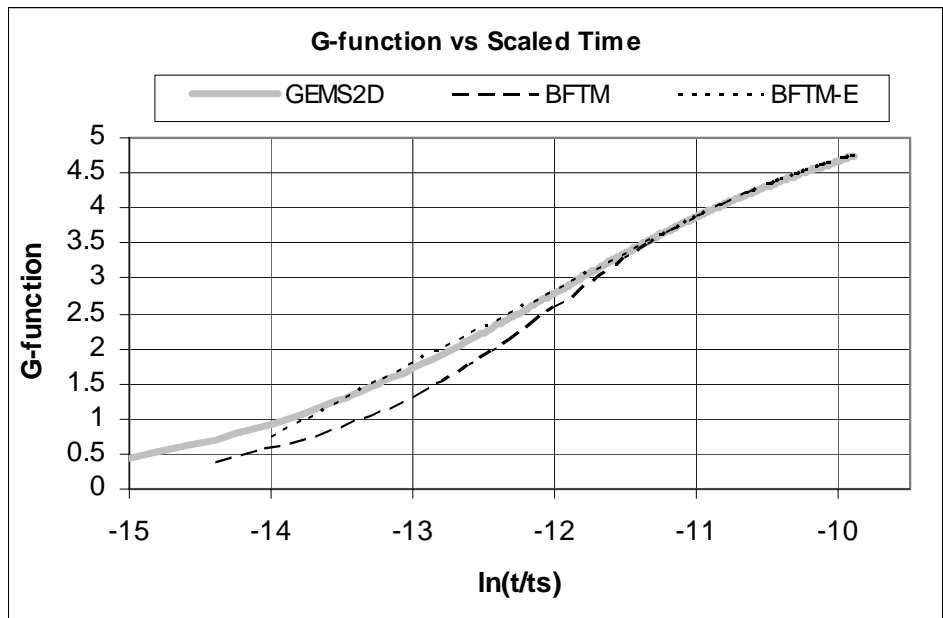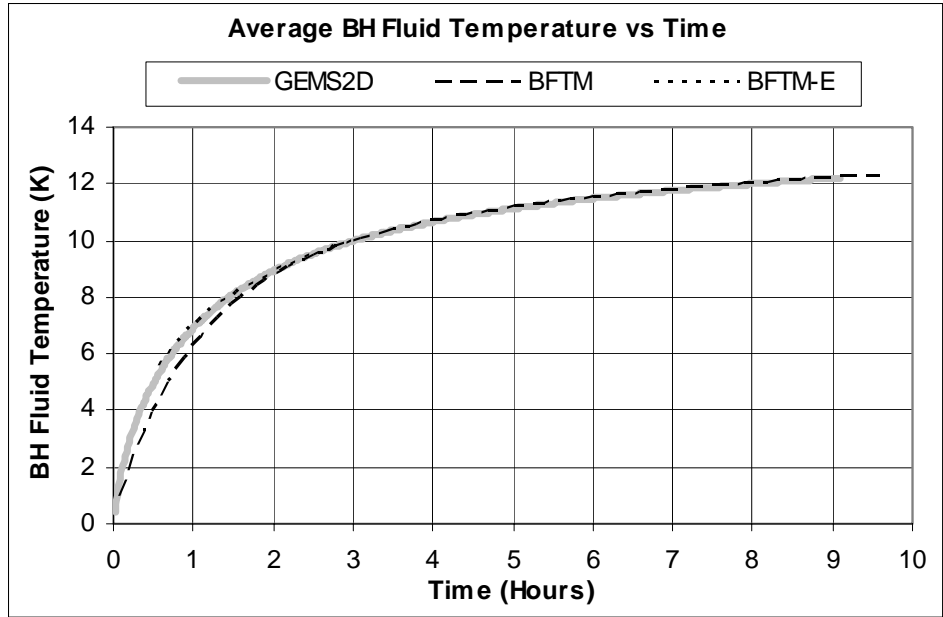
Figure 4-12 Validation of the BFTM Model Using a GEMS2D Simulation with a 0.316 cm (0.125 in) Shank Spacing
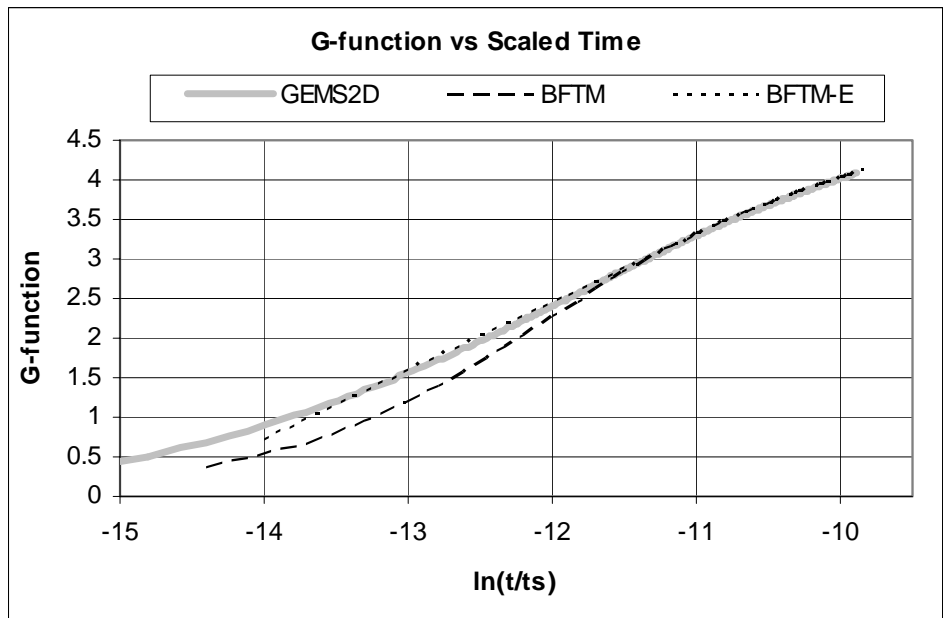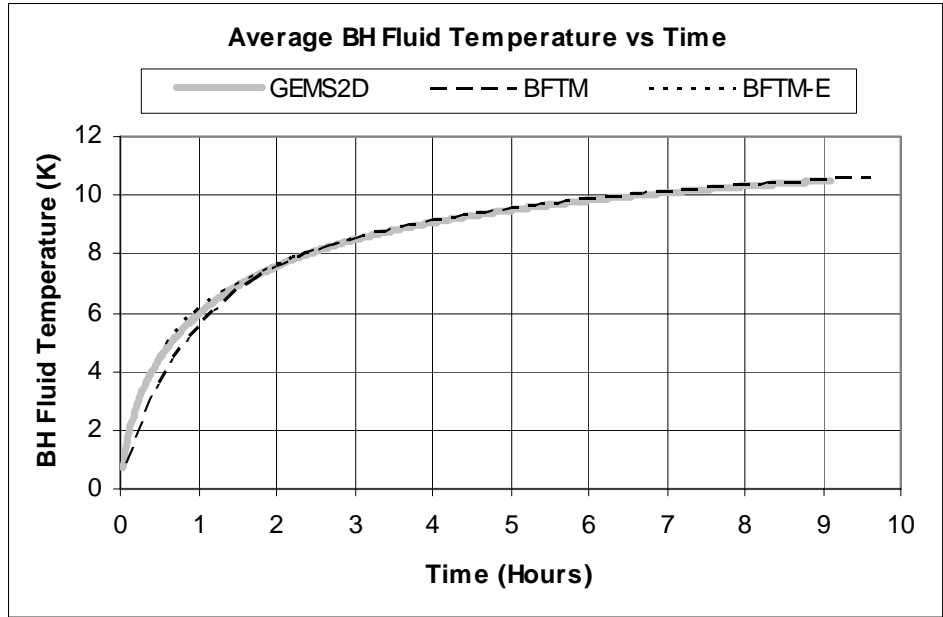
Figure 4-13 Validation of the BFTM Model Using a GEMS2D Simulation with a 2.25 cm (0.89 in) Shank Spacing

Average BH Fluid Temperature vs Time

G-function vs Scaled Time
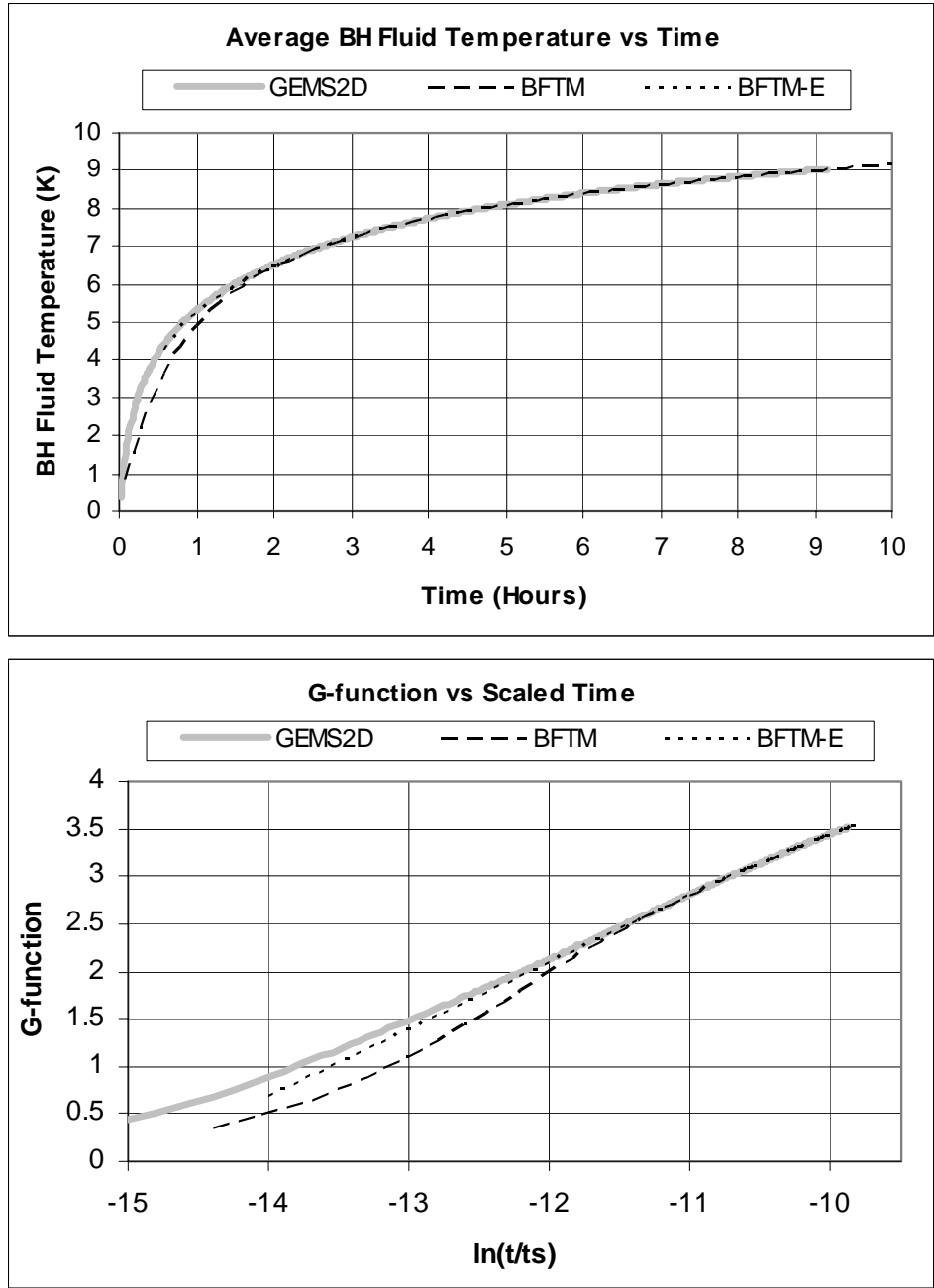
Figure 4-14 Validation of the BFTM Model Using a GEMS2D Simulation with a 1 4.13 cm (5/8 in) Shank Spacing

4.5   Grout Conductivity Validation

Figures 4-15 and 4-16 indicate the performance of the BFTM model with respect to changes in grout conductivity. The grout conductivity was changed from 0.25 to 1.5 (W/(m·K)) (0.144 to 0.867 (Btu/(h·ft·°F))) which covers the typical ranges for grout conductivity. As the grout conductivity increases, the fluid temperature decreases, however, the accuracy of the model is relatively unaffected by the change. The error is slightly worse for the 0.25 W/m·K (0.144 Btu/(h·ft·°F)) case. This case is designed to test the limits of the BFTM model, since the conductivity in this case is one third the actual conductivity of regular bentonite grout.

As shown in Figure 4-15, exponential extrapolation only slightly reduces the error for very small grout conductivities. There is a noticeable improvement, however, for larger grout conductivities, as shown in Figure 4-16.

Table 4-6 shows the borehole resistances for the different grout conductivities used in the BFTM model. The plot for the 0.75 W/mK (0.6232 $Btu/°F \cdot ft \cdot h$) grout conductivity is shown in Figure 4-9.

Table 4-6 Borehole Resistances for Shank Spacing Validation Tests

Grout Conductivity	0.25 W/mK 0.144 $Btu/°F \cdot ft \cdot h$	0.75 W/mK 0.6232 $Btu/°F \cdot ft \cdot h$	1.5 W/mK 1.123 $Btu/°F \cdot ft \cdot h$
Borehole Resistance	0.4383 mK/W 0.7586 $°F \cdot ft \cdot h / Btu$	0.1822 mK/W 0.3153 $°F \cdot ft \cdot h / Btu$	0.1155 mK/W 0.1999 $°F \cdot ft \cdot h / Btu$
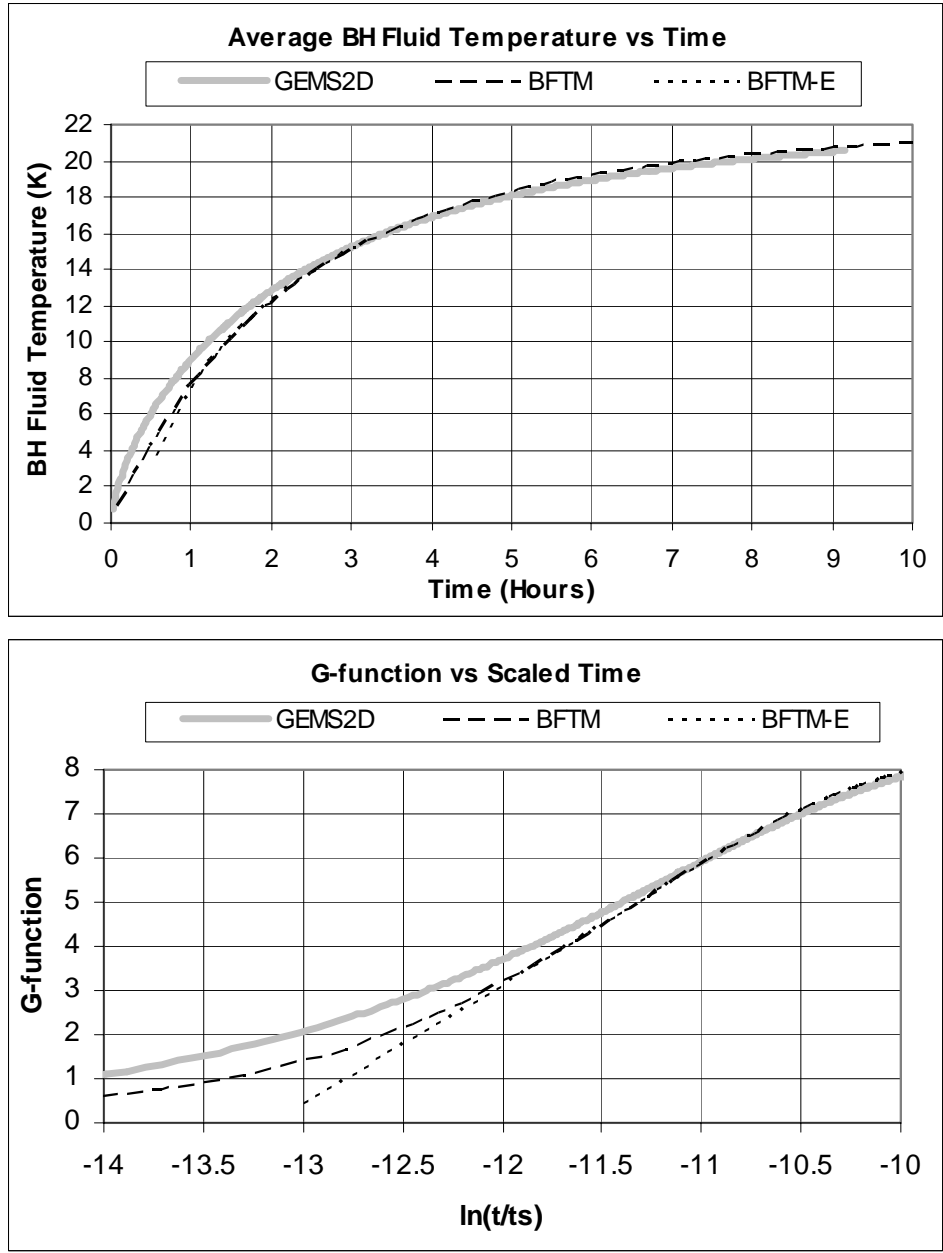
Figure 4-15 Validation of the BFTM Model Using a GEMS2D Simulation with Grout Conductivity of 0.25 W/(m·K) (0.144 Btu/(h·ft·°F))
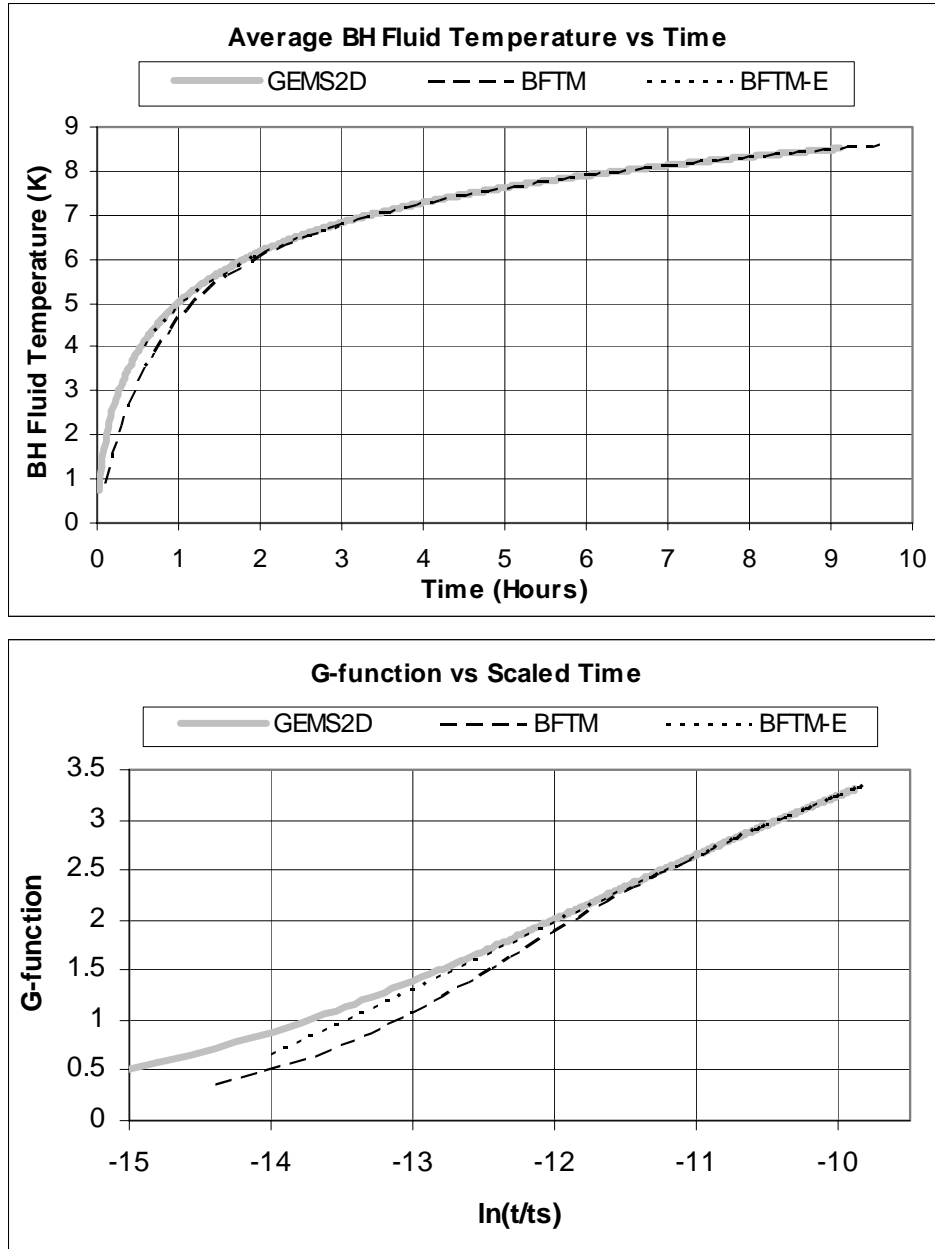
Figure 4-16 Validation of the BFTM Model Using a GEMS2D Simulation with Grout Conductivity of 1.5 W/m·K (0.867 Btu/(h·ft·°F))

4.6 Soil Conductivity Validation

Figures 4-17 through 4-19 show the effect (or lack of effect) of changing the soil

conductivity on the performance of the BFTM model. The tests were conducted between

soil conductivities of 0.5 and 8 W/m·K (0.289 to 4.62 Btu/(h·ft·°F))) to cover a wide

range of soil conductivity. This test showed that the BFTM model is insensitive to the

soil conductivity. As noted in the prior tests the BFTM model very closely estimates the fluid temperature especially after 2 hours.

As can be seen in the g-function plots in figure 4-17 through 19 the BFTM model is linear between -13 to -12 for small soil conductivities but has increasing curvature between -12 to -10 for very high soil conductivities such as 8.0 W/mK (4.62 $(Btu/^{\circ}F \cdot ft \cdot h)$). Also, it should be noted that linear extrapolation underestimates the temperature profile for small soil conductivities but overestimates it for large soil conductivities. For Figure 4-19 the soil conductivity has approximately the same error as the BFTM model at two hours. For the very low soil conductivity shown in Figure 4-17, linear extrapolation is slightly less accurate. For all other cases, linear extrapolation is an improvement

Table 4-7 shows the borehole resistance used in the BFTM model. As can be seen the soil conductivity has a very small effect on borehole resistance. The plot for the 2.5 W/mK (1.44 $Btu/^{\circ}F \cdot ft \cdot h$) soil conductivity is shown in Figure 4-9.

Table 4-7 Borehole Resistances for Soil Conductivity Validation Tests

Soil Conductivity	0.5 (.289)	1.5 (.866)	2.5 (1.44)	8 (4.62)	W/mK $(Btu/^{\circ}F \cdot ft \cdot h)$
Borehole Resistance	0.1856 (0.3212)	0.1833 (0.3172)	0.1822 (0.3153)	0.1806 (0.3126)	mK/W $(^{\circ}F \cdot ft \cdot h / Btu)$
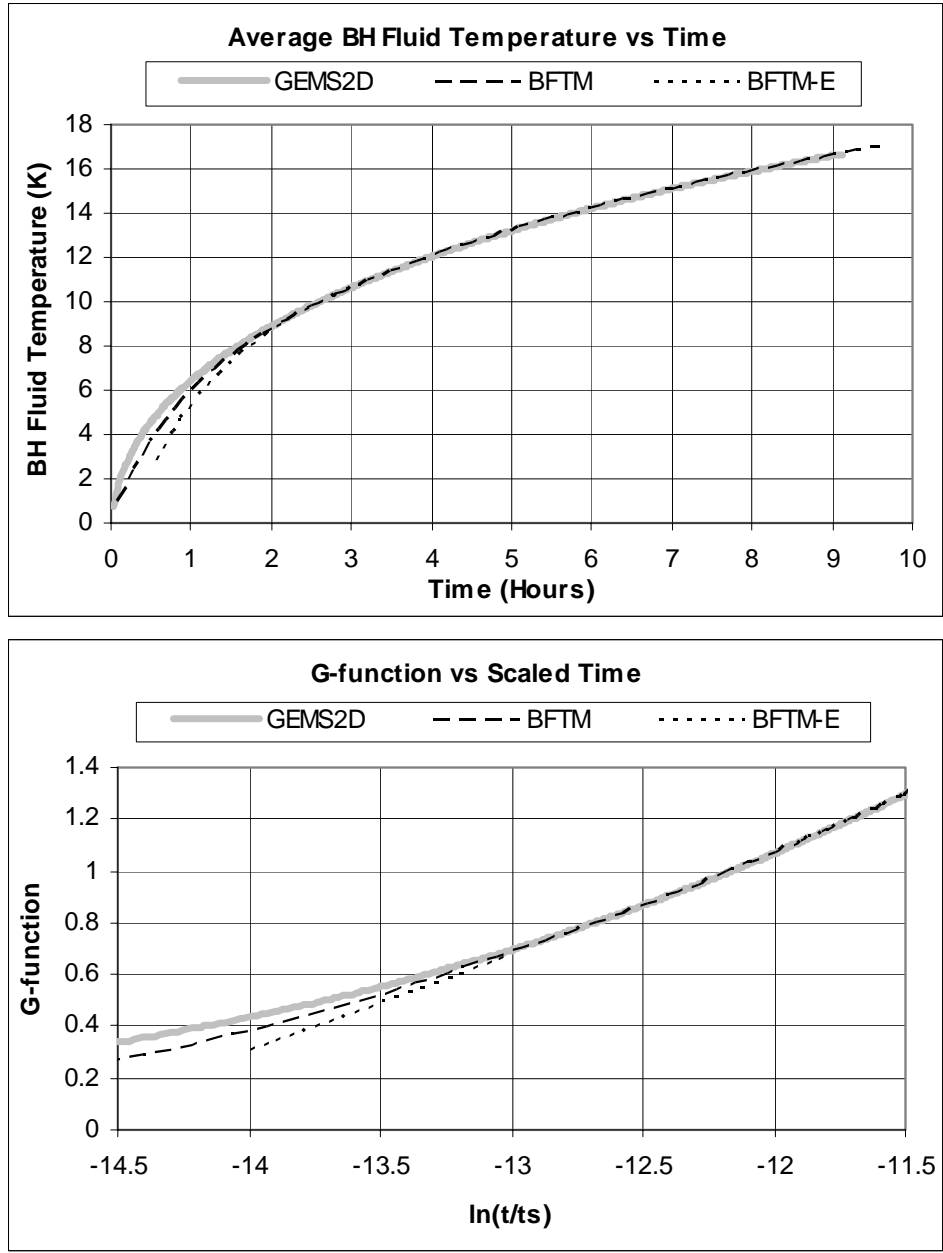
Figure 4-17 Validation of the BFTM Model Using a GEMS2D Simulation With Soil Conductivity of 0.5 W/m·K (0.289 Btu/(h·ft·°F))
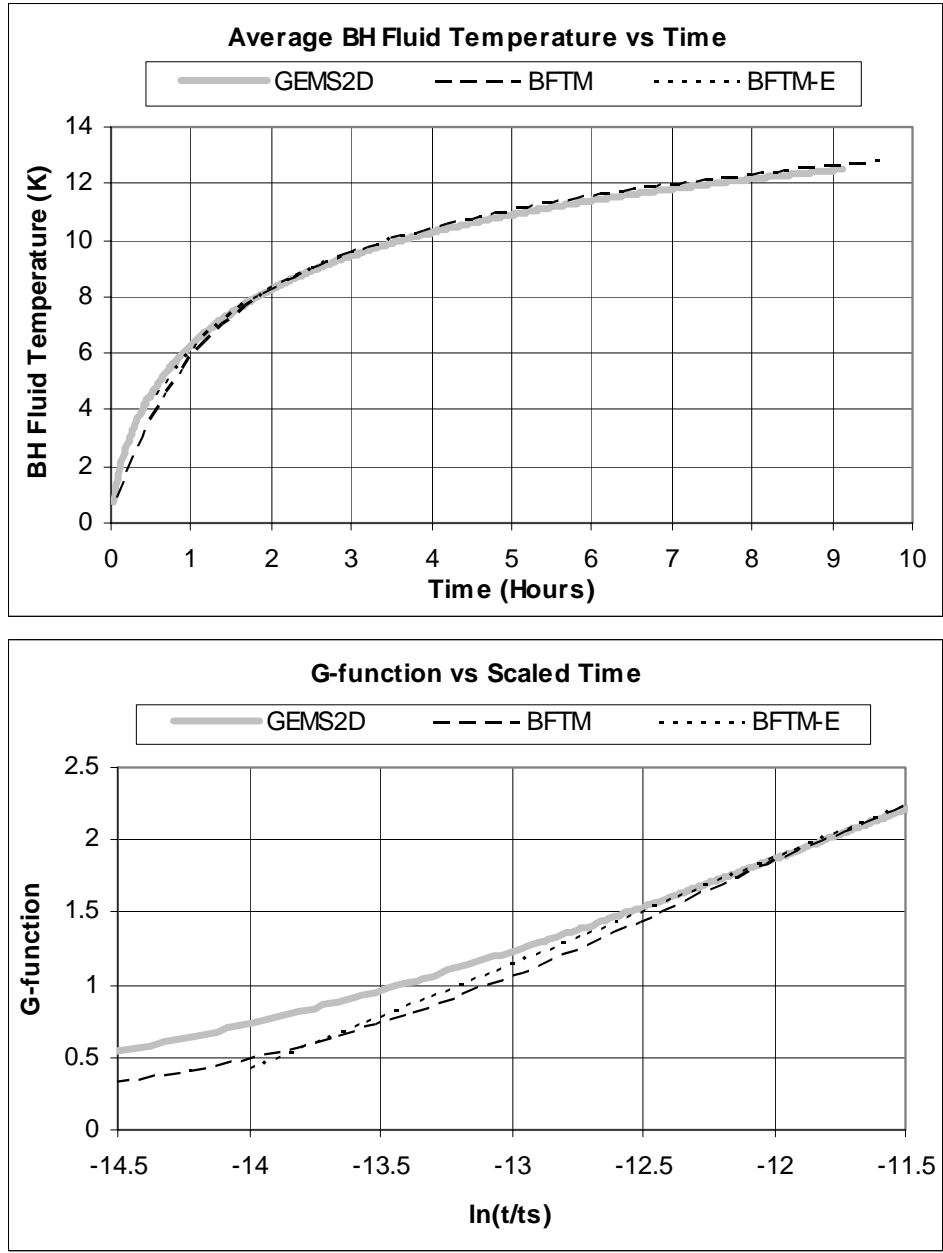
Figure 4-18 Validation of the BFTM Model Using a GEMS2D Simulation with a Soil Conductivity of 1.5 W/m·K (0.867 Btu/(h·ft·°F))
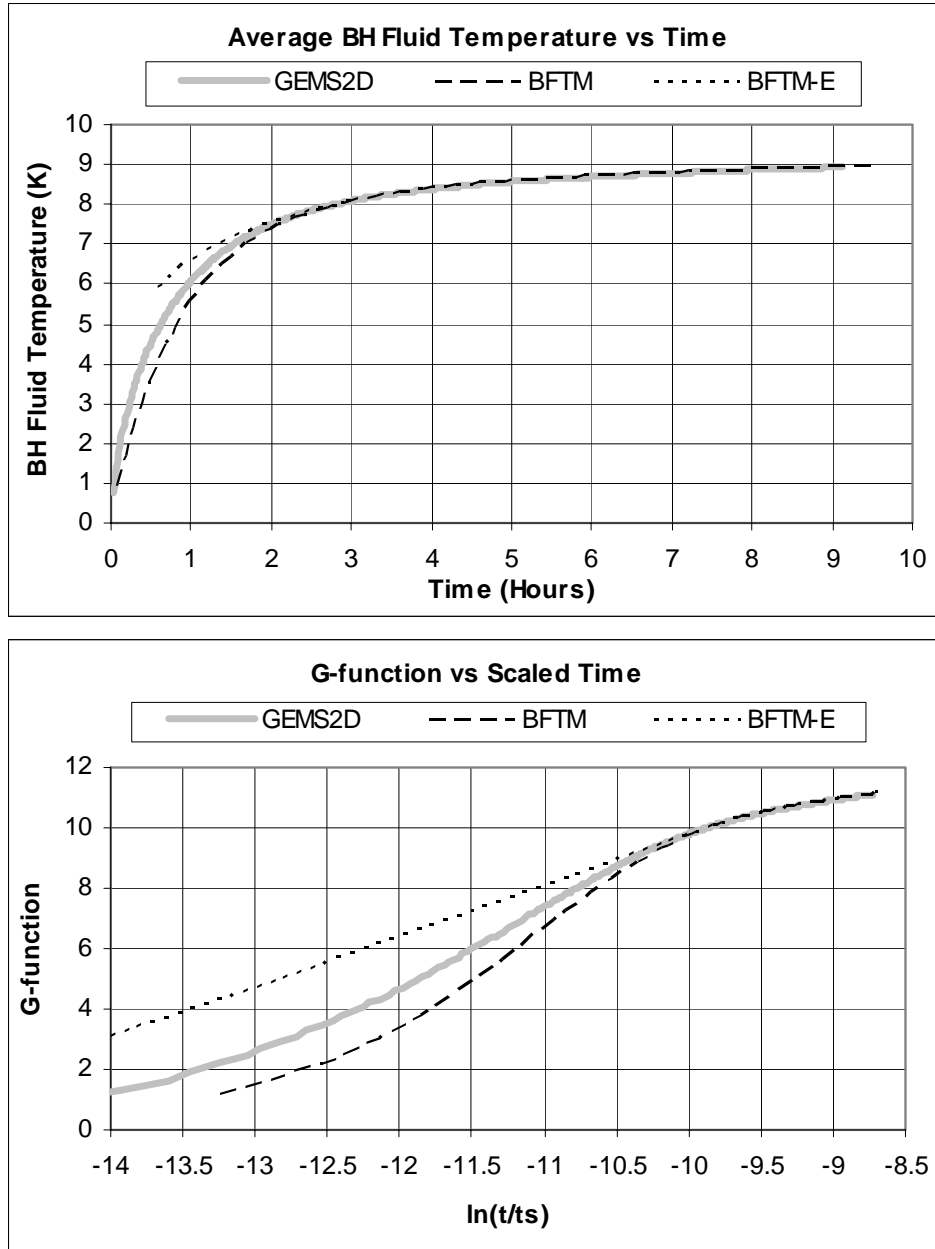
Figure 4-19 Validation of the BFTM Model Using a GEMS2D Simulation with a Soil Conductivity of 8 W/m·K (4.62 Btu/(h·ft·°F))

4.7 Grout Volumetric Heat Capacity Validation

Figures 4-20 and 21 show the grout volumetric heat capacity validation simulations. The figures show that the overall fluid temperature profile is slightly lowered as the grout volumetric heat capacity increases. The typical values for the grout

volumetric heat capacity are 3.9 $MJ / m^3 \cdot K$ (58.2 $Btu / ft^3 \cdot {}^{\circ}F$) for bentonite and 3.4

$MJ / m^3 \cdot K$ (50.7 $Btu / ft^3 \cdot {}^{\circ}F$) for thermally enhanced grout. Grout volumetric heat

capacities of 2, 3.9, and 8 $MJ / m^3 \cdot K$ (29.8, 58.2, and 119 $Btu / ft^3 \cdot {}^{\circ}F$) were simulated

to test the limits of the BFTM model.

As can be seen the grout volumetric heat capacity significantly changes the

temperature profile created by the BFTM model. For very low grout volumetric heat

capacity such as in Figure 4-20 the BFTM is very accurate after two hours, however for

very large heat capacities there is 0.5 °C (0.9 °F) difference between the two models.

Similar to the prior sections the BFTM model slightly under predicts the fluid

temperature. Since the steady state borehole resistance does not change with grout

volumetric heat capacity, 0.1822 mK/W (0.3153 (${}^{\circ}F \cdot ft \cdot h / Btu$)) was used in the BFTM

model.

Linear extrapolation is not much of an advantage with very small grout

volumetric heat capacities since the BFTM model is very accurate. There is a slight

increase in error using linear extrapolation before 2 hours as seen in Figure 4-20.

However for very large grout volumetric heat capacity as seen in Figure 4-21 linear

extrapolation has the same error. These errors are tolerable since volumetric heat

capacities specified are extreme cases.
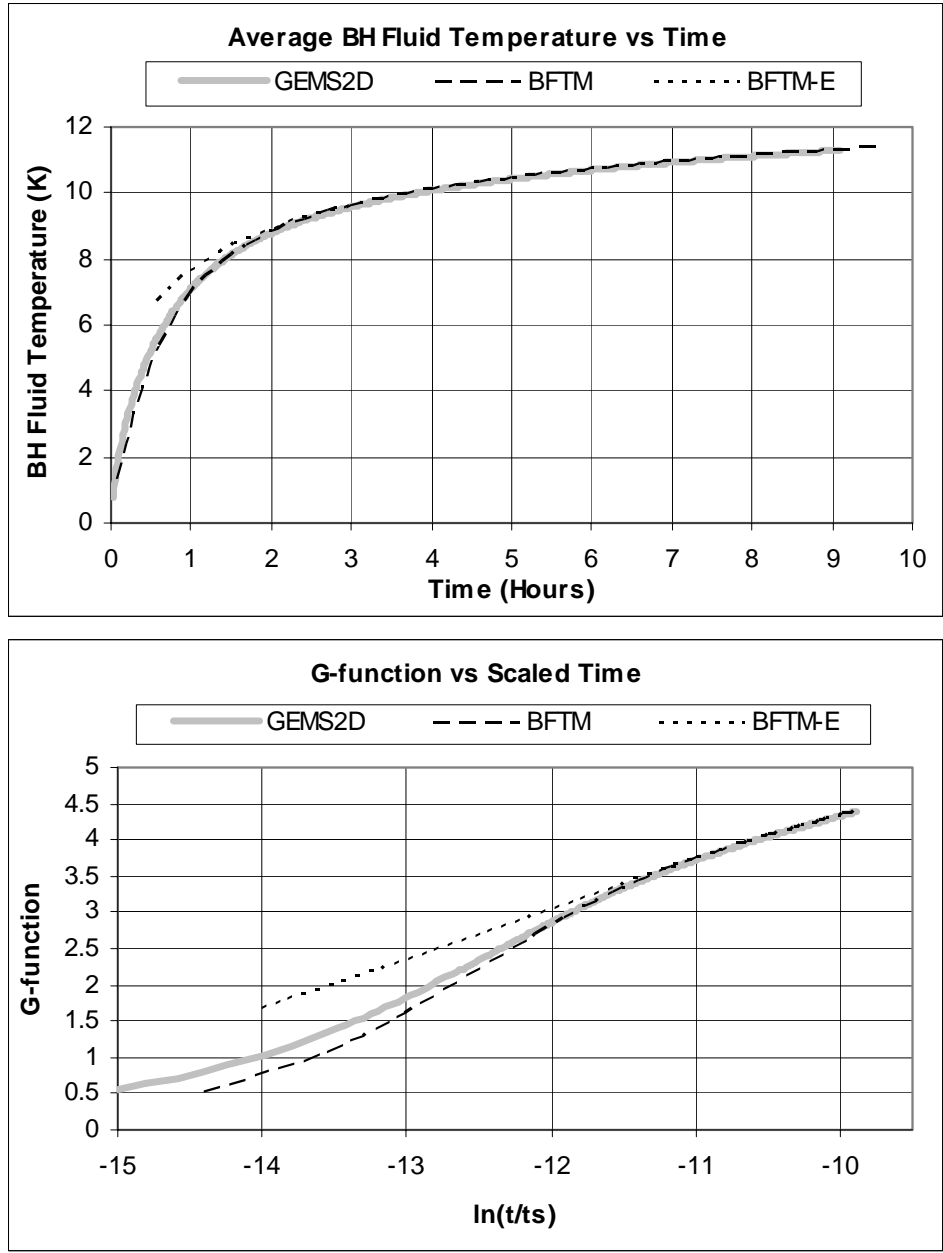
Figure 4-20 Validation of the BFTM Model Using a GEMS2D Simulation with a Grout Volumetric Heat Capacity of 2 MJ/m³·K (29.8 Btu/ft³·F)
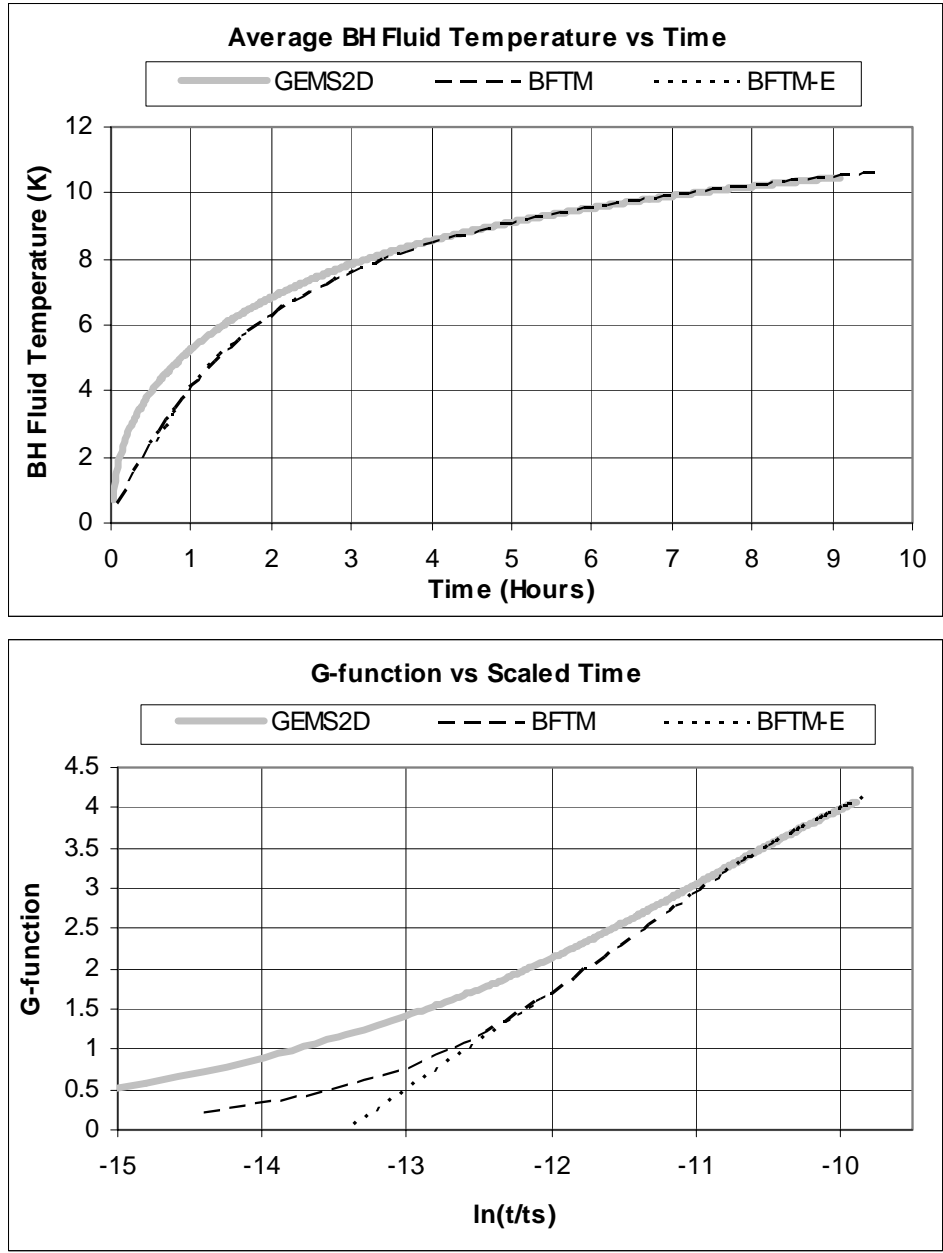
Figure 4-21 Validation of the BFTM Model Using a GEMS2D Simulation with a Grout Volumetric Heat Capacity of 8 MJ/m^3-K (119 Btu/ft^3·F)

119

4.8 BFTM Model Fluid Factor Validation with GEMS2D

Simulations were created to analyze the BFTM model's ability to accurately predict the fluid temperature of systems with different fluid factors. As discussed in Section 3.3, changing fluid factor is analogous to changing the thermal mass per unit length of the fluid. Figures 4-22 and 4-24 show two systems in which the fluid has been doubled and figures 4-23 and 4-25 show a system in which the fluid has been quadrupled.

In Figure 4-22 and 4-23 the BFTM model is very close to the GEMS2D solution thus the exponential curve fit does not improve accuracy. For the 19.1 cm (7.5 in) borehole in Figure 4-24 and 4-25 the BFTM significantly underestimates the temperature by more than 0.65 °C (1.2 °F) at two hours. For these two cases logarithmic extrapolation improves the accuracy to less than 0.1 °C (0.18 °F) error at 2 hours.
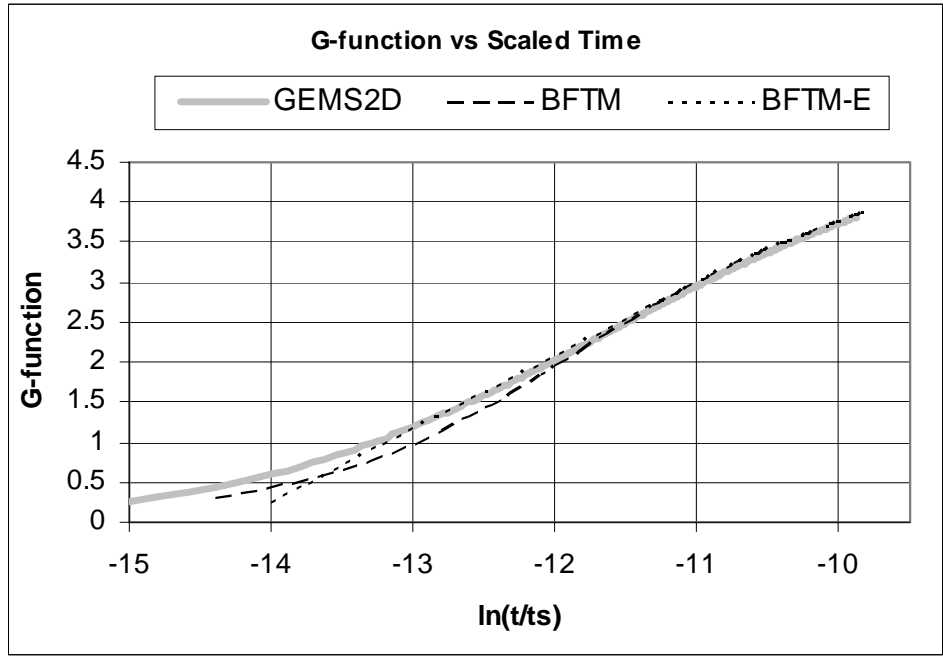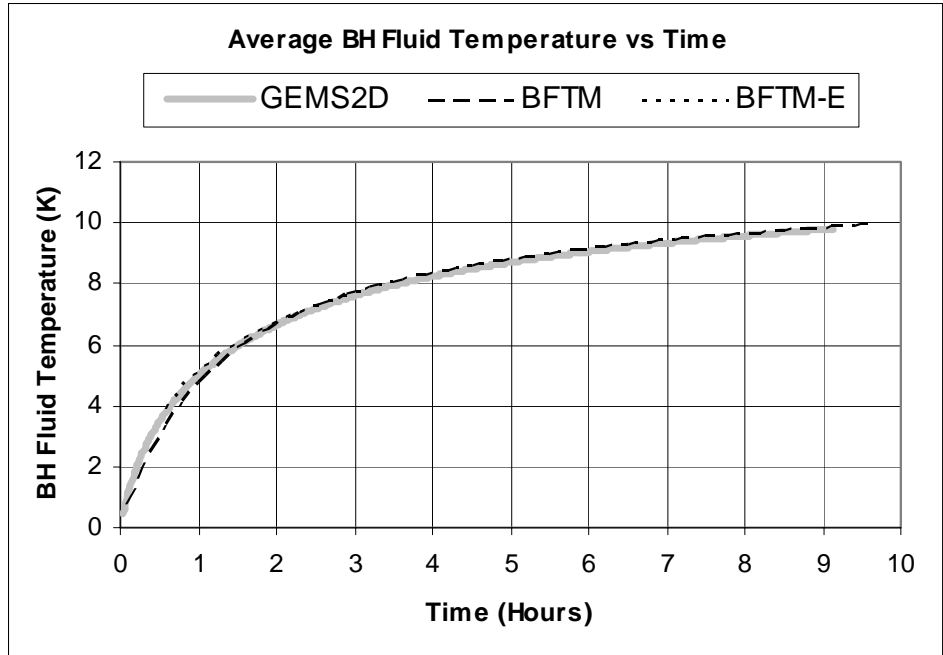
Figure 4-22 Validation of the BFTM Model Using a GEMS2D Simulation with a 11.4 cm (4.5 in) BH Diameter 3 cm (1.18 in) Shank Spacing and 2 Times the Fluid.

121
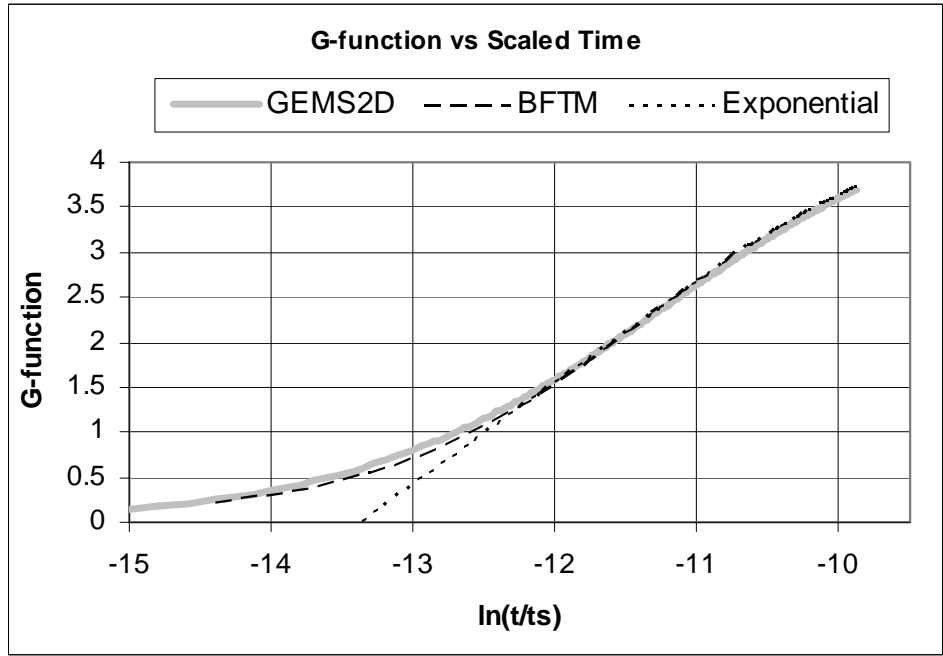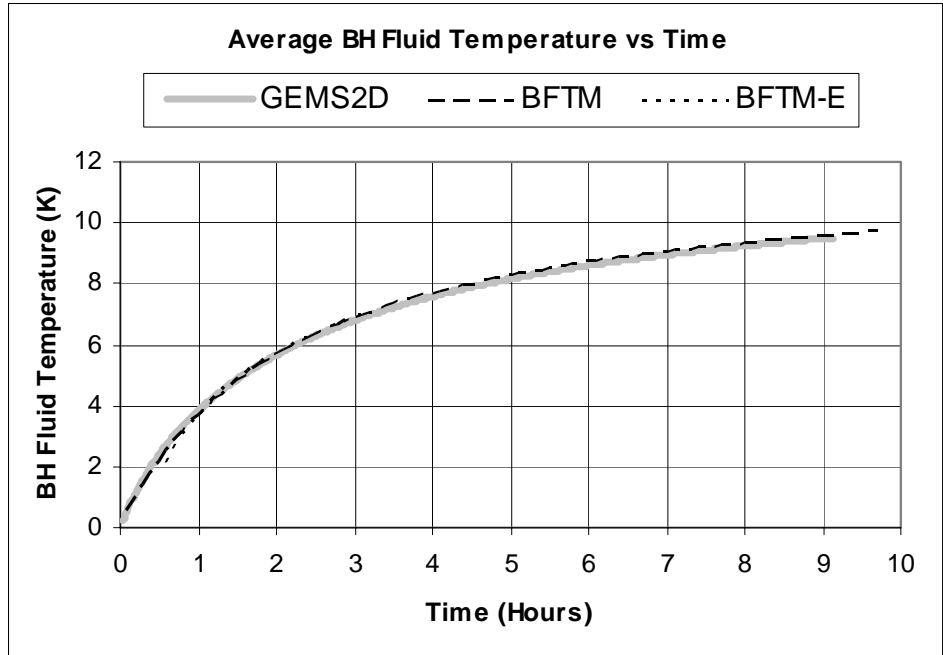
Figure 4-23 Validation of the BFTM Model Using a GEMS2D Simulation with a 11.4 cm (4.5 in) BH Diameter 3 cm (1.18 in) Shank Spacing and 4 Times the Fluid
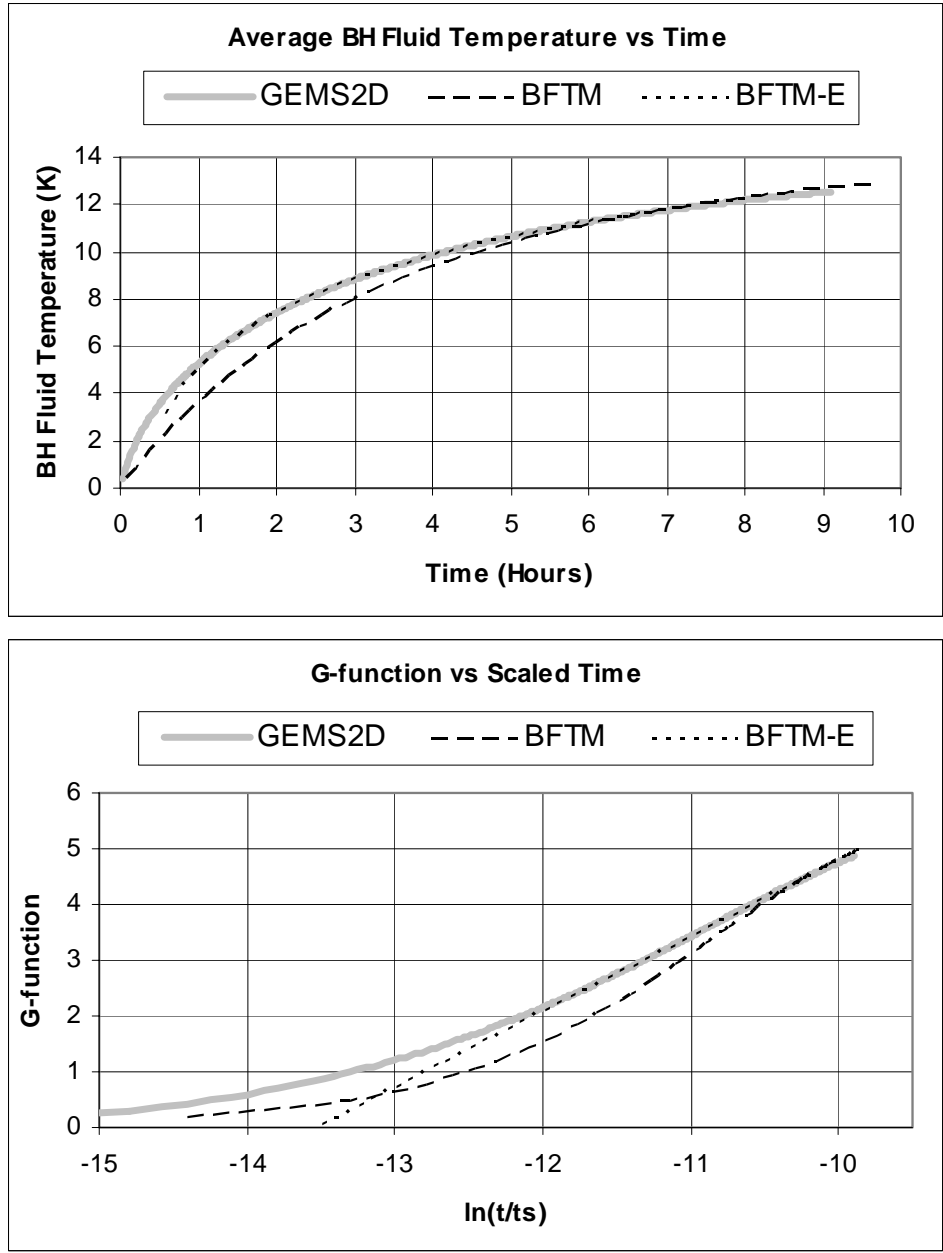
Figure 4-24 Validation of the BFTM Model Using a GEMS2D Simulation with a 19.05 cm (7.5 in) BH Diameter 2.25 cm (0.886 in) Shank Spacing and 2 Times the Fluid
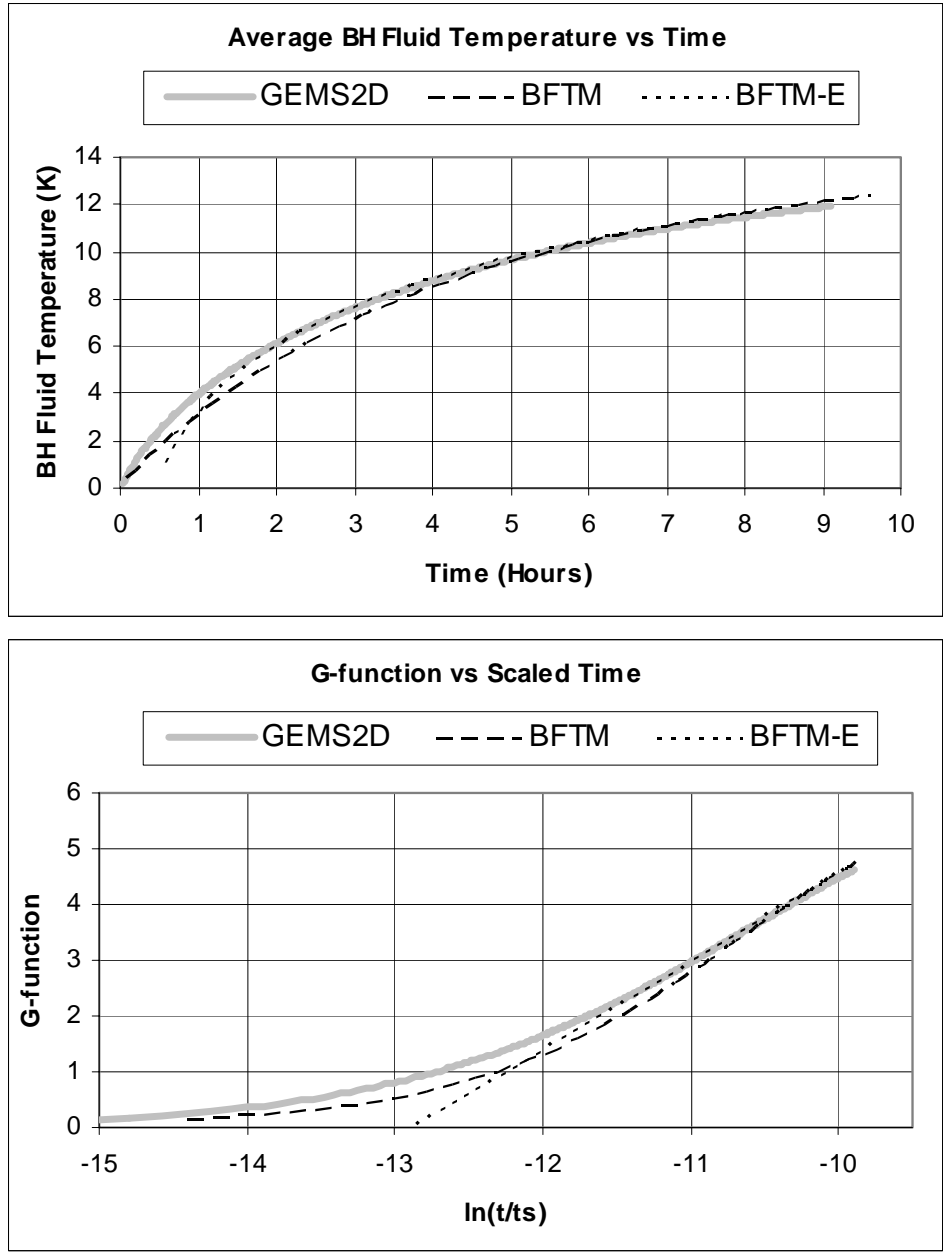
Figure 4-25 Validation of the BFTM Model Using a GEMS2D Simulation with a 19.05 cm (7.5 in) BH Diameter 2.25 cm (0.886 in) Shank Spacing and 4 Times the Fluid

4.9   Implementation and Validation of the BFTM-E Model

Chapters 5 and 6 use the BFTM-E model within GLHEPRO. This section

describes the implementation of the BFTM-E model within GLHEPRO and also shows

the accuracy that can be attained with an example case using a 17.8 cm (7 in) diameter borehole.

The implementation in GLHEPRO used a non-dimensionalized version of Tables 4-2 and 4-3. The equations for non-dimensionalizing borehole diameter and shank spacing are shown in Equation 4-1 and 4-2 respectively. In Table 4-2, instead of extrapolation time represented as a function of borehole diameter, extrapolation time was represented as a ratio of twice the U-tube outside diameter divided by the borehole diameter. Thus, as this ratio approaches zero, the U-tubes approach zero diameter and as the U-tubes approach the maximum size possible, the ratio approaches one.

The non-dimensional shank spacing is equal to the shank spacing divided by the maximum possible shank spacing. When the shank spacing is zero, the non-dimensional shank spacing is zero and when the U-tubes are touching the borehole radius the non-dimensional shank spacing is 1. Both non-dimensional parameters range between zero and one.

$$Ratio_{Dia} = \frac{2 \cdot D_{U-tube}}{D_{BH}} \tag{4-1}$$

$$Ratio_S = \frac{S}{D_{BH} - 2 \cdot D_{U-tube}} \tag{4-2}$$

Where,

$Ratio_S$ = shank spacing ratio (non-dimensional)

$Ratio_{Dia}$ = borehole diameter ratio (non-dimensional)

D_{U-tube} = U-tube outside diameter (cm or in)

D_{BH} = borehole diameter (cm or in)

S = shank spacing (cm or in)

Using Equation 4-1 an extrapolation time can be found by linearly interpolating within Table 4-2.

Table 4-8 Non-Dimensional Borehole Diameter vs Time for Slope Matching

Non-Dimensional BH Diameter	Time (hours)
0.877	2
0.586	3
0.438	5
0.350	8

Table 4-9 GAF Dependent on Non-Dimensional Borehole Diameter, Non-Dimensional Shank Spacing and Fluid Factor

Non-Dimensional BH Diameter = 0.586			
Non-Dimensional Shank Spacing	1xfluid	2xfluid	4xfluid
0.067	0.260	0.240	0.220
0.211	0.285	0.250	0.230
0.477	0.285	None	None
0.636	0.285	0.250	0.230
0.742	0.290	None	None
0.871	0.290	0.250	0.230

Non-Dimensional BH Diameter = 0.438			
Non-Dimensional Shank Spacing	1xfluid	2xfluid	4xfluid
0.117	0.245	0.225	0.200
0.263	0.270	0.240	0.215
0.351	0.270	0.248	0.230
0.409	0.270	None	None
0.480	0.270	0.255	0.230
0.738	0.270	None	None

Non-Dimensional BH Diameter = 0.350			
Non-Dimensional Shank Spacing	1xfluid	2xfluid	4xfluid
0.081	0.220	0.205	0.185
0.181	0.235	0.225	0.200
0.243	0.245	0.230	0.205
0.282	0.250	None	None
0.332	0.255	0.239	0.210
0.667	0.255	None	None

Using Equations 4-1 and 2 as well as the fluid factor a GAF can be found by linearly interpolating within the GAF values given in Table 4-9. The extrapolation time can be found by using interpolating within table Table 4-8 once the non-dimensional borehole diameter is calculated with equation 4-1.

As an example, a borehole was chosen with 17.8 cm (7 in) diameter, 4 cm (1.57 in) shank spacing and all other properties specified in Table 4-1. The borehole resistance for this system is 0.235 mK/W (0.4067 °F·ft·hr/Btu). In this example the GAF and extrapolation time will be calculated using the ratios defined in Equation 4-1 and 2.   The borehole diameter ratio equals 0.37581 and the shank spacing ratio equals 0.3604. The calculation for the extrapolation time is as follows.

Calculation of extrapolation time using diameter ratio		
Diameter Ratio	Time	
0.43845	5 hours	
0.37581	7.14 hours	←Linearly Interpolated Time
0.35076	8 hours	

The calculation of GAF is three dimensional interpolation using the $Ratio_{Dia}$, $Ratio_{S}$ as well as the fluid factor. Since the fluid factor is equal to 1 in this example this calculation becomes two dimensional interpolation. The first interpolation uses the shank spacing ratio (which is 0.3604) to interpolate within the data in Table 4-3 for the 15.2 cm (6 in) and 19.1 cm (7.5 in) diameter boreholes. This yields a GAF of 0.27 for the 15.2 cm (6 in) diameter borehole and 0.255 for the 19.1 cm (7.5 in) diameter borehole.   Next, using the borehole diameter ratio (0.37581), the actual GAF for our test case can be found as follows.

Calculation of GAF		
Diameter Ratio	GAF	
0.43845	0.27	
0.37581	0.2593	←Linearly Interpolated Time
0.35076	0.255	

Figure 4-26 shows the GEMS2D temperature profile and g-function plotted with the BFTM-E model using the extrapolation time of 7.14 hours and a GAF of 0.2593.
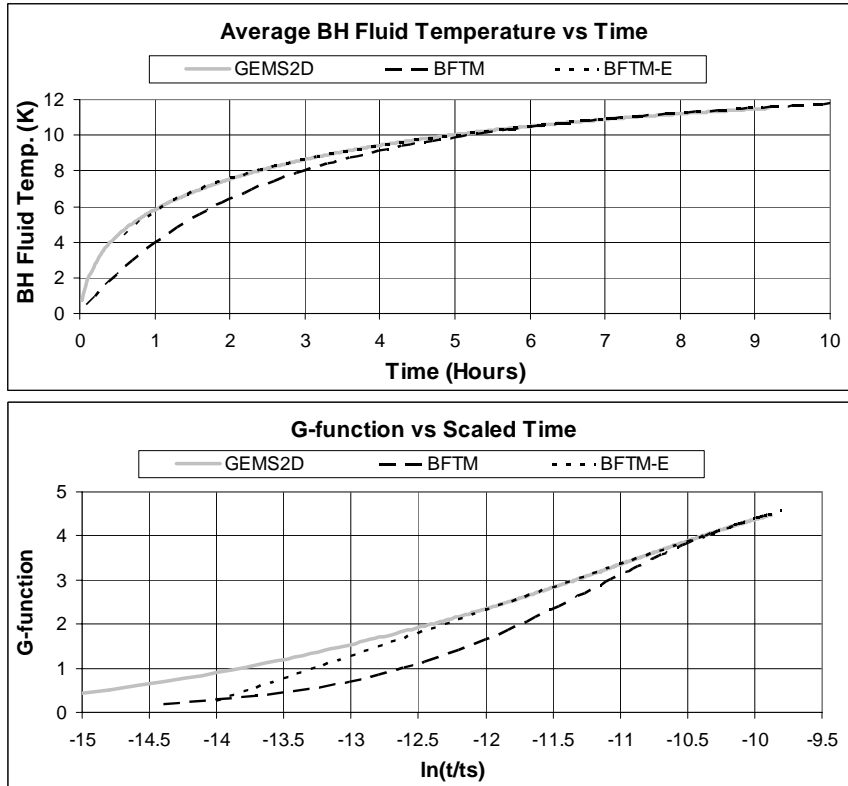
Figure 4-26 Temperature Profile for the BFTM-E and GEMS2D Models with a 17.8 cm (7 in) Borehole Diameter and 4 cm (1.57 in) Shank Spacing Using an Interpolated GAF Value

As can be seen in Figure 4-26, the error between the BFTM-E and GEMS2D temperature profile is very small, overestimating the GEMS2D temperature by only 0.04ºC (0.08 ºF) at two hours.

To validate shank spacing a 11.4 cm (4.5 in) borehole diameter with a 1.58 cm (0.623 in) shank spacing was created. The resulting GEMS2D and BFTM-E data is shown in Figure 4-9. The temperature was overestimated by approximately 0.08 °C (0.14 °F) at two hours. The error increase for interpolated values of GAF is expected to be negligible.

128

4.10 Conclusion of BFTM Model Validation

Over 60 different GEMS2D simulations were created to validate the accuracy of the BFTM model. As shown in Figures 4-8 through 4-11 the BFTM model is much more accurate than the line source model. The grout allocation factor (GAF) is used very successfully to reduce the difference between the BFTM model and the GEMS2D model. A three dimensional matrix of GAF values is shown in Table 4-3 to be a function of borehole diameter, shank spacing, and fluid factor. The BFTM model can be further improved by using linear extrapolation to reduce the error to less than 0.1 °C (0.9 °F) for the cases, which have realistic inputs, at 2 hours of heat injection or extraction.

A non-dimensionalized version of the extrapolation time and GAF matrix is shown in Table 4-8 and 4-9 respectively. Table 4-8 shows GAF as a function of non-dimensionalized BH diameter and shank spacing which are defined by equations 4-1 and 4-2. Representing GAF in terms of non-dimensional variables generalizes the GAF so that it can be found for borehole diameters and shank spacings that are not represented in Table 4-3.

To validate the non-dimensional version for BH diameter and shank spacings that are not included in the data set shown in Table 4-8 and 4-9 two simulations were used. To validate BH diameter accuracy a 17.8 cm (7 in) diameter borehole case was created. The resulting GEMS2D and BFTM-E data is shown in Figure 4-26. To validate shank spacing a 11.4 cm (4.5 in) borehole diameter with a 1.58 cm (0.623 in) shank spacing was created. The resulting GEMS2D and BFTM-E data is shown in Figure 4-9. In both cases the error at two hours was less than 0.1 °C (0.9 °F). Thus the error increase for interpolated values of GAF is expected to be negligible.

5 THE EFFECT OF THE BFTM MODEL ON GLHE DESIGN

This chapter uses a modified version of GLHEPRO 3.0 to evaluate the impact of the borehole fluid thermal mass (BFTM) model on system design. To do this, a peak-load-dominant church building and a non-peak-load-dominant small office building have been selected. Ground loop heat pump loads for the church have been created using BLAST (1986) with weather data from Detroit, MI; Dayton, OH; Lexington, KY; Birmingham, AL; and Mobile, AL. Likewise, ground loop heat pump loads have been created using BLAST (1986) for the small office building, for Houston, TX and Tulsa, OK. For each building BLAST (1986) produced one year of hourly heat pump loads. The loads were aggregated into monthly and peak, heating and cooling loads. The aggregated loads were then used in GLHEPRO for ten year simulations.

For both buildings, the borehole diameter, shank spacing, grout conductivity, and fluid factor were changed to give a better understanding of the influence of these parameters on designing GLHE systems.

5.1 Test Buildings

Section 5.1.1 and 5.1.2 give a physical description of the church and small office building. Section 5.1.3 gives a description of the loads on each of the two buildings for there corresponding locations.

5.1.1 Church

The church building was created to represent the main auditorium of a typical medium or small size church. It does not model a specific building that is currently in

existence. The church building is intentionally skewed to represent a very peak-load-dominant building.

The peak loading condition imposed on the building occurs on a weekly basis for a duration of two hours and is a result of 348 occupants and the indoor lighting. The lighting in this simulation accounts for approximately 5.5% of the total peak loads on the system whereas the people account for approximately 94.5% of the peak loads. Table 5-1 presents general information on the church building, including dimensions and building materials.

Table 5-1 Church Building Description

BUILDING DESCRIPTION		
Description		
Four Metal Walls		
Double Pane Tinted Window on Two of the Four Walls, 30.5 m² (100 ft²) on Each Wall		
Slab Floor		
Flat Roof		
Mineral Fiber Insulation on all Four Walls		
Geometry		
Width	28 m	92 ft
Length	19.5 m	64 ft
Ceiling Height	4.88 m	16 ft
Floor Area	547 m²	5888 ft²
Building Volume	2667 m³	94210 ft³
		R-value
MATERIALS DESCRIPTION	°C·m²/W	°F·ft²·h/Btu
Metal Building Wall	0.0090	0.051
Metal - galvanized steel (0.159 cm or 1/16 in)	887.2	5038
Insulation - Mineral Fiber Fibrous (15.2 cm or 6 in)	0.0093	0.053
BLBD - Gypsum Plaster (0.953 cm or 3/8 in)	0.5278	2.997
Double Pane Tinted Window	0.1675	0.951
Glass - Grey Plate (0.953 cm or 3/8 in)	2.487	14.120
Airspace Resistance	0.1935	1.099
Slab Floor	0.0171	0.097
Dirt (30.5 cm or 12 in)	0.0176	0.100
Concrete - Sand and Gravel (10.2 in or 4 in)	0.5289	3.003
Metal Building Roof	0.0069	0.039
Steel Siding	915.8	5200
Ceiling Airspace	0.1761	1.000
Mineral Fiber Fill (18.4 cm or 7.25 in)	0.0074	0.042
Acoustic Tile (0.953 cm or 3/8 in)	0.1856	1.054

5.1.2 Small Office Building

The following description is taken from Yavuzturk (1999). The small office building example was completed in 1997 and is located in Stillwater, Oklahoma. The total area of the building is approximately 14,205 ft^2 (1,320 m^2). In order to determine the annual building loads for the example building using BLAST (1986), the following approach was taken:

i) Eight different thermal zones were identified in the building. For each zone, a single zone draw through fan system is specified as a surrogate for a ground source heat pump. The coil loads on this system are equivalent to those of a ground source heat pump system.

ii) The office occupancy is set to 1 person per 9.3 m^2 (100 ft^2) with a heat gain of 450 BTU/hr (131.9 W) 70% of which is radiant, on an officer occupancy schedule.

iii) The office equipment heat gains are set to 1.1 W/ ft^2 (12.2 W/ m^2), on an office equipment schedule, on an office equipment schedule.

iv) The lighting heat gains are set to 1 W/ ft^2 (11.1W/ m^2), on an office lighting schedule.

v) Day time (8am-6pm, Monday-Friday), night time and weekend thermostat settings are specified for each zone. During the day, the temperature set point is 20.0°C (68.0°F). For the night, only heating is provided, if necessary, and the set point is 14.4°C (58.0°F).

The example building is analyzed considering two different climatic regions each represented by the Typical Meteorological Year (TMY) weather data: A typical hot and

humid climate is simulated using Houston, TX; a more moderate climate is simulated using Tulsa, OK.

5.1.3   Annual Loading

The amount of heat rejected or extracted to and from the ground varies continuously over time due to the weather and the internal heat gains imposed on the building such as people and lighting. These changes result in ground loop temperatures that vary with time. With regards to heat pump performance, this causes a range of COP values for the water-to-air heat pump.

For design purposes, the heat pump that was used is the Climate Master VS200 water to air heat exchanger. This heat pump has a COP of cooling of 4.8 at 10°C (50 °F) and of 3.2 at 32.2°C (90 °F). In heating the COP is 3.2 at 4.44 °C (40 °F) and 3.9 at 26.7 °C (80 °F).   Table 5-2 shows the raw heating and cooling loads and the approximate heat rejection and heat extraction loads, assuming fixed COP values of 4.4, for cooling and 3.6 for heating which comes from the performance data at 15.6 °C (60 °F).

Table 5-2 Church Building Load Table for Different Locations

City Location	Annual				
	Heating Load KBTU (MW-hr)	Cooling Load KBTU (MW-hr)	Nominal Heat Extraction KBTU (MW-hr)	Nominal Heat Rejection KBTU (MW-hr)	Ratio Heat extraction to Heat Rejection
Detroit	84930 (24.9)	2315 (0.679)	117595 (34.5)	2995 (0.878)	39
Dayton	71598 (21)	3328 (0.975)	99135 (29.1)	4306 (1.26)	23
Lexington	53339 (15.6)	3479 (1.02)	73854 (21.6)	4502 (1.32)	16
Nashville	41814 (12.3)	4876 (1.43)	57896 (17)	6310 (1.85)	9
Birmingham	29654 (8.69)	5690 (1.67)	41059 (12)	7363 (2.16)	6
Mobile	13807 (4.05)	7632 (2.24)	19117 (5.6)	9876 (2.89)	2
Lexington*	31201 (9.14)	12923 (3.79)	43201 (12.7)	16724 (6.97)	2.6
Nashville*	20424 (5.98)	18396 (5.39	28279 (8.28)	23807 (6.97)	1.2
Birmingham*	11836 (3.47)	21453 (6.29)	16388 (4.8)	27763 (8.13)	0.59
Mobile*	1954 (0.572)	27915 (8.18)	2706 (0.793)	36125 (10.6)	0.08

This shows that for all church locations the systems are heating dominant. As can be seen, the cooler locations produce greater heat load dominance.

In Table 5-2, Lexington*, Nashville*, Birmingham* and Mobile* show buildings in which the building descriptions have been modified so that the annual heating loads have been reduced and cooling loads have been increased. These buildings have the same geometry as the ones with more heating except the ground heat transfer has been eliminated by replacing the slab-on-grade with a perfectly insulated crawlspace. Thus, in winter less heating load is required since there is less heat lost to the ground and in summer more cooling is required for the same reason. The lighting load has also been changed by slightly decreasing the load and distributing it throughout the week for the buildings with more cooling, whereas the lighting load coincides with ~~on~~ the two hour peak each week for the buildings with more heating. The lighting load is a minor

influence on the systems loads. The net effect produces buildings with a smaller ratio of heat extraction to heat rejection.

The monthly heating and cooling loads on the system are as follows. The aggregated monthly heating and cooling loads for the church building for all locations are plotted in Figure 5-1 and Figure 5-2 respectively.
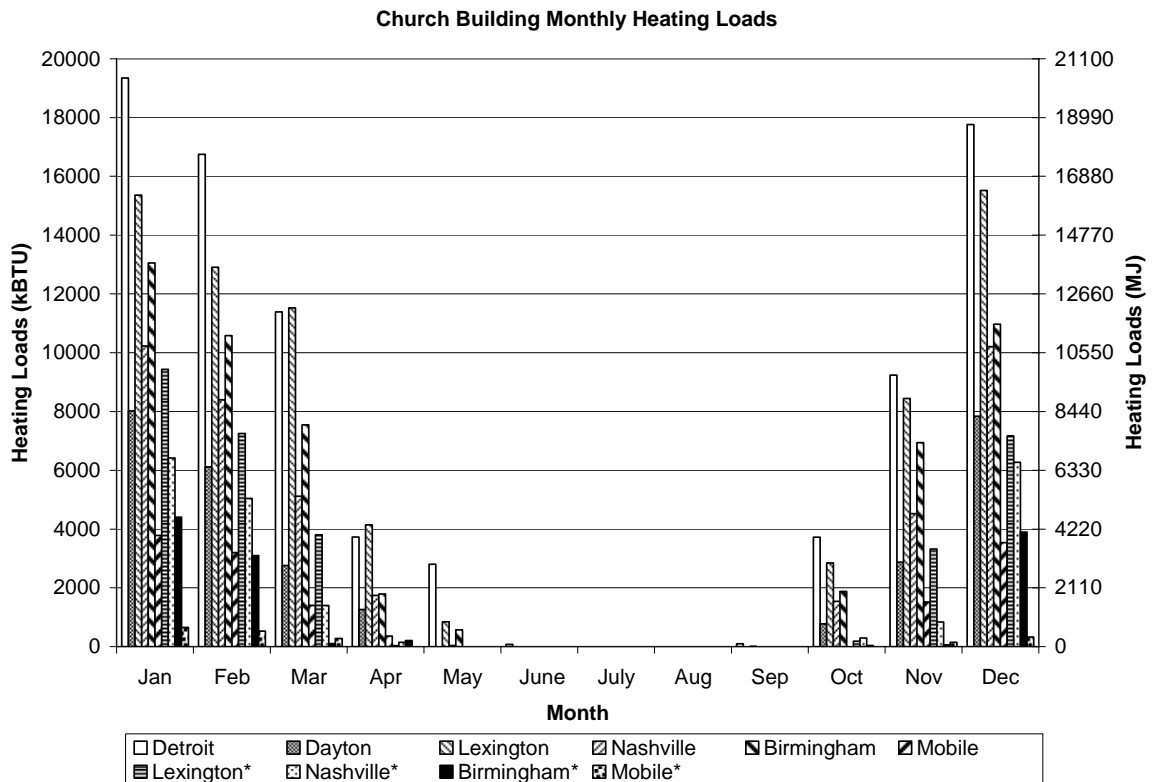
Figure 5-1 Monthly Church Heating Loads
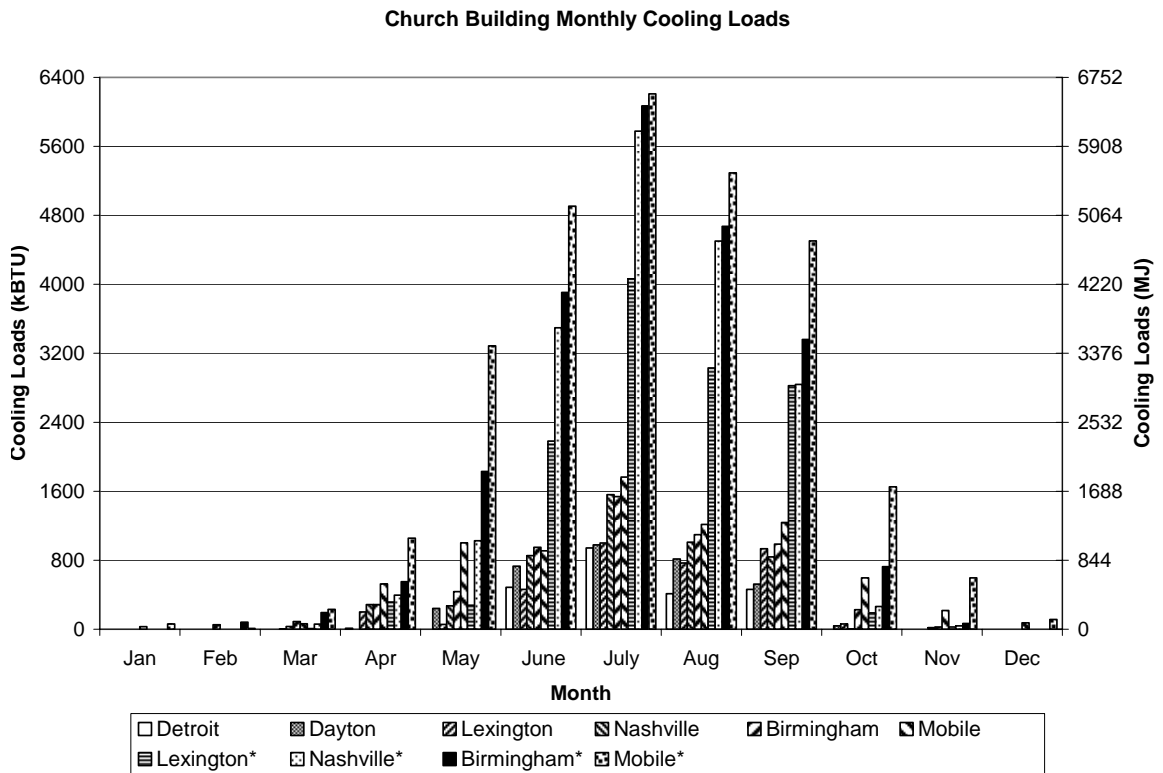
Figure 5-2 Monthly Church Cooling Loads

The peak monthly heating and cooling loads for the church building are shown in Figure 5-3 and Figure 5-4.
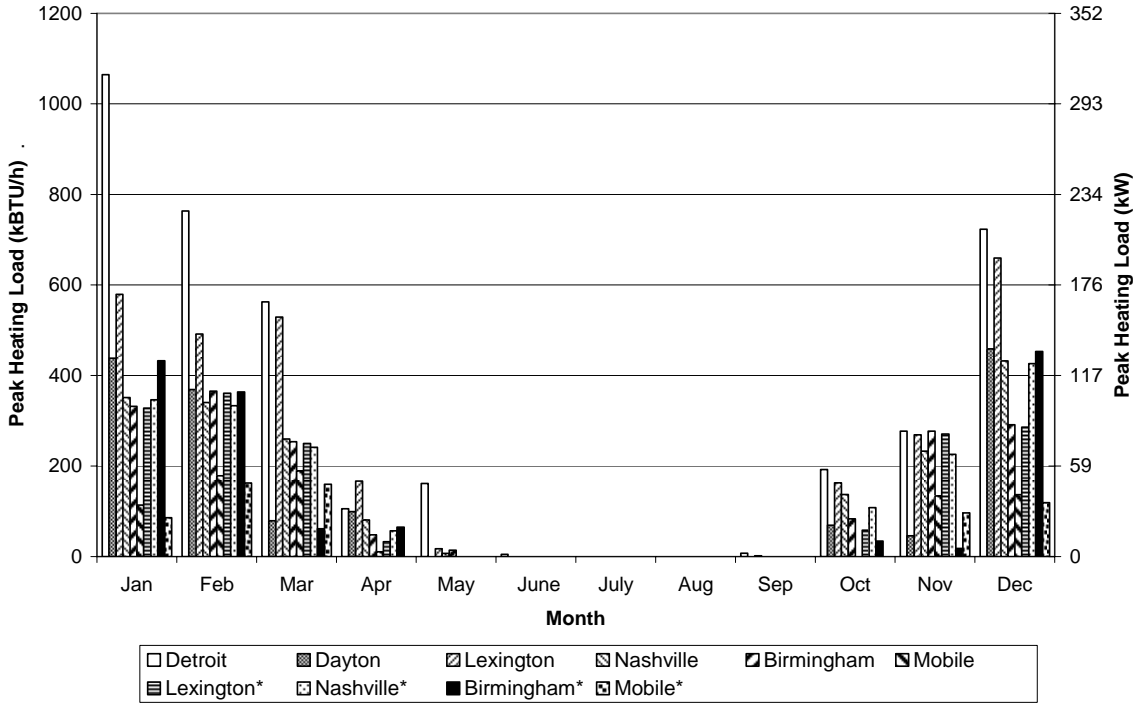
Figure 5-3 Monthly Church Peak Heating Loads

Church Building Monthly Peak Cooling Loads
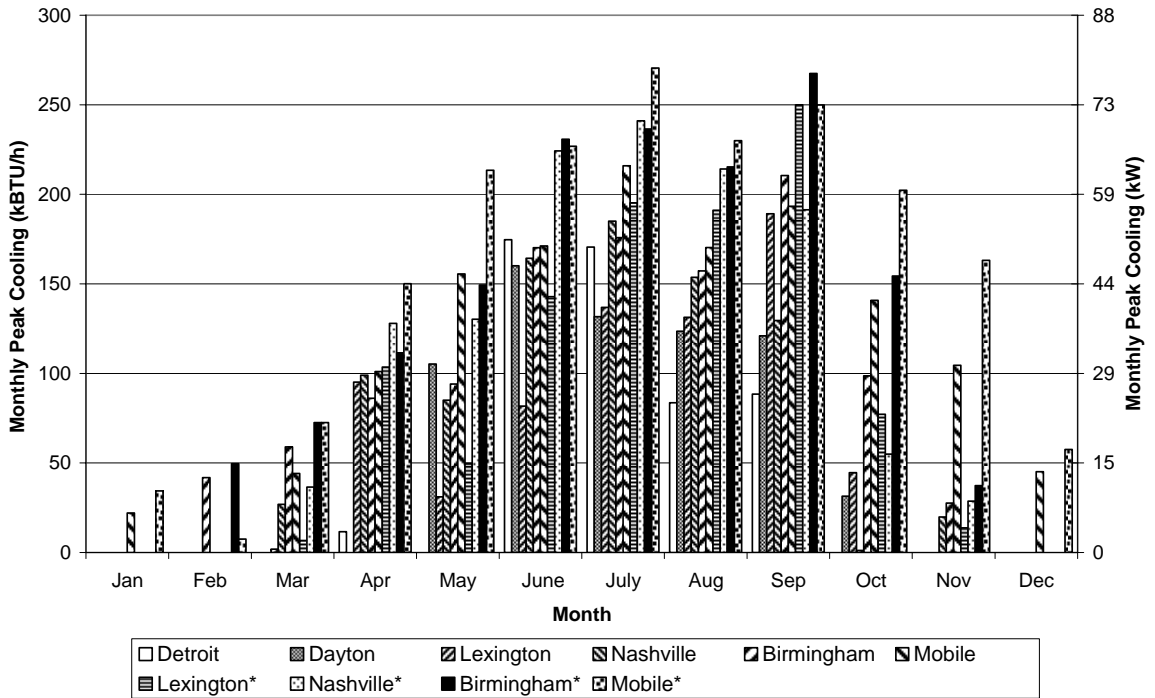
Figure 5-4 Monthly Church Peak Cooling Loads

137

The small office building simulated in BLAST produced the loads shown in Table 5-3. Similar to Table 5-2, the same Climate Master VS200 COP values are used to determine the heat extraction or rejection.

Table 5-3 Building Load Table for the Small Office Building

City Location	Annual Loading				
	Heating Load kBTU (kWh)	Cooling Load kBTU (kWh)	Nominal Heat Extraction kBTU (kWh)	Nominal Heat Rejection kBTU (kWh)	Ratio Heat Extraction to Rejection
Houston	7517 (2203)	181656 (53238)	9728 (2851)	251526 (73715)	0.039
Tulsa	50141 (14695)	133797 (39212)	64892 (19018)	185255 (54293)	0.35

Since Houston and Tulsa have warm climates the ratio of heat extraction to heat rejection is small, especially for Houston. The small office building for both locations is cooling load dominant. Tulsa has approximately three times as much heat rejection as extraction whereas Houston has approximately 25 times as much heat rejection as extraction.

The monthly heating and cooling loads that were aggregated from the hourly BLAST simulation are shown in Figures 5-5 and 5-6. The heating and cooling peak loads are shown in Figures 5-7 and 5-8.
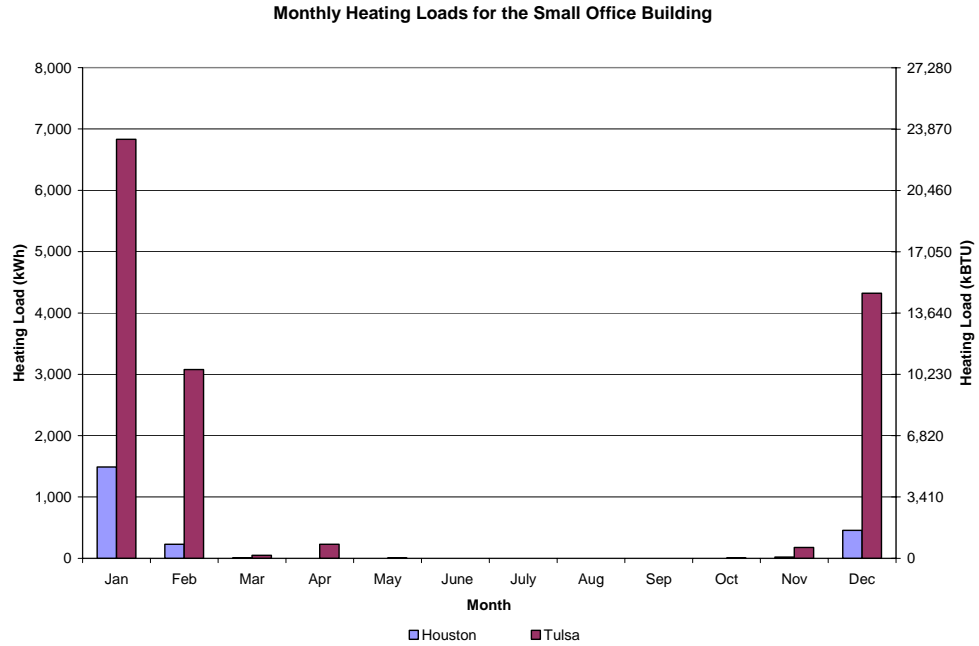
Figure 5-5 Monthly Heating Loads for the Small Office Building
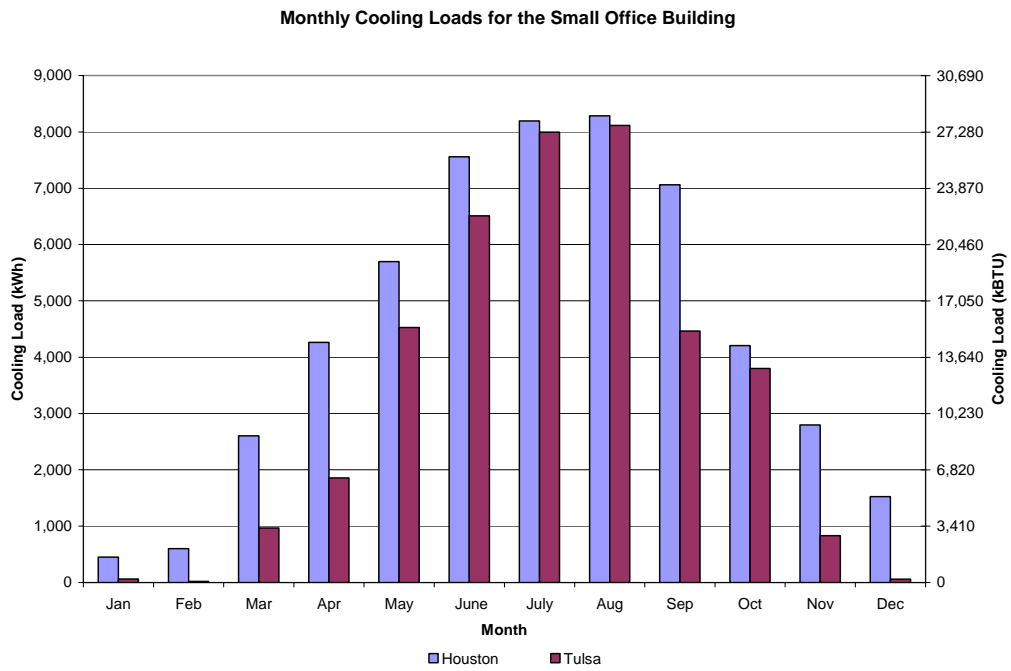
Figure 5-6 Monthly Cooling Loads for the Small Office Building

139

Monthly Peak Heating Loads for the Small Office Building
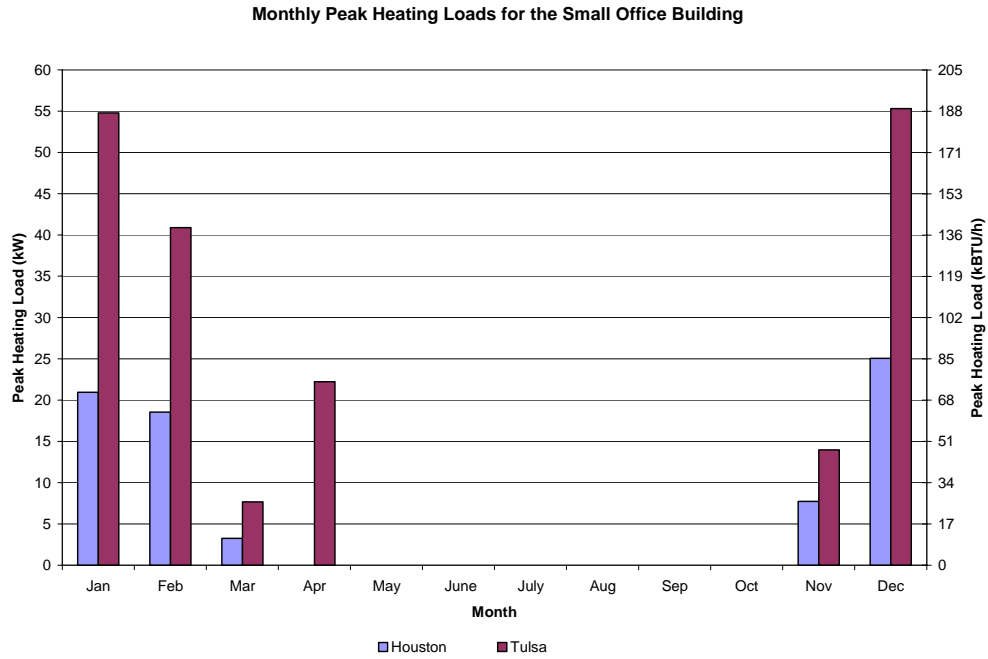
Figure 5-7 Monthly Peak Heating Loads for the Small Office Building

Monthly Peak Cooling Loads for the Small Office Building
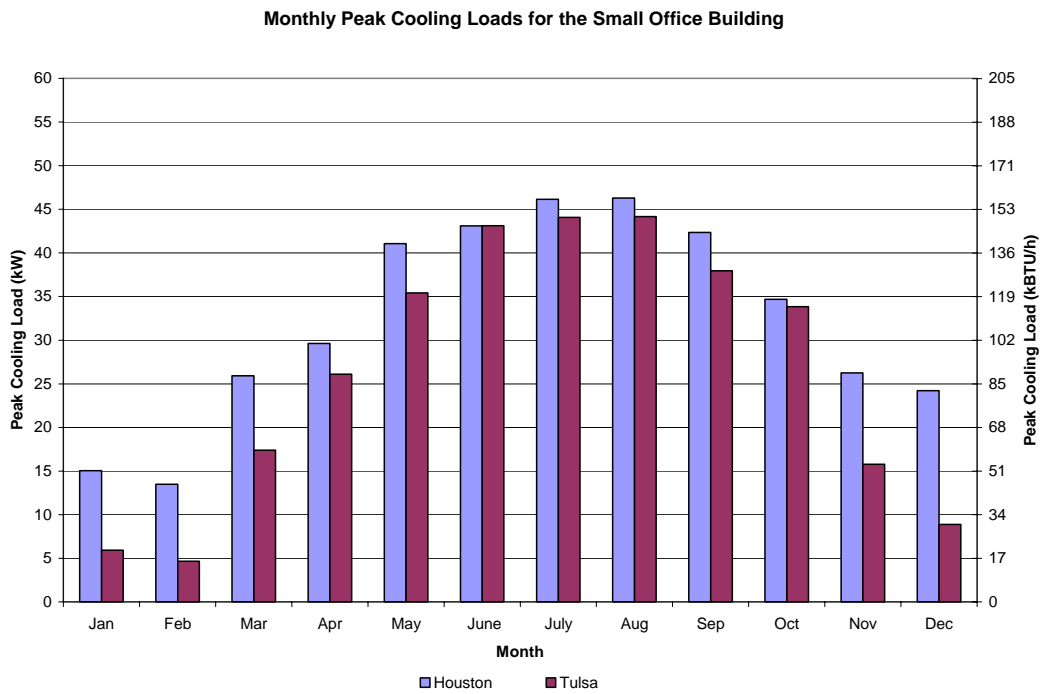
Figure 5-8 Monthly Peak Cooling Loads for the Small Office Building

5.2 GLHE Design Procedures

The baseline GLHE design that was chosen for the church building and small office building is shown in Table 5-4.

Table 5-4 GLHE Properties for the Church and Small Office Building

Borehole Configuration		
Spacing	15 ft	4.57 m
Configuration	6x6	6x6
Depth	250 ft	76.2 m
Borehole Geometric Properties		
Diameter	4.5, 6, 7.5 in	11.4, 15.2, 19.1 cm
U-tube Shank Spacing	A, B, C3, C	A, B, C3, C
U-tube ID	1.08 in	2.74 cm
U-tube OD	1.315 in	3.34 cm
U-Tube Properties		
Conductivity	0.225 Btu/hr-ft-F	0.389 W/(mk)
Volumetric Heat Capacity	26.4 Btu/ft^3-F	1.77 MJ/(m^3*k)
Soil Properties		
Conductivity	1.44 Btu/hr-ft-F	2.5 W/(mk)
Volumetric Heat Capacity	37.28 Btu/ft^3-F	2.500 MJ/(m^3*k)
Grout Properties		
Thermally Enhanced		
Conductivity	0.87 Btu/hr-ft-F	1.5 W/(mk)
Volumetric Heat Capacity	50.7 Btu/ft^3-F	3.400 MJ/(m^3*k)
Standard Bentonite		
Conductivity	0.43 Btu/hr-ft-F	0.75 W/(mk)
Volumetric Heat Capacity	58.16 Btu/ft^3-F	3.900 MJ/(m^3*k)
Fluid Properties		
Type	100% Water	100% Water
Flowrate	230 gal/min	870 L/min
Fluid Factor	0.1, 1, 2, 3, 4	0.1, 1, 2, 3, 4
Convection Coefficient	298 Btu/(hr-ft^2-F)	1690 W/(m^2-k)

A 6x6 borehole configuration, with 4.57 m (15ft) spacing and 76.2 m (250ft) depth was chosen to handle the yearly loads on the system for all church locations and the small office building location as shown in Table 5-4. For the GLHEPRO sizing depth simulations the 76.2 m (250 ft) depth was used as the preliminary guess depth. The borehole properties and configuration were standardized for all locations so that a comparison can be made between the different loading conditions. Of the borehole

parameters shown in Table 5-4, the parameters that were varied are the grout

conductivity, shank spacing and fluid mass since they influence the STS g-function.

For all locations the soil is assumed to have the same conductivity and volumetric

heat capacity of saturated sand. The conductivity and volumetric heat capacity of the soil

was also standardized for all the simulations so that they can be compared for various

locations without the influence of soil type.

The heat pump chosen for the church and small office building is the Climate

Master VS200 water to air heat pump. The recommended heat pump temperature range

is between 4.4 and 37.8 °C (40 and 90 °F) for heating and cooling. This temperature

range limits the GLHEPRO, sizing bounds to between 4.44 and 32.2 °C (40 and 100 °F).

Using GLHEPRO, both the sizing and simulation function were performed over 10 years

for both buildings.

The steady state ground temperatures for the various church and small office

locations greatly effect the ground loop fluid temperatures in a GLHEPRO simulation.

The steady state ground temperatures are shown for the church and small office locations

in Table 5-5.

Table 5-5 Undisturbed Ground Temperature Table for Various Cities

Building Type	City Location	Ground Temperature (F)	Ground Temperature (C)
Church	Detroit	49	9.44
Church	Dayton	53	11.7
Church	Lexington	58	14.4
Church	Nashville	60	15.5
Church	Birmingham	65	18.3
Church	Mobile	68	20
Small Office	Tulsa	62	16.7
Small Office	Houston	71	21.7

Since, for all the church locations, accept Birmingham* and Mobile*, the systems

are heating load dominant, as shown in Table 5-2, the lower bound of 4.4 °C (40 °F) for

the Climate Master VS200 will typically be the limiting fluid temperature for the church GLHEPRO simulations. As shown in Table 5-5, the steady state ground temperature for the church building located in Detroit is only 9 degrees above the minimum temperature set by the Climate Master VS200. This small delta temperature coupled with a ratio of heat extraction to heat rejection of 39, as shown in Table 5-2 means that the ground loop will need to be much larger than all the other locations. In practice, a heat pump with a wider operating temperature would be chosen for such a location.

Since the small office building located in both Tulsa and Houston is cooling load dominant and the ground temperatures are relatively high, especially in Houston, the upper bound for the fluid temperature of 37.8 °C (100 °F) set by the Climate Master VS200 will govern the depth of the borehole.

For the church, the peak loads chosen for the system occur weekly for a 2 hour duration. The two hour peak duration for one heat extraction pulse is shown in Figure 5-9 for Birmingham, AL. Figure 5-10 shows multiple peaks with heating loads. The heating loads are much larger than the cooling loads for all church locations. For Birmingham, AL the typical building heating load is between 0 and 10.3 MJ/h (0 and 35,000 BTU/h) with peak loads that range typically between -32.2 and 240 MJ/h (-110,000 and 820,000 BTU/h).
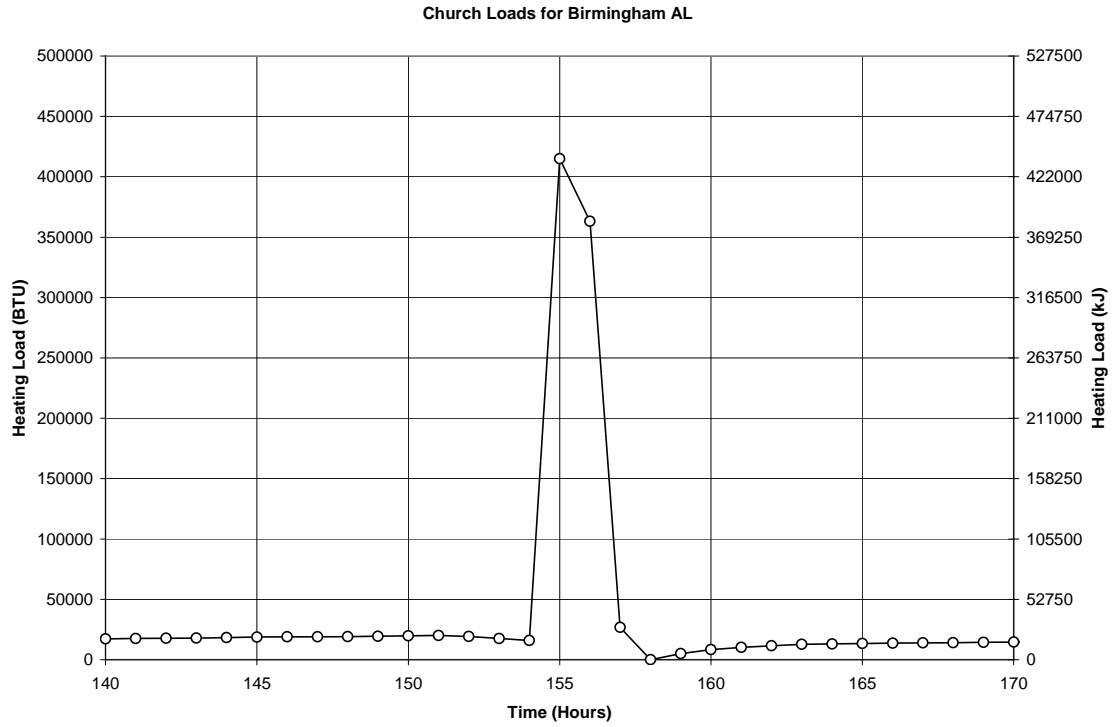
Figure 5-9 Raw Church Loads Single 2 Hour Peak Heat Load
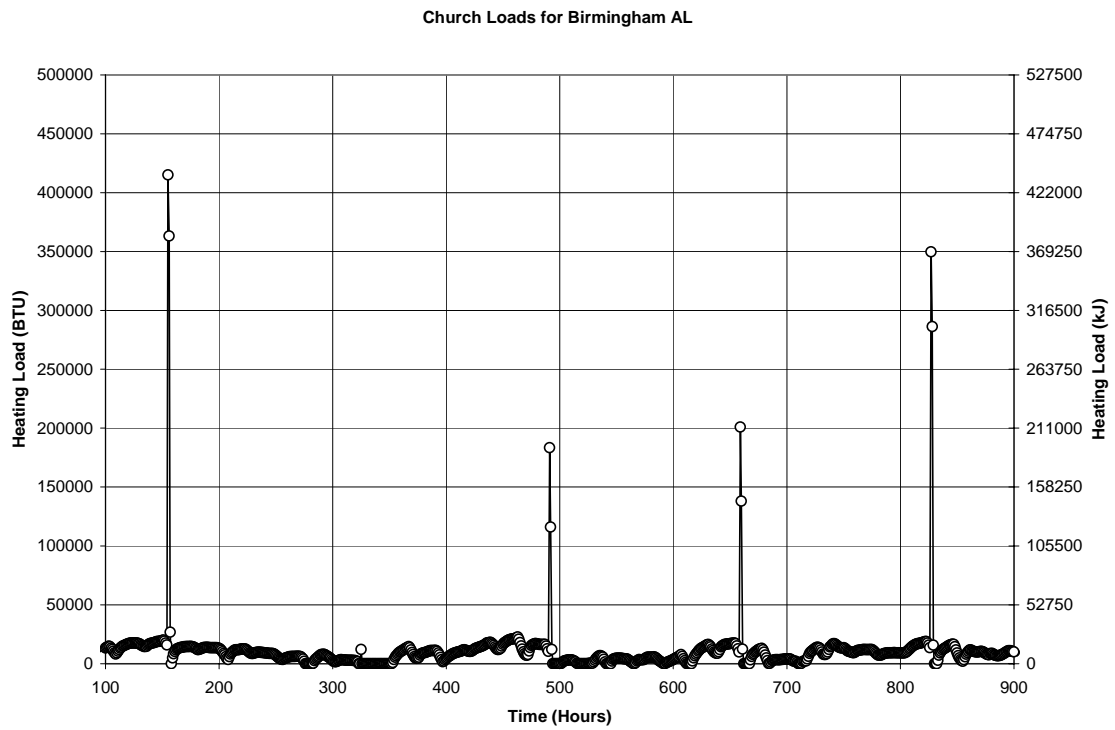
Figure 5-10 Raw Church Loads for Birmingham AL

144

The peak loads for the small office building are very different from the church loads. The small office building has internal heat gain profiles like a typical office building. The peak cooling loads are of 10 hour durations and occur five times a week. A typical 10 hour heat pulse can be seen in Figure 5-11 and a typical week is shown in 5-12.
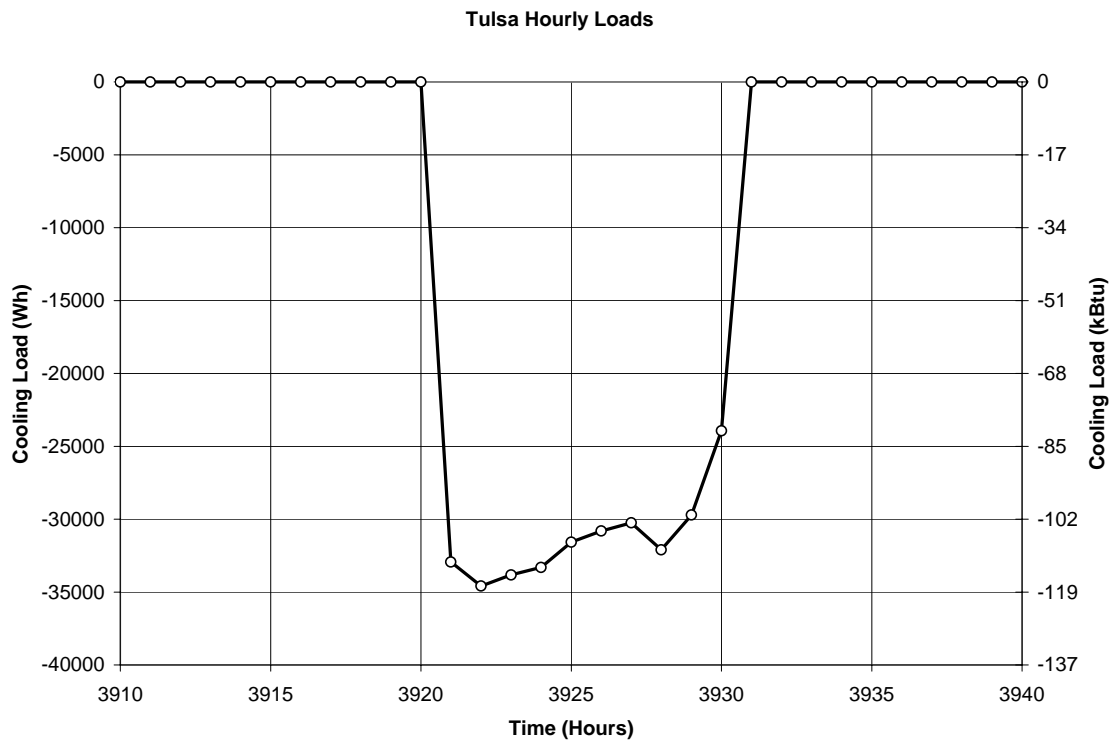
Tulsa Hourly Loads

Figure 5-11 One Peak of Hourly Loads for Tulsa Small Office Building
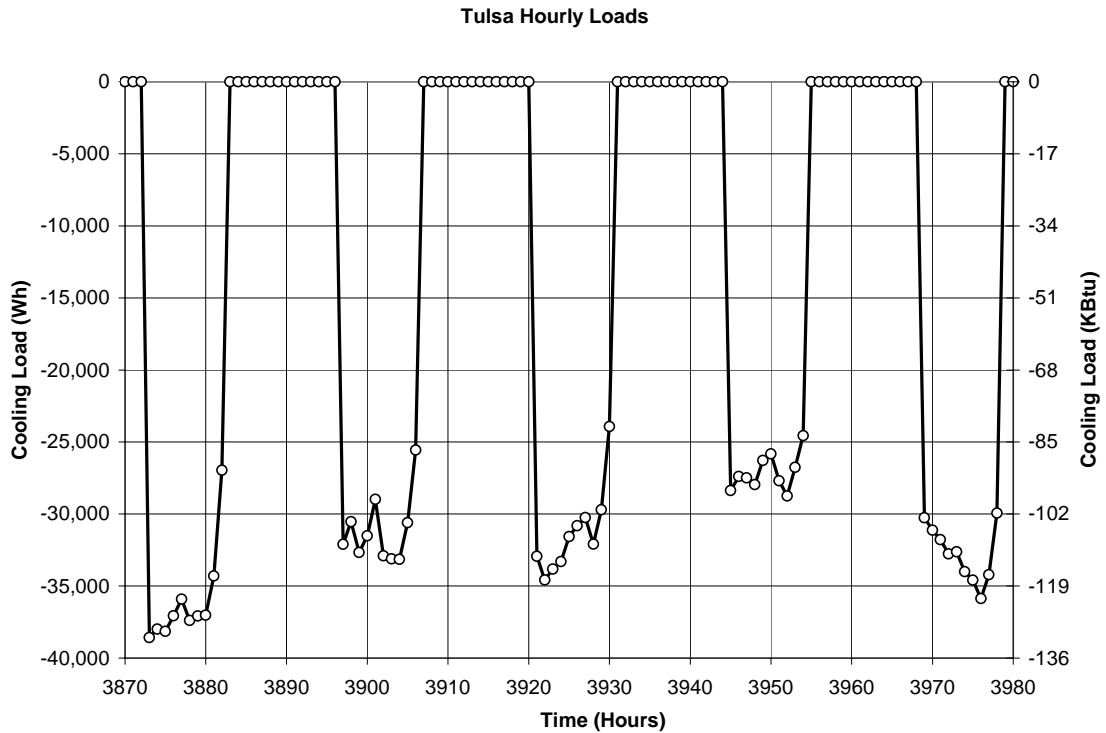
Figure 5-12 One Work Week of Hourly Loads for Tulsa Small Office Building

As shown in Table 5-4, the fluid factors that were simulated are 0.1, 1, 2, 3 and 4.

Figure 5-13 show g-functions created from the line source as well as the BFTM model.

As can be seen the 0.1 x fluid factor is about half way between the line source and the

BFTM model with 1 x fluid factor. As the fluid factor approaches zero the BFTM g-

function will approach the line source g-function. Inputting a fluid factor of zero will

make the simulation crash, so simulations at zero fluid factor were not possible.

Therefore, simulations using the line source method were used to approximate the zero

fluid factor case.

146
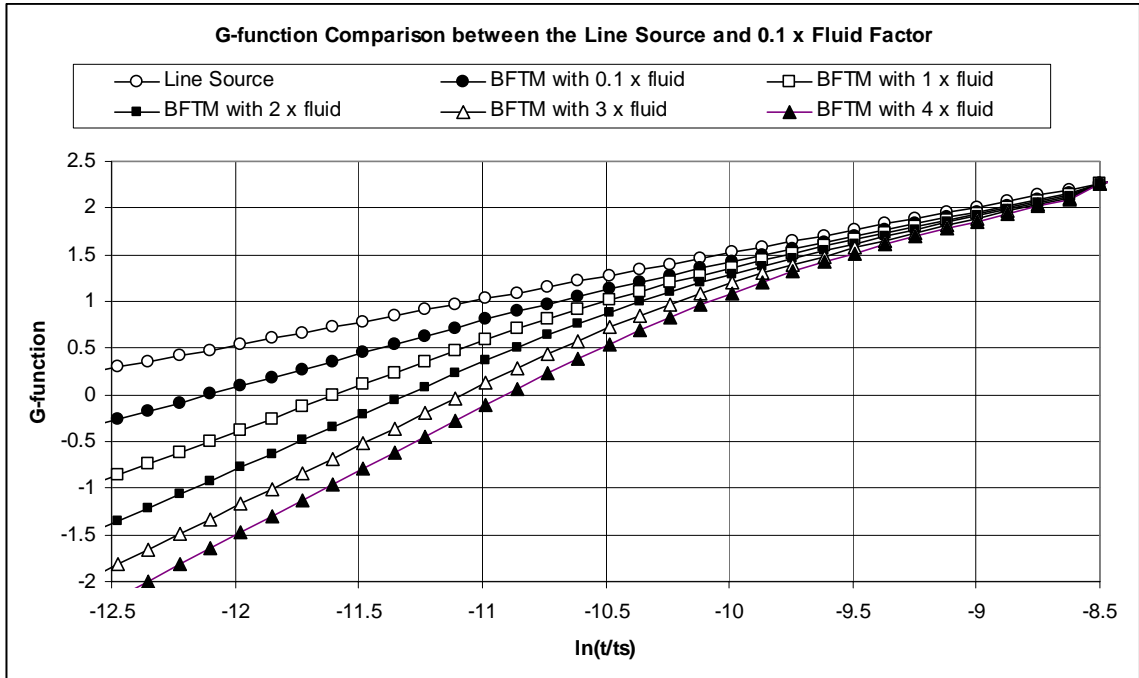
Figure 5-13 Short Time Step G-Function Comparison between the Line Source and the BFTM Model with 0.1, 1, 2, 3 and 4 x Fluid Factor

For the GLHEPRO simulations, the peak loads for the church building are set to 2 hours which, for the base case, is -11.4 log time in Figure 5-13 and for the small office building the peak loads were set to 8 hours which, for the base case, is -10.0 log time in Figure 5-13.

5.3   Simulation Results

This section gives the results of the church and small office GLHEPRO ten year simulations. A comparison is given between the two buildings to determine the impact of the BFTM model on typical non-peak-load-dominant systems such as the small office building and peak-load-dominant systems such as the church building. To more deeply analyze and understand the effect of varying specific parameters within the borehole fluid thermal mass models the fluid factor, shank spacing, borehole diameter, and grout conductivity were varied for both the church and small office buildings. The parameters

147

impact on designing actual GLHE systems was determined using the GLHEPRO sizing function.

5.3.1 Fluid Factor Results

Increasing the fluid factor, while keeping all other borehole parameters constant, unilaterally increased the performance of the borehole system for both the church building and the small office building. This can be seen in the GLHEPRO sizing results shown in Figure 5-14 to 17 for a 11.4 cm (4.5 in) diameter borehole. Figures 5-14 and 5-15 are for thermally enhanced grout and Figures 5-16 and 5-17 are for standard grout. Shank spacing is varied with values of 0.318 and 4.75 cm (0.125 and 1.87 in).

As can be seen in Figure 5-14 and 5-15, as the fluid factor increases the required depth of the borehole system decreased. Also for every church location, as the shank spacing increases, the required depth of the borehole decreases.
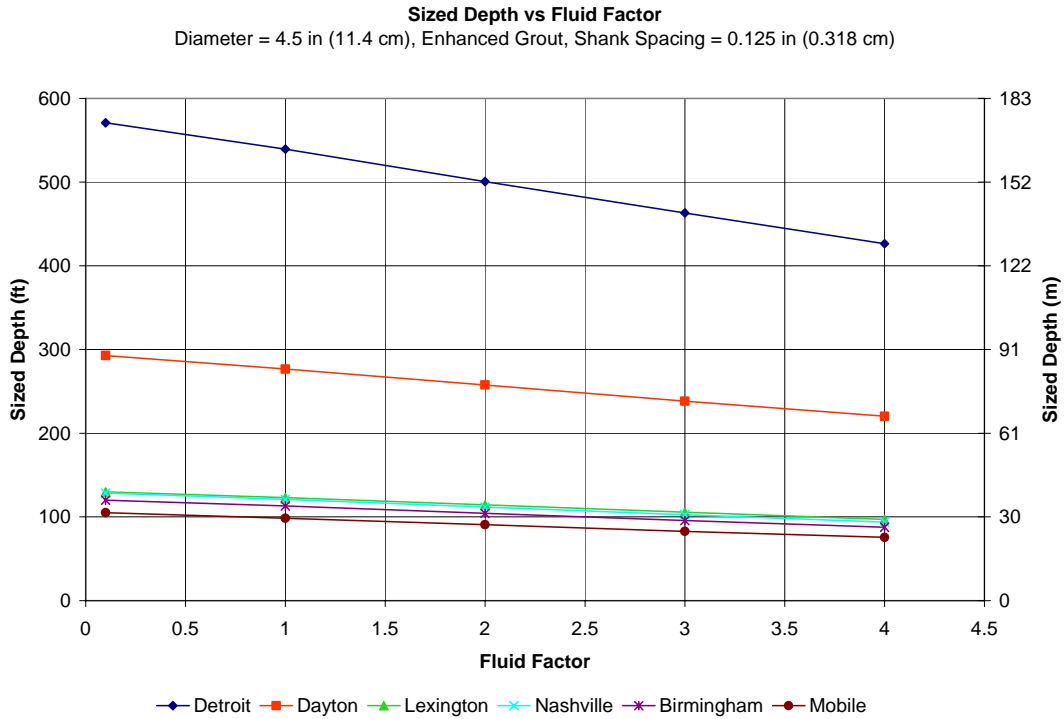
Figure 5-14 GLHEPRO Sized Depth vs Fluid Factor for a Church Building with a Borehole Diameter of 4.5 in (11.4 cm), Enhanced Grout, and Shank Spacing of 0.125 in (0.318 cm)
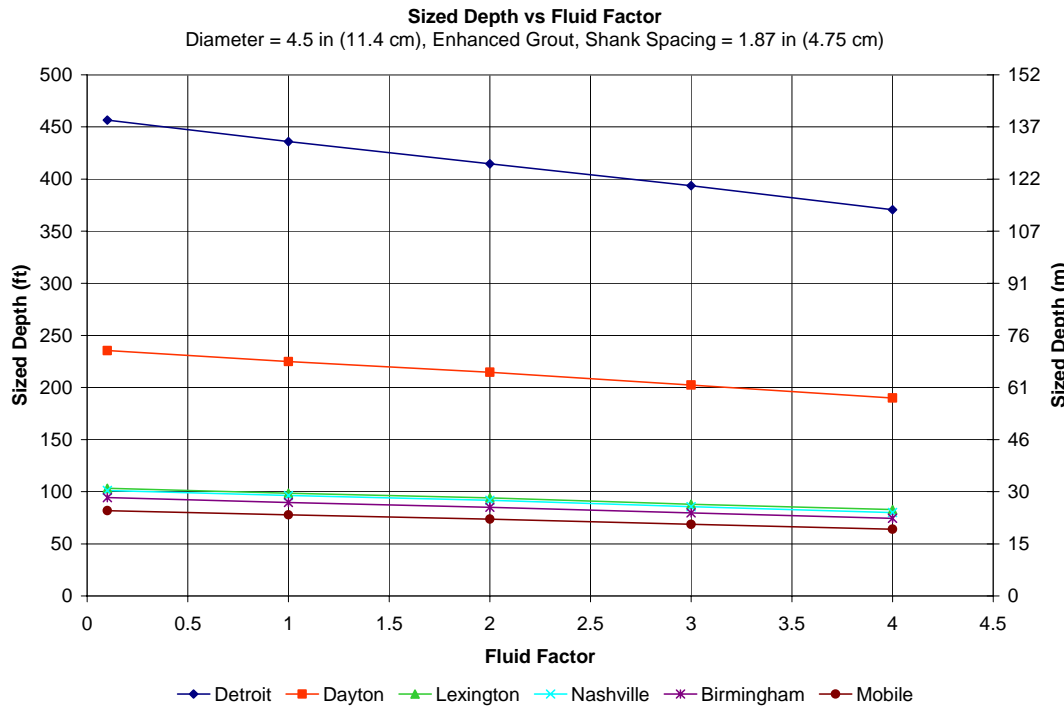
Figure 5-15 GLHEPRO Sized Depth vs Fluid Factor for Church Building with a Borehole Diameter of 4.5 in (11.4 cm), Enhanced Grout, and Shank Spacing of 1.87 in (4.75 cm)

149

Figures 5-16 and 5-17 show GLHEPRO sized borehole depths vs fluid factor for standard grout as well as two different shank spacing for the church building. The borehole depth percent reduction due to increasing fluid factor or shank spacing is also larger for standard grout vs thermally enhanced grout.

Sized Depth vs Fluid Factor
Diameter = 4.5 in (11.4 cm), Standard Bentonite Grout, Shank Spacing = 0.125 in (0.318 cm)
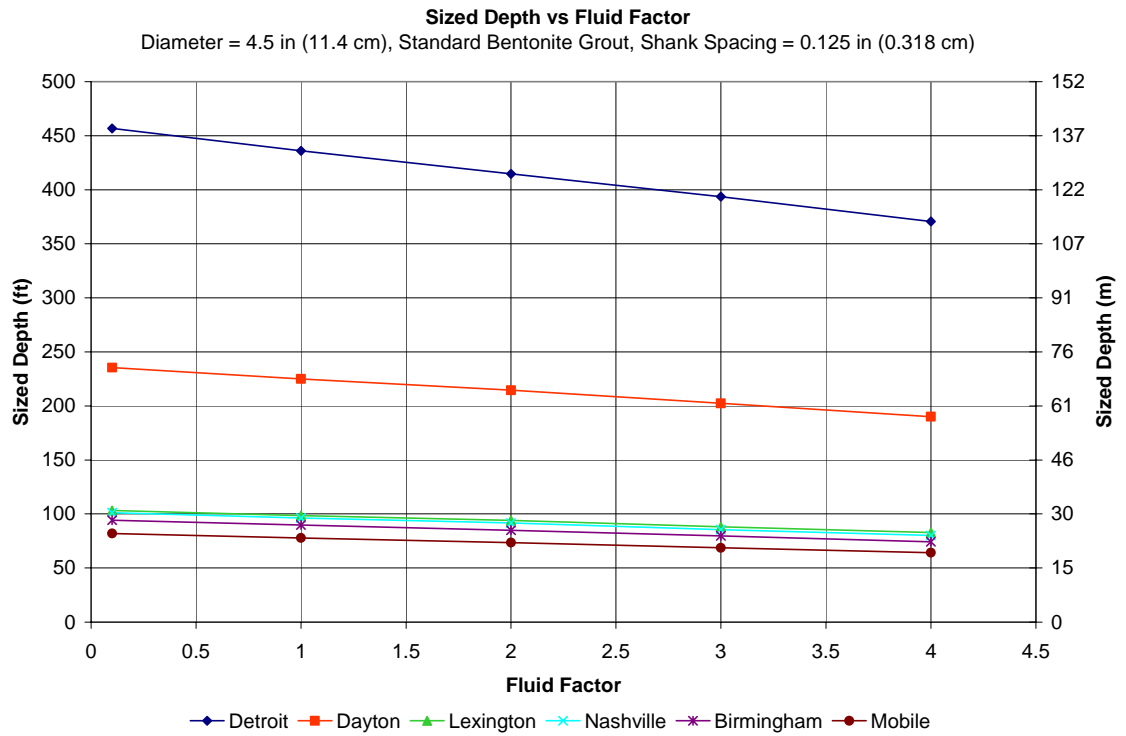
Figure 5-16 GLHEPRO Sized Depth vs Fluid Factor for a Church Building with a Borehole Diameter of 4.5 in (11.4 cm), Standard Bentonite Grout, and Shank Spacing of 0.125 in (0.318 cm)

Sized Depth vs Fluid Factor
Diameter = 4.5 in (11.4 cm), Standard Bentonite Grout, Shank Spacing = 1.87 in (4.75 cm)

Legend: Detroit — Dayton — Lexington — Nashville — Birmingham — Mobile
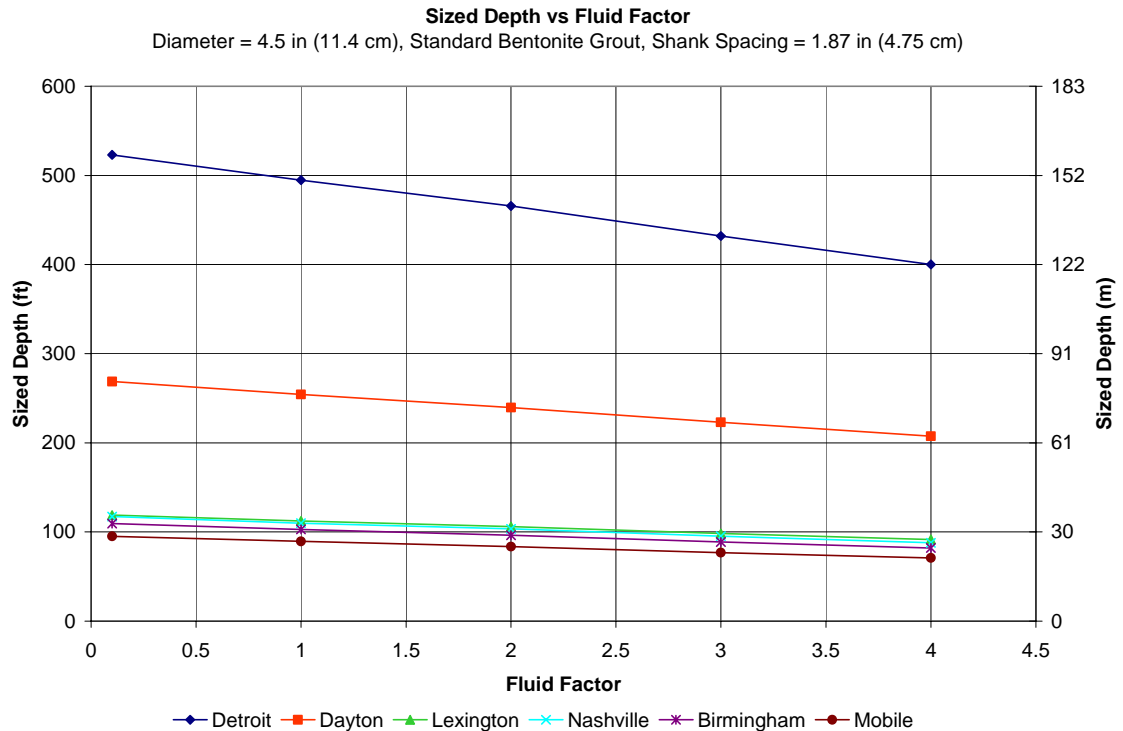
Figure 5-17 GLHEPRO Sized Depth vs Fluid Factor for Church Building with a Borehole Diameter of 4.5 in (11.4 cm), Standard Bentonite Grout, and Shank Spacing of 1.87 in (4.75 cm)

Figure 5-18 and 19 show GLHEPRO sized depths vs fluid factor for the non-peak- load-dominant small office building. The most noticeable difference that can be seen between the church and office building is that the fluid factor impacts the necessary depth of the borehole much less for the office building. The reduction in depth gained by varying shank spacing is also less for the small office building than for the church building.   Similarly, Figure 5-18 and 19 show that the reduction in depth due to changing grout type is also lessened for the small office building.

151

Sized Depth vs Fluid Factor
Diameter = 4.5 in (11.4 cm), Standard Grout, Shank Spacing= 0.125 in (0.318 cm)
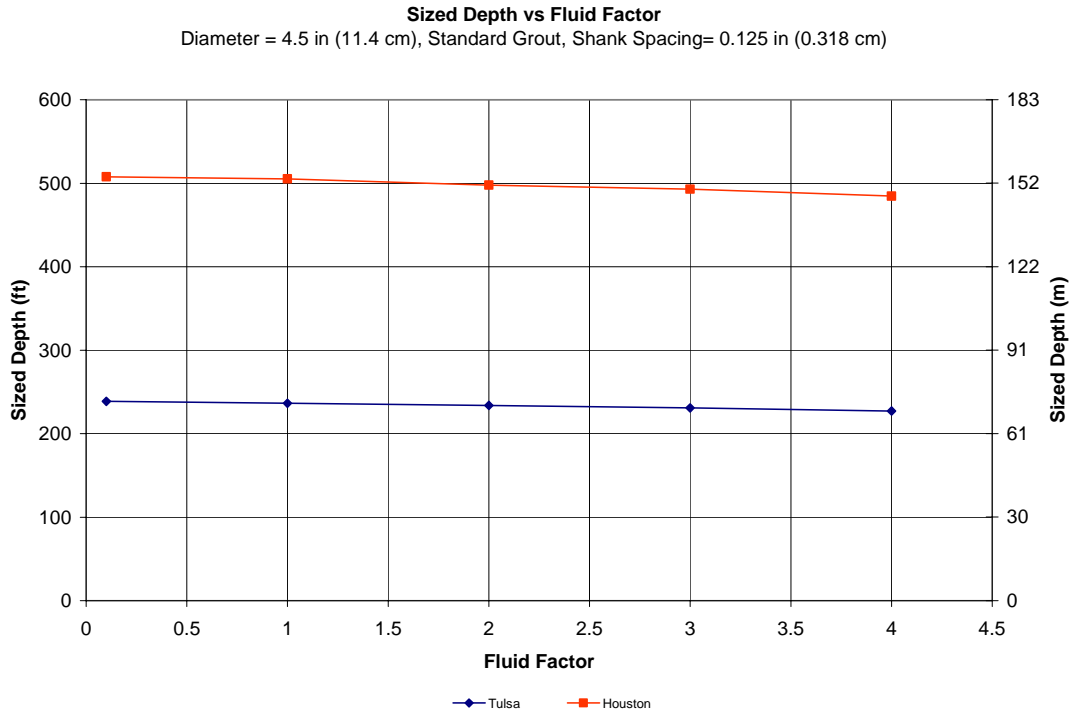
Figure 5-18 GLHEPRO Sized Depth vs Fluid Factor for Small Office Building with a Borehole Diameter of 4.5 in (11.4 cm), Standard Bentonite Grout, and Shank Spacing of 0.125 in (0.318 cm)

Sized Depth vs Fluid Factor
Diameter = 4.5 in (11.4 cm), Thermally Enhanced Grout, Shank Spacing = 1.87 in (4.75 cm)
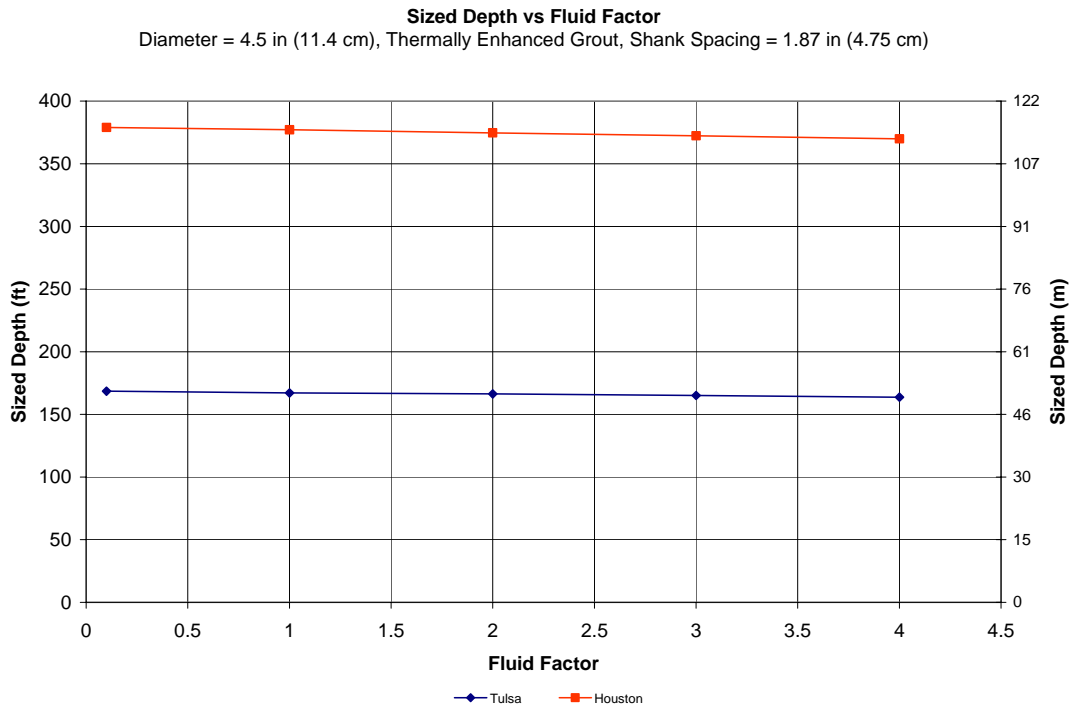
Figure 5-19 GLHEPRO Sized Depth vs Fluid Factor for Small Office Building with a Borehole Diameter of 4.5 in (11.4 cm), Thermally Enhanced Grout, and Shank Spacing of 1.87 in (4.75 cm)

152

Using the BFTM model, the peak-load-dominant church building has much more sensitivity to internal borehole properties, such as fluid factor, shank spacing and grout type, than the non-peak-load-dominant small office building. For non-peak-load-dominant systems, the effects of grout conductivity and shank spacing on the sized depths produced by GLHEPRO are significant. The impact of grout conductivity and shank spacing on non-peak-load-dominant system's sized depth is significant because of the sensitivity of borehole resistance to these parameters.

To more closely evaluate the fluid factors impact on the BFTM model results Tables 5-6 and 5-7 were created. Tables 5-6 and 5-7 show percent changes in sized depth when changing the fluid factor from 0.1 to 1, 1 to 2, 2 to 3, and 3 to 4 for different shank spacing, grout type, all ten church locations, and two office building locations. Table 5-8 and 5-9 show the actual required depths in feet for thermally and non-thermally enhanced grout.

Table 5-6 Percent Change in GLHEPRO Sizing Depth with Respect to Varying Fluid Factor for Peak-Load-Dominant and Non-Peak-Load-Dominant Buildings with Standard Grout

Borehole Diameter in and (cm)	Shank Spacing	Fluid Factor	Birming-ham	Dayton	Detroit	Lexing-ton	Nashville	Mobile	Birming-ham*	Lexing-ton*	Mobile*	Nashville*	Tulsa	Houston
4.5 (11.4)	A	(0.1-1)	11.2	10.1	10.3	10.9	11.6	11.3	11.5	11.8	10.6	12.0	0.9	0.5
4.5 (11.4)	A	(1-2)	12.4	11.5	11.2	11.7	12.1	12.7	12.0	11.5	12.1	12.4	1.1	1.5
4.5 (11.4)	A	(2-3)	12.3	11.5	12.0	11.0	12.2	12.7	12.6	12.0	12.4	13.0	1.3	1.0
4.5 (11.4)	A	(3-4)	11.6	10.5	10.8	10.5	11.6	12.1	11.5	11.2	11.6	12.0	1.6	1.7
4.5 (11.4)	B	(0.1-1)	9.5	9.2	8.6	9.4	9.8	9.7	9.4	9.2	9.5	10.1	0.8	0.7
4.5 (11.4)	B	(1-2)	10.1	9.1	9.8	8.7	9.3	10.4	9.9	9.4	10.1	9.8	0.8	0.8
4.5 (11.4)	B	(2-3)	11.2	10.1	10.4	10.2	11.0	11.5	11.3	11.2	10.5	11.9	1.2	1.1
4.5 (11.4)	B	(3-4)	10.6	9.5	9.5	9.6	11.0	11.0	10.2	9.9	10.8	11.1	1.4	1.2
4.5 (11.4)	C3	(0.1-1)	7.1	6.1	5.8	6.4	6.7	7.1	6.9	6.7	6.6	7.0	0.7	0.1
4.5 (11.4)	C3	(1-2)	6.9	6.2	7.0	6.6	7.1	7.3	7.0	7.0	6.9	7.4	0.8	0.8
4.5 (11.4)	C3	(2-3)	9.0	7.9	7.9	7.8	8.6	9.0	8.6	7.8	8.5	9.2	1.0	1.0
4.5 (11.4)	C3	(3-4)	8.7	7.7	8.1	7.9	8.2	8.9	8.6	8.8	8.6	9.1	1.1	1.1
4.5 (11.4)	C	(0.1-1)	6.1	5.6	5.6	5.8	6.5	6.3	6.0	6.1	6.2	6.7	0.7	0.3
4.5 (11.4)	C	(1-2)	6.8	5.9	6.0	5.8	6.1	6.8	6.6	5.9	6.1	6.7	0.8	0.6
4.5 (11.4)	C	(2-3)	8.3	7.2	7.5	7.4	8.2	8.3	8.1	7.8	8.4	8.4	0.9	1.2
4.5 (11.4)	C	(3-4)	8.1	7.3	7.7	7.2	8.0	8.2	8.0	7.7	7.7	8.2	0.9	0.7
6 (15.2)	A	(0.1-1)	13.3	11.4	11.4	11.5	12.2	13.6	12.6	12.3	12.1	13.0	1.1	1.1
6 (15.2)	A	(1-2)	14.9	13.9	14.2	14.0	16.0	15.2	15.1	15.2	14.2	15.7	1.6	1.0
6 (15.2)	A	(2-3)	16.1	14.7	14.8	14.9	14.9	16.5	15.5	15.1	16.2	16.6	1.8	1.8
6 (15.2)	A	(3-4)	14.6	13.7	13.6	13.6	15.2	15.3	15.1	14.2	14.5	15.3	2.1	2.1
6 (15.2)	B	(0.1-1)	11.5	11.0	11.1	11.5	11.9	12.0	11.3	10.9	12.6	11.6	1.1	1.3
6 (15.2)	B	(1-2)	10.1	8.9	9.0	8.5	9.3	10.0	9.8	9.3	8.5	9.9	1.1	0.9
6 (15.2)	B	(2-3)	11.8	10.8	11.2	10.9	12.5	12.3	12.1	11.7	11.7	13.0	1.5	1.3
6 (15.2)	B	(3-4)	11.9	10.6	10.7	10.6	11.6	12.6	11.4	11.4	11.9	12.1	1.6	1.4
6 (15.2)	C3	(0.1-1)	6.6	5.8	6.2	6.2	6.4	7.0	6.2	6.3	6.4	6.8	0.8	0.3
6 (15.2)	C3	(1-2)	6.7	6.0	6.0	5.9	6.7	6.6	6.6	6.1	6.7	7.1	0.8	0.6
6 (15.2)	C3	(2-3)	7.7	6.8	7.1	7.1	7.4	8.0	7.6	7.8	7.2	8.0	0.9	1.3
6 (15.2)	C3	(3-4)	7.8	7.0	6.2	6.8	7.9	8.2	7.8	7.4	7.7	8.2	0.9	0.6
6 (15.2)	C	(0.1-1)	6.3	5.5	6.0	5.3	6.0	6.3	6.0	5.3	5.8	6.1	0.8	0.5
6 (15.2)	C	(1-2)	6.3	5.4	5.7	5.6	6.2	6.2	6.0	6.1	6.3	6.7	0.8	0.6
6 (15.2)	C	(2-3)	7.1	6.4	6.0	6.1	6.7	7.4	7.2	7.1	6.4	7.2	0.9	0.7
6 (15.2)	C	(3-4)	7.5	6.6	6.3	7.3	7.6	7.6	7.4	7.2	7.1	7.8	0.9	0.7
7.5 (19.1)	A	(0.1-1)	12.5	11.9	11.3	10.8	11.8	13.0	12.0	11.9	11.8	12.6	1.6	1.9
7.5 (19.1)	A	(1-2)	15.6	13.5	13.6	13.9	14.8	15.7	15.3	15.9	14.4	16.1	2.1	1.8
7.5 (19.1)	A	(2-3)	17.2	16.0	16.3	16.7	17.5	17.8	17.2	15.6	17.7	17.5	2.4	2.1
7.5 (19.1)	A	(3-4)	17.8	16.1	16.3	15.8	17.6	18.2	17.5	17.4	16.8	18.7	2.4	2.3
7.5 (19.1)	B	(0.1-1)	12.1	11.2	11.5	11.0	11.1	12.1	11.7	11.2	12.5	12.2	1.6	1.1
7.5 (19.1)	B	(1-2)	10.2	9.1	9.6	9.2	10.2	10.8	10.2	10.0	9.5	10.6	1.4	1.5
7.5 (19.1)	B	(2-3)	9.9	9.1	9.2	9.0	9.8	10.2	9.9	9.4	9.8	10.4	1.4	1.2
7.5 (19.1)	B	(3-4)	10.1	9.0	9.0	9.0	10.1	10.6	9.7	9.6	10.0	10.5	1.3	1.2
7.5 (19.1)	C3	(0.1-1)	5.9	5.1	5.3	5.1	6.0	6.1	5.7	5.3	5.9	6.1	0.9	0.7
7.5 (19.1)	C3	(1-2)	5.6	4.9	5.0	4.9	5.2	5.4	5.2	5.3	5.4	5.8	0.7	0.6
7.5 (19.1)	C3	(2-3)	5.5	4.8	5.0	4.7	5.2	5.7	5.5	5.5	5.2	5.5	0.9	0.6
7.5 (19.1)	C3	(3-4)	5.7	5.3	4.4	5.4	5.9	5.9	5.7	5.4	5.5	6.2	0.9	0.7
7.5 (19.1)	C	(0.1-1)	5.4	4.8	4.9	4.8	5.1	5.8	5.1	5.2	5.3	5.8	0.9	0.6
7.5 (19.1)	C	(1-2)	4.9	4.2	4.5	4.2	4.4	5.0	5.0	5.0	4.6	5.0	0.7	0.6
7.5 (19.1)	C	(2-3)	4.9	4.6	3.8	4.9	5.2	5.1	4.5	4.4	4.7	5.2	0.9	0.5
7.5 (19.1)	C	(3-4)	5.3	4.6	4.5	4.9	5.2	5.4	5.5	5.3	4.7	5.3	0.8	0.7

Table 5-7 Percent Change in GLHEPRO Sizing Depth with Respect to Varying Fluid Factor for Peak-Load-Dominant and Non-Peak-Load-Dominant Buildings with Thermally Enhanced Grout

Borehole Diameter in and	Shank Spacing	Fluid Factor	Birmingham	Dayton	Detroit	Lexington	Nashville	Mobile	Birmingham*	Lexington*	Mobile*	Nashville*	Tulsa	Houston
4.5 (11.4)	A	(0.1-1)	6.6	5.6	5.6	5.6	6.2	6.5	6.0	6.2	5.8	6.5	0.7	0.6
4.5 (11.4)	A	(1-2)	7.8	7.1	7.5	7.1	7.7	8.1	8.1	7.4	7.5	7.9	0.8	0.2
4.5 (11.4)	A	(2-3)	8.9	7.9	7.7	8.1	8.7	9.4	8.6	8.7	8.6	9.5	1.0	1.0
4.5 (11.4)	A	(3-4)	9.0	7.8	8.3	8.4	8.9	9.0	8.9	8.6	9.0	9.2	1.1	1.1
4.5 (11.4)	B	(0.1-1)	5.8	5.4	5.5	5.3	6.0	6.0	5.8	5.6	5.6	6.1	0.7	0.5
4.5 (11.4)	B	(1-2)	7.0	6.0	5.9	6.0	6.6	6.9	6.5	6.3	6.3	7.1	0.7	0.9
4.5 (11.4)	B	(2-3)	7.9	7.1	7.4	7.4	7.9	8.2	7.9	7.8	8.3	8.3	0.9	0.9
4.5 (11.4)	B	(3-4)	8.5	7.3	7.0	7.1	7.6	8.5	8.2	8.0	7.7	8.4	0.9	0.6
4.5 (11.4)	C3	(0.1-1)	5.0	4.6	4.7	4.9	4.9	4.9	4.8	5.3	4.9	5.4	0.9	0.6
4.5 (11.4)	C3	(1-2)	5.7	4.8	5.1	4.5	5.3	5.9	5.6	5.3	5.4	5.9	0.9	0.5
4.5 (11.4)	C3	(2-3)	6.8	6.2	5.4	6.4	7.0	6.9	6.6	6.6	6.7	7.0	0.6	0.7
4.5 (11.4)	C3	(3-4)	7.0	6.2	6.1	6.6	6.5	7.2	7.1	6.7	6.4	7.1	0.9	0.7
4.5 (11.4)	C	(0.1-1)	5.0	4.6	4.6	4.6	5.0	5.1	4.9	5.0	5.1	5.1	0.8	0.5
4.5 (11.4)	C	(1-2)	5.6	4.7	5.0	4.7	4.9	5.5	5.4	5.5	5.1	6.0	0.4	0.6
4.5 (11.4)	C	(2-3)	6.5	5.8	5.2	6.6	6.9	6.9	6.5	6.1	6.3	6.8	0.8	0.6
4.5 (11.4)	C	(3-4)	7.0	6.3	6.0	6.1	6.7	6.9	6.9	6.8	6.6	7.0	0.9	0.7
6 (15.2)	A	(0.1-1)	6.0	5.3	5.2	5.3	5.6	5.6	5.9	5.7	5.2	5.9	0.7	0.6
6 (15.2)	A	(1-2)	7.4	6.7	6.9	7.0	7.6	8.2	7.4	7.6	7.3	8.0	0.9	0.7
6 (15.2)	A	(2-3)	9.4	8.5	8.0	8.5	9.2	9.5	9.1	8.8	9.0	9.6	1.0	0.9
6 (15.2)	A	(3-4)	9.8	8.8	9.5	9.0	9.5	10.0	9.9	9.0	9.5	10.3	1.0	1.0
6 (15.2)	B	(0.1-1)	5.7	5.4	5.7	5.7	5.9	6.0	5.8	5.9	5.9	6.2	0.8	0.8
6 (15.2)	B	(1-2)	6.1	5.3	5.2	5.0	5.7	6.1	5.7	5.3	5.6	5.9	0.7	0.8
6 (15.2)	B	(2-3)	7.7	6.8	7.1	6.8	7.6	7.8	7.5	7.7	7.8	8.2	0.8	0.6
6 (15.2)	B	(3-4)	8.1	7.2	6.8	7.4	7.8	8.3	8.0	7.4	7.6	7.9	1.1	0.8
6 (15.2)	C3	(0.1-1)	4.5	4.2	3.7	4.4	4.6	4.7	4.5	3.9	4.7	4.6	0.7	0.5
6 (15.2)	C3	(1-2)	4.7	4.2	3.9	4.8	5.1	4.9	4.9	5.2	4.6	5.1	0.7	0.5
6 (15.2)	C3	(2-3)	5.8	4.9	5.0	5.1	5.4	5.8	5.4	5.2	5.5	5.8	0.8	0.6
6 (15.2)	C3	(3-4)	5.9	5.4	5.4	5.6	6.1	6.0	5.7	5.5	5.7	6.1	0.8	0.6
6 (15.2)	C	(0.1-1)	4.5	4.2	4.5	4.4	5.0	4.4	4.5	4.0	4.5	4.6	0.7	0.5
6 (15.2)	C	(1-2)	5.0	4.2	3.0	4.7	4.7	5.1	4.8	5.1	4.5	5.0	0.7	0.5
6 (15.2)	C	(2-3)	5.4	4.8	5.0	4.5	5.3	5.8	5.4	5.1	5.5	5.8	0.8	0.6
6 (15.2)	C	(3-4)	5.9	5.3	5.4	6.0	6.1	6.1	5.9	5.5	5.7	6.0	0.8	0.7
7.5 (19.1)	A	(0.1-1)	4.7	4.5	5.0	4.0	4.3	5.0	4.6	4.4	5.5	4.6	0.8	0.7
7.5 (19.1)	A	(1-2)	6.6	5.9	5.8	5.8	6.1	6.2	6.4	6.2	5.8	6.5	1.0	0.8
7.5 (19.1)	A	(2-3)	7.9	6.9	7.3	7.4	7.8	8.4	8.0	7.8	7.5	8.1	1.2	0.9
7.5 (19.1)	A	(3-4)	9.2	8.3	8.3	8.4	9.4	9.4	9.0	8.7	8.8	9.9	1.2	1.1
7.5 (19.1)	B	(0.1-1)	5.7	4.8	4.7	4.9	5.5	5.4	5.0	5.0	5.0	5.7	0.8	0.7
7.5 (19.1)	B	(1-2)	5.3	4.6	4.8	4.8	5.0	5.2	5.4	5.0	5.5	5.2	0.8	0.6
7.5 (19.1)	B	(2-3)	5.7	5.0	5.1	4.9	5.3	5.8	5.5	5.7	5.5	5.9	0.7	0.6
7.5 (19.1)	B	(3-4)	5.9	5.3	5.2	5.1	5.6	6.2	5.8	5.6	5.2	5.9	0.9	0.7
7.5 (19.1)	C3	(0.1-1)	4.3	3.6	3.4	3.8	3.9	4.0	4.1	3.9	3.3	4.4	0.6	0.6
7.5 (19.1)	C3	(1-2)	3.8	3.3	3.5	3.5	3.6	3.9	3.7	3.6	4.3	4.0	0.6	0.5
7.5 (19.1)	C3	(2-3)	3.9	3.7	3.5	3.5	4.1	4.3	3.8	3.7	3.8	3.9	0.4	0.5
7.5 (19.1)	C3	(3-4)	4.3	3.8	3.9	4.1	4.2	4.3	4.2	4.1	4.1	4.5	0.9	0.5
7.5 (19.1)	C	(0.1-1)	3.7	3.3	3.4	3.5	3.5	3.9	3.7	3.6	3.6	4.0	0.9	0.5
7.5 (19.1)	C	(1-2)	3.7	3.5	3.5	3.2	4.1	4.0	3.6	3.4	3.9	3.6	0.6	0.5
7.5 (19.1)	C	(2-3)	4.0	3.4	3.5	4.0	3.8	3.7	3.7	3.7	3.7	4.2	0.6	0.5
7.5 (19.1)	C	(3-4)	4.2	3.7	3.8	3.6	4.0	4.3	4.1	3.9	3.9	4.2	0.7	0.5

155

Table 5-8 Required Depth (ft) for Thermally Enhanced Grout, Calculated with GLHEPRO

Borehole Diameter in and (cm)	Shank Spacing	Fluid Factor	Birming-ham	Dayton	Detroit	Lexing-ton	Nashville	Mobile	Birming-ham*	Lexing-ton*	Mobile*	Nashville*	Tulsa	Houston
4.5 (11.4)	A	0.1	107	293	571	130	129	105	120	119	141	118	194	424
4.5 (11.4)	A	1	100	277	540	123	121	99	113	111	133	111	193	421
4.5 (11.4)	A	2	92	258	501	114	112	91	104	104	123	102	191	421
4.5 (11.4)	A	3	85	238	463	106	103	83	96	95	113	93	189	417
4.5 (11.4)	A	4	77	220	426	97	94	76	88	87	103	85	187	412
4.5 (11.4)	B	0.1	98	270	526	119	118	96	110	108	129	108	185	408
4.5 (11.4)	B	1	92	256	498	113	111	90	104	103	122	102	183	406
4.5 (11.4)	B	2	86	241	469	107	104	84	97	96	115	95	182	402
4.5 (11.4)	B	3	79	225	436	99	96	77	90	89	105	87	180	398
4.5 (11.4)	B	4	73	209	406	92	89	71	83	82	98	80	179	396
4.5 (11.4)	C3	0.1	85	239	463	105	103	83	96	95	113	94	170	382
4.5 (11.4)	C3	1	81	228	442	100	98	79	91	90	107	89	169	379
4.5 (11.4)	C3	2	76	217	420	95	93	75	86	85	102	84	167	377
4.5 (11.4)	C3	3	71	204	398	89	87	70	81	80	95	78	166	375
4.5 (11.4)	C3	4	66	192	374	84	81	65	75	75	89	73	165	372
4.5 (11.4)	C	0.1	84	235	457	103	101	82	94	94	111	93	168	379
4.5 (11.4)	C	1	80	225	436	99	96	78	90	89	106	88	167	377
4.5 (11.4)	C	2	75	215	415	94	92	74	85	84	100	83	166	375
4.5 (11.4)	C	3	71	202	394	88	86	69	80	79	94	77	165	372
4.5 (11.4)	C	4	66	190	371	83	80	64	74	74	88	72	164	370
6 (15.2)	A	0.1	113	308	601	137	136	111	127	126	148	125	200	436
6 (15.2)	A	1	106	292	570	130	128	105	120	119	141	118	199	433
6 (15.2)	A	2	98	273	532	121	119	97	111	110	131	109	197	430
6 (15.2)	A	3	90	251	491	112	108	88	102	101	119	99	195	426
6 (15.2)	A	4	81	230	447	102	99	79	92	92	109	89	193	422
6 (15.2)	B	0.1	94	263	513	116	115	93	106	106	126	105	184	406
6 (15.2)	B	1	89	249	484	110	108	87	101	100	118	99	183	403
6 (15.2)	B	2	84	236	459	104	102	82	95	94	112	93	181	399
6 (15.2)	B	3	78	221	428	98	95	76	88	87	104	86	180	397
6 (15.2)	B	4	71	205	400	91	87	70	81	81	96	79	178	394
6 (15.2)	C3	0.1	76	218	421	96	93	75	87	86	102	84	162	367
6 (15.2)	C3	1	73	209	406	91	89	72	83	82	98	80	161	365
6 (15.2)	C3	2	70	200	391	87	85	68	79	78	93	76	160	363
6 (15.2)	C3	3	66	191	371	83	80	64	75	74	88	72	158	361
6 (15.2)	C3	4	62	181	352	78	75	61	71	70	83	68	157	359
6 (15.2)	C	0.1	76	216	418	95	93	74	86	85	101	84	161	366
6 (15.2)	C	1	73	207	400	91	88	71	82	82	97	80	160	364
6 (15.2)	C	2	69	199	388	87	84	68	78	78	93	76	159	362
6 (15.2)	C	3	65	189	369	83	80	64	74	74	88	72	158	360
6 (15.2)	C	4	62	179	350	78	75	60	70	70	83	67	156	357
7.5 (19.1)	A	0.1	117	321	630	143	141	116	133	131	156	130	205	445
7.5 (19.1)	A	1	112	306	599	137	135	110	127	125	148	124	204	442
7.5 (19.1)	A	2	105	289	565	129	127	104	119	118	139	116	202	438
7.5 (19.1)	A	3	97	269	526	120	117	95	110	109	129	107	199	434
7.5 (19.1)	A	4	88	248	484	110	107	87	100	100	118	97	197	430
7.5 (19.1)	B	0.1	92	256	498	113	111	90	104	103	122	102	182	402
7.5 (19.1)	B	1	87	244	475	108	105	85	99	98	116	96	181	399
7.5 (19.1)	B	2	82	233	453	103	100	81	94	93	110	91	179	397
7.5 (19.1)	B	3	78	221	430	98	95	76	89	88	104	86	178	394
7.5 (19.1)	B	4	73	210	408	93	90	72	84	83	99	81	177	392
7.5 (19.1)	C3	0.1	71	204	399	89	87	70	81	80	95	79	147	358
7.5 (19.1)	C3	1	68	197	385	86	83	67	78	77	92	75	146	356
7.5 (19.1)	C3	2	66	191	372	83	80	65	75	74	88	72	145	354
7.5 (19.1)	C3	3	63	184	359	80	77	62	72	72	85	70	145	352
7.5 (19.1)	C3	4	61	177	346	77	74	59	69	69	82	67	143	350
7.5 (19.1)	C	0.1	69	199	389	87	84	68	79	78	93	76	145	353
7.5 (19.1)	C	1	67	193	376	84	81	65	76	75	90	73	144	351
7.5 (19.1)	C	2	64	186	363	81	78	63	73	73	86	71	143	350
7.5 (19.1)	C	3	62	180	351	78	75	60	70	70	83	68	142	348
7.5 (19.1)	C	4	59	173	337	75	72	58	68	67	80	65	141	346

Table 5-9 Required Depth (ft) for Standard Grout, Calculated with GLHEPRO

Borehole Diameter in and (cm)	Shank Spacing	Fluid Factor	Birming-ham	Dayton	Detroit	Lexing-ton	Nashville	Mobile	Birming-ham*	Lexing-ton*	Mobile*	Nashville*	Tulsa	Houston
4.5 (11.4)	A	0.1	145	390	765	177	175	143	164	162	192	162	239	508
4.5 (11.4)	A	1	130	352	690	158	156	128	146	144	173	144	236	505
4.5 (11.4)	A	2	114	314	617	141	138	113	130	129	153	127	234	498
4.5 (11.4)	A	3	101	280	547	126	122	99	114	114	135	112	231	493
4.5 (11.4)	A	4	90	252	491	114	109	88	102	102	120	99	227	485
4.5 (11.4)	B	0.1	129	351	688	157	156	128	146	144	172	144	222	476
4.5 (11.4)	B	1	117	320	631	143	141	116	133	131	156	130	220	473
4.5 (11.4)	B	2	106	292	572	131	128	104	120	119	141	118	219	469
4.5 (11.4)	B	3	95	264	515	118	115	93	107	107	127	105	216	464
4.5 (11.4)	B	4	85	241	468	108	103	83	97	96	114	94	213	459
4.5 (11.4)	C3	0.1	103	283	553	126	124	101	116	115	136	114	192	421
4.5 (11.4)	C3	1	96	266	522	118	116	94	108	107	128	106	191	420
4.5 (11.4)	C3	2	89	250	486	111	108	88	101	100	119	99	189	417
4.5 (11.4)	C3	3	82	231	450	102	99	80	93	92	109	90	188	413
4.5 (11.4)	C3	4	75	214	415	94	92	73	85	85	100	82	186	408
4.5 (11.4)	C	0.1	97	269	523	119	117	95	109	108	129	107	186	408
4.5 (11.4)	C	1	91	254	495	112	110	89	103	102	121	100	184	407
4.5 (11.4)	C	2	85	240	466	106	103	83	96	96	114	94	183	405
4.5 (11.4)	C	3	78	223	432	98	95	77	89	89	105	86	181	400
4.5 (11.4)	C	4	72	207	400	91	88	71	82	82	97	80	180	397
6 (15.2)	A	0.1	163	432	850	197	195	162	184	182	214	182	261	553
6 (15.2)	A	1	143	385	758	176	173	141	162	161	190	159	258	548
6 (15.2)	A	2	123	335	658	153	147	121	139	138	164	136	254	542
6 (15.2)	A	3	105	290	567	132	127	103	119	119	140	115	249	532
6 (15.2)	A	4	90	253	495	115	109	88	102	103	121	99	244	521
6 (15.2)	B	0.1	128	347	682	157	154	126	144	142	170	141	231	494
6 (15.2)	B	1	114	311	610	140	137	112	129	128	150	126	229	488
6 (15.2)	B	2	103	284	557	128	125	101	117	116	137	114	226	483
6 (15.2)	B	3	91	255	498	115	110	89	103	103	122	100	223	477
6 (15.2)	B	4	81	229	447	103	98	79	92	92	108	89	219	470
6 (15.2)	C3	0.1	94	261	510	116	114	92	106	105	125	104	186	408
6 (15.2)	C3	1	88	246	479	109	106	86	100	99	117	97	184	407
6 (15.2)	C3	2	82	232	451	103	100	81	93	93	110	90	183	405
6 (15.2)	C3	3	76	217	420	96	92	74	86	86	102	84	181	399
6 (15.2)	C3	4	70	202	395	89	85	69	80	80	95	77	179	397
6 (15.2)	C	0.1	89	250	489	110	108	88	101	100	119	99	180	398
6 (15.2)	C	1	84	236	460	105	102	82	95	95	112	93	179	396
6 (15.2)	C	2	79	224	435	99	96	77	90	89	105	87	177	393
6 (15.2)	C	3	73	210	409	93	89	72	83	83	99	81	176	391
6 (15.2)	C	4	68	197	384	86	83	67	77	77	92	75	174	388
7.5 (19.1)	A	0.1	176	465	910	212	210	175	199	197	231	196	276	585
7.5 (19.1)	A	1	155	413	813	190	187	153	176	175	205	173	272	574
7.5 (19.1)	A	2	133	361	710	166	161	131	151	149	177	147	266	564
7.5 (19.1)	A	3	112	308	603	140	135	110	127	127	149	123	260	552
7.5 (19.1)	A	4	94	262	512	120	113	91	107	107	126	102	254	539
7.5 (19.1)	B	0.1	124	337	664	152	148	122	140	138	165	137	235	499
7.5 (19.1)	B	1	109	301	592	136	132	108	124	124	146	121	231	493
7.5 (19.1)	B	2	99	275	537	124	119	97	112	112	132	109	228	486
7.5 (19.1)	B	3	89	251	490	114	108	88	102	102	120	98	225	481
7.5 (19.1)	B	4	81	229	448	104	98	79	92	93	108	88	222	475
7.5 (19.1)	C3	0.1	88	247	481	109	107	87	100	99	118	97	181	400
7.5 (19.1)	C3	1	83	235	456	104	100	81	94	94	111	92	179	397
7.5 (19.1)	C3	2	79	223	434	99	95	77	90	89	105	86	178	395
7.5 (19.1)	C3	3	74	213	413	94	91	73	85	84	100	82	177	393
7.5 (19.1)	C3	4	70	202	395	89	85	69	80	80	95	77	175	390
7.5 (19.1)	C	0.1	83	234	455	103	100	82	94	94	111	92	174	388
7.5 (19.1)	C	1	79	223	433	99	95	77	89	89	105	86	173	386
7.5 (19.1)	C	2	75	214	414	95	91	73	85	84	100	82	172	383
7.5 (19.1)	C	3	71	204	399	90	87	70	81	81	96	78	170	381
7.5 (19.1)	C	4	68	195	381	86	82	66	77	77	91	74	169	379

As can be seen in Table 5-6 and 5-7, the 1x fluid factor significantly influences the sized borehole depth versus the 0.1 x fluid factor. The improvement going from 0.1 to 1 x fluid factor for all church locations was a minimum of 3.3% for thermally enhanced grout. The improvement was as large as 13.6% for a system with standard grout. The improvement for changing the fluid factor from 1 to 2 ranged between 3.0% for a system with enhanced grout to 16.1% for a system with standard grout. Similar improvements are shown when increasing the fluid factor from 2 to 3 and 3 to 4. Accounting for the fluid thermal mass in the borehole and connecting pipes using the BFTM model, versus using the line source, which does not account for the fluid, produces an increase in accuracy approximately equivalent to that of changing fluid factor from 0.1 to 2. Table 5-6 and 5-7 shows that this can be between a 6 and 30 percent accuracy improvement between the BFTM and the line source models. Also, for a peak-load-dominant system adding a storage tank that increases the fluid factor from 2 to 4, will allow 30 percent reduction to the necessary borehole depth, if regular grout is used.

The reduction in depth of the borehole field for the small office and church simulations, shown in Table 5-6 and 5-7, does not change greatly with location.

The percent decrease in sized depth for the non-peak-load-dominant church building is a maximum of 1.9% going from 1 to 2 x fluid factor and a minimum of 0.3% going from 0.1 to 1 x fluid factor. The lack of improvement in the sizing function for the small office building regarding the fluid thermal mass model is due to a peak duration of 8 hours. The office building, which is represented by the Tulsa and Houston columns of Table 5-7, show that the BFTM model has a minor impact on systems that have peak

158

loads of 8 hours. However for systems that have very short peak loads such as the church building example the borehole fluid thermal mass model can have a large impact.

5.3.2 U-Tube Shank Spacing Results

The shank spacing primarily affects the steady state borehole resistance. Figure 5-20 shows borehole resistance as a function of shank spacing. The relationship between shank spacing and borehole resistance for standard bentonite is very linear however for thermally enhanced grout, which is not shown here, the relationship is less linear.

Borehole Resistance vs Shank Spacing
Standard Bentonite Grout, Diameter 4.5 in (11.4 cm)
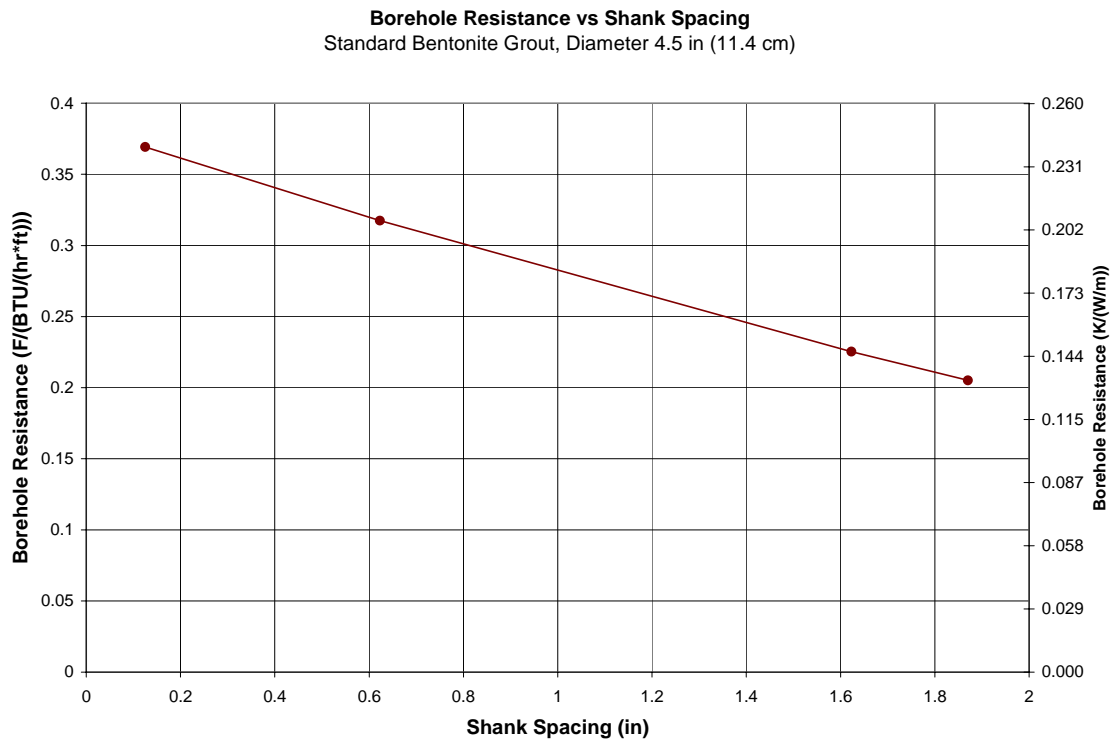
Figure 5-20 Borehole Resistance vs Shank Spacing for Church Building Using Standard Bentonite Grout and a Diameter of 4.5 in (11.4 cm)

Figures 5-21 and 5-22 show church GLHEPRO sized borehole depths as a function of shank spacing for standard grout as well as fluid factors of 1 and 2 respectively. Figures 5-23 and 5-24 show office building GLHEPRO sized borehole depths as a function of shank spacing for standard grout as well as fluid factors of 1 and 2

respectively. As can be seen the change in borehole resistance caused by the change in shank spacing has a large impact on the overall sized depth of the borehole system for both the peak-load-dominant church building simulations and the non-peak-load-dominant office building simulations.

Sized Depth vs Shank Spacing
Standard Bentonite Grout, Diameter 4.5 in (11.4 cm), Fluid Factor = 1
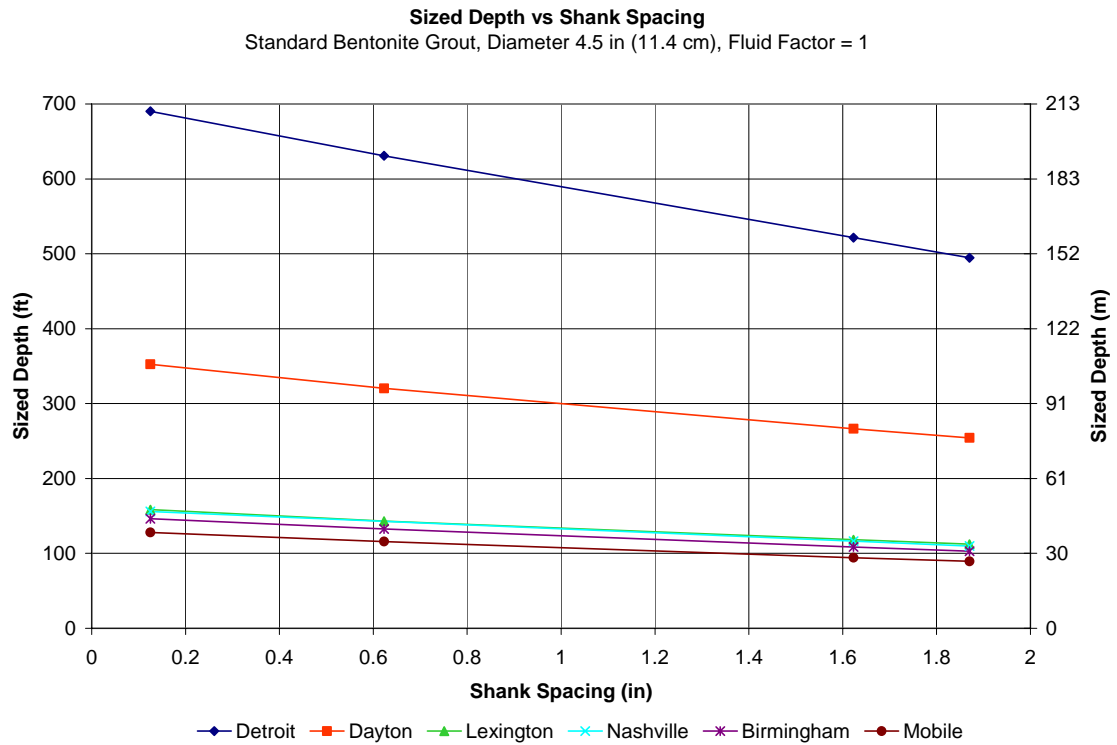
Figure 5-21 Sized Borehole Depth vs Shank Spacing for Church Building Using Standard Bentonite Grout, Diameter of 4.5 in (11.4 cm), Fluid Factor of 1
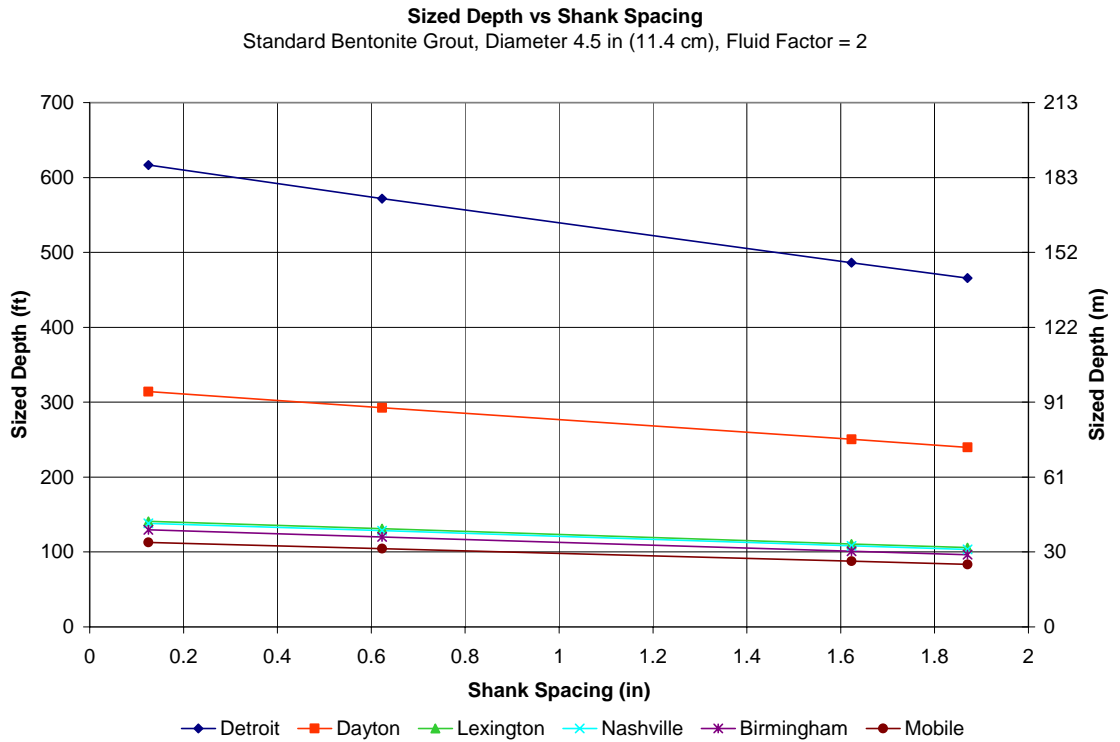
Figure 5-22 Sized Borehole Depth vs Shank Spacing for Church Building Using Standard Bentonite Grout, Diameter of 4.5 in (11.4 cm), Fluid Factor of 2
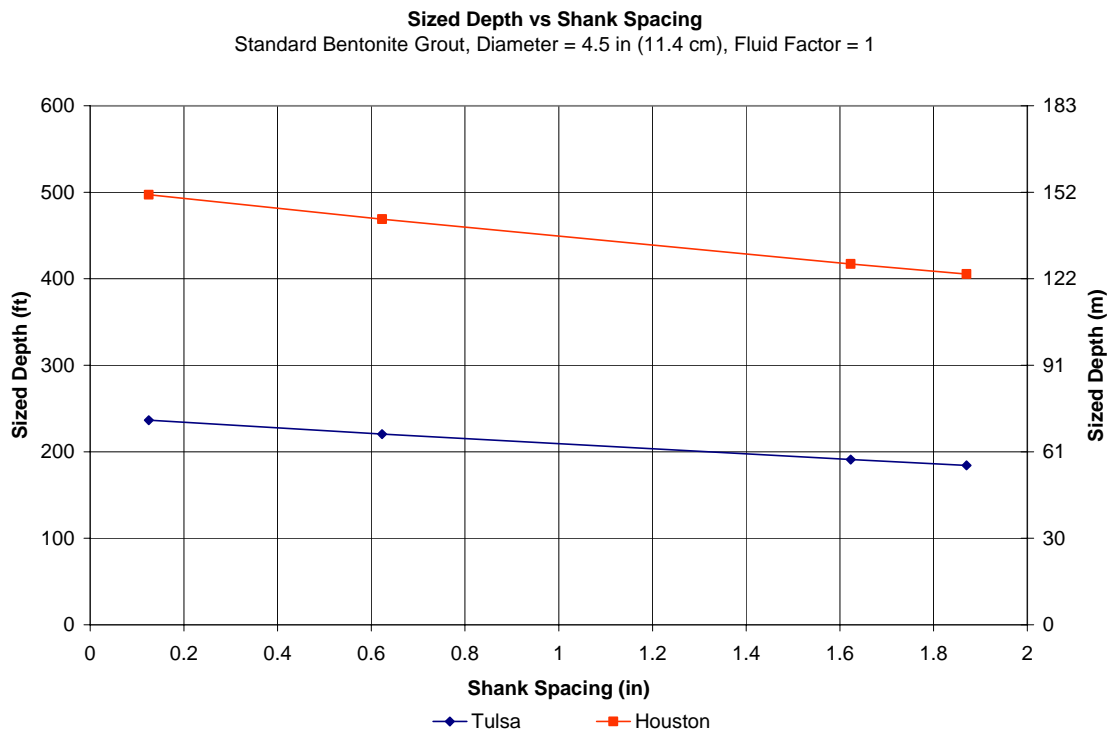
Figure 5-23 Sized Borehole Depth vs Shank Spacing for Office Building Using Standard Bentonite Grout, Diameter of 4.5 in (11.4 cm), Fluid Factor of 1

Sized Depth vs Shank Spacing
Standard Bentonite Grout, Diameter = 4.5 in (11.4 cm), Fluid Factor = 2
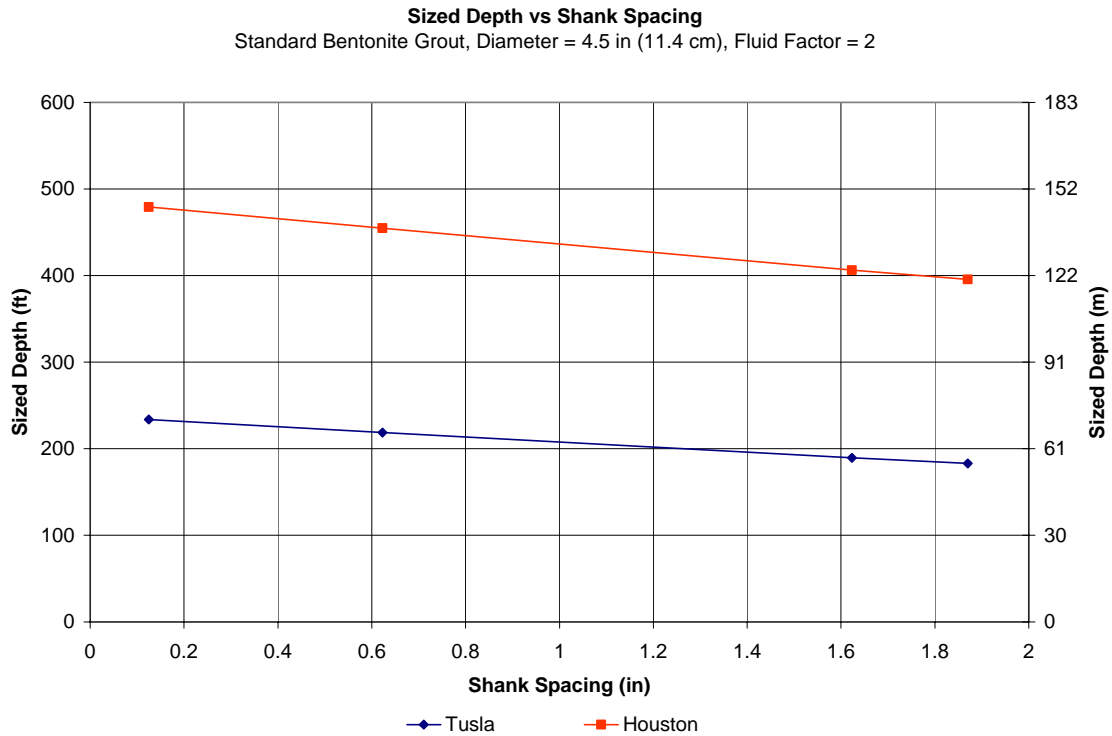
Figure 5-24 Sized Borehole Depth vs Shank Spacing for Office Building Using Standard Bentonite Grout, Diameter of 4.5 in (11.4 cm), Fluid Factor of 2

Table 5-10 provides a comparison between the percent change in borehole resistance and how it relates to the percent change in GLHEPRO sized depth as shank spacing is changed. Shank spacing has a very large impact on borehole depth. The percent difference from A to C3 for a borehole system with 19.1 cm (7.5 in) boreholes, standard grout and fluid factor equal to 1, produces between 55.0% and 61.4% difference in depth for the church building. The percent difference for the office building for the same borehole configuration is between 41.7% and 31.5% difference. The percentages decrease for thermally enhanced grout and small borehole diameters.

Table 5-10 Percent Change in GLHEPRO Sizing Depth for Changes in Borehole Shank Spacing

Borehole Diameter in and (cm)	Shank Spacing	Fluid Factor	Birming-ham	Dayton	Detroit	Lexing-ton	Nashville	Mobile	Birming-ham*	Lexing-ton*	Mobile*	Nashville*	Tulsa	Houston
						Regular Grout								
4.5 (11.4)	(A-C3)	0.1	33.9	31.7	32.2	33.5	34.1	34.5	34.2	34.5	33.9	35.0	21.4	18.8
4.5 (11.4)	(A-C3)	1	29.9	27.8	27.8	29.1	29.3	30.4	29.7	29.5	29.9	30.0	21.3	18.4
4.5 (11.4)	(A-C3)	2	24.5	22.6	23.6	24.1	24.3	25.1	24.8	25.1	24.9	25.1	21.0	17.7
4.5 (11.4)	(A-C3)	3	21.2	19.0	19.5	20.9	20.7	21.4	20.9	21.0	21.0	21.3	20.7	17.7
4.5 (11.4)	(A-C3)	4	18.3	16.2	16.9	18.3	17.2	18.2	18.0	18.5	18.0	18.3	20.1	17.1
6 (15.2)	(A-C3)	0.1	54.0	49.3	49.9	52.0	52.9	54.4	53.8	53.7	52.5	54.4	33.7	30.2
6 (15.2)	(A-C3)	1	47.7	44.0	45.1	47.0	47.5	48.2	47.8	48.1	47.1	48.5	33.4	29.4
6 (15.2)	(A-C3)	2	39.9	36.4	37.2	39.2	38.6	40.0	39.6	39.4	40.0	40.3	32.6	29.0
6 (15.2)	(A-C3)	3	31.7	28.7	29.7	31.6	31.4	31.7	31.9	32.2	31.2	31.9	31.7	28.5
6 (15.2)	(A-C3)	4	25.0	22.2	22.4	25.0	24.2	24.7	24.7	25.6	24.5	24.9	30.6	27.0
7.5 (19.1)	(A-C3)	0.1	66.6	61.3	61.7	64.0	65.4	67.4	66.2	66.1	64.9	67.3	41.7	37.5
7.5 (19.1)	(A-C3)	1	60.7	55.1	56.2	58.8	60.1	61.2	60.5	60.2	59.5	61.4	41.0	36.4
7.5 (19.1)	(A-C3)	2	51.4	47.1	48.2	50.5	51.2	51.7	51.2	50.4	51.2	52.0	39.7	35.2
7.5 (19.1)	(A-C3)	3	40.3	36.3	37.4	39.1	39.4	40.2	40.0	40.7	39.2	40.5	38.2	33.7
7.5 (19.1)	(A-C3)	4	28.5	25.8	25.7	29.0	28.0	28.2	28.6	29.1	28.2	28.2	36.7	32.2
4.5 (11.4)	(B-C3)	0.1	22.7	21.5	21.8	22.0	22.4	23.3	22.5	22.4	23.0	23.0	14.4	12.4
4.5 (11.4)	(B-C3)	1	20.3	18.4	19.0	19.1	19.3	20.6	20.1	19.9	20.1	20.0	14.3	11.8
4.5 (11.4)	(B-C3)	2	17.0	15.5	16.1	17.0	17.1	17.5	17.3	17.5	16.9	17.6	14.3	11.8
4.5 (11.4)	(B-C3)	3	14.8	13.3	13.6	14.6	14.7	14.9	14.7	14.2	14.9	14.9	14.1	11.7
4.5 (11.4)	(B-C3)	4	13.0	11.6	12.2	13.0	11.9	12.9	13.0	13.1	12.7	12.9	13.7	11.6
6 (15.2)	(B-C3)	0.1	30.5	28.2	28.8	30.0	30.4	30.8	30.5	30.0	30.3	30.5	21.8	18.9
6 (15.2)	(B-C3)	1	25.7	23.1	23.9	24.7	25.0	25.9	25.5	25.6	24.2	25.7	21.6	18.0
6 (15.2)	(B-C3)	2	22.3	20.2	20.9	22.1	22.4	22.5	22.4	22.5	22.4	22.9	21.3	17.7
6 (15.2)	(B-C3)	3	18.2	16.2	16.9	18.3	17.4	18.2	17.9	18.5	17.9	18.0	20.7	17.7
6 (15.2)	(B-C3)	4	14.2	12.7	12.4	14.6	13.7	13.9	14.3	14.5	13.6	14.1	20.0	17.0
7.5 (19.1)	(B-C3)	0.1	33.5	30.7	32.0	32.7	32.2	33.8	33.3	33.2	33.5	33.6	25.8	22.0
7.5 (19.1)	(B-C3)	1	27.4	24.8	25.8	27.0	27.3	28.0	27.4	27.5	27.0	27.6	25.2	21.6
7.5 (19.1)	(B-C3)	2	22.9	20.6	21.3	22.8	22.3	22.7	22.5	22.9	22.9	23.0	24.5	20.8
7.5 (19.1)	(B-C3)	3	18.4	16.3	17.1	18.6	17.8	18.2	18.2	19.0	18.3	18.0	24.0	20.2
7.5 (19.1)	(B-C3)	4	14.1	12.7	12.5	15.0	13.5	13.6	14.3	14.9	13.7	13.7	23.5	19.7
						Thermally Enhanced Grout								
4.5 (11.4)	(A-C3)	0.1	22.9	20.4	20.9	21.5	22.2	23.4	22.6	22.2	21.9	22.8	13.1	10.5
4.5 (11.4)	(A-C3)	1	21.3	19.4	19.9	20.8	20.9	21.8	21.5	21.3	21.1	21.8	13.3	10.5
4.5 (11.4)	(A-C3)	2	19.2	17.1	17.6	18.2	18.6	19.6	19.0	19.2	18.9	19.8	13.3	10.8
4.5 (11.4)	(A-C3)	3	17.1	15.5	15.3	16.5	16.9	17.2	17.0	17.1	17.0	17.3	12.9	10.6
4.5 (11.4)	(A-C3)	4	15.1	13.8	13.1	14.8	14.6	15.4	15.2	15.1	14.5	15.2	12.7	10.2
6 (15.2)	(A-C3)	0.1	38.3	34.4	35.1	35.9	37.0	38.7	38.0	37.8	36.6	38.9	21.2	17.2
6 (15.2)	(A-C3)	1.1	36.9	33.3	33.6	35.0	36.1	37.9	36.7	36.1	36.1	37.7	21.2	17.1
6 (15.2)	(A-C3)	2.1	34.2	30.8	30.7	32.8	33.7	34.6	34.2	33.7	33.5	34.9	21.1	16.9
6 (15.2)	(A-C3)	3.1	30.7	27.3	27.8	29.5	30.0	31.0	30.6	30.2	30.1	31.2	20.8	16.6
6 (15.2)	(A-C3)	4.1	26.9	23.9	23.8	26.1	26.7	27.0	26.5	26.7	26.4	27.1	20.6	16.2
7.5 (19.1)	(A-C3)	0.1	48.6	44.3	44.9	45.9	47.7	49.6	48.3	48.0	48.2	49.2	33.3	21.7
7.5 (19.1)	(A-C3)	1	48.2	43.4	43.3	45.8	47.4	48.6	47.9	47.5	46.0	49.0	33.1	21.6
7.5 (19.1)	(A-C3)	2	45.6	40.9	41.2	43.6	45.0	46.5	45.4	45.0	44.6	46.6	32.7	21.3
7.5 (19.1)	(A-C3)	3	41.7	37.8	37.6	39.8	41.5	42.5	41.5	41.1	41.1	42.6	31.9	20.9
7.5 (19.1)	(A-C3)	4	37.0	33.5	33.2	35.7	36.5	37.6	36.9	36.7	36.5	37.4	31.6	20.3
4.5 (11.4)	(B-C3)	0.1	13.9	12.5	12.7	13.0	13.5	14.0	13.7	13.3	13.4	13.9	8.0	6.6
4.5 (11.4)	(B-C3)	1	13.1	11.8	11.9	12.6	12.5	13.0	12.7	13.0	12.7	13.2	8.2	6.7
4.5 (11.4)	(B-C3)	2	11.8	10.5	11.1	11.1	11.1	12.0	11.8	12.0	11.8	12.1	8.3	6.3
4.5 (11.4)	(B-C3)	3	10.8	9.7	9.1	10.1	10.3	10.6	10.5	10.8	10.2	10.7	8.0	6.1
4.5 (11.4)	(B-C3)	4	9.4	8.5	8.2	9.6	9.3	9.3	9.4	9.4	8.9	9.4	8.0	6.1
6 (15.2)	(B-C3)	0.1	20.9	18.8	19.6	19.6	20.5	21.1	20.6	20.8	20.5	21.8	12.7	10.2
6 (15.2)	(B-C3)	1.1	19.7	17.6	17.5	18.3	19.3	19.8	19.3	18.8	19.3	20.3	12.6	9.9
6 (15.2)	(B-C3)	2.1	18.3	16.5	16.2	18.0	18.7	18.6	18.6	18.7	18.2	19.5	12.6	9.5
6 (15.2)	(B-C3)	3.1	16.4	14.6	14.2	16.3	16.5	16.7	16.4	16.3	16.0	17.0	12.6	9.5
6 (15.2)	(B-C3)	4.1	14.2	12.8	12.8	14.4	14.8	14.3	14.1	14.4	14.2	15.2	12.4	9.3
7.5 (19.1)	(B-C3)	0.1	25.0	22.4	22.1	23.7	24.9	25.2	24.6	24.7	24.6	25.5	21.7	11.6
7.5 (19.1)	(B-C3)	1	23.6	21.2	20.8	22.7	23.3	23.8	23.7	23.6	22.9	24.2	21.4	11.5
7.5 (19.1)	(B-C3)	2	22.2	19.9	19.5	21.4	21.9	22.5	22.1	22.3	21.6	23.0	21.2	11.5
7.5 (19.1)	(B-C3)	3	20.4	18.6	17.9	20.0	20.8	21.0	20.4	20.2	20.0	21.0	20.9	11.3
7.5 (19.1)	(B-C3)	4	18.7	17.2	16.6	18.9	19.4	19.0	18.9	18.7	18.9	19.7	20.8	11.2

5.3.3 Borehole Diameter Results

As can be seen in Figures 5-26 and 5-27 increasing the borehole diameter from 7.62 cm (3 in) to 15.24 cm (6 in), while holding shank spacing constant, for both the church and small office substantially increases the required borehole depth. Since the conductivity of the grout is much smaller than the conductivity of the soil, increasing borehole diameter also increases borehole resistance. Thus the increase in borehole length due to an increase in borehole resistance is shown in Figure 5-25. The change in borehole resistance with diameter causes a significant change in sized depth for both peak-load-dominant and non-peak-load-dominant systems.
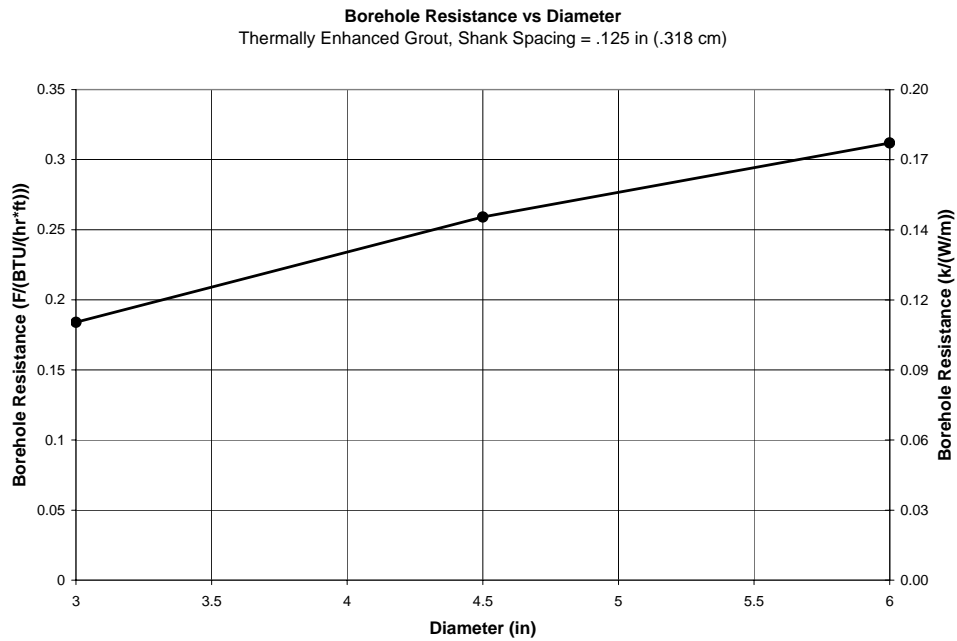
Figure 5-25 Borehole Resistance vs Diameter Using Thermally Enhanced Grout, Shank Spacing of 0.125 in (0.318 cm)

Sized Depth vs Diameter
Thermally-Enhanced Grout, Fluid Factor = 1, Shank Spacing =.125 in (.318 cm)
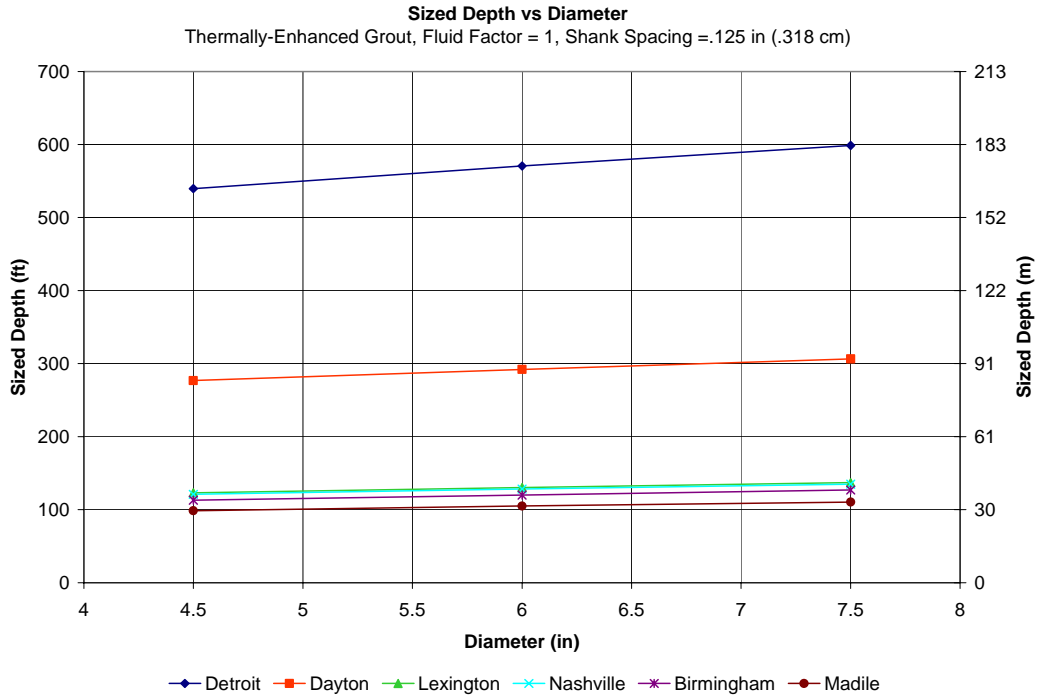
Figure 5-26 Sized Borehole Depth vs Diameter for Church Building Using Thermally Enhanced Grout, Shank Spacing of 0.125 in (0.318 cm), and Fluid Factor of 1

Sized Depth vs Diameter
Standard Bentonite Grout, Fluid Factor = 1, Shank Spacing = .125 in (.318 cm)
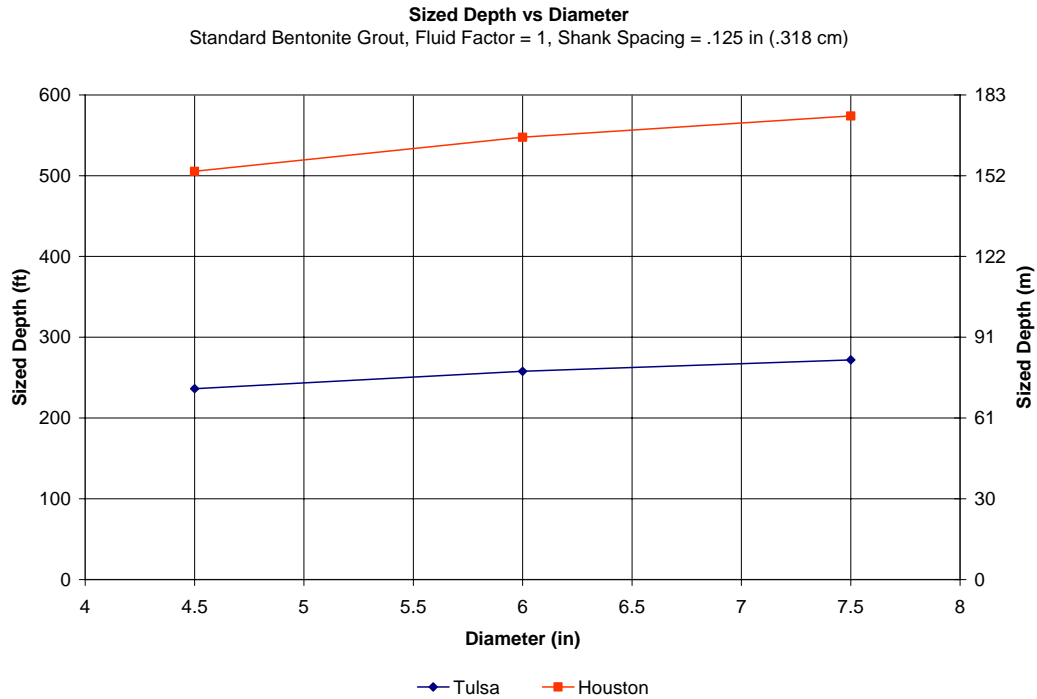
Figure 5-27 Sized Borehole Depth vs Diameter for Small Office Building Using Standard Bentonite Grout , Shank Spacing of 0.125 in (0.318 cm), and Fluid Factor of 1

165

Table 5-11 shows borehole depths (left side) and percent changes in borehole resistance (right side) due to changing the borehole diameter from 11.4 cm to 15.2 cm (4.5 to 6 in) and 15.2 cm to 19.1 cm (6 to 7.5 in). Shank spacing was held constant. As can be seen by the negative numbers, increasing the borehole diameters increases the required depth. Table 5-9 shows that changing the borehole diameter has less of an influence on GLHEPRO's sized depth as fluid factor is increased.

Table 5-11 Percent Change in GLHEPRO Sizing Depth for Changes in Borehole Diameter

Birmingham

Fluid Factor	Shank Spacing cm (in)	Regular Grout BH Diameter cm (in) 11.4 (4.5)	15.2 (6)	19.1 (7.5)	Thermally Enhanced Grout BH Diameter cm (in) 11.4 (4.5)	15.2 (6)	19.1 (7.5)
0.1	.318 (0.125)	144	163	176	107	113	117
1	.318 (0.125)	129	142	155	100	106	112
2	.318 (0.125)	114	123	133	92	99	105
3	.318 (0.125)	101	104	111	85	90	97
4	.318 (0.125)	90	90	93	77	81	88
0.1	1 (0.394)	135	143	147	101	104	108
1	1 (0.394)	122	125	127	95	98	102
2	1 (0.394)	109	111	112	89	92	96
3	1 (0.394)	97	97	97	82	84	89
4	1 (0.394)	86	86	86	75	77	81
0.1	3 (1.181)	115	127	130	90	94	97
1	3 (1.181)	106	113	115	85	89	92
2	3 (1.181)	97	102	103	80	83	87
3	3 (1.181)	88	91	92	75	77	82
4	3 (1.181)	80	81	81	69	71	76
0.1	4.11 (1.618)	103	120	123	85	90	92
1	4.11 (1.618)	96	108	109	81	85	87
2	4.11 (1.618)	90	98	99	76	80	83
3	4.11 (1.618)	82	88	89	71	74	78
4	4.11 (1.618)	75	79	81	66	69	74

Fluid Factor	Shank Spacing cm (in)	Regular Grout BH Diameter cm (in) 15.2 (6) to 11.4 (4.5)	19.1 (7.5) to 15.2 (6)	Enhanced Grout BH Diameter cm (in) 15.2 (6) to 11.4 (4.5)	19.1 (7.5) to 15.2 (6)
0.1	3.18 (0.125)	-12.1	-7.6	-5.4	-4.1
1	3.18 (0.125)	-9.5	-8.2	-6.3	-5.0
2	3.18 (0.125)	-7.2	-7.7	-6.4	-6.1
3	3.18 (0.125)	-3.5	-6.7	-5.9	-7.7
4	3.18 (0.125)	0.0	-3.6	-5.1	-8.2
0.1	1 (0.394)	-5.5	-2.7	-3.3	-3.2
1	1 (0.394)	-2.9	-1.8	-3.3	-3.4
2	1 (0.394)	-1.6	-0.7	-3.4	-3.9
3	1 (0.394)	-0.1	-0.1	-3.1	-5.4
4	1 (0.394)	0.0	-0.1	-3.0	-5.7
0.1	3 (1.181)	-9.9	-2.5	-3.9	-2.9
1	3 (1.181)	-6.8	-1.5	-3.8	-3.4
2	3 (1.181)	-5.2	-1.0	-3.5	-4.2
3	3 (1.181)	-3.3	-0.7	-3.4	-5.7
4	3 (1.181)	-0.9	-0.5	-3.0	-6.0
0.1	4.11 (1.618)	-14.9	-2.9	-5.6	-2.9
1	4.11 (1.618)	-11.8	-0.9	-4.9	-2.8
2	4.11 (1.618)	-8.8	-0.8	-4.8	-3.4
3	4.11 (1.618)	-6.9	-1.7	-4.2	-4.9
4	4.11 (1.618)	-4.7	-2.1	-4.0	-6.3

Birmingham*

Fluid Factor	Shank Spacing cm (in)	Regular Grout BH Diameter cm (in) 11.4 (4.5)	15.2 (6)	19.1 (7.5)	Thermally Enhanced Grout BH Diameter cm (in) 11.4 (4.5)	15.2 (6)	19.1 (7.5)
0.1	.318 (0.125)	164	184	199	120	127	133
1	.318 (0.125)	146	162	176	113	120	127
2	.318 (0.125)	130	139	151	104	111	119
3	.318 (0.125)	114	119	127	96	102	110
4	.318 (0.125)	102	102	107	88	92	100
0.1	1 (0.394)	152	163	168	114	118	122
1	1 (0.394)	138	142	145	107	111	115
2	1 (0.394)	124	126	128	100	104	109
3	1 (0.394)	110	111	111	92	96	101
4	1 (0.394)	98	98	98	85	88	93
0.1	3 (1.181)	129	143	148	102	106	109
1	3 (1.181)	119	128	130	96	100	104
2	3 (1.181)	110	116	118	91	94	99
3	3 (1.181)	100	103	104	84	88	93
4	3 (1.181)	91	92	92	78	81	86
0.1	4.11 (1.618)	116	136	140	96	101	104
1	4.11 (1.618)	109	123	124	91	96	99
2	4.11 (1.618)	101	111	112	86	91	94
3	4.11 (1.618)	93	100	102	81	85	89
4	4.11 (1.618)	85	90	92	75	79	84

Fluid Factor	Shank Spacing cm (in)	Regular Grout BH Diameter cm (in) 15.2 (6) to 11.4 (4.5)	19.1 (7.5) to 15.2 (6)	Enhanced Grout BH Diameter cm (in) 15.2 (6) to 11.4 (4.5)	19.1 (7.5) to 15.2 (6)
0.1	3.18 (0.125)	-11.5	-7.7	-5.9	-4.2
1	3.18 (0.125)	-10.3	-8.4	-6.0	-5.5
2	3.18 (0.125)	-7.2	-8.2	-6.6	-6.6
3	3.18 (0.125)	-4.3	-6.5	-6.1	-7.7
4	3.18 (0.125)	-0.6	-4.1	-5.1	-8.6
0.1	1 (0.394)	-6.6	-3.0	-3.6	-3.1
1	1 (0.394)	-3.0	-2.2	-3.2	-3.7
2	1 (0.394)	-2.0	-1.3	-3.6	-4.6
3	1 (0.394)	-0.6	-0.2	-3.6	-5.2
4	1 (0.394)	-0.1	-0.3	-3.4	-5.9
0.1	3 (1.181)	-10.2	-2.9	-4.0	-3.3
1	3 (1.181)	-7.0	-1.6	-3.7	-3.6
2	3 (1.181)	-5.7	-1.8	-3.8	-4.5
3	3 (1.181)	-3.3	-1.2	-3.7	-5.4
4	3 (1.181)	-1.1	-0.3	-3.5	-6.0
0.1	4.11 (1.618)	-15.4	-2.7	-5.7	-2.8
1	4.11 (1.618)	-12.3	-1.1	-5.1	-3.1
2	4.11 (1.618)	-9.5	-0.8	-5.1	-3.5
3	4.11 (1.618)	-7.2	-1.8	-4.7	-5.3
4	4.11 (1.618)	-5.6	-2.2	-4.5	-6.5

Detroit

Fluid Factor	Shank Spacing cm (in)	Regular Grout BH Diameter cm (in) 11.4 (4.5)	15.2 (6)	19.1 (7.5)	Thermally Enhanced Grout BH Diameter cm (in) 11.4 (4.5)	15.2 (6)	19.1 (7.5)
0.1	.318 (0.125)	765	850	910	571	601	630
1	.318 (0.125)	690	758	813	540	570	599
2	.318 (0.125)	617	658	710	501	532	565
3	.318 (0.125)	547	567	603	463	491	526
4	.318 (0.125)	491	495	512	426	447	484
0.1	1 (0.394)	717	760	779	544	563	582
1	1 (0.394)	649	673	685	517	530	549
2	1 (0.394)	591	599	605	482	498	522
3	1 (0.394)	527	529	530	447	462	485
4	1 (0.394)	475	475	475	413	426	450
0.1	3 (1.181)	614	678	695	491	509	523
1	3 (1.181)	568	607	620	466	482	498
2	3 (1.181)	527	555	563	441	457	476
3	3 (1.181)	481	497	500	412	426	448
4	3 (1.181)	441	446	447	389	399	419
0.1	4.11 (1.618)	554	646	664	463	490	499
1	4.11 (1.618)	520	582	592	442	464	476
2	4.11 (1.618)	488	532	537	420	439	454
3	4.11 (1.618)	451	483	490	397	412	432
4	4.11 (1.618)	416	438	447	374	390	409

Fluid Factor	Shank Spacing cm (in)	Regular Grout BH Diameter cm (in) 15.2 (6) to 11.4 (4.5)	19.1 (7.5) to 15.2 (6)	Enhanced Grout BH Diameter cm (in) 15.2 (6) to 11.4 (4.5)	19.1 (7.5) to 15.2 (6)
0.1	3.18 (0.125)	-10.5	-6.9	-5.1	-4.7
1	3.18 (0.125)	-9.4	-7.0	-5.6	-4.8
2	3.18 (0.125)	-6.4	-7.6	-6.1	-6.0
3	3.18 (0.125)	-3.6	-6.1	-5.9	-6.7
4	3.18 (0.125)	-0.8	-3.4	-4.6	-7.9
0.1	1 (0.394)	-5.8	-2.5	-3.3	-3.4
1	1 (0.394)	-3.7	-1.7	-2.6	-3.5
2	1 (0.394)	-1.4	-1.0	-3.2	-4.6
3	1 (0.394)	-0.4	-0.1	-3.3	-4.7
4	1 (0.394)	-0.1	0.0	-3.1	-5.5
0.1	3 (1.181)	-9.9	-2.4	-3.7	-2.7
1	3 (1.181)	-6.5	-2.2	-3.4	-3.2
2	3 (1.181)	-5.3	-1.4	-3.7	-3.9
3	3 (1.181)	-3.2	-0.7	-3.4	-5.0
4	3 (1.181)	-1.2	-0.3	-2.6	-4.9
0.1	4.11 (1.618)	-15.3	-2.8	-5.6	-1.9
1	4.11 (1.618)	-11.1	-1.7	-4.9	-2.7
2	4.11 (1.618)	-8.8	-0.8	-4.6	-3.4
3	4.11 (1.618)	-6.8	-1.5	-3.6	-4.6
4	4.11 (1.618)	-5.1	-2.2	-4.1	-4.9

167

5.1.4   Discussion of GLHEPRO Sizing Results

As can be seen in Figures 5-14 through 5-17 very different GLHEPRO sized depths can be found for the same building placed in different locations. This is because building loads can vary greatly for a building in different locations as shown in Table 5-1 and 5-4. Because of the load differences between locations a single borehole configuration should not be used in all locations for one specific building.

 As shown in Table 5-6 and 5-7 the BFTM model improves the accuracy of the GLHEPRO sized borehole depth, over the accuracy of the line source solution, on the order of 6 to 30% for peak-load-dominant systems such as the Church building. This improvement in accuracy is caused by changing the fluid factor from 0.1, which approximates the line source, to 2, which is closer to an actual system's fluid factor.

Improvements in borehole depth can be made if a buffer tank is used to increase the fluid factor from a value of 2 to 4. Table 5-6 and 5-7 show this improvement to be typically between 6 and 30% for the church building. However, for typical systems such as an office building, represented by the Houston and Tulsa columns of Table 5-6 and 5-7, the influence of using the borehole fluid thermal mass model produces only minor changes. These changes typically range between 1 and 4 percent reduction for a fluid factor change of 2 to 4.

When designing a GLHE system for a peak-load-dominant system the internal borehole properties (such as the borehole diameter, shank spacing, grout type, and fluid factor) should be carefully chosen since they greatly affect the sized depth output from GLHEPRO. The influence of shank spacing and borehole diameter can be seen in Table 5-10 and 5-11 respectively. In some cases for standard bentonite grout, fluid factor of 1,

and 11.4 cm (4.5 in) borehole diameter, when the U-tubes were moved from the A to the C3 spacing, the sized depth changed by over 30%. This large change occurs because the borehole resistance changes greatly as can be seen in Figure 5-20. The relative magnitudes of the percent sized depth reduction do not change for church location.

An important observation from the data in this chapter is that reductions in borehole depth are not additive with respect to borehole improvement. When an internal borehole parameter is changed to increase the performance of the borehole, it decreases the percent reduction in borehole depth that can be achieved by changing another internal borehole parameter.

6 HOURLY SIMULATION USING THE BFTM MODEL

This chapter evaluates the impact of the BFTM model on simulation of ground source heat pump systems through a detailed model in HVACSIM+ (Varanasi 2002). Additional locations where HVACSIM+ was implemented include Khan, et al. (2003), Park, et al. (1985), and Clark (1985).

The detailed model in this chapter incorporates a heat pump, a pump, and a GLHE. Using this model, an hourly comparison is made between g-functions derived from the line source and g-functions derived from the BFTM model using the Tulsa, Oklahoma small office building described in Chapter 5. Comparing the BFTM model with the line source is useful since the line source was used in GLHEPRO for simulating borehole systems due to its speed and simplicity.

Also a seven year and ten year study was conducted using the BFTM model within HVACSIM+ and GLHEPRO. The performance of these two models are compared for two different systems, a peak-load-dominant and a non-peak-load-dominant case. The peak-load-dominant case was simulated with fluid factors of 1, 2 and 4. The non-peak-load-dominant case was simulated with fluid factors of 1 and 2. For comparison with GLHEPRO the fluid pump was removed from the detailed HVACSIM+ model leaving a two-component model composed of a heat pump and ground loop. The heating and cooling loads for the two systems will come from BLAST simulations of the small office building located in Tulsa, Oklahoma and the church building located in Nashville Tennessee. The properties of each building were discussed in detail in section 5.1.

6.1   HVACSIM+ Hourly Simulation

An HVACSIM+ model was created that consists of three components: a heat pump, a fluid pump, and a ground loop heat exchanger. This three component model was created using the Visual Modeling Tool for HVACSIM+ and is displayed in Figure 6-1.
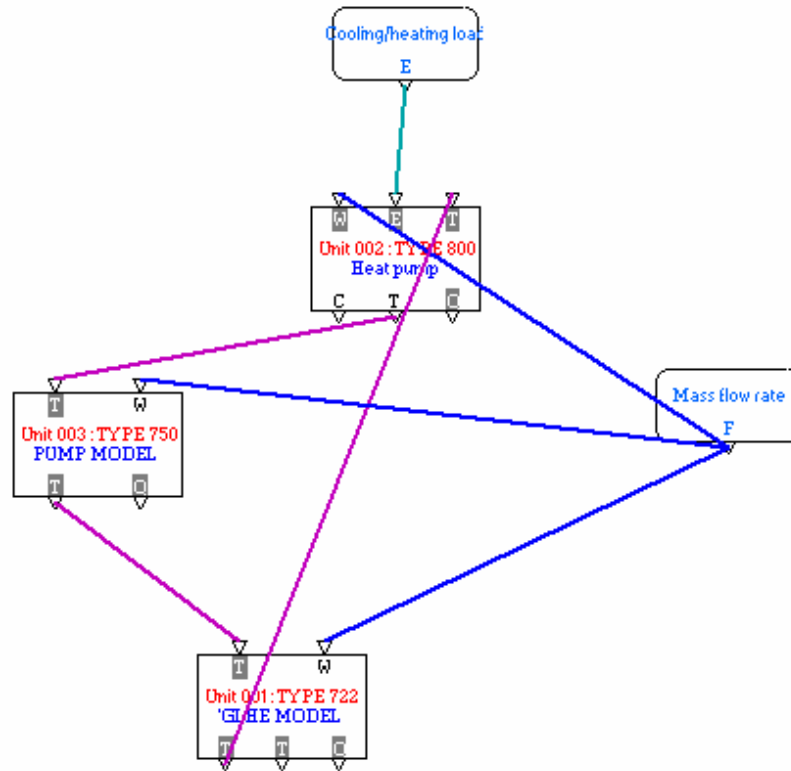
Figure 6-1 Three Component Model of a GLHE System in HVACSIM+

The heat pump is a Climate Master VS200 water to air heat pump with a nominal capacity of 7000 SCFM (standard ft^3/min), capable of meeting the design capacity required for the small office building. The VS200 is modeled within HVACSIM+ using coefficients for four polynomial curve fit equations shown in Equations 6-1 and 6-2 with coefficients shown in Table 6-1. Since the fluid flow was held at a constant rate the coefficients P_4, P_5, P_9, and P_{10}, are set to zero. Also, since the second order term is very small, the Ratio and COP change almost linearly with the EWT to the heat pump.

$$Ratio = P_1 + P_2 \cdot EWT + P_3 \cdot EWT^2 + P_4 \cdot \dot{M} + P_5 \cdot \dot{M} \cdot EWT \qquad \textbf{(6-1)}$$

$$\textbf{(6-2)}$$

$$COP = P_6 + P_7 \cdot EWT + P_8 \cdot EWT^2 + P_9 \cdot \dot{M} + P_{10} \cdot \dot{M} \cdot EWT$$

where,

P =	Array of curve fit coefficients
EWT =	Entering water temperature to the heat pump (ºC)
$\dot{M}$ =	Mass flow rate $\left(\dfrac{kg}{s}\right)$
$Ratio$ =	Heat extraction to heating or heat rejection to cooling (non-dimensional)
COP =	COP coefficient in heating or cooling

Table 6-1 Coefficients for the VS200 Climate Master Heat Pump

	P_1	P_2	P_3	P_4	P_5	P_6	P_7	P_8	P_9	P_{10}
Heating	1.4812	-.0081	.0001	0	0	2.9926	.0468	.0005	0	0
Cooling	1.176	.0025	.00005	0	0	6.816	-.1033	.0004	0	0

These coefficients are valid for a flow rate of 0.00328 M³/s (52 gal/min) and a temperature range from 4.44 °C (40 °F) to 37.8 °C (100 °F).

The next component that was created for the model is the pump. The pump has a constant 80% efficiency and produces a pressure rise of 100 KPa (14.5 psi) at a flow rate of 0.00328 M³/s (52 gal/min).

The third and final component is the GLHE represents the ground loop. The same configuration shown in Table 4-1 is used here. There are 16 boreholes, each 76.2 m (250 ft) in length. The undisturbed ground temperature is 17.22 °C (63 °F). The HVACSIM+ component requires a g-function to be specified in a separate text file. The borehole resistance is specified as 0.183 K/(W/M) (0.317 F/(BTU/(hr·ft))). The specific properties in Table 4-1 were used to make the combined long and short time step g-function.
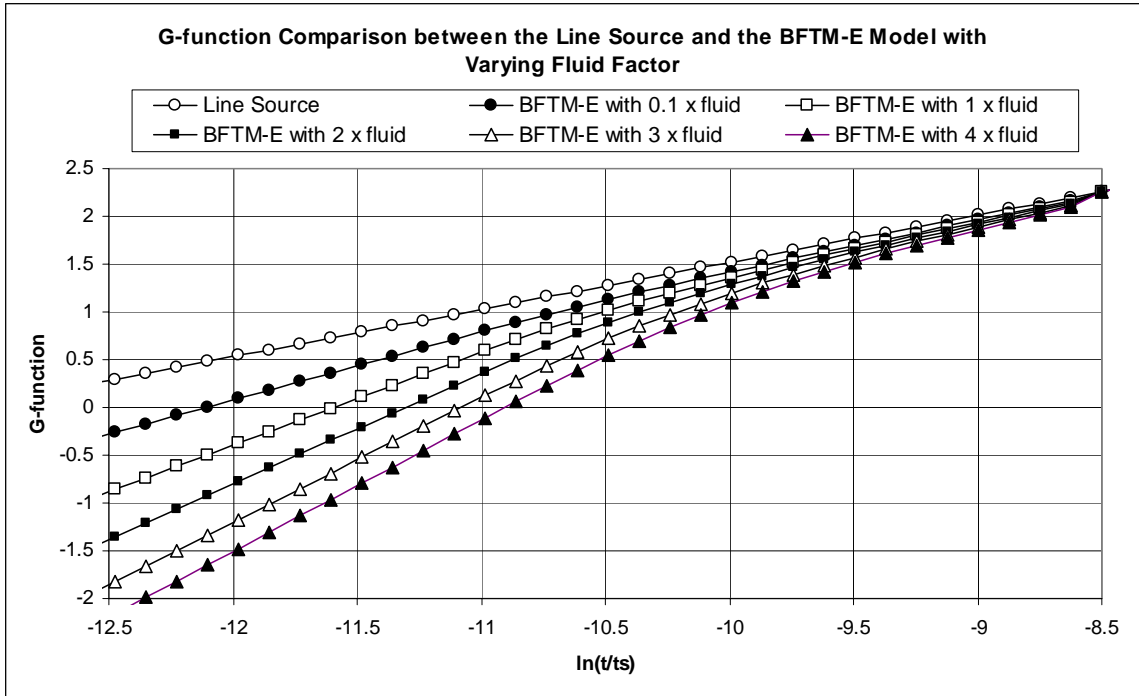
Figure 6-2 G-function's for Various Fluid Factors

The two inputs to the system are the fluid flow rate and hourly loads. The mass flow rate is constant through the entire length of the simulation. The assumption within the borehole resistance calculation is that the fluid is in the turbulent flow regime for the entire simulation. The hourly loads are treated as boundary conditions on the Climate Master VS200 Heat Pump.

6.2 Line source and BFTM Model Comparison Using a Detailed HVACSIM+ Model

Since hourly heating/cooling loads are available, the BFTM model will be evaluated with hourly time steps. In Section 5.3 the BFTM model will be compared to the line source since the line source is consistent with what has been used in GLHEPRO to simulate a boreholes short time step thermal response.

173

The small office building located in Tulsa, with hourly loads created in a BLAST simulation is used to show the difference between the line source and the BFTM model with fluid factor equal to 1. The model was run for one year using the hourly heating and cooling loads calculated by BLAST.

Some buildings such as churches, stadiums, concert halls, and community centers as well as the smart bridge application might have loading that is almost entirely peak-load-dominant. Even though the small office building is not peak load dominant, Figures 6-3 and 6-4 show times of the year where the minimum temperature is governed by peak loads. These times do not govern the size of the GLHE, however they do provide data showing the temperature differential between the line source and the BFTM-E models for peak loading conditions.

Two different segments of data are shown in Figures 6-3 and 6-4 for the GLHE outlet temperature. In both of these plots, the peak loads that control the minimum temperature of the time period shown are 1 to 2 hours duration. Both show that the line source over predicts the peak temperature by as much as 1.3 °C (2.3 °F) for the time range shown. This can be seen at time 345 hours in Figure 6-3 and at 535 hours in Figure 6-4. The peak temperature occurs in the first hour of the peak heat pulse for the line source and sometimes occurs on the second hour for the BFTM-E model. This is due to the thermal dampening which was created by modeling the fluid mass for the given heat extraction.
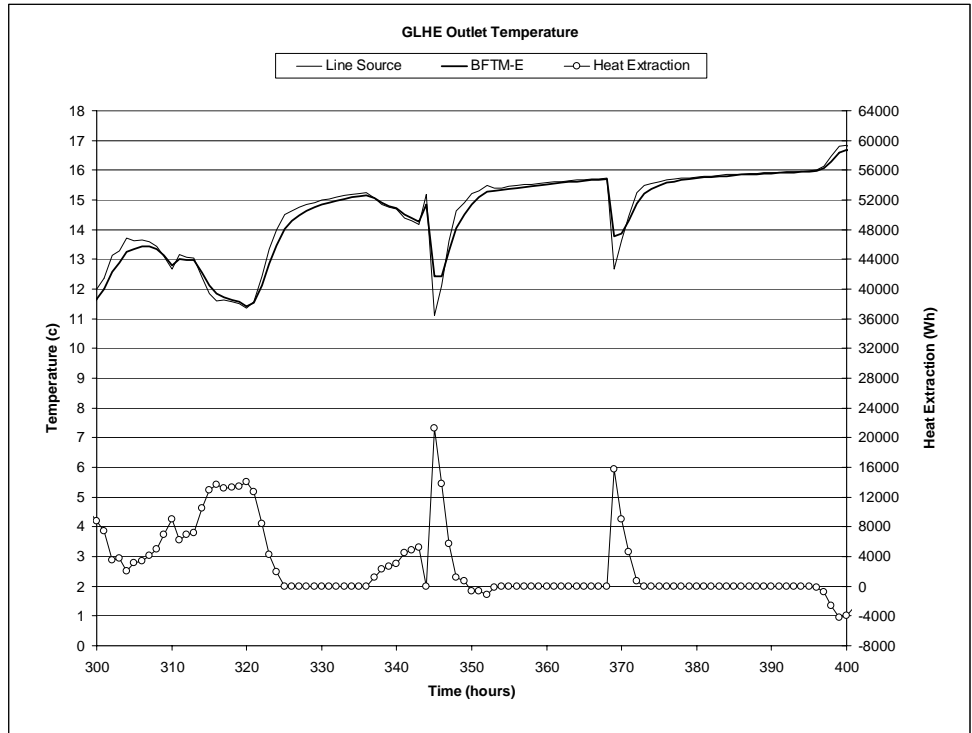
Figure 6-3 Detailed HVACSIM+ Model with Tulsa Loads for Peak-Load-Dominant Times
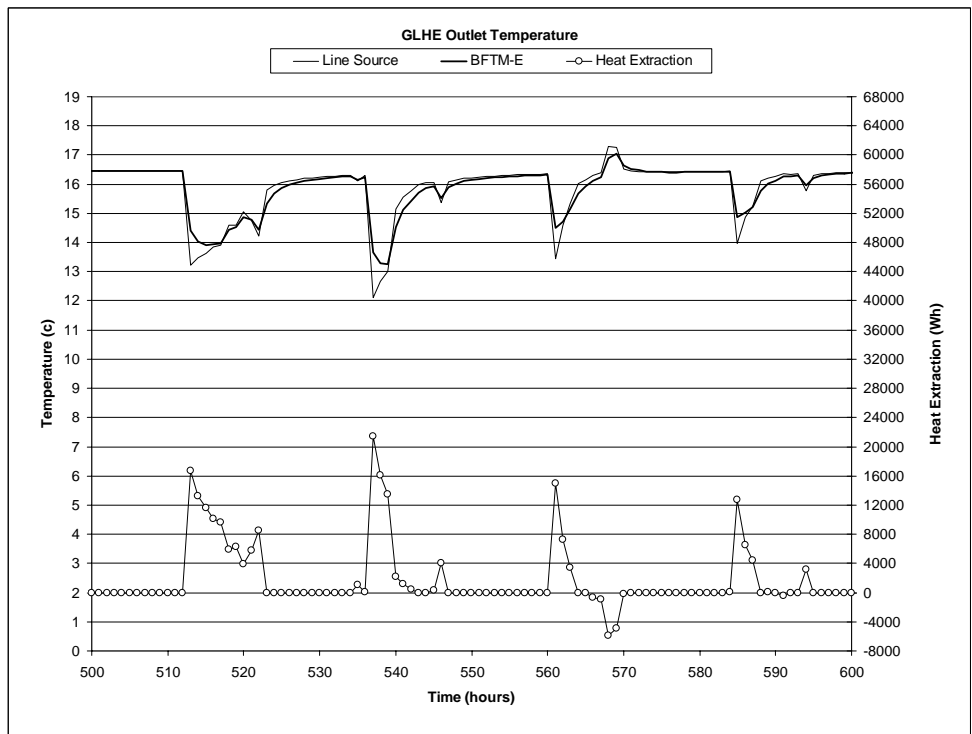
Figure 6-4 Detailed HVACSIM+ Model with Tulsa Loads for Peak-Load-Dominant Times

175

Figure 6-5 shows a slightly longer peak load than those shown in Figure 6-3 and
6-4. The peak loads in Figure 6-5 are of 5 to 7 hours duration. For these peak loads there
is only a 0.35 °C (0.63 °F) temperature difference between the line source and the
BFTM-E model. This temperature difference is much lower than the 1.3 °C (2.3 °F)
temperature differences shown in Figure 6-3 and 6-4.
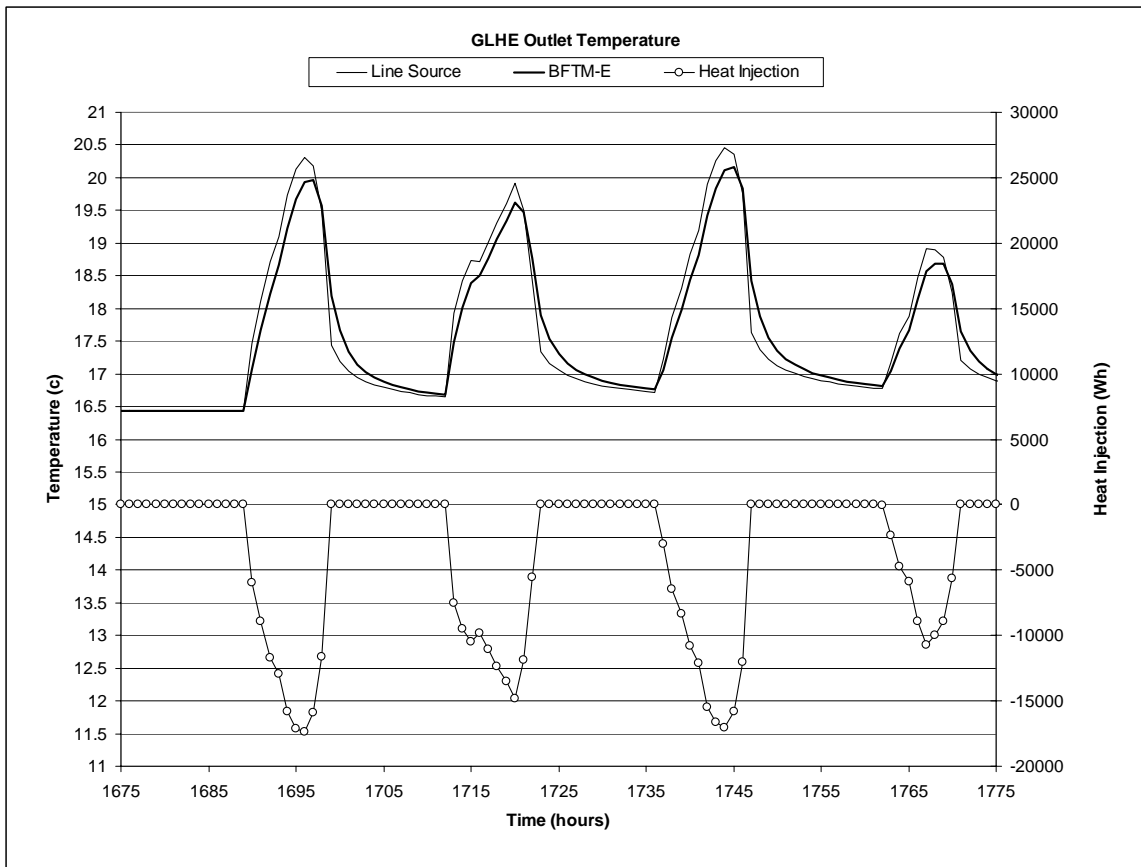
Figure 6-5 Detailed HVACSIM+ with Tulsa Loads

Figure 6-6 shows a time of the year where a short duration peak is superimposed
on a long duration heat pulse. A gradually changing heating load occurs between 645
and 680 hours. During this period there is less than 0.5 °C (0.9 °F) between the two
models. At 681 hours the magnitude of the heating load jumps from about 10,000 to
30,000 W/h (34,000 to 102,000 Btu/hr). This sudden heating load creates a 1.0 °C (1.8

176

°F) temperature difference between the line source and the fluid thermal mass model. This shows that the maximum or minimum temperature of a system can be significantly influenced by heat flux transients riding on a long duration heat pulse.
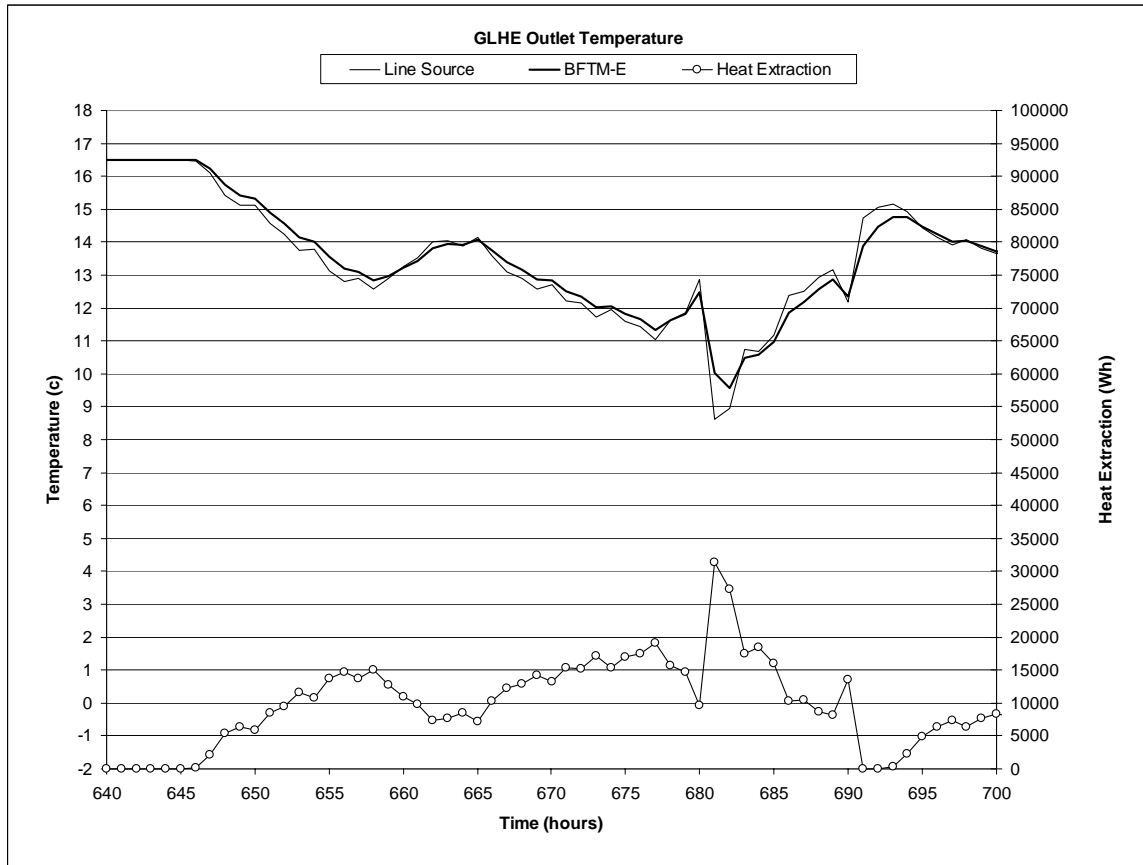
Figure 6-6 Detailed HVACSIM+ with Tulsa Loads for a Short Duration Heat Pulse on a Long Duration Heat Pulse

A longer heat load than those shown in 6-3 and 6-4 will dominate the profile of most buildings such as an office buildings. Peak loads for many buildings will be around 10 hours. Figure 6-7 shows a typical load for the small office building where the load is of 10 hour duration. Each of these plots show five days in summer where heat is injected in the ground for approximately ten hours per day. Since the heating load drops off after approximately 8 hours the maximum temperature that is reached for each ten hour heat

177

pulse is at roughly the 8th hour mark. Thus the maximum temperature differential

between the line source and the BFTM-E model behaves similar to an 8 hour heat pulse.

Since the heat pulses are long, the temperature difference is approximately 0.3 °C (0.54

°F) between the line source and the BFTM solution at hour 4050.

The line source solution is typically less smooth than the BFTM model as can be

seen in the jaggedness of the first two ten hour duration cooling loads in Figure 6-7. The

BFTM better predicts a real systems fluid temperature by modeling the mass of the fluid

which damps the response of the GLHE extraction.
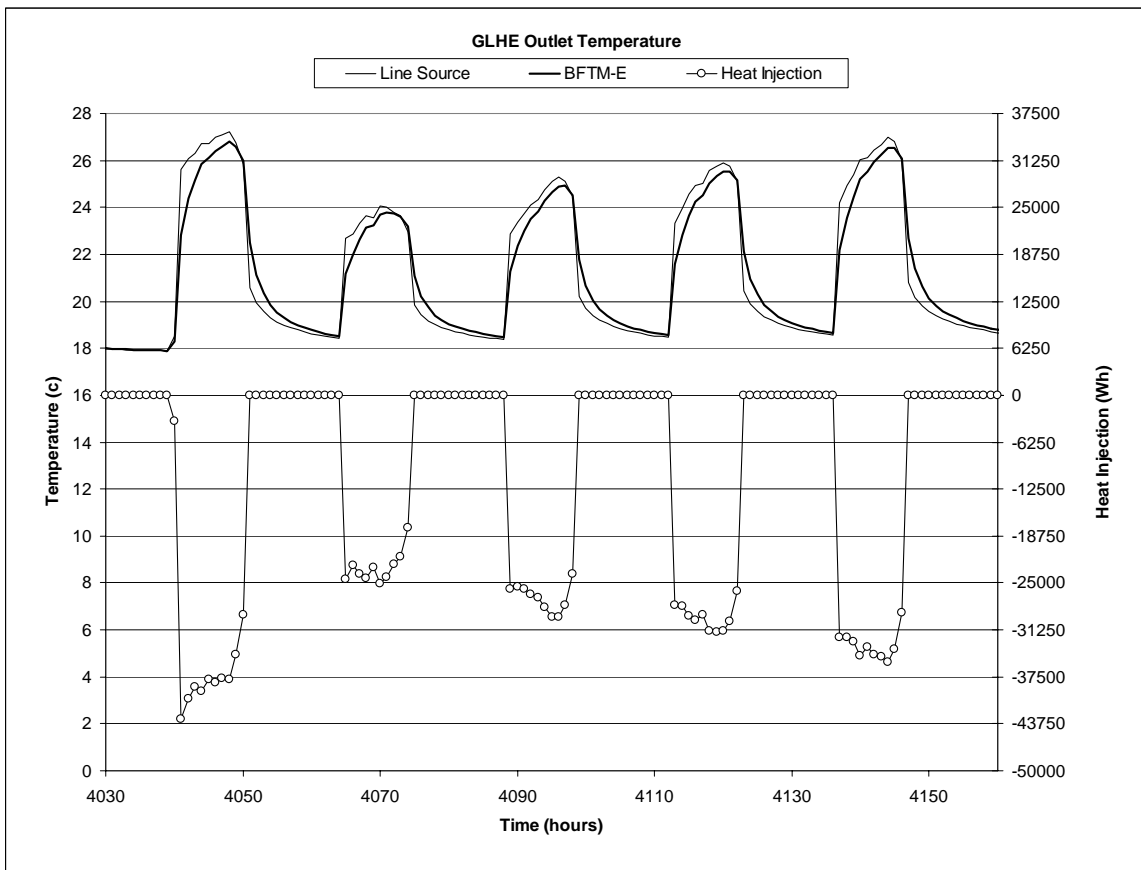
Figure 6-7 Detailed HVACSIM+ with Tulsa Loads for Long Duration Heat Pulses

Figure 6-8 shows the difference in temperature over the course of 5 days between the line source and the BFTM model. Several times a year the temperature difference between the two methods is greater than 2.5 °C (4.5 °F).
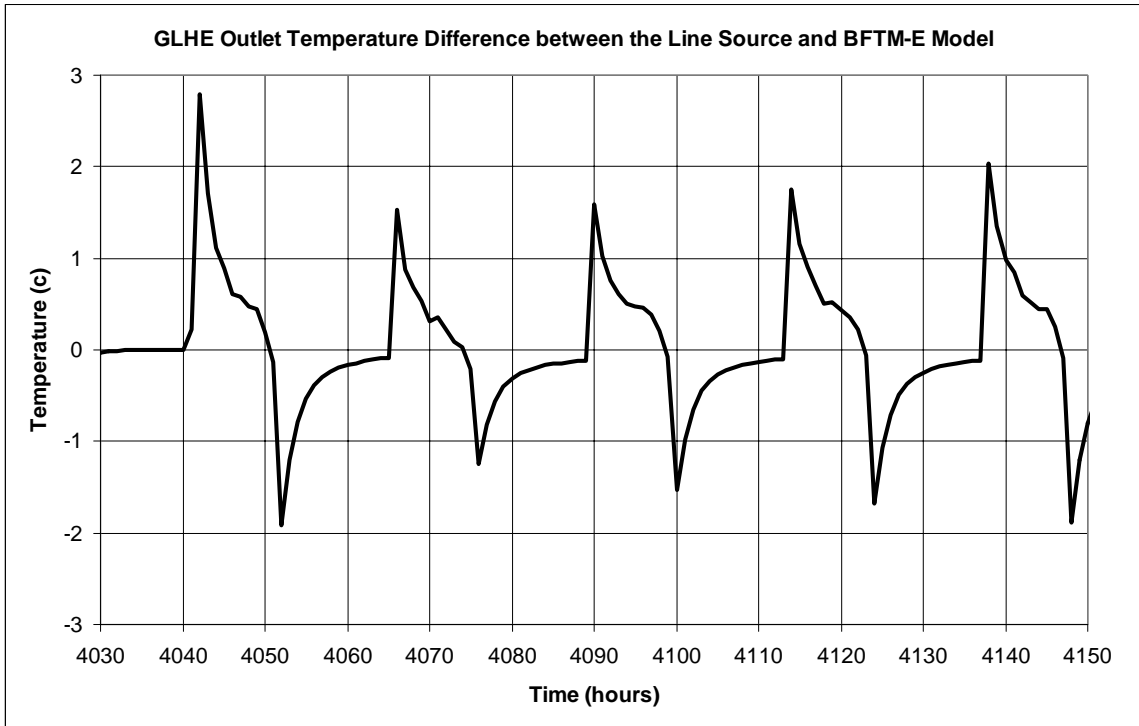
Figure 6-8 Difference in Temperature between the LS and BFTM Models

Figures 6-9 and 6-10 are the heat pump power consumption curves for the line source and BFTM model. Figure 6-9 shows the power consumption for the time of the year where the maximum temperature occurs and Figure 6-10 shows the time which the maximum yearly power consumption occurs. Figures 6-9 and 6-10 show relatively little difference between the heat pump power consumption for the line source and the fluid thermal mass model, producing less than a 1% difference in heat pump power consumption between the two models. The annual electrical energy consumption predicted by the line source is 13.09 MW·h (44.7 MBtu) whereas the annual electrical

energy consumption predicted by the BFTM model is 12.97 MW·h (44.2 MBtu). Thus the line source is reasonably accurate for energy consumption predictions.
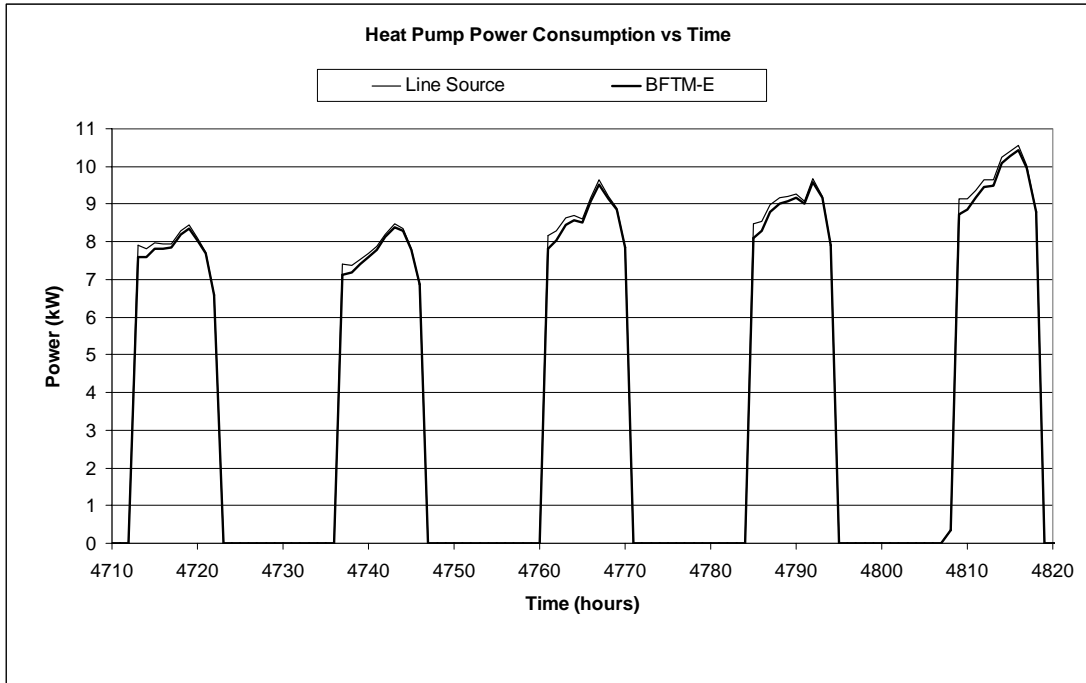
Figure 6-9 Heat Pump Power Curve for the LS and BFTM Models
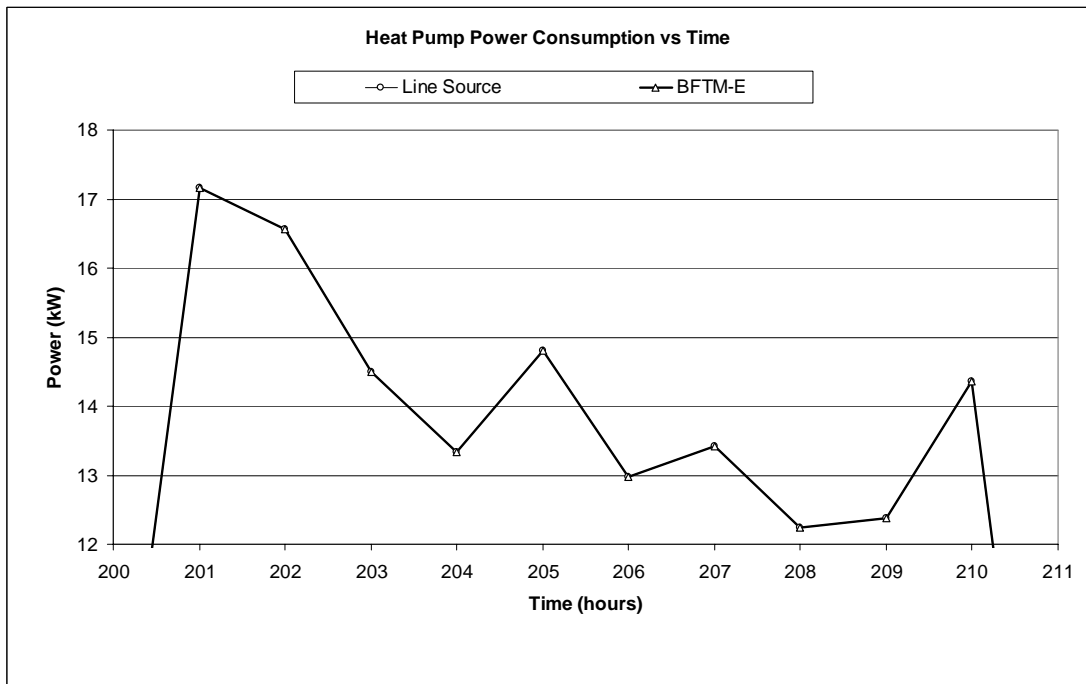
Figure 6-10 Heat Pump Power Curve for the LS and BFTM Models

Figure 6-11 shows the time over which the maximum temperature occurs for the first year. Since this peak is almost 8 hours in length there is a 0.5 °C (0.9 °F) difference between the two models.
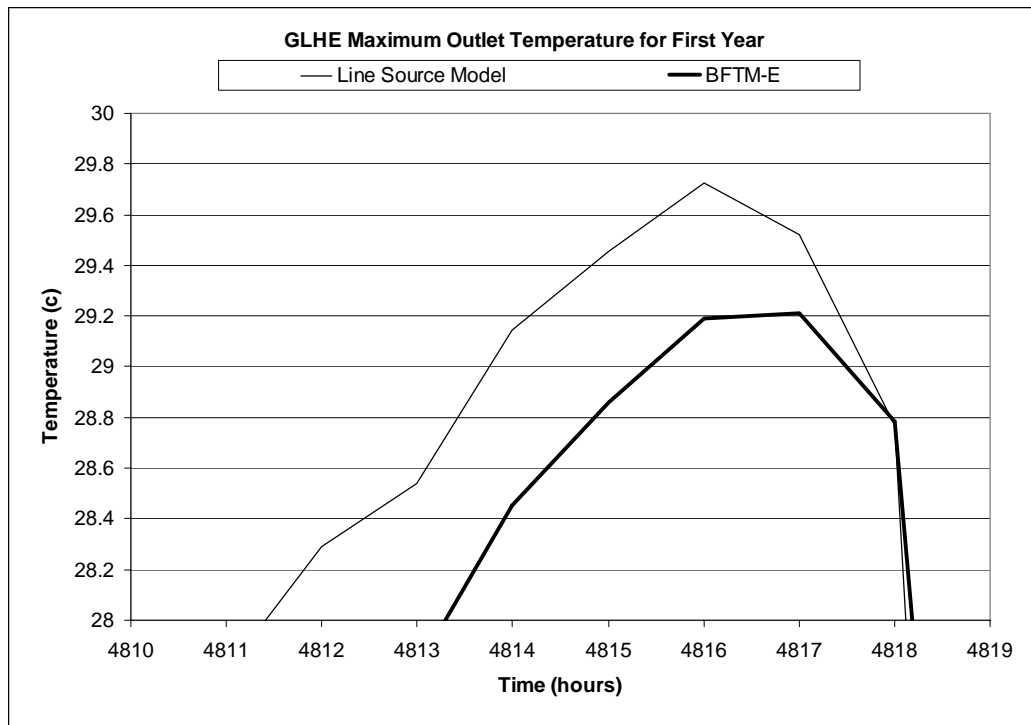
Figure 6-11 Detailed HVACSIM+ Model with Tulsa Loads

As shown in Figures 6-3 and 6-4, a simulation with a more peak-load-dominant loading condition will show larger difference between the line source and the BFTM-E models for the maximum yearly temperature.

6.3 Influence of the Fluid Multiplication Factor on System Design

This section uses the three component HVACSIM+ model shown in Figure 6-1 and a GLHEPRO model with various magnitudes of the fluid multiplication factor to analyze its impact on system design. The general pump, heat pump, and borehole

configuration used in HVACSIM+ is identical to the one described in section 6.1. The

loads for this model however, are from a different BLAST simulation of the small office

building located in Houston, Texas.

Figure 6-2 shows 6 g-functions for different fluid factors of 0.1, 1, 2, 3 and 4 and

the line source based g-function. All curves approach a common beginning point at -14.6

log time and converge to approximately the same ending point at -8.5 log time. Also, as

the fluid factor increases the short time step g-function curves decrease.

6.3.1 Fluid Factor Analysis with HVACSIM+ Simulation Tools

Four hourly HVACSIM+ simulations were run with each of the g-function curves

shown in Figure 6-2 except the 0.1 fluid factor and the line source curves since a

comparison of the line source to the BFTM model was made in section 6.2. Figures 6-12

through 6-14 shows the fluid temperature exiting the ground loop.

Figure 6-12 shows the temperature response for five heat pulses where heat is

injected into the ground for approximately 10 hours. The temperature of the fluid rises

during the day and falls during the night.

Figure 6-12 shows the fluid acting as a damper in the GLHE system by causing its

temperature to respond slower to heat inputs. The larger the fluid factor, the slower the

fluid temperature will rise for a heat rejection and the slower the fluid temperature will

recover when there is no heat rejection.
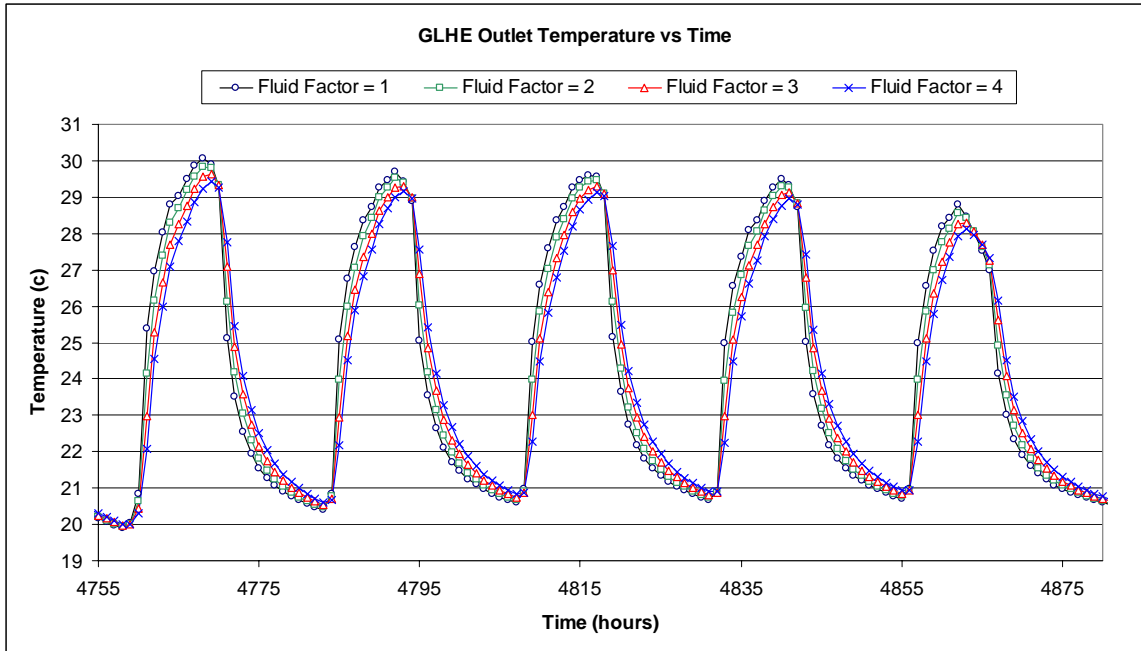
Figure 6-12 GLHE Inlet Temperature for Different Fluid Factors

Figure 6-13 shows the ten hour heat rejection cycle where the maximum temperature occurs for the first year. An increasing phase shift can be seen in the systems thermal response as the fluid factor increases. This phenomena is similar to most simple dynamic systems in that as dampening is increased the phase shift between the input and output also increases. In Figure 6-13 the maximum peak temperature with a fluid factor of one or two occurs at 4768 hours. When the fluid factor increases to three or four the peak temperature occurs at 4769 hours.
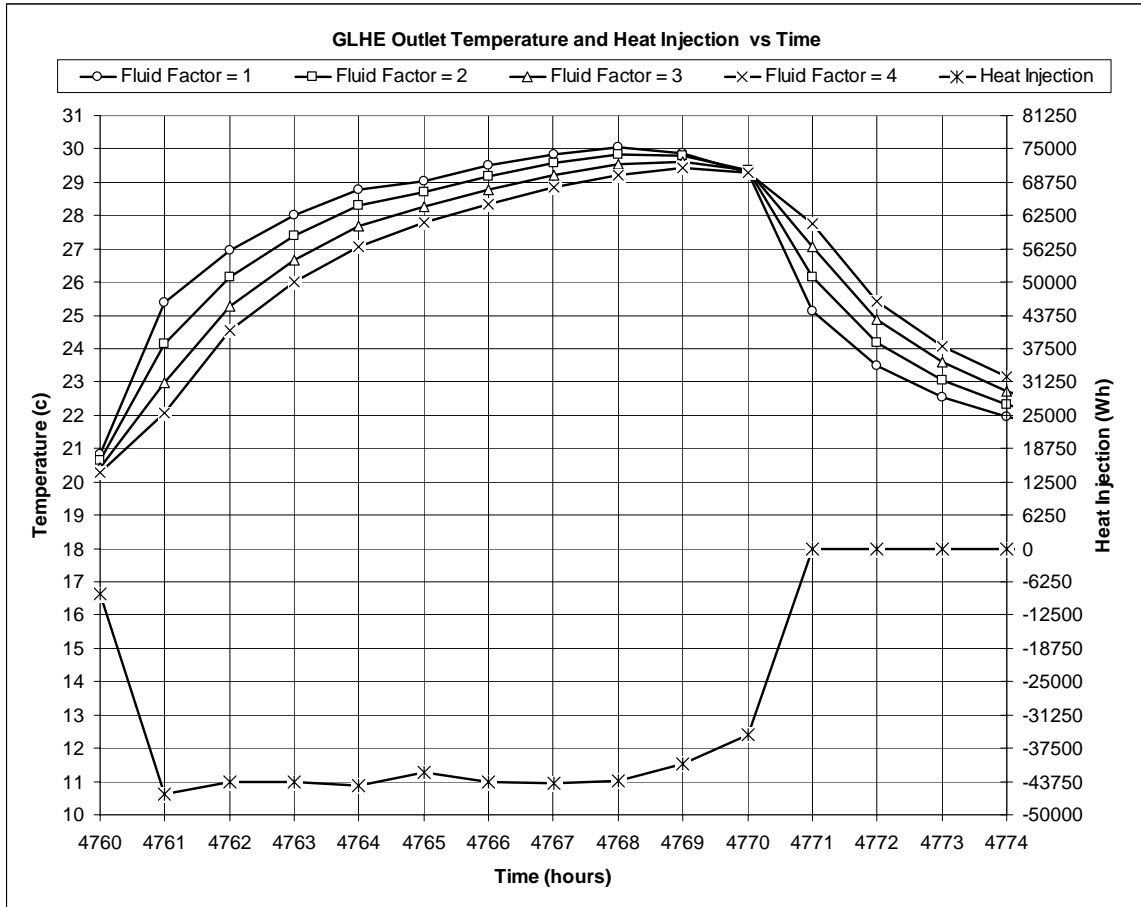
Figure 6-13 GLHE Inlet Temperature for Different Fluid Factor

The maximum inlet fluid temperature for the first year of simulation is 30.1 °C

(86.2 °F) for a fluid factor of 1, 29.8 °C (85.6 °F) for a fluid factor of 2, 29.5 °C (85.1 °F)

for a fluid factor of 3 and 29.3 °C (84.7 °F) for a fluid factor of 4. Thus increasing the

fluid factor from 1 to 2 produces a drop of 0.3 °C (0.5 °F), increasing it from 2 to 3

produces another drop of 0.3 °C (0.5 °F), and from 3 to 4 produces a drop of 0.2 °C (0.4

°F). The general trend is that there are diminishing returns for increasing the fluid mass

in the system.
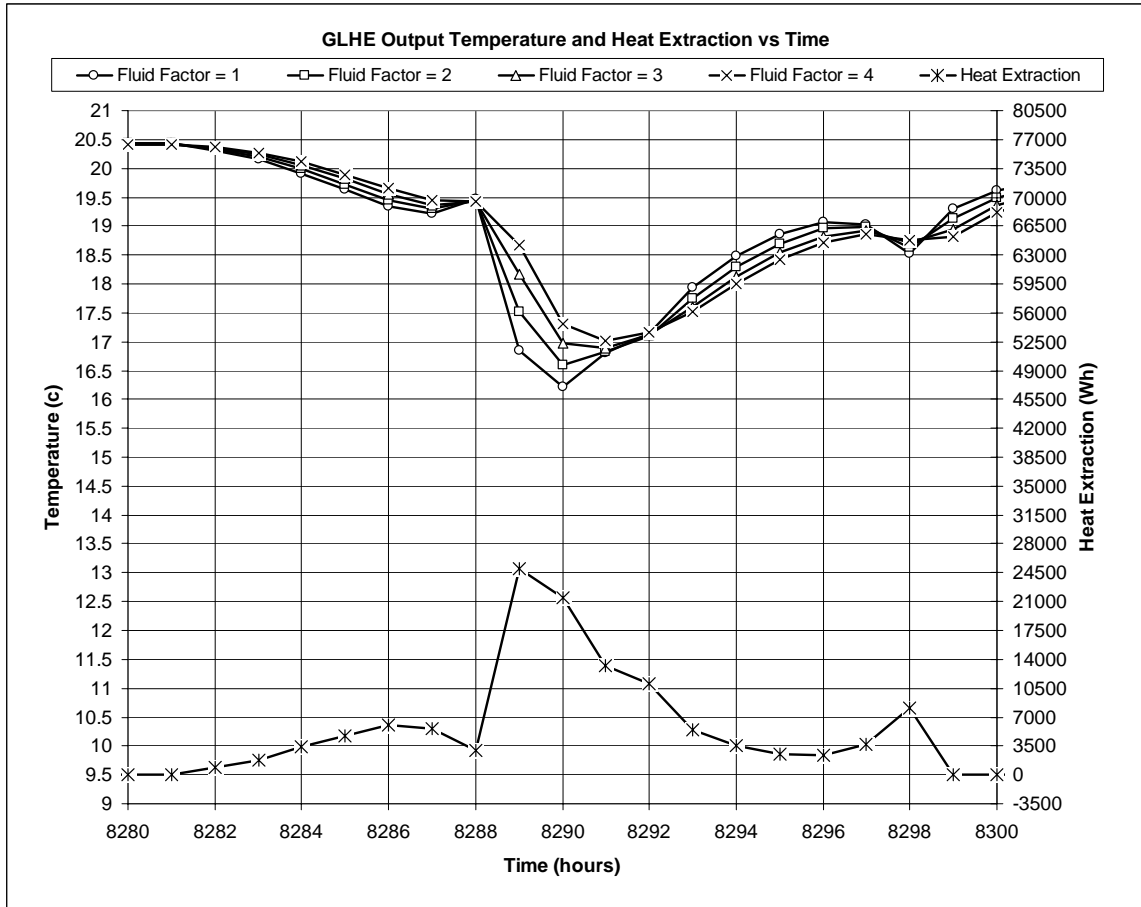
Figure 6-14 GLHE Inlet Temperature for Different Fluid Factors

For a shorter duration peak load in Figure 6-14 there is a 0.4 °C (0.7 °F) temperature increase between a fluid factor of 1 and 2. The same temperature drop occurs when fluid factor is increased from 2 to 3 and from 3 to 4.

6.4   HVACSIM+ and GLHEPRO Comparison

This section will compare results between GLHEPRO and HVACSIM+ for three different seven year peak-load-dominant simulations and two different ten year non-peak-load-dominant simulations. The section will show the BFTM model for longer multiple year GLHEPRO simulations as compared to the higher resolution HVACSIM+ hourly simulations. The three seven year simulations use BLAST loads from the church

185

building located in Nashville for fluid factors of 1, 2, and 4. The two ten year simulations use BLAST loads from the small office building located in Houston for fluid factors of 1 and 2. The buildings and loads are described in detail in Chapter 5.1 along with the aggregated monthly loads for GLHEPRO.

For the small office building, 8 hour peak loads for heat injection were used in GLHEPRO. Figure 6-15 shows five days of a typical week where the heat injection loads have a duration of ten hours, however, as can be seen in Figure 6-7, the peak temperature occurs on the 8th hour due to the reduction in heat injection for the last two hours. Thus 8 hour heat pulses were used in GLHEPRO for the small office building
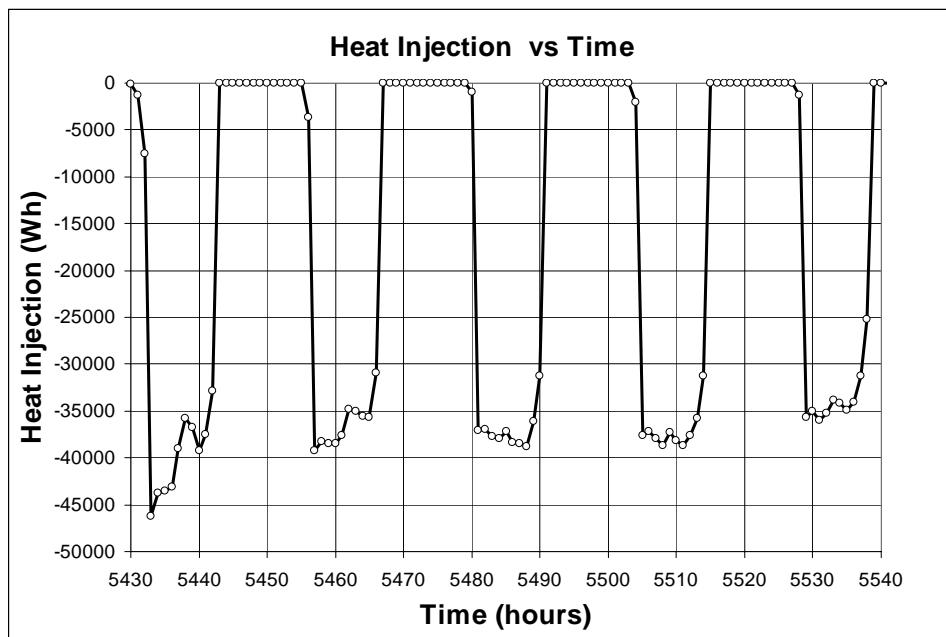

Figure 6-15 Typical Peak Loads for Small Office Building in Houston

For the church building in Nashville, a 2 hour peak load was used for heat injection in GLHEPRO. Figure 6-16 shows a typical heat injection of 2 hour duration that occurs once a week.
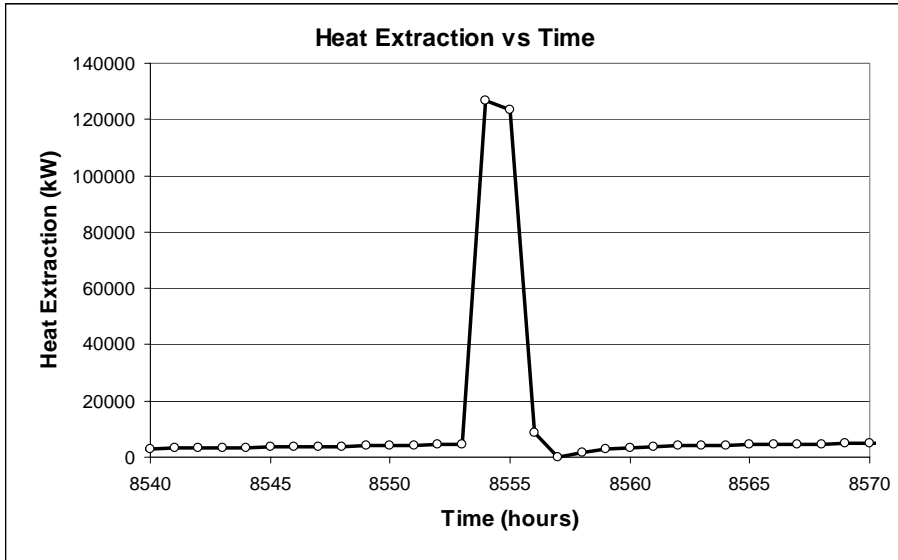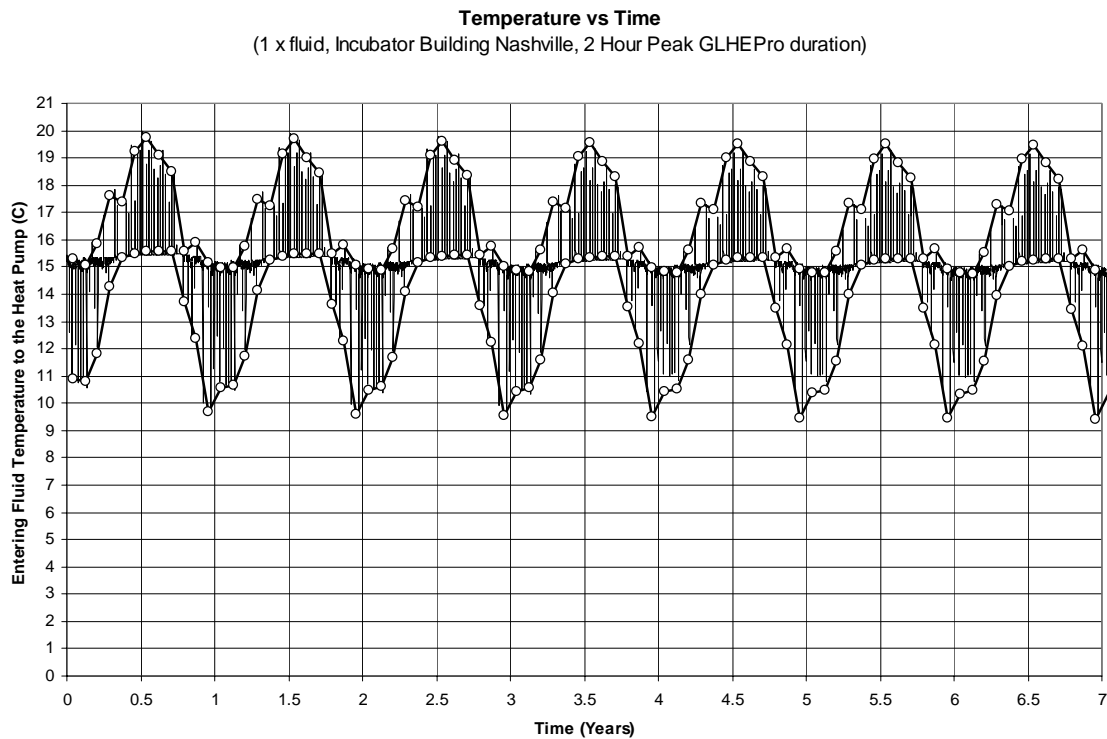
Figure 6-16 Typical Peak Loads for Church Building in Nashville

In order to compare the GLHEPRO and HVACSIM+ models the HVACSIM+ model was changed to a two component model consisting of a GLHE module and a water to air heat pump module. Figure 6-17 shows the two component model. The heat pump and GLHE components in this model are identical to those in Figure 6-1.
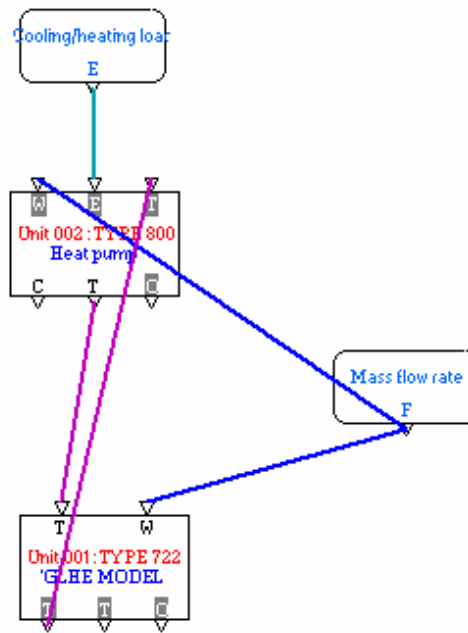
**Figure 6-17 Two Component GLHE Model**

Figures 6-18, 19, and 20 show the entering fluid temperature to the heat pump for the peak-load-dominant church building located in Nashville.   In all three cases, the maximum and minimum monthly GLHEPRO curves can be seen bounding the hourly HVACSIM+ simulations. The net change over seven years in yearly maximum and minimum temperature is less than 0.25°C (0.45°F) for both HVACSIM+ and GLHEPRO. As can be seen in Figures 6-18, 19 and 20 as the fluid factor increases, the yearly maximum temperature decreases, and yearly minimum temperature increases. Thus, for the first seven years of simulation the fluid temperatures for the 1 x fluid factor are between 19.9 and 9.2 °C (67.8 and 48.6 °F), for the 2 x fluid factor are between 19.4 and 10.0 °C (66.9 and 50 °F), and for the 4 x fluid factor are between 18.5 and 11.0 °C (65.3 and 51.8 °F).
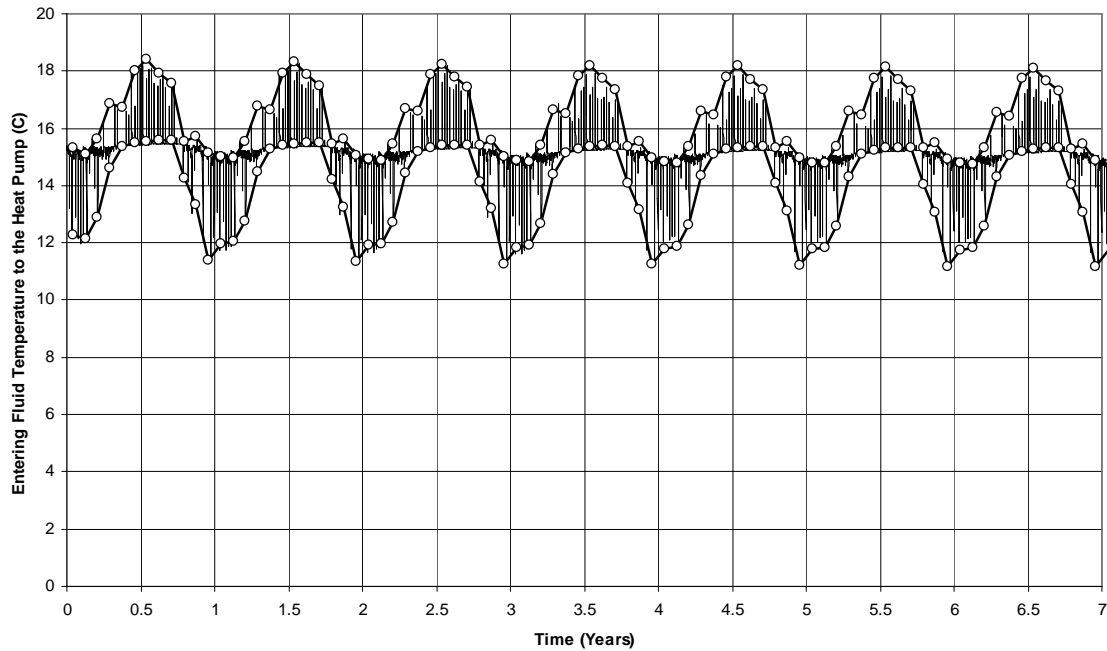
Temperature vs Time
(1 x fluid, Incubator Building Nashville, 2 Hour Peak GLHEPro duration)

Figure 6-18 Entering Temperature to the Heat Pump for a Church Building Located in Nashville, 1 x fluid, and 2 hour GLHEPRO Peak Duration

Temperature vs Time
(2 x fluid, Incubator Building Nashville, 2 Hour Peak GLHEPro duration)
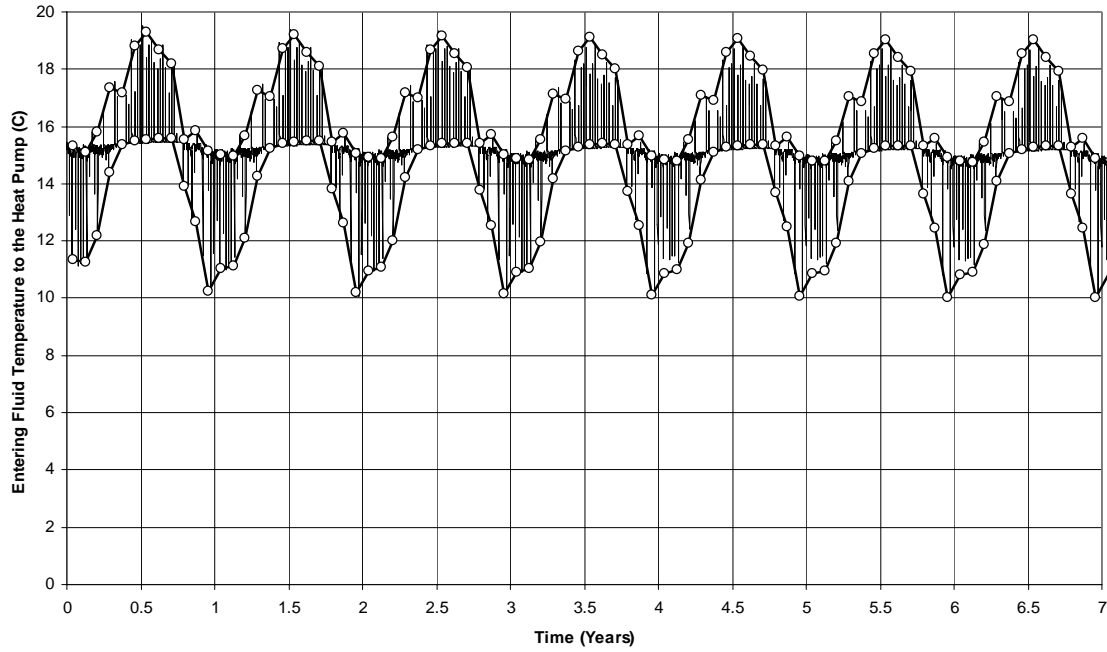
Figure 6-19 Entering Temperature to the Heat Pump for a Church Building Located in Nashville, 2 x fluid, and 2 hour GLHEPRO Peak Duration

Temperature vs Time
(4 x fluid, Incubator Building Nashville, 2 Hour Peak GLHEPro duration)

Figure 6-20 Entering Temperature to the Heat Pump for a Church Building Located in Nashville, 4 x fluid, and 2 hour GLHEPRO Peak Duration

189

Figure 6-21 and 6-22 shows the maximum and minimum yearly fluid temperature entering the heat exchanger. As can be seen the difference in the two models for the maximum yearly temperature is approximately 0.25 °C (0.45 °F). The difference between the two models for the minimum yearly temperature can be seen to be much smaller on the order of 0.1 °C (0.18 °F) for the 2 x fluid factor case. As can be seen in Figure 6-21 and 6-22, the error slightly increases as the fluid factor is increased. However, the GLHEPRO temperatures for all cases are very close to the HVACSIM+ temperatures.
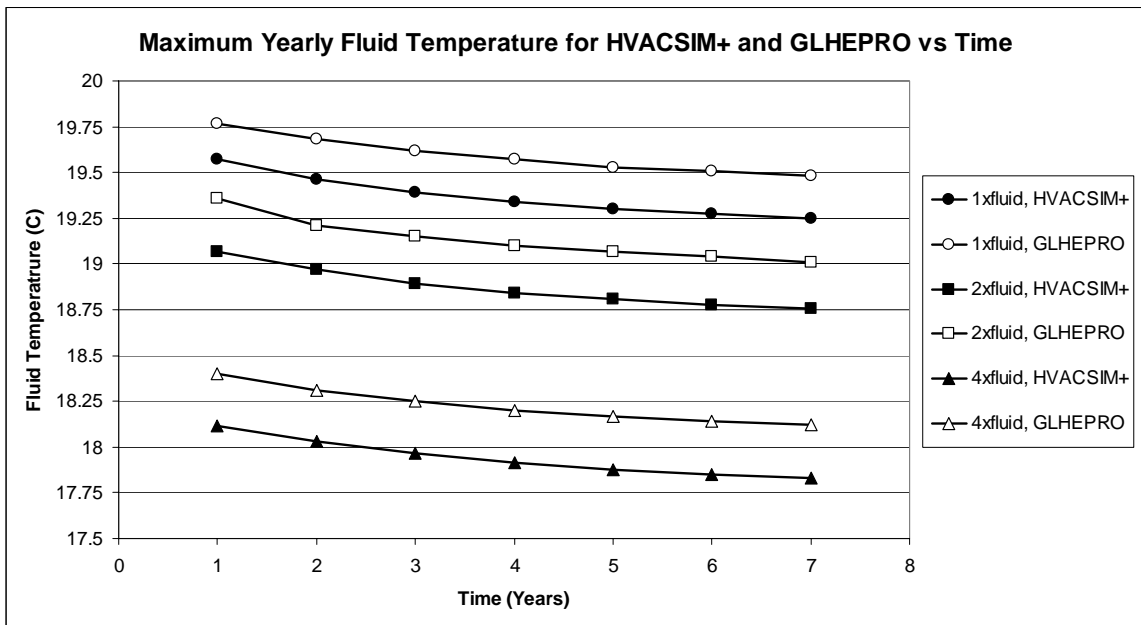

Figure 6-21 GLHEPRO and HVACSIM+ Maximum Yearly Entering Temperature to the Heat Pump for a Church Building Located in Nashville
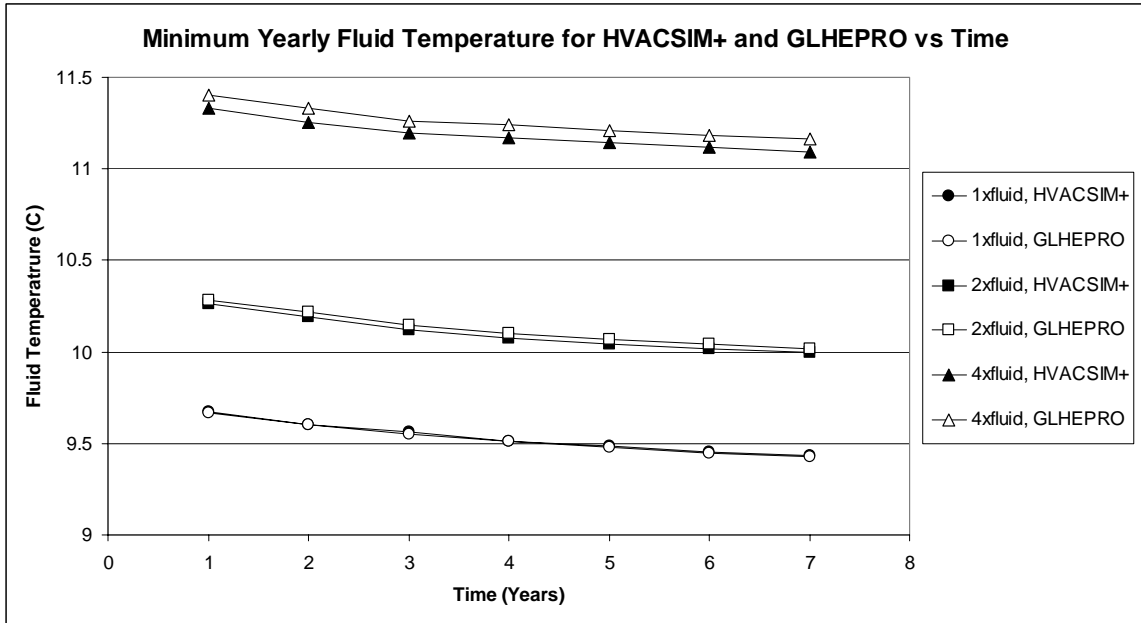
Figure 6-22 GLHEPRO and HVACSIM+ Minimum Yearly Entering Temperature to the Heat Pump for a Church Building Located in Nashville

The next three comparisons between GLHEPRO and HVACSIM+ are shown in Figure 6-23 and 6-24. These comparisons are of the small office building located in Houston. Since the building is cooling load dominant, the maximum and minimum fluid temperature rises over the duration of the seven years. Unlike the church building, this building is not peak-load-dominant. The influence of the borehole fluid mass is minimized causing the entering fluid temperature to the heat pump to change very little when the fluid factor is increased. The maximum temperature in the first year for HVACSIM+ for 1, and 2 x fluid factors is 31.8 and 31.5 °C (89.2 and 88.7 °F) respectively. This difference is approximately a fourth of the difference shown for the church building. Similar to the prior comparison, the maximum and minimum yearly temperatures in GLHEPRO and HVACSIM+ have less than 0.3 °C (5.4 °F) of difference.

Temperature vs Time
(1 x fluid, Small Office Building Houston, 8 Hour Peak GLHEPro duration)
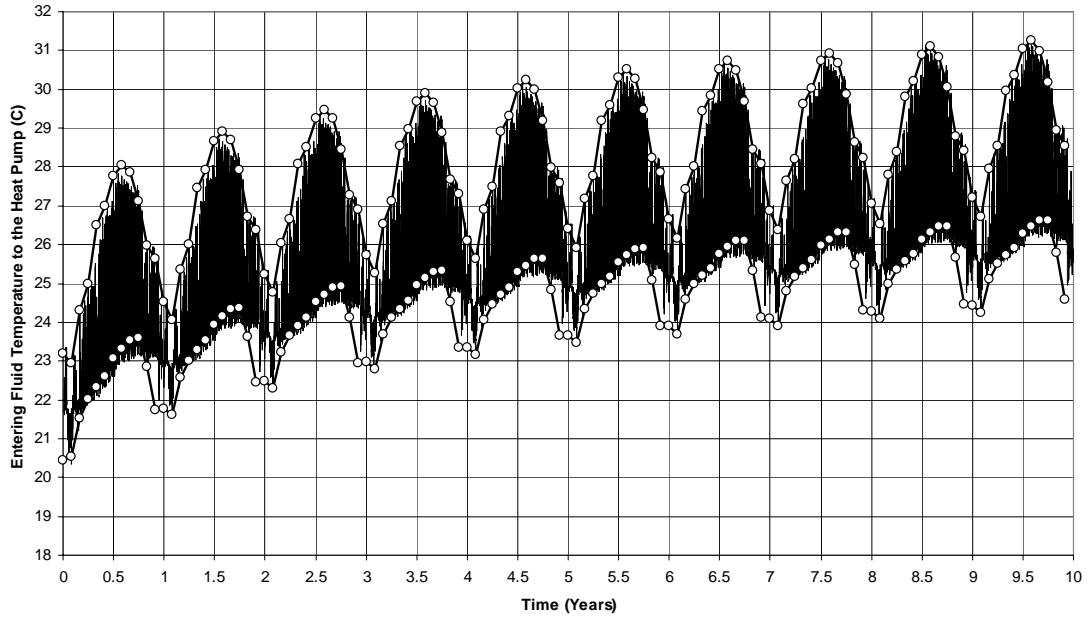
Figure 6-23 Entering Temperature to the Heat Pump for a Small Office Building Located in Houston, 1 x fluid, and 8 hour GLHEPRO Peak Duration

Temperature vs Time
(2 x Fluid, Small Office Building Houston, 8 Hour Peak GLHEPro duration)
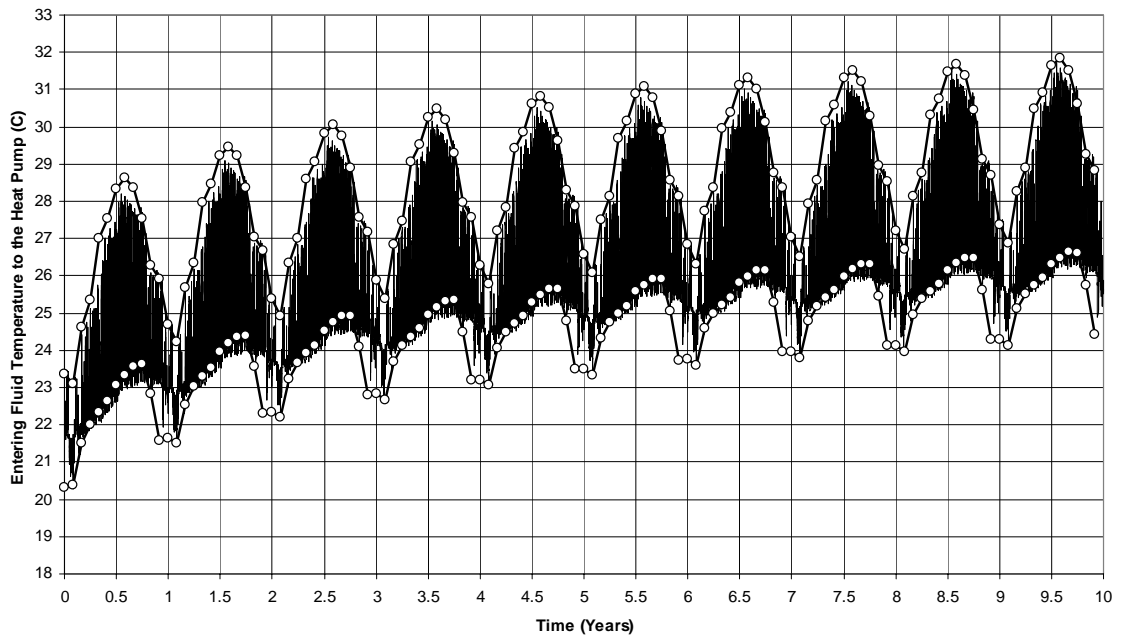
Figure 6-24 Entering Temperature to the Heat Pump for a Small Office Building Located in Houston, 2 x fluid, and 8 hour GLHEPRO Peak Duration

6.5   Conclusion

The effect of peak-load duration on the fluid temperature profile was studied by comparing the line source and BFTM-E models within a three component hourly HVACSIM+ model. For very short duration peak loads of 1 to 2 hours, there can be a 1.3 °C (2.3 °F) difference in peak temperatures between the line source and the BFTM model. For large peak loads of 8 hours duration the difference between the line source and the BFTM model is 0.3 °C (0.5 °F). However, for calculating energy consumption, the line source provides accurate solutions.

Using a two component HVACSIM+ model, GLHEPRO, when used with correct peak load durations, is shown to accurately predict the peak entering fluid temperatures. For all simulations the maximum and minimum yearly fluid temperature calculated by GLHEPRO were within 0.30°C (0.54 °F) of the temperatures calculated by the HVACSIM+ simulation.

7   CONCLUSIONS AND RECOMMENDATIONS

The primary objective, as stated in Section 1.3, is to develop and implement a system whereby engineers can accurately model and optimize short time step heat-pulse systems without time consuming numerical modeling. Within this main objective are five minor objectives. They are stated in section 1.3 but are listed again as follows:

1. Determine an appropriate method for calculating the steady state borehole resistance and implementing it in GLHEPRO.

2. Enhance the short-time-step (STS) GLHE simulation methodology to account for thermal mass of the fluid to yield more accurate designs via simulations.

3. Develop an automated method for producing the combined short and long time step g-function.

4. Evaluate the impact of the more accurate g-function calculation methodologies on the design of GSHP systems.

5. Evaluate the impact of the more accurate g-function methodologies on the simulation of GSHP.

This chapter details the completion of each of these objectives and recommendations for future work.

7.1   Conclusions

The multipole method was chosen for the steady state borehole resistance calculation. This method is very accurate and correlates with the GEMS2D solution to 3 or 4 significant digits. Unlike GEMS2D, the multipole method is an analytical solution, so it is very fast computationally, taking much less than a second to calculate the

borehole resistance. Since the borehole resistance is calculated once at the beginning of a simulation this makes the multipole method ideal for incorporating in GLHEPRO 3.

The objective of obtaining a methodology that will account for the thermal mass of the fluid was also attained. This method is derived from an analytical equation for heat transfer outside of an electrical cable buried in soil. This new method is called the borehole fluid thermal mass (BFTM) model. The BFTM model was fine tuned to provide better accuracy with a grout allocation factor (GAF) and logarithmic extrapolation. Using a fluid multiplication factor within the BFTM model allows GLHE systems to be designed to account for extra fluid in the system. The fluid factor also enables engineers to design systems which store extra water purposely to increase the efficiency of the GLHE with regards to peak loads. This thesis shows that increasing the amount of fluid in a GLHE gives a borehole system better performance by decreasing the amount of a temperature spiking due to short heat pulses.

Uniting the short and long time step g-functions became simple after the borehole resistance comparison showed that the multipole method should be used to calculate the borehole resistance. When the correct steady state borehole resistance is subtracted from the overall ground and borehole resistance from the BFTM model, the long time step and short time step g-functions will merge.

A comparison was also made between the line source and the more accurate BFTM model using one year's worth of hourly heating/cooling loads for the Houston small office building. The comparison shows that there are numerous times during the year when the delta temperature difference between the line source and the BFTM model

is over 2.5 °C (4.5 °F) however, since the small office building is not peak-load-dominant, the maximum difference in the first year's peak temperature is 0.5 °C (0.9 °F).

The final objective was to evaluate the impact of incorporating the BFTM model inside GLHEPRO. This comparison was made through 3 seven year and 2 ten year HVACSIM+ comparisons using hourly loads. Three of the simulations used a peak-load-dominant building for fluid factors of 1, 2, and 4 and two simulations used a non-peak-load-dominant building for fluid factors of 1 and 2. The BFTM model showed very similar results between HVACSIM+ and GLHEPRO. The maximum yearly fluid temperature exiting the ground loop was less than 0.3 °C (0.54 °F) difference.

7.2   Recommendations

This research introduces a method whereby the thermal mass of the fluid in a borehole can be modeled. It can be used in conjunction with any simulation that uses g-functions to model the thermal response of the ground to heat inputs. The method has been shown to be highly accurate for heat pulses of 2 or more hours. There are several research areas that could be undertaken to improve current GLHE simulations.

1. In this study the circulating fluid was assumed well mixed and turbulent. For actual systems the flow regime is dependent on fluid flow rates. Since the heat transfer properties between laminar and turbulent flow are very different the flow regime might greatly influence the performance of a GLHE system. A study determining the flow regime's impact on system design could be conducted. Assuming it is shown to be significant , a model could be developed which accounted for both laminar and turbulent flow.

196

2. The BFTM-E model which requires GAF and extrapolation time might not be

   the best application of the BEC model. A purely numerical solution to the

   BEC model might provide suitably accurate results.

References

Abramowitz, M., and I. Stegun, 1972. *Handbook of Mathematical Functions with Formulas, Graphs, and Mathematical Tables, 9th printing.* New York: Dover Publications, pp 890.

Bennet, J., J. Claesson, and G. Hellström, 1987. *Multipole Method to Compute the Conductive Heat Flows to and Between Pipes in a Composite Cylinder.* University of Lund, Department of Building Technology and Mathematical Physics. Lund, Sweden.

BLAST., 1986. *BLAST (Building Loads and System Thermodynamics).* University of Illinois, Urbana-Champaign.

Carslaw, H.S., and J.C. Jaeger, 1947. *Conduction of Heat in Solids*, Oxford, U.K.: Claremore Press.

Chiasson, A. 1999. *Advances in Modeling of Ground-Source Heat Pump Systems.* M.S. Thesis. Oklahoma State University. Stillwater, OK.

Chiasson, A. and J.D. Spitler. 2000. *A Modeling Approach To Design Of A Ground-Source Heat Pump Bridge Deck Heating System.* Proceedings of the 5th International Symposium on Snow Removal and Ice Control Technology. Roanoke, VA. September 5-8, 2000.

Chiasson, A. and J.D. Spitler. 2001. *Modeling Approach to Design of a Ground-Source Heat Pump Bridge Deck Heating System. Transportation Research Record.* 1741:207-215

Chiasson, A.D., J.D. Spitler, S.J. Rees, M.D. Smith. 2000. *A Model for Simulating the Performance of a Pavement Heating System as a Supplemental Heat Rejecter With Closed-Loop Ground-Source Heat Pump Systems. ASME Journal of Solar Energy Engineering.* November 2000. 122:183-191

Chiasson, A.D., J.D. Spitler, S.J. Rees, M.D. Smith. 2000. *A Model For Simulating The Performance Of A Shallow Pond As A Supplemental Heat Rejecter With Closed-Loop Ground-Source Heat Pump Systems.* ASHRAE Transactions. 106(2):107-121.

Claesson, J., and P. Eskilson, 1988. *Simulation Model for Thermally Interacting Heat Extraction Boreholes*.

Clark, D. R. *HVACSIM+ Building Systems and Equipment Simulation Program Reference Manual.* NBSIR 84-2996. National Bureau of Standards, January, 1985.

Drake, R., and E. Eckert, 1972. *Analysis of Heat and Mass Transfer*. New York: McGraw-Hill Book Company.

Eskilson, P., 1987. *Thermal Analysis of Heat Extraction Boreholes*. Ph.D. Thesis. Department of Mathematical Physics, Lund Institute of Technology.

a) Gu, Y., and D. O'Neal, 1998. *Development of an Equivalent Diameter Expression for Vertical U-Tubes Used in Ground-Coupled Heat Pumps*. ASHRAE Transactions 104(2): 347-355.

b) Gu, Y., and D. O'Neal, 1998. *Modeling the Effect of Backfills on U-Tube Ground Coil Performance.* ASHRAE Transactions. Volume 104(2), 356-365.

Hellstrom, G., 1991. *Ground Heat Storage: Thermal Analyses of Duct Storage Systems.* University of Lund, Department of Mathematical Physics. Lund, Sweden.

Ingersoll, R., and H. Plass, 1948. *Theory of the Ground Pipe Heat Source for the Heat Pump. Heating Piping and Air Conditioning*. July. pp. 119-122.

Ingersoll, L.R., O.J. Zobel, and A.C. Ingersoll, 1954. *Heat Conduction with Engineering, Geological, and Other Applications.* New York: McGraw-Hill.

Khan, M.H., A. Varanasi, J.D. Spitler, D.E. Fisher, R.D. Delahoussaye. 2003. *Hybrid Ground Source Heat Pump System Simulation Using Visual Modeling Tool For Hvacsim+.* Proceedings of Building Simulation 2003 pp. 641-648. Eindhoven, Netherlands, August 11-14, 2003.

Press, W.H., B.P. Flannery, S.A. Teukolsky, and W.T. Vetterling, 1989. *Numerical Recipes*. New York: Press Syndicate of the University of Cambridge.

Kavanaugh, S.P., and J.D. Deerman, 1991. *Simulation of vertical U tube ground coupled heat pump systems,* ASHRAE Transactions, Volume 97, 287-295.

Park, C., Clark D. R., Kelly G. E. 1985. *An Overview of HVACSIM+, a Dynamic Building/HVAC/Control Systems Simulation Program.* Building Energy Simulation Conference, Seattle, Washington. August 21-22, 1985.

Patankar, S.V., 1980. *Numerical Heat Transfer and Fluid Flow,* Hemisphere, New York, NY.

Paul, N.D., 1996. *The Effect of Grout Thermal Conductivity on Vertical Geothermal Heat Exchanger Design and Performance*. Master of Science Thesis. South Dakota State University.

Ramamoorthy, M. H. Jin, A. Chiasson, J.D. Spitler. 2001. *Optimal Sizing of Hybrid Ground-Source Heat Pump Systems that use a Cooling Pond as a Supplemental Heat Rejecter – A System Simulation Approach*. ASHRAE Transactions. 107(1):26-38.

Rees, S. 2001. Personal Communications. Oklahoma State University, Stillwater, OK

Rees, S.J., J.D. Spitler and X. Xiao, X 2002. *Transient Analysis of Snow-melting System Performance. ASHRAE Transactions.* 108(2):406-423.

Spitler, J.D., 2000. GLHEPRO 3.0 for Windows Users Guide. School of Mechanical and Aerospace Engineering, Oklahoma State University.

Spitler, J.D., S.J. Rees, C. Yavuzturk. 1999. *More Comments on In-situ Borehole Thermal Conductivity Testing.* The Source. Vol. 12, No. 2, March/April 1999. pp. 4-6.

Spitler, J.D, S.J. Rees, C. Yavuzturk. 2000. *Recent Developments in Ground Source Heat Pump System Design, Modeling and Applications.* Proceedings of the Dublin 2000 Conference. Dublin, September 2000.

Spitler, J.D, S.J. Rees, C. Yavuzturk. 2000. *Recent Developments in Ground Source Heat Pump System Design, Modeling and Applications.* Proceedings of the Dublin 2000 Conference. Dublin, September 2000.

SEL. 1997. *TRNSYS Manual, a transient simulation program. Madison:* Solar Engineering Laboratory, University of Wisconsin-Madison.

Varanasi, A. *Development Of A Visual Tool For HVACSIM+.* M.S. Thesis December 2002.

Yavuzturk, C., 1999. *Modeling of Vertical Ground Loop Heat Exchangers for Ground Source Heat Pump Systems*. Ph.D. Thesis. Mechanical and Aerospace Engineering, Oklahoma State University.

Yavuzturk, C., and J. Spitler, 1999. *A Short Time Step Response Factor Model for Vertical Ground Loop Heat Exchangers*. ASHRAE Transactions. 105(2): 475-485.

Yavuzturk, C., J.D. Spitler. 2000. *Comparative Study to Investigate Operating and control Strategies for Hybrid Ground Source Heat Pump Systems Using a Short Time-step Simulation Model.* ASHRAE Transactions. 106(2):192-209.

Yavuzturk, C., J. Spitler, and S. Rees. 1999. *A Transient Two-dimensional Finite Volume Model for the Simulation of Vertical U-tube Ground Heat Exchangers.* ASHRAE Transactions. 105(2):465-474.

VITA

Ray Young

Candidate for the Degree of

Master of Science

Thesis: DEVELOPMENT, VERIFICATION, AND DESIGN ANALYSIS OF THE

BOREHOLE FLUID THERMAL MASS MODEL FOR APPROXIMATING

SHORT TERM BOREHOLE THERMAL RESPONSE

Major Field: Mechanical Engineering

Biographical:

Personal: Born in Waterloo, Iowa, on Jun 26, 1977, to Grant and Janice Young.

Education: Received Bachelor of Science in Mechanical Engineering from Oklahoma State University, Stillwater, Oklahoma in June 2001. Completed the requirements for the Master of Science degree with a major in Mechanical Engineering at Oklahoma State University in December, 2004

Experience: Employed by Oklahoma State University, Department of Mechanical Engineering as a research assistant June 2001 to July 2002. Employed by Lockheed Martin as an Aeronautical Engineer from July 2002 to December 2004.

Professional Memberships: None